

1992

Painleve singularity analysis applied to charged particle dynamics during reconnection

Jay Walter Larson
College of William & Mary - Arts & Sciences

Follow this and additional works at: <https://scholarworks.wm.edu/etd>



Part of the [Astrophysics and Astronomy Commons](#), and the [Plasma and Beam Physics Commons](#)

Recommended Citation

Larson, Jay Walter, "Painleve singularity analysis applied to charged particle dynamics during reconnection" (1992). *Dissertations, Theses, and Masters Projects*. Paper 1539623818.
<https://dx.doi.org/doi:10.21220/s2-c0jn-9756>

This Dissertation is brought to you for free and open access by the Theses, Dissertations, & Master Projects at W&M ScholarWorks. It has been accepted for inclusion in Dissertations, Theses, and Masters Projects by an authorized administrator of W&M ScholarWorks. For more information, please contact scholarworks@wm.edu.

INFORMATION TO USERS

This manuscript has been reproduced from the microfilm master. UMI films the text directly from the original or copy submitted. Thus, some thesis and dissertation copies are in typewriter face, while others may be from any type of computer printer.

The quality of this reproduction is dependent upon the quality of the copy submitted. Broken or indistinct print, colored or poor quality illustrations and photographs, print bleedthrough, substandard margins, and improper alignment can adversely affect reproduction.

In the unlikely event that the author did not send UMI a complete manuscript and there are missing pages, these will be noted. Also, if unauthorized copyright material had to be removed, a note will indicate the deletion.

Oversize materials (e.g., maps, drawings, charts) are reproduced by sectioning the original, beginning at the upper left-hand corner and continuing from left to right in equal sections with small overlaps. Each original is also photographed in one exposure and is included in reduced form at the back of the book.

Photographs included in the original manuscript have been reproduced xerographically in this copy. Higher quality 6" x 9" black and white photographic prints are available for any photographs or illustrations appearing in this copy for an additional charge. Contact UMI directly to order.

U·M·I

University Microfilms International
A Bell & Howell Information Company
300 North Zeeb Road, Ann Arbor, MI 48106-1346 USA
313/761-4700 800/521-0600

Order Number 9236129

**Painlevé singularity analysis applied to charged particle
dynamics during reconnection**

Larson, Jay Walter, Ph.D.

The College of William and Mary, 1992

U·M·I
300 N. Zeeb Rd.
Ann Arbor, MI 48106



**PAINLEVÉ SINGULARITY ANALYSIS
APPLIED TO CHARGED PARTICLE DYNAMICS
DURING RECONNECTION**

A Dissertation

Presented to

The Faculty of the Department of Physics
The College of William and Mary in Virginia

In Partial Fulfillment

Of the Requirements for the Degree of
Doctor of Philosophy

by


J. Walter Larson

1992

APPROVAL SHEET

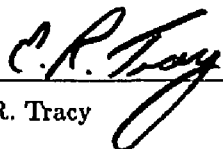
This dissertation is submitted in partial fulfillment of the
requirements for the degree of

Doctor of Philosophy

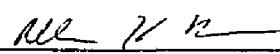


J. Walter Larson


Approved, April 1992



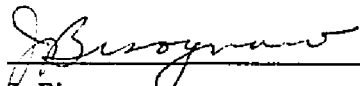
E. R. Tracy



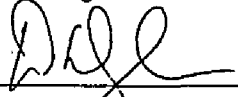
A. H. Boozer



G. Vahala



J. Bisognano



D. Douglas
CEBAF, Newport News, VA

To My Mother Joyce Larson,

who gave me so many years of her life,

and My Father Walter "Bud" Larson,

whom I miss very much...

THANKS!

CONTENTS

TABLE OF CONTENTS	iv
ACKNOWLEDGEMENTS	vii
LIST OF TABLES	x
LIST OF FIGURES	xi
ABSTRACT	xvi
Chapter One: Reconnection and Magnetic Nulls	
§1.1a What is Reconnection?	2
§1.1b Test-Particle Modelling of Reconnection	7
§1.2a Basics of Particle Orbit Theory in Plasmas	9
§1.2b Drift Motions	12
§1.2c Adiabatic Invariants	16
§1.3a The Magnetic Field Near a Null	22
§1.3b Test-Particle Motion Near a Magnetic Null	23
§1.4 A Simple Model For Neutral Lines and Neutral Sheets	27
Chapter Two: Integrability and Singularity Analysis	
§2.1 Dynamical Systems and Integrability	36
§2.2 Singularity Analysis	41

§2.3 The Ablowitz-Ramani-Segur (ARS) Algorithm	48
§2.4 Tests For Nonintegrability	58
§2.5 Direct Methods for the Construction of Integrals	62
Chapter Three: Singularity Analysis Applied to Test-Particle Equations of Motion	
§3.1 A Simple Model and its Symmetries	64
§3.2 Painlevé Property Test of (3.1.5a-e)	69
§3.4 Yoshida Analysis of (3.1.4a-f)	91
§3.5 Summary	94
Chapter Four: Trajectories, Asymptotic Behavior, and Invariants;	
Part I: The Weak Painlevé Candidates	
§4.1a Agenda for Testing the Singularity Analysis Results	96
§4.1b Plan of the Numerical Experiments	98
§4.1c Simulations of Ensembles of Test Particles	101
§4.2 Properties of Trajectories in X-Line Configurations	104
§4.3 Properties of Trajectories in Elliptical O-Line Configurations	121
§4.4 Summary of the Properties of the Weak Painlevé Candidates	138
Chapter Five: Trajectories, Asymptotic Behavior, and Invariants;	
Part I: Cases that Possess the Painlevé Property	

§5.1 What the Painlevé Property Implies	140
§5.2 The Neutral Sheet Configuration	141
§5.3 The Circular O-Line Geometry	150
§5.4 More About the Second Painlevé Transcendent	158
§5.5 Exact Solutions to the Kinetic Equation	167

APPENDICES:

Appendix One: Determination of the Leading Order Behaviors for Equations (3.2.2a-c)	169
Appendix Two: The Slab ($\delta = 0$) Geometry	180
Appendix Three: Proof that the Radial Equation Possesses The Painlevé Prop- erty	185
Appendix Four: Symplectic Integration	
§A4.1 Introduction	190
§A4.2 Constructing Symplectic Schemes	192
§A4.3 Numerical Scheme for Equations (1.4.8a-f)	205
§A4.4 Symplectic Scheme for the Reduced System (5.3.12)	208
Appendix Five: Computer Code XOSsim.f	212
References	243
Vita	250

ACKNOWLEDGEMENTS

This is precisely how I wanted it to end: up all night, fingers flailing at the keyboard. It's now 4:57 A. M., and I'm sitting here trying to wrap up my graduate career in a page or so—not an easy task. This is, after all, The Biggest Thing I've Done, and something I could not have done without help from so many people. What follows is an incomplete list...

My defense committee: Drs. Joseph Bisognano, Allen Boozer, David Douglas, and George Vahala. Thank you for taking the time to read this document, offering constructive criticisms, and making my defense an interesting experience.

My Advisor: Dr. Gene Tracy. Thank you for the time, effort, good humor, guidance, and above all, PATIENCE. Thanks for introducing me to soliton theory and the wonderful world of singularity analysis. Thanks for pulling the strings needed to get me to Santa Fe. Thanks from rescuing me from unemployment, and providing the opportunity to find out what's so bad/good about neural nets. It has been hard work and great fun. I must also thank Gene's wife Maureen, for the wonderful party, and a fantastic cake.

Dr. John Finn of the University of Maryland: Much thanks for the introduction to the technique of symplectic integration, the substantial help with our numerical simulation effort, and the useful discussions.

Dr. Barbara Abraham-Shrauner of Washington University: Thanks for the useful correspondence, advice, and involvement in our work.

The Staff Faculty and of the Physics Department: Thank you for the hospitality, coffee, photocopying, use of the key to the supply closet, and above all, the relaxed atmosphere that normally prevails.

April: Thank you for the support, love, patience and company. The past several

months have been absolutely miserable, but they would have been much worse without you. Thanks for being so good about the skiing trip we missed over spring break, '92 (I was stuck in the 'burg, writing at a furious pace).

My Many Friends/Partners in Crime: Benny Bach, Doug Baker, Jim Fedchak, Matt Coffey, Computer Science Matt (Johnson), and everyone else here. It's been a lot of fun 1) climbing radio towers, 2) making fireworks, 3) slam dancing, 4) drinking, 5) kayaking in the pool at Governor's Square, 6) talking when we all should be working, and 7) anything else to relieve the tedium that comes with living in Williamsburg. In particular, much thanks go to Alastair Neil, who has been great company and help these (too!) many years, and thanks for teaching me that GOTO statements *are EVIL*.

My Parents and Family: I can never repay the support and love that my parents have given to me. Words fail to express the good fortune that I have had in the Great Lottery. Any good in me is due to them. I only wish that my father had lived to see this day.

The City and People of Williamsburg: Where history is "sanitized for Your Protection." Thanks for showing me that there are much worse places than Des Moines, Iowa. If you live here, I have only three things to say: 1) burn down your house, 2) collect the insurance money, and 3) move to Santa Fe.

Others: Hunter S. Thompson, William S. Burroughs, Jello Biafra, The Replacements, Black Flag, The Flaming Lips, David Lynch, The Pixies, Brian Eno, The Velvet Underground, Laurie Anderson, the Marquis de Sade, Mark Rothko, the Marx Brothers, the Residents, the Jesus Lizard, Big Black, WCWM, Hassan Chop, Kissy Burdock, John Lee Hooker, Johnny Cash, Harry Belafonte, and Mojo Nixon (not necessarily in that order).

My Future Employer: Wherever you are (don't worry gang, I have a great summer job!).

LIST OF TABLES

Table	Page
TABLE OF CONTENTS	iv
3.2.1 Allowed Values of δ for Rational $\beta_y \in (-1, 0)$	74
3.2.2 Allowed Values of δ for Rational $\beta_y \in (0, 1)$	75
3.2.3 Allowed Values of δ for Rational $\beta_y > 1$	76
3.2.4 Allowed Values of δ for Rational $\beta_y \in (0, \frac{1}{2})$	83
A1.1 Filter Comparing (A1.1a) and (A1.1b)	175

LIST OF ILLUSTRATIONS

Figure	Page
1.1.1 X-Line Magnetic Fields for Various δ	4
1.1.2 O-Line Magnetic Fields for Various δ	5
1.1.3 The Neutral Sheet ($\delta = 0$)	5
1.1.4 Plasma Flow Field for an X-Line Magnetic Field	6
1.2.1 The Pitch Angle θ	19
1.2.2 Mirror Points and Magnetic Field Strength	20
1.4.1 Unit Vectors \hat{b} , $\hat{e}_{\perp 1}$, and $\hat{e}_{\perp 2}$	30
1.4.2 Unmagnetized Regions for Various δ	32
1.4.3a Final Kinetic Energy vs. y_{gc_0} ($\delta = 1$)	33
1.4.3b Detail of Figure 1.4.3a	34
2.1.1 Natural Boundaries for the Hénon-Heiles System	45
2.3.1 The Ablowitz-Ramani-Segur (ARS) Algorithm	57
3.3.1 Angles θ_1 and θ_2 for an X-Line Field ($\delta = \frac{1}{4}$)	66
3.4.1 Distribution in δ of the Painlevé and Weak Painlevé Cases	95
4.1.1 Initializing the Test Particle	99

4.2.1 x - y Trajectory ($\delta = \frac{1}{8}$)	106
4.2.2 x - z Trajectory ($\delta = \frac{1}{8}$)	106
4.2.3 x -Phase Space Trajectory Trajectory ($\delta = \frac{1}{8}$)	107
4.2.4 z -Phase Space Trajectory Trajectory ($\delta = \frac{1}{8}$)	108
4.2.5 The Magnetic Moment μ vs. t ($\delta = \frac{1}{8}$)	109
4.2.6a Exit Kinetic Energy vs. Initial Position ($\delta = \frac{1}{8}$)	110
4.2.6b Detail of Figure 4.2.6a	110
4.2.7 Exit Kinetic Energy vs. Initial Position ($\delta = \frac{15}{128}$)	111
4.2.8 Exit Kinetic Energy vs. Initial Position ($\delta = \frac{17}{128}$)	112
4.2.9 x - y Trajectory ($\delta = 4.95 \times 10^{-3}$)	114
4.2.10 x - z Trajectory ($\delta = 4.95 \times 10^{-3}$)	114
4.2.11 x -Phase Space Trajectory Trajectory ($\delta = 4.95 \times 10^{-3}$)	115
4.2.12 z -Phase Space Trajectory Trajectory ($\delta = 4.95 \times 10^{-3}$)	115
4.2.13 y -Phase Space Trajectory Trajectory ($\delta = 4.95 \times 10^{-3}$)	116
4.2.14 The Magnetic Moment μ vs. t ($\delta = 4.95 \times 10^{-3}$)	116
4.2.15a Exit Kinetic Energy vs. y_{gc_0} ($\delta = 4.95 \times 10^{-3}$)	117
4.2.15b Detail of Figure 4.2.15a	117
4.2.16 Exit Kinetic Energy vs. y_{gc_0} ($\delta = 5.0 \times 10^{-3}$)	118

4.2.17 y -Phase Space Trajectory Trajectory ($\delta = 4.995 \times 10^{-4}$)	119
4.2.18 Test Particle Kinetic Energy vs. Time ($\delta = \frac{17}{128}$)	120
4.2.19 Test Particle Kinetic Energy vs. Time ($\delta = 4.95 \times 10^{-3}$)	121
4.3.1 Frequency of the x -Oscillations ($\delta = -\frac{1}{8}$)	125
4.3.2 Amplitude of the x -Oscillations ($\delta = -\frac{1}{8}$)	126
4.3.3 A Typical x - y Trajectory ($\delta = -\frac{1}{8}$)	127
4.3.4 A Typical x - z Trajectory ($\delta = -\frac{1}{8}$)	127
4.3.5 A Typical x -Phase Space Trajectory ($\delta = -\frac{1}{8}$)	128
4.3.6 A Typical y -Phase Space Trajectory ($\delta = -\frac{1}{8}$)	129
4.3.7 A Typical z -Phase Space Trajectory ($\delta = -\frac{1}{8}$)	129
4.3.8 Quasiperiodic x - y Trajectory ($\delta = -\frac{1}{16}$)	130
4.3.9 x - y Trajectory ($\delta = -4.95 \times 10^{-3}$)	130
4.3.10 x - z Trajectory ($\delta = -4.95 \times 10^{-3}$)	131
4.3.11 x -Phase Space Trajectory Trajectory ($\delta = -4.95 \times 10^{-3}$)	131
4.3.12 y -Phase Space Trajectory Trajectory ($\delta = -4.95 \times 10^{-3}$)	132
4.3.13 Magnetic Moment μ vs. time ($\delta = -\frac{1}{8}$)	133
4.3.14 Action Integral in x , J_x , vs. Time ($\delta = -\frac{1}{8}$)	134
4.3.15 Action Integral in y , J_y , vs. Time ($\delta = -\frac{1}{8}$)	134

4.3.16 Test-Particle Kinetic Energy vs. Time ($\delta = -\frac{1}{8}$)	135
4.3.17 Log-log Plot of E_K vs. t ($\delta = -\frac{1}{16}$)	136
4.3.18 Exit Kinetic Energy vs. Initial Position ($\delta = -\frac{1}{8}$)	137
4.3.19 Detail of Figure 4.3.18	137
5.2.1 Frequency of the x -Oscillations in the Neutral Sheet	145
5.2.2 A Typical x - y Trajectory	145
5.2.3 A Typical x -Phase Space Trajectory ($\epsilon > 0$)	146
5.2.4 Action integral in x , J_x vs. Time ($\epsilon > 0$)	147
5.2.5 A Typical x - y Trajectory ($\epsilon < 0$)	148
5.2.6 A Typical x -Phase Space Trajectory ($\epsilon < 0$)	148
5.2.7 Action integral in x , J_x vs. Time ($\epsilon < 0$)	149
5.2.8 Magnetic Moment μ vs. Time ($\epsilon < 0$)	149
5.3.1 A Typical ρ -Phase Space Trajectory ($\epsilon > 0$)	156
5.3.2 Radial Action integral J_ρ vs. Time ($\epsilon > 0$)	157
5.4.1 Sectoring of the Complex ζ -Plane Near $\zeta = \infty$	161
5.4.2 Contours for the Inverse Problem	165
A4.2.1 Relative Error in H_x vs. Time	200
A4.2.2 Relative Error in H_y vs. Time	201

A4.2.3 Relative Error in H_z vs. Time	201
A4.3.1 Relative Error in H vs. Time	208
A4.4.1 Extended Phase Space Hamiltonian vs. Time	211

ABSTRACT

For a plasma in the collisionless régime, test-particle modelling can lend some insight into the macroscopic behavior of the plasma, e.g conductivity and heating. A common example for which this technique is used is a system with electric and magnetic fields given by $\mathbf{B} = \delta y \hat{x} + x \hat{y} + \gamma \hat{z}$ and $\mathbf{E} = \epsilon \hat{z}$, where δ , γ , and ϵ are constant parameters. This model can be used to model plasma behavior near neutral lines, ($\gamma = 0$), as well as current sheets ($\gamma = 0, \delta = 0$). The integrability properties of the particle motion in such fields might affect the plasma's macroscopic behavior, and we have asked the question "*For what values of δ , γ , and ϵ is the system integrable?*" To answer this question, we have employed *Painlevé singularity analysis*, which is an examination of the singularity properties of a test particle's equations of motion in the complex time plane. This analysis has identified two field geometries for which the system's particle dynamics are integrable in terms of the second Painlevé transcendent: the circular O-line case and the case of the neutral sheet configuration. These geometries yield particle dynamics that are integrable in the Liouville sense (i.e. there exist the proper number of integrals in involution) in an extended phase space which includes the time as a canonical coordinate, and this property is also true for nonzero γ . The singularity property tests also identified a large, dense set of X-line and O-line field geometries that yield dynamics that may possess the weak Painlevé property. In the case of the X-line geometries, this result shows little relevance to to the physical nature of the system, but the existence of

a dense set of elliptical O-line geometries with this property may be related to the fact that for ϵ positive, one can construct asymptotic solutions in the limit $t \rightarrow \infty$.

Painlevé Singularity Analysis
Applied to Charged Particle Motion
During Reconnection

CHAPTER ONE

RECONNECTION AND MAGNETIC NULLS

§1.1a What Is Reconnection?

The first mention of the phenomenon of magnetic reconnection can be traced to Giovanelli's work on solar flares [1-3]. Magnetic reconnection is a plasma process that has seen intense interest over the past thirty-five years [4]. In our solar system, reconnection is considered to be an important mechanism for plasma heating in the solar corona [5,6], the Earth's and other planetary magnetospheres [7-9], as well as the study of plasma behavior in comet tails [10]. Outside of our solar system, reconnection may be of importance in the study of accretion disks, as well as current sheets that occur in interstellar and intergalactic space [11]. In the field of magnetic confinement fusion devices, such as tokamaks and stellarators, reconnection can lead to instabilities and loss of confinement [12].

A basic understanding of the process of reconnection can be gained by considering a plasma which obeys the generalized version of Ohm's law[13]:

$$\mathbf{E} + \frac{1}{c} \mathbf{v} \times \mathbf{B} = \frac{1}{\sigma} \mathbf{j}. \quad (1.1.1a)$$

$$\nabla \times \mathbf{E} = -\frac{1}{c} \frac{\partial \mathbf{B}}{\partial t} \quad (1.1.1b)$$

$$\nabla \times \mathbf{B} = -\frac{1}{c} \frac{\partial \mathbf{E}}{\partial t} + \frac{4\pi}{c} \mathbf{j}, \quad (1.1.1c)$$

where \mathbf{E} is the electric field in the plasma's rest frame, \mathbf{v} is the plasma flow velocity field, \mathbf{B} is the magnetic field, \mathbf{j} is the current, σ is the scalar electrical conductivity

of the plasma, and c is the speed of light. The complete picture of plasma processes must also include force and energy balance equations, as well as mass and charge conservation laws, but for our purposes, (1.1.1a-c) are all we need for the present discussion.

Taking the curl of (1.1.2), and applying both Faraday's and Ampère's laws (1.1.1b,c), and neglecting the displacement current term present in (1.1.1c), yields an expression for the temporal evolution of \mathbf{B} :

$$\frac{\partial \mathbf{B}}{\partial t} = \nabla \times \mathbf{v} \times \mathbf{B} + \frac{\nabla^2 \mathbf{B}}{\sigma}. \quad (1.1.2)$$

The term $\nabla \times \mathbf{v} \times \mathbf{B}$ is related to the convection of the magnetic field with the plasma flow, while the term involving the Laplacian of \mathbf{B} describes the diffusion of magnetic field lines through the plasma. In the limit of ideal plasma conductivity—i.e. $\sigma \rightarrow \infty$ —the dominant field evolution process is convection, meaning that the plasma and field lines are “frozen” together. This bonding between the magnetic field and plasma is a basic component of ideal magnetohydrodynamics (MHD), where a fluid element is associated with a single magnetic field line during the system's evolution.

When the second term on the RHS of (1.1.2) is dominant over the convection term, the plasma has a finite conductivity, and ideal MHD breaks down. This can lead to changes in the magnetic field topology, which can in turn produce strong electric fields capable of driving currents and heating the plasma.

From the point of view of magnetic field topology, reconnection will occur wherever sudden changes in the magnetic field geometry take place [8]. In particular,

points, curves, or surfaces at which the magnetic field strength is zero will lead to reconnection [14]. These regions are called *magnetic nulls* [15], and are of great importance in the study of reconnection in astrophysical plasmas. A simple example of a magnetic and electric field combination that will yield a null is

$$\mathbf{B} = \frac{B_0}{L}(\delta y\hat{x} + x\hat{y}) \quad \mathbf{E} = E_0\hat{z}, \quad (1.1.3)$$

where B_0 , δ and L are constant parameters.

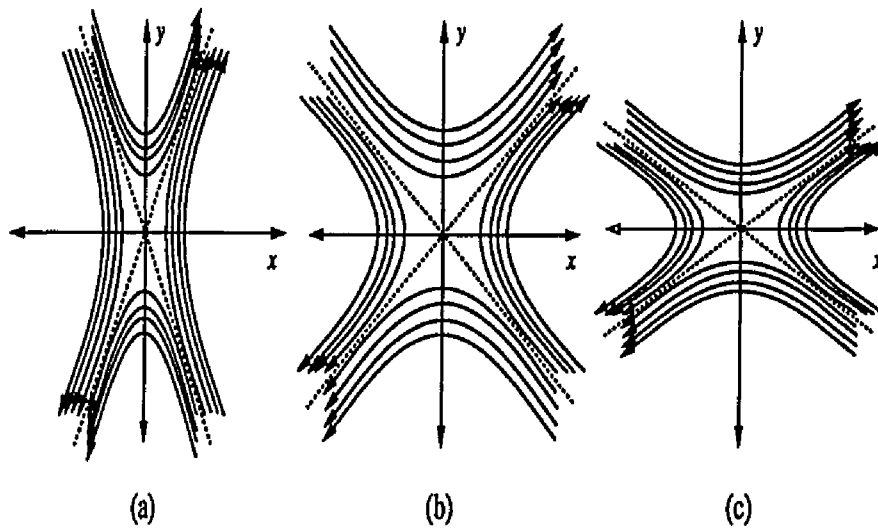


Figure 1.1.1. X-Line Magnetic Fields for Various δ :

a) $\delta = \frac{1}{4}$, b) $\delta = 1$, c) $\delta = 4$.

For $\delta > 0$, the magnetic field lines are hyperbolic, and the z -axis is a neutral line, called an *X-type null line*. The asymptotes for these hyperbolae, indicated by the dotted lines in Figure 1.1.1, are called *field line separatrices*. For $\delta < 0$, the field lines are closed and elliptical (Figure 1.1.2), with zero magnetic field along the z -axis a neutral line, which is called an *O-type neutral line*. For the O-line geometry, the z -axis is the field line separatrix. Finally, for the case $\delta = 0$ (or

$\delta \rightarrow \pm\infty$), the magnetic field lines become straight lines, and the plane $x = 0$ (or $y = 0$) is a neutral sheet, as shown in Figure 1.1.3. For the neutral sheet, the field line separatrix is the neutral plane itself.

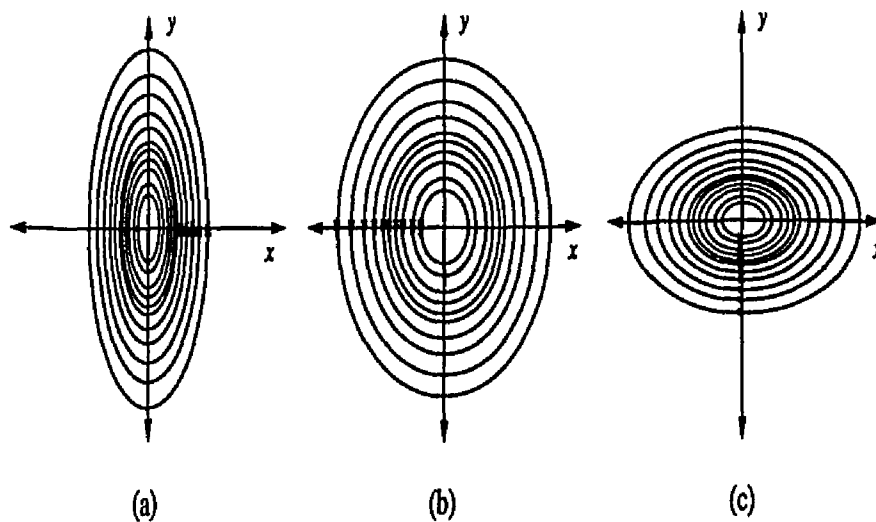


Figure 1.1.2. O-Line Magnetic Fields for Various δ :

a) $\delta = -\frac{1}{4}$, b) $\delta = -1$, c) $\delta = -4$.

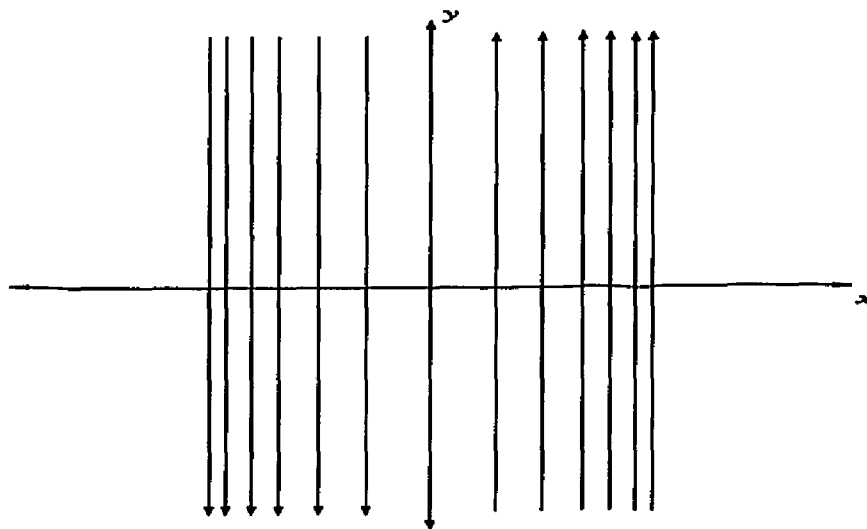


Figure 1.1.3. The Neutral Sheet ($\delta = 0$).

The connection between these field structures and reconnection can be seen by examining the plasma flow near the nulls. If we take E_0 , B_0 , and L to be positive quantities, the wholesale motion of the plasma can be viewed in terms of the $\mathbf{E} \times \mathbf{B}$ drift, which will be derived in the next section. In Figure 1.1.4 the plasma flow field lines are represented by bold lines, and depict the trajectories of the $\mathbf{E} \times \mathbf{B}$ drift for $\delta = 1$, which is the vector field

$$\mathbf{v}_E = \frac{c}{\delta^2 y^2 + x^2} (-x\hat{x} + \delta y\hat{y}).$$

Note that for X-type configurations, the plasma flows in towards the null in regions I and III, and away from the null in regions II and IV. For the O-type null, the plasma flow is much more simple, with the plasma is focused in towards the null, which is also the case for the neutral sheet.

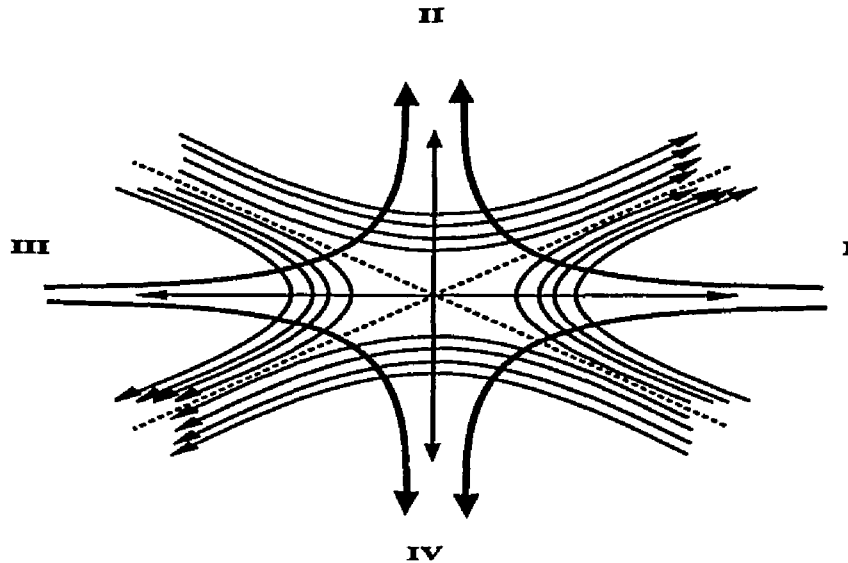


Figure 1.1.4. Plasma Flow Field for an X-Line Field.

The aforementioned situation leads to two more specific definitions of recon-

nection. Dungey [16] defines reconnection as a phenomenon which occurs if an electric field exists along an X-type null line. Vasylunas [17] views reconnection as a process which occurs when a plasma flow crosses a magnetic field line separatrix.

Magnetic nulls are not the only types of field structures that will allow reconnection to take place. In fact, in most applications relevant to magnetic confinement fusion, magnetic nulls are not the source of reconnection, but rather a sudden change in magnetic field topology. In the case of tearing modes [12], fields given by (1.1.3) have an additional shear magnetic field component along the z -axis, and reconnection can still occur. In plasma fusion devices, reconnection will occur when the poloidal components of the field exhibit nulls, but the toroidal component of the magnetic field, will be nonzero.

§1.1b Test-Particle Modelling of Reconnection

The study of plasmas in the low-collisionality régime lends itself well to test-particle modelling [18]. A large ensemble of particles representing the plasma are modelled using single-particle equations of motion, and macroscopic quantities such as currents and temperature are obtained via appropriate averages over the ensemble. This approach has been used to calculate the self-consistent electric field and finite conductivity of plasma in an X-line configuration [19,20], as well as plasma heating [21].

The test-particle approach simplifies the task of modelling the plasma greatly, but the approach raises another set of questions:

Q1: What is the generic behavior of the single-particle equations of motion?

These equations may or may not be integrable. In the case of the X-line case of (1.1.3), the particle dynamics appear to be chaotic [20,22]. For O-lines and neutral slabs, we will find that the motion is quite regular, and in some cases, it is integrable in the Hamiltonian sense (i.e. there exist an appropriate number of integrals that are in involution). It is this question that is the central focus of this dissertation.

Q2: What effect does the answer of Q1 have on the macroscopic quantities associated with the plasma?

We might find for instance that the transport properties (e.g. electrical conductivity σ) of the plasma depend on the integrability properties of our test-particle system. These issues are outside of the scope of our present work, but we feel that they are worthy of investigation. In particular, we would like to apply the results of the work contained in this dissertation to the study of neutral sheets [23] and O-type neutral lines [24], which are also believed to play important roles in the magnetosphere.

The macroscopic behavior of a plasma can be studied in terms of a *distribution function* $f(\mathbf{q}, \mathbf{p}, t)$. In the noncollisional limit, the plasma's distribution function will satisfy the kinetic equation [13]

$$\frac{\partial f}{\partial t} + \dot{\mathbf{q}} \cdot \frac{\partial f}{\partial \mathbf{q}} + \dot{\mathbf{p}} \cdot \frac{\partial f}{\partial \mathbf{p}} = 0. \quad (1.1.4)$$

Here, \mathbf{q} are spatial coordinates, \mathbf{p} are their canonical conjugate momenta, and t is the time variable. The test particle trajectories are the characteristics for the kinetic equation, which implies that if we know the integrals associated with the test-particle motion, we will be able to construct exact solutions to (1.1.4). This fact

gives impetus to the investigation of the integrability properties of the test-particle equations of motion for a plasma. There are methods which fall under the title of *singularity analysis*, which can be applied to a system of differential equations to determine its propensity for exact solutions. The subject of singularity analysis will be developed in the next chapter, and applied to a test-particle model associated with reconnection in Chapter Three.

For now, we shall spend the next section reviewing some of the basic concepts of plasma physics which are applicable to the present work. This review is included for the sake of completeness, and readers who are familiar with the basics of particle orbit theory and the use of adiabatic invariants can skip this section, and move on to § 1.3, where a test-particle model for reconnection is derived.

§1.2a Basics of Particle Orbit Theory in Plasmas

The motion of charged particles in magnetic and electric fields is a basic problem in plasma physics. The particle's equations of motion in Newtonian form are given by

$$m \frac{d^2 \mathbf{r}}{dt^2} = q \mathbf{E} + \frac{q}{c} \mathbf{v} \times \mathbf{B}, \quad (1.2.1)$$

where \mathbf{r} is the particle's position, \mathbf{v} its velocity, and m and q are the particle's mass and charge, respectively. The electric field \mathbf{E} and magnetic field \mathbf{B} are generally functions of both the particle's position \mathbf{r} and the time t . Within the scope of this dissertation, however, we shall take \mathbf{E} to be uniform, and \mathbf{B} will be a function of the coordinate vector \mathbf{r} . It is important to note that we are taking the fields \mathbf{E} and \mathbf{B} in (1.1.1) as given, and will not be attempting to solve for the self-consistent

magnetic and electric fields.

The most elementary case of (1.2.1) arises when \mathbf{E} is uniform and $\mathbf{B} = 0$, which leads to acceleration of the charged particle along the electric field line on which its initial position lies. If $\mathbf{E} = 0$ and \mathbf{B} is uniform, the motion is simple, but more interesting. Let $\mathbf{B} = B_0 \hat{y}$, which gives us equations of motion for a test particle of mass m and charge q of the form

$$m \frac{d^2 x}{dt^2} = -\frac{qB_0}{c} v_z \quad (1.2.2a)$$

$$\frac{d^2 y}{dt^2} = 0 \quad (1.2.2b)$$

$$m \frac{d^2 z}{dt^2} = \frac{qB_0}{c} v_x. \quad (1.2.2c)$$

The second equation in this system tells us that the particle's velocity along the magnetic field, v_y is a constant. The remaining equations form a coupled system that can be simplified to obtain equations for v_x and v_z :

$$\frac{d^2 v_x}{dt^2} + \Omega_0 v_x = 0 \quad (1.2.3a)$$

$$\frac{d^2 v_z}{dt^2} + \Omega_0 v_z = 0, \quad (1.2.3b)$$

where the quantity Ω_0 is called the particle's *gyrofrequency*, and is defined as

$$\Omega_0 = \frac{qB_0}{mc}. \quad (1.2.3c)$$

The above system can be solved readily to obtain

$$v_x(t) = v_{\perp} \cos(\Omega_0 t + \gamma) \quad (1.2.4a)$$

$$v_z(t) = v_{\perp} \sin(\Omega_0 t + \gamma), \quad (1.2.4a)$$

where γ is a constant phase, and the quantity v_{\perp} is the magnitude of the components of the velocity in the x - z plane, which is called the *perpendicular velocity*.

The position of the particle is thus given by

$$x(t) = x_0 + \rho_g \sin(\Omega_0 t + \gamma) \quad (1.2.5a)$$

$$y(t) = y_0 + v_y t \quad (1.2.5b)$$

$$z(t) = z_0 - \rho_g \cos(\Omega_0 t + \gamma), \quad (1.2.5c)$$

where the particle's initial position is given by (x_0, y_0, z_0) , and the quantity ρ_g is called the particle's *gyroradius*, or *Larmor radius*, and is defined by

$$\rho_g = \frac{v_{\perp}}{\Omega_0}. \quad (1.2.5d)$$

The particle's trajectory is thus a simple helix, whose axis is the magnetic field line running through the point (x_0, y_0, z_0) , with radius ρ_g . The point (x_0, z_0) , is called the particle's *guiding center*. As we shall see, the system (1.2.1) can be studied from the point of view of tracking the particle's guiding center motion if the length scale L over which the magnetic field changes noticeably is greater than the Larmor radius ρ_g :

$$\rho_g \ll L \equiv \frac{B}{|\nabla B|} \quad (1.2.6)$$

Though the equations of motion (1.2.1) may appear simple, in practice, they form a coupled, nonlinear system of ordinary differential equations (ODE's), that will produce particle motion that is complicated, and even chaotic [19,24]. It is for this reason that, whenever possible, the study of particle motion in magnetic

and electric fields is studied in terms of *drift motion*, as mentioned above. If the condition (1.2.6) is satisfied, the individual drift motions can be used to replace the the system's full equations of motion with a set of equations called the *drift*, or *guiding center* equations of motion. What follows is a description of the basic drift motions that will be encountered in the course of this dissertation.

§1.2b Drift Motions

The presence of both magnetic and electric fields will lead to a drift motion that is called the $\mathbf{E} \times \mathbf{B}$ drift, whose associated velocity is denoted by \mathbf{v}_E . A simple example of this motion can be seen by considering charged-particle motion in a uniform magnetic field, such as the system (1.2.2a-c), but with the addition of a uniform electric field given by $\mathbf{E} = E_0 \hat{z}$. The test-particle equations of motion are then

$$m \frac{d^2 x}{dt^2} = -\frac{qB_0}{c} v_z \quad (1.2.7a)$$

$$\frac{d^2 y}{dt^2} = 0 \quad (1.2.7b)$$

$$m \frac{d^2 z}{dt^2} = \frac{qB_0}{c} v_x + \frac{qE_0}{c}. \quad (1.2.7c)$$

Again, we find that v_y is a constant, and (1.2.7a,c) can be decoupled to obtain

$$\frac{d^2 v_x}{dt^2} + \Omega_0^2 v_x + \frac{\Omega_0^2}{cB_0^2} E_0 B_0 = 0 \quad (1.2.8a)$$

$$\frac{d^2 v_z}{dt^2} + \Omega_0^2 v_z = 0. \quad (1.2.8b)$$

Solving for v_x and v_z yields

$$v_x(t) = v_{\perp} \cos(\Omega_0 t + \gamma) - \frac{cE_0}{B_0} \quad (1.2.9a)$$

$$v_z(t) = v_{\perp} \sin(\Omega_0 t + \gamma), \quad (1.2.9a)$$

where the second term in (1.2.9a) is a drift motion along the $-x$ direction, and is called the $\mathbf{E} \times \mathbf{B}$ drift. The resulting motion for this example is a simple gyromotion in the x - z plane, with the particle's guiding center moving with constant velocity $\mathbf{v}_g = (v_E, v_{y_0}, 0)$. In general, this drift velocity is written as

$$\mathbf{v}_E = \frac{c}{B^2} \mathbf{E} \times \mathbf{B}. \quad (1.2.10)$$

It is interesting to note that this drift velocity is independent of the charge of the test particle.

Two types of drift motion will arise if we allow the magnetic field to be inhomogeneous; i.e. $\mathbf{B} = \mathbf{B}(x, y, z)$. One type of drift motion is a consequence of the fact that the gradient of the field strength is nonzero—the ∇B drift, while the other appears if the field lines are curved, and is called the *curvature drift*. As we shall see, both of these drifts differ from the $\mathbf{E} \times \mathbf{B}$ drift in that they depend on the charge of the test particle.

The ∇B drift can be understood by considering the following simple example. Let $\mathbf{E} = 0$ and $\mathbf{B} = B(x)\hat{y}$. Following the steps used to derive (1.2.8a,b) we find

$$\frac{d^2 v_x}{dt^2} + \Omega^2(x)v_x + v_x v_z \frac{d\Omega}{dx} = 0 \quad (1.2.11a)$$

$$\frac{d^2 v_z}{dt^2} + \Omega^2(x)v_z + v_x^2 \frac{d\Omega}{dx} = 0. \quad (1.2.11b)$$

Given the assumption that B is varying slowly over the length scale associated with

the particle's motion, we may expand $\Omega(x)$ as a Taylor series about the particle's guiding center located at (X, Y, Z) :

$$\begin{aligned}\Omega(x) &= \Omega(X) + (x - X) \left. \frac{d\Omega}{dx} \right|_{x=X} + \mathcal{O}(\rho_g^2) \\ &= \Omega(X) + (x - X)\Omega'(X) + \mathcal{O}(\rho_g^2).\end{aligned}$$

Using this expansion converts (1.2.11a,b) into

$$\frac{d^2 v_x}{dt^2} + \Omega^2(X)v_x = -\Omega'(X)v_x v_z - 2\Omega(X)\Omega'(X)(x - X)v_x + \mathcal{O}(\rho_g^2) \quad (1.2.12a)$$

$$\frac{d^2 v_z}{dt^2} + \Omega^2(X)v_z = \Omega'(X)v_x^2 - 2\Omega(X)\Omega'(X)(x - X)v_z + \mathcal{O}(\rho_g^2). \quad (1.2.12b)$$

The terms on the right hand sides of (1.2.12a,b) are small compared to the terms on the left hand sides, and can be approximated by using the guiding center values for these quantities. Using (1.2.4a,b) and (1.2.5a) to eliminate these terms, and applying basic trigonometric identities leads to a pair of inhomogeneous, linear second order ODE's:

$$\frac{d^2 v_x}{dt^2} + \Omega^2(X)v_x = -\frac{3}{2}\Omega'(X)v_\perp^2 \sin[2(\Omega(X)t + \gamma)] \quad (1.2.13a)$$

$$\frac{d^2 v_z}{dt^2} + \Omega^2(X)v_z = \frac{1}{2}\Omega'(X)v_\perp^2 \left(3 \cos[2(\Omega(X)t + \gamma)] - 1 \right) \quad (1.2.13b)$$

The above equations can be solved by using standard techniques, which leads to the solutions

$$v_x(t) = v_\perp \cos(\Omega(X)t + \gamma) + \frac{\Omega'(X)v_\perp^2}{2\Omega^2(X)} \sin[2(\Omega(X)t + \gamma)] \quad (1.2.14a)$$

$$v_z(t) = v_\perp \sin(\Omega(X)t + \gamma) - \frac{\Omega'(X)v_\perp^2}{2\Omega^2(X)} \left(\cos[2(\Omega(X)t + \gamma)] + 1 \right). \quad (1.2.14b)$$

The motion illustrated by (1.2.14a,b) consists locally of the standard guiding center oscillations of frequency $\Omega(X)$, along with an additional oscillation of frequency

$2\Omega(X)$, and the z -component of the velocity also has a zero-frequency term which is of particular interest. Averaging (1.2.14a,b) over one local gyroperiod (i.e. over a period of time equal to $2\pi/\Omega(X)$), we find that the average velocity is

$$\begin{aligned}\langle v_x \rangle &= 0 \\ \langle v_y \rangle &= v_{\parallel} \\ \langle v_z \rangle &= -\frac{\Omega'(X)v_{\perp}^2}{2\Omega^2(X)}.\end{aligned}$$

The z component of the above equation is called the *grad B drift*. Recalling the definition of the gyrofrequency from (1.2.3c), we may write the above expression in a more general form

$$\mathbf{v}_{\nabla B} = cW_{\perp} \frac{(\mathbf{B} \times \nabla)\mathbf{B}}{qB^3}, \quad (1.2.15)$$

where $W_{\perp} = mv_{\perp}^2/2$, the kinetic energy of the test particle due to motion perpendicular to \mathbf{B} .

The drift effects on a particle due to magnetic field line curvature may be derived in a similar fashion, and the general form of the drift velocity associated with field line curvature, the *curvature drift* has a general expression given by

$$\mathbf{v}_C = 2cW_{\parallel} \frac{\mathbf{B} \times (\mathbf{B} \cdot \nabla)\mathbf{B}}{qB^4}, \quad (1.2.16)$$

where $W_{\parallel} = mv_{\parallel}^2/2$, the kinetic energy of the test particle due to motion parallel to the magnetic field.

Given the aforementioned types of drift motion, it is possible to express the guiding center velocity \mathbf{v}_d as

$$\mathbf{v}_d = \mathbf{v}_E + \mathbf{v}_{\nabla B} + \mathbf{v}_C,$$

The drift motion can be derived from a Hamiltonian given by [25]

$$H_d = \frac{mv_{\parallel}^2}{2} + \mu B + q\Phi,$$

where v_{\parallel} is the component of the velocity parallel to the magnetic field and μ is a quantity called the particle's *magnetic moment*. The magnetic moment is the action integral associated with the particle's gyromotion about the field line, and is discussed in greater detail in the next section.

§1.2c Adiabatic Invariants

As we saw in the previous section, it is possible to simplify the study of particle orbits in electric and magnetic fields if these fields are uniform, or vary significantly on length scales that are much larger than the test particle's gyroradius. The ability to perform this simplification in some regions of the phase space is linked to the existence of near-constants that are called *adiabatic invariants* [26,27]. These are quantities that will remain nearly constant during the system's evolution, as long as the magnetic field varies slowly. The two invariants that the system (1.2.1a-c) possesses are the *magnetic moment invariant* μ , and the *parallel invariant* J_{\parallel} . Using the constancy of these quantities, it is possible to simplify the system's motion by averaging out the fast oscillations in the system, and study only its drift motion.

The most common application of adiabatic invariants in plasma physics is the use of the conservation of the magnetic moment μ to average out the rapid gyration

of a particle about a field line in favor of its drift motion along and perpendicular to the magnetic field. This picture of plasma behavior is called *guiding center theory*. Another common use of an adiabatic invariant to simplify the study of plasma phenomena is the use of the parallel invariant J_{\parallel} to study the mirroring of charged particles trapped in a magnetic field, which is the case in the Earth's radiation belts [28,29], as well as in some fusion devices, such as tokamaks and mirror machines [30]. The existence of the parallel invariant as a good adiabatic invariant allows the elimination of the bounce motion of a particle between its mirror points in favor of the slower relative motion of the mirror points themselves.

The Magnetic Moment μ

The calculation of drift motions found in §1.2b hinged upon the assumption that the spatio-temporal variation of the system's magnetic field was slow, which leads to the conservation of a quantity called the *magnetic moment* μ , which is, as mentioned previously, the action associated with a charged particle's gyromotion about a magnetic field line:

$$\mu = \oint p_{\perp} dq_{\perp},$$

where p_{\perp} and q_{\perp} are the momentum and coordinate perpendicular to the magnetic field. This quantity can be written more directly as [13]:

$$\mu = \frac{v_{\perp}^2}{2B}, \quad (1.2.17)$$

where v_{\perp} is the component of the velocity that is perpendicular to the magnetic field.

The quantity μ , as defined in (1.2.17), is a good adiabatic invariant if the magnetic field has slow spatio-temporal variations compared to a test particle's gyromotion; i.e. \mathbf{B} varies on a time scale much longer than a test particle's gyroperiod, and the local length scale over which the magnetic field varies is large compared to the particle's gyroradius. Since we are considering only time-independent magnetic fields in this dissertation, only the second criterion mentioned above is relevant. An estimate of the length scale L over which the magnetic field changes significantly can be obtained by taking the ratio of the magnitude of the gradient of B to B :

$$L \equiv \frac{B}{|\nabla B|}. \quad (1.2.18)$$

Clearly, L is a function of the system's coordinates.

The ratio of ρ_g to L will determine how well the magnetic moment is conserved, and hence, how well guiding-center theory applies to the system. Since both the scale length L and the particle's gyroradius ρ_g are functions of the coordinates and momenta, we shall call the ratio ρ_g/L the *magnetization function* $\Upsilon(x, y, z, p_x, p_y, p_z)$:

$$\Upsilon(x, y, z, p_x, p_y, p_z) = \frac{\rho_g(x, y, z, p_x, p_y, p_z)}{L(x, y, z, p_x, p_y, p_z)}. \quad (1.2.19)$$

When $\Upsilon(x, y, p_x, p_y, p_z) \ll 1$, the particle will be magnetized, and μ will be a good invariant. When $\Upsilon(x, y, p_x, p_y, p_z) \sim 1$, the adiabatic invariance of μ will begin to break, and the particle will become demagnetized, and the guiding-center

approximation will not be valid. Note that the concept of the gyroradius, as defined in §1.2a will only have precise meaning if the particle is strongly magnetized; i.e. $\Upsilon \ll 1$.

An interesting consequence of the adiabatic invariance of μ is the phenomenon of *mirroring*. In order to see this, we introduce the concept of the *pitch angle* θ , which relates the relative sizes of the perpendicular and parallel components of a particle's velocity \mathbf{v} with respect to the magnetic field (Figure 1.2.1):

$$\theta = \arctan\left(\frac{v_{\perp}}{v_{\parallel}}\right). \quad (1.2.20)$$

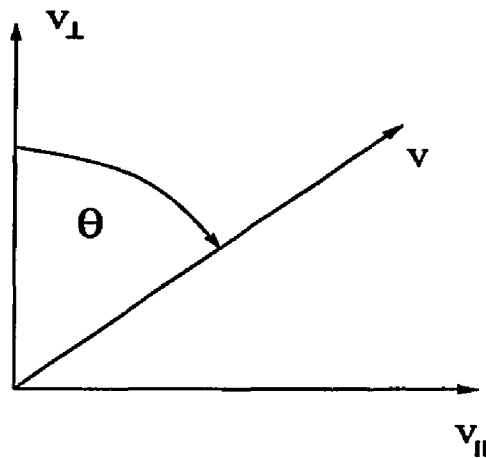


Figure 1.2.1. The Pitch Angle θ .

In the absence of an electric field, the existence of mirroring is easy to see by considering a charged particle at some position s_0 on a field line with pitch angle θ . If the magnetic field strength at this point is B_0 , then the magnetic moment for this particle is

$$\mu = \frac{v^2 \sin^2 \theta}{2B_0} = \text{constant}. \quad (1.2.21)$$

Now suppose we have the situation illustrated in Figure 1.2.2, where we have the magnetic field strength increasing as the particle moves away from s_0 , reaching a maximum at the points s_{M_1} and s_{M_2} , at which the field strength takes on the value B_M .

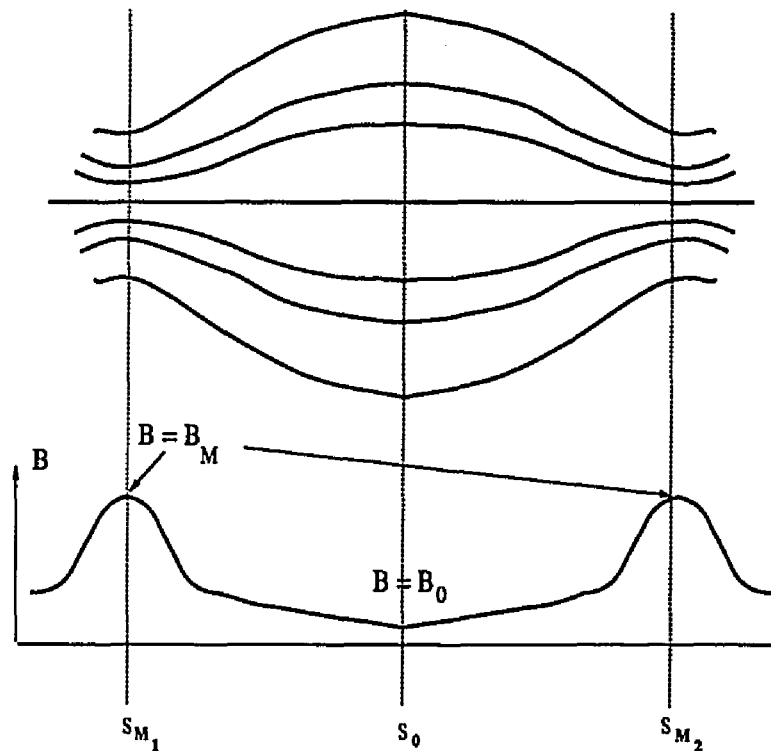


Figure 1.2.2. Mirror Points and Magnetic Field Strength.

Since the magnetic moment is a constant, we must have an increase in v_{\perp} . The fact that the particle's energy is a constant means that this increase in v_{\perp} must be accompanied by a corresponding decrease in v_{\parallel} , and there is the possibility, if B_M is sufficiently large, that eventually, all of the particle's kinetic energy will be in its perpendicular motion, and we will have $v_{\parallel} = 0$, leading to the reflection of the particle at or before the points s_{m_1} and s_{m_2} . At these *mirror points*, the

particle's perpendicular velocity is $v_{\perp} = v$, leading us to rewrite the expression for the particle's pitch angle at s_0 as

$$\sin^2 \theta = \frac{v_{\perp}^2}{v^2} = \frac{B_0}{B_M}. \quad (1.2.22)$$

From (1.2.22), we see that if we start at the point s_0 with $|\sin \theta| > \sqrt{B_0/B_M}$, the particle will be reflected, or *trapped*, whereas particles with $|\sin \theta| < \sqrt{B_0/B_M}$ will not be reflected, and are called *passing* particles.

The Parallel Invariant J_{\parallel}

For the trapped particles, the periodic motion between the mirror points is related to another conserved quantity that the system possesses, which is called the parallel invariant J_{\parallel} :

$$J_{\parallel} = \oint p_{\parallel} dq_{\parallel}, \quad (1.2.23)$$

where p_{\parallel} and q_{\parallel} are the components of the momentum and coordinate that are along the magnetic field, and the integration is performed over one period in this motion. Typically, the period of the oscillation of the parallel motion will be somewhat longer than the particle's gyroperiod, which means that field strength variations that occur on the same time scale as the particle's bounce frequency or the same length scale as the distance between the mirror points will break this invariant. Since the particle's gyromotion takes place on much shorter spatio-temporal scales, the parallel invariant is less robust than the magnetic moment.

Now that we have some understanding about the basic principles of charged particle motion in electric and magnetic fields, we can turn our attention to the description of magnetic and electric fields associated with reconnection, and the test particle dynamics they generate.

§1.3a The Magnetic Field Near a Null

As we saw in §1.1a, the topic of reconnection is closely related to the existence of magnetic null spaces, such as null points, neutral lines, or neutral sheets. All three types of the aforementioned field structures can be described in terms of a simple local model of the magnetic field. Consider a magnetic null that includes the origin of a Cartesian coordinate system (x,y,z) . Near the null, we can write the magnetic induction field \mathbf{B} as a Taylor series in the coordinate vector \mathbf{r} :

$$\mathbf{B}(\mathbf{r}) = \mathbf{B}_0 + \nabla\mathbf{B}\mathbf{r} + \nabla\nabla\mathbf{B} : \mathbf{r}\mathbf{r} + \dots \quad (1.3.1)$$

Since we are interested in nulls, we will let $\mathbf{B}_0 = 0$, and given that we wish to focus on magnetic field structure near the null itself, we may truncate this expression at first order in \mathbf{r} , which yields an expression that can be written in matrix form:

$$\mathbf{B} = \mathbf{L}\mathbf{r} = \begin{pmatrix} L_{11} & L_{12} & L_{13} \\ L_{21} & L_{22} & L_{23} \\ L_{31} & L_{32} & L_{33} \end{pmatrix} \begin{pmatrix} x \\ y \\ z \end{pmatrix}.$$

With no loss of generality, we can, through the appropriate change of variables, express \mathbf{B} in such a fashion that one of the eigenvectors of \mathbf{L} is parallel to the z -axis.

This allows us to write \mathbf{L} in this new basis as a new matrix \mathbf{M} :

$$\mathbf{B} = \mathbf{M}\mathbf{r} = \begin{pmatrix} M_{11} & M_{12} & 0 \\ M_{21} & M_{22} & 0 \\ M_{31} & M_{32} & M_{33} \end{pmatrix} \begin{pmatrix} x \\ y \\ z \end{pmatrix}. \quad (1.3.2)$$

The elements of the matrix \mathbf{M} must satisfy the condition that the magnetic field is solenoidal, specifically

$$\nabla \cdot \mathbf{B} = 0,$$

or

$$\text{Tr}(\mathbf{M}) = 0. \quad (1.3.3)$$

A complete study of the relationship between the eigenvalues of \mathbf{M} and their resulting field line topologies can be found in the work of Fukao [32].

§1.3b Test-Particle Motion Near a Magnetic Null

Now we turn our attention to the issue of charged particle motion in a magnetic field as defined by (1.3.2). Consider a particle with mass m and charge q placed in the magnetic field defined by (1.3.2). In addition to this magnetic field we assume an electrostatic field $\mathbf{E}(x, y, z) = -\nabla\Phi(x, y, z)$, where Φ is the electrostatic potential.

The equations of motion in Newtonian form are:

$$m \frac{d^2 \mathbf{r}}{dt^2} = \frac{q}{c} \dot{\mathbf{r}} \times \mathbf{B} + q\mathbf{E},$$

or,

$$\frac{d^2 x}{dt^2} = -\frac{q}{mc} \dot{z} B_y + \frac{q E_x}{m} \quad (1.3.4a)$$

$$\frac{d^2 y}{dt^2} = \frac{q}{mc} \dot{z} B_x + \frac{q E_y}{m} \quad (1.3.4b)$$

$$\frac{d^2 z}{dt^2} = \frac{q}{mc} (\dot{x} B_y - \dot{y} B_x) + \frac{q E_z}{m}. \quad (1.3.4c)$$

This set of equations describes the test particle's motion in this field configuration, and can be integrated to produce particle trajectories. If, however, we wish to

understand more about the system's dynamical properties, such as its phase space structure and its constants of the motion, we are best served by examining the system in a Hamiltonian formulation. The first step in this process is to construct the test-particle Hamiltonian $H(x, y, z, p_x, p_y, p_z)$.

$$H(x, y, z, p_x, p_y, p_z) = \frac{1}{2m}(\mathbf{p} - \mathbf{A})^2 - q\Phi(x, y, z), \quad (1.3.5a)$$

Where $\Phi(x, y, z)$ and \mathbf{A} are the electrostatic and magnetic vector potentials, respectively:

$$\mathbf{E} = -\nabla\Phi(x, y, z) \quad (1.3.5b)$$

$$\mathbf{B} = \nabla \times \mathbf{A}. \quad (1.3.5c)$$

The system's motion is then governed by Hamilton's equations:

$$\dot{x}_i = \frac{\partial H}{\partial p_i} \quad (1.3.6a)$$

$$\dot{p}_i = -\frac{\partial H}{\partial x_i}. \quad (1.3.6b)$$

Before we can construct the Hamiltonian and write down Hamilton's equations, we must construct the magnetic vector potential \mathbf{A} appropriate to the field given by (1.3.2). One way to accomplish this is to write each of the components of \mathbf{A} as a quadratic polynomial in the Cartesian coordinates x , y , and z :

$$A_i = \frac{1}{2}\Gamma_{ijk}x_jx_k, \quad (1.3.7)$$

where Γ is a third-rank symmetric tensor; $\Gamma_{ijk} = \Gamma_{ikj}$. Note that we are summing over repeated indices, and will adopt this as convention unless we specify otherwise.

Since $\mathbf{B} = \nabla \times \mathbf{A}$, it is possible to solve for the elements of Γ in terms of the elements of \mathbf{B} :

$$B_i = \frac{1}{2} \epsilon_{ijk} \frac{\partial}{\partial x_j} \Gamma_{klm} x_l x_m. \quad (1.3.8)$$

Since these relations must hold for all (x, y, z) , (1.3.8) leads to nine equations involving the elements of Γ :

$$\begin{aligned} M_{11} &= \Gamma_{312} - \Gamma_{213} & M_{12} &= \Gamma_{322} - \Gamma_{223} & M_{13} &= \Gamma_{323} - \Gamma_{233} \\ M_{21} &= \Gamma_{113} - \Gamma_{311} & M_{22} &= \Gamma_{123} - \Gamma_{312} & M_{23} &= \Gamma_{133} - \Gamma_{313} \\ M_{31} &= \Gamma_{211} - \Gamma_{112} & M_{32} &= \Gamma_{212} - \Gamma_{122} & M_{33} &= \Gamma_{213} - \Gamma_{123} \end{aligned} \quad (1.3.9)$$

Note that in this formulation of \mathbf{A} , the condition that \mathbf{B} be solenoidal is satisfied identically, as expected:

$$\begin{aligned} \nabla \cdot \mathbf{B} &= M_{11} + M_{22} + M_{33} \\ &= (\Gamma_{312} - \Gamma_{213}) + (\Gamma_{123} - \Gamma_{312}) + (\Gamma_{213} - \Gamma_{123}) = 0. \end{aligned} \quad (1.3.10)$$

In addition to the nine equations described above in (1.3.9), we impose the gauge restriction that \mathbf{A} and the electric potential $\Phi(x, y, z)$ satisfy the Lorentz condition:

$$\nabla \cdot \mathbf{A} + \frac{\partial \Phi}{\partial t} = 0,$$

which, for an electrostatic system, implies

$$\nabla \cdot \mathbf{A} = 0. \quad (1.3.11)$$

In terms of the tensor Γ_{ijk} , we have

$$\delta_{jk} \frac{\partial}{\partial x_j} \Gamma_{klm} x_l x_m = 0. \quad (1.3.12)$$

Since this equation must apply for all (x, y, z) , this leads to three conditions on the elements of Γ :

$$\Gamma_{111} + \Gamma_{212} + \Gamma_{313} = 0$$

$$\Gamma_{112} + \Gamma_{222} + \Gamma_{323} = 0$$

$$\Gamma_{113} + \Gamma_{223} + \Gamma_{333} = 0$$

(1.3.13)

The tensor Γ_{ijk} has $3^3 = 27$ elements, nine of which can be determined by the fact that Γ_{ijk} is symmetric in its second and third indices. Equations (1.3.9) and (1.3.13) comprise a set of twelve equations which must be satisfied for all (x, y, z) . This means that six of the remaining elements of Γ_{ijk} are undetermined, and must be provided in order to determine Γ_{ijk} completely. These six constants are related to gauge freedom, since we can always perform a gauge transformation $\mathbf{A} \rightarrow \mathbf{A}' = \mathbf{A} + \nabla\Lambda$, where the gauge function $\Lambda(x, y, z)$ is

$$\Lambda(x, y, z) = G_1 x^3 + G_2 y^3 + G_3 z^3 + G_4 x^2 y + G_5 x^2 z + G_6 y^2 x + G_7 y^2 z + G_8 z^2 x + G_9 z^2 y,$$

where the parameters $\{G_1, \dots, G_9\}$ are constants. The condition $\nabla \cdot \mathbf{A}' = 0$ will determine three of these constants, and the remaining six are arbitrary.

Given the vector potential \mathbf{A} and the electrostatic potential $\Phi(x, y, z)$, it is a simple task to construct the system's Hamiltonian $H(x, y, z, p_x, p_y, p_z)$:

$$H(x, y, z, p_x, p_y, p_z) = \frac{1}{2m} \sum_{i=1}^3 \left(p_i - \frac{q}{2c} \Gamma_{ijk} x_j x_k \right)^2 + q\Phi(x, y, z). \quad (1.3.14)$$

The equations of motion in Hamiltonian form are thus

$$\dot{x}_i = \frac{1}{m} \left(p_i - \frac{q}{2c} \Gamma_{ijk} x_j x_k \right) \quad (1.3.15a)$$

$$\dot{p}_i = \frac{q}{mc} \left(p_i - \frac{q}{2c} \Gamma_{ijk} x_j x_k \right) \frac{\partial}{\partial x_i} \Gamma_{ijk} x_j x_k - \frac{\partial \Phi}{\partial x_i}. \quad (1.3.15b)$$

where in the second equation, the index i is fixed (no summation is performed over this index).

§1.4 A Simple Model For Neutral Lines and Neutral Sheets

A simple model that produces the reconnection process described in § 1.1 is the field combination

$$\mathbf{B} = \frac{B_0}{L} (\delta y \hat{x} + x \hat{y}) \quad (1.4.1a)$$

$$\mathbf{E} = E_0 \hat{z}, \quad (1.4.1b)$$

where B_0 , E_0 , δ , and L are constant parameters. A vector potential associated with (1.4.1a) is

$$\begin{aligned} \mathbf{A} &= \frac{1}{2} (\delta y^2 - x^2) \hat{z} \\ &= \Psi(x, y) \hat{z}, \end{aligned} \quad (1.4.2a)$$

i.e.

$$\Gamma_{322} = \delta, \quad \Gamma_{311} = -1,$$

and the rest of the Γ_{ijk} are zero. The function $\Psi(x, y)$ is called the *flux function*.

An electrostatic potential that generates (1.4.1b) is given by

$$\Phi(x, y, z) = -E_0 z. \quad (1.4.2b)$$

The Hamiltonian for a charged test particle moving in the fields given by (1.4.1a,b) is

$$H = \frac{1}{2m} \left[p_x^2 + p_y^2 + \left(p_z - \frac{q}{c} \Psi(x, y) \right)^2 \right] - qE_0 z \quad (1.4.3)$$

The Hamiltonian equations of motion are thus

$$\dot{x} = \frac{p_x}{m} \quad (1.4.4a)$$

$$\dot{y} = \frac{p_y}{m} \quad (1.4.4b)$$

$$\dot{z} = \frac{p_z}{m} + \frac{\Omega_0}{2L}(x^2 - \delta y^2), \quad (1.4.4c)$$

$$\dot{p}_x = -\frac{\Omega_0}{L}xp_z + \frac{m\Omega_0}{2L^2}x(\delta y^2 - x^2) \quad (1.4.4d)$$

$$\dot{p}_y = \delta\frac{\Omega_0}{L}yp_z - \delta\frac{m\Omega_0}{2L^2}y(\delta y^2 - x^2) \quad (1.4.4e)$$

$$\dot{p}_z = qE_0, \quad (1.4.4f)$$

where the quantity Ω_0 is defined as

$$\Omega_0 = \frac{qB_0}{mc}.$$

The above set of equations can be simplified by transforming the system to dimensionless variables:

$$\begin{aligned} x &= L\tilde{x} & p_x &= mL\Omega_0\tilde{p}_x \\ t &= \frac{\tilde{t}}{\Omega_0} & y &= L\tilde{y} & p_y &= mL\Omega_0\tilde{p}_y \\ q &= \sqrt{mL^3}\Omega_0\tilde{q} & z &= L\tilde{z} & p_z &= mL\Omega_0\tilde{p}_z \\ H &= mL\Omega_0^2\tilde{H} & \mathbf{B} &= \sqrt{\frac{m}{L}}\Omega_0\tilde{\mathbf{B}} & \mathbf{E} &= \sqrt{\frac{m}{L}}\Omega_0\tilde{\mathbf{E}} \end{aligned} \quad (1.4.5)$$

This transformation leads to the dimensionless system whose magnetic and electric fields are given by

$$\tilde{\mathbf{B}} = \delta\tilde{y}\hat{x} + \tilde{x}\hat{y} \quad (1.4.6)$$

$$\tilde{\mathbf{E}} = \epsilon\hat{z},$$

where $\epsilon \equiv \sqrt{\frac{L}{m}}\Omega_0^{-1}E_0$ is a dimensionless constant.

The test particle Hamiltonian in our set of dimensionless variables is

$$\tilde{H} = \frac{1}{2} \left[\tilde{p}_x^2 + \tilde{p}_y^2 + \left(\tilde{p}_z - \frac{1}{2}(\delta\tilde{y}^2 - \tilde{x}^2) \right)^2 \right] - \kappa\tilde{z}, \quad (1.4.7)$$

where $\kappa = \epsilon\tilde{q}$. The Hamiltonian equations of motion are thus

$$\frac{d\tilde{x}}{d\tilde{t}} = \tilde{p}_x \quad (1.4.8a)$$

$$\frac{d\tilde{y}}{d\tilde{t}} = \tilde{p}_y \quad (1.4.8b)$$

$$\frac{d\tilde{z}}{d\tilde{t}} = \tilde{p}_z + \frac{1}{2}(\tilde{x}^2 - \delta\tilde{y}^2), \quad (1.4.8c)$$

$$\frac{d\tilde{p}_x}{d\tilde{t}} = -\tilde{x}\tilde{p}_z + \frac{1}{2}\tilde{x}(\delta\tilde{y}^2 - \tilde{x}^2) \quad (1.4.8d)$$

$$\frac{d\tilde{p}_y}{d\tilde{t}} = \delta\tilde{y}\tilde{p}_z - \delta\frac{1}{2}\tilde{y}(\delta\tilde{y}^2 - \tilde{x}^2) \quad (1.4.8e)$$

$$\frac{d\tilde{p}_z}{d\tilde{t}} = \kappa, \quad (1.4.8f)$$

From this point forward, we shall drop the tildes from our variables, and use only the dimensionless variables defined in (1.4.6) for the rest of this discussion.

It is worthwhile to discuss briefly some of the basic quantities associated with the test particle model given by (1.4.6-8). The magnitude of \mathbf{B} is simply $B = \sqrt{\delta^2 y^2 + x^2}$, and the unit vectors parallel and perpendicular to \mathbf{B} are

$$\begin{aligned} \hat{\mathbf{b}} &= \frac{\mathbf{B}}{B} = \frac{\delta y}{B}\hat{\mathbf{x}} + \frac{x}{B}\hat{\mathbf{y}} \\ \hat{\mathbf{e}}_{\perp 1} &= -\frac{x}{B}\hat{\mathbf{x}} + \frac{\delta y}{B}\hat{\mathbf{y}} \end{aligned} \quad (1.4.9)$$

$$\hat{\mathbf{e}}_{\perp 2} = \hat{\mathbf{z}}.$$

These unit vectors, along with a sample field line are illustrated in Figure 1.4.1.

Note that this set of unit vectors $\{\hat{\mathbf{b}}, \hat{\mathbf{e}}_{\perp 1}, \hat{\mathbf{e}}_{\perp 2}\}$ form a right-handed frame, and in particular,

$$\hat{\mathbf{b}} \times \hat{\mathbf{e}}_{\perp 1} = \hat{\mathbf{e}}_{\perp 2}, \quad \hat{\mathbf{e}}_{\perp 1} \times \hat{\mathbf{e}}_{\perp 2} = \hat{\mathbf{b}}, \quad \hat{\mathbf{e}}_{\perp 2} \times \hat{\mathbf{b}} = \hat{\mathbf{e}}_{\perp 1}. \quad (1.4.10)$$

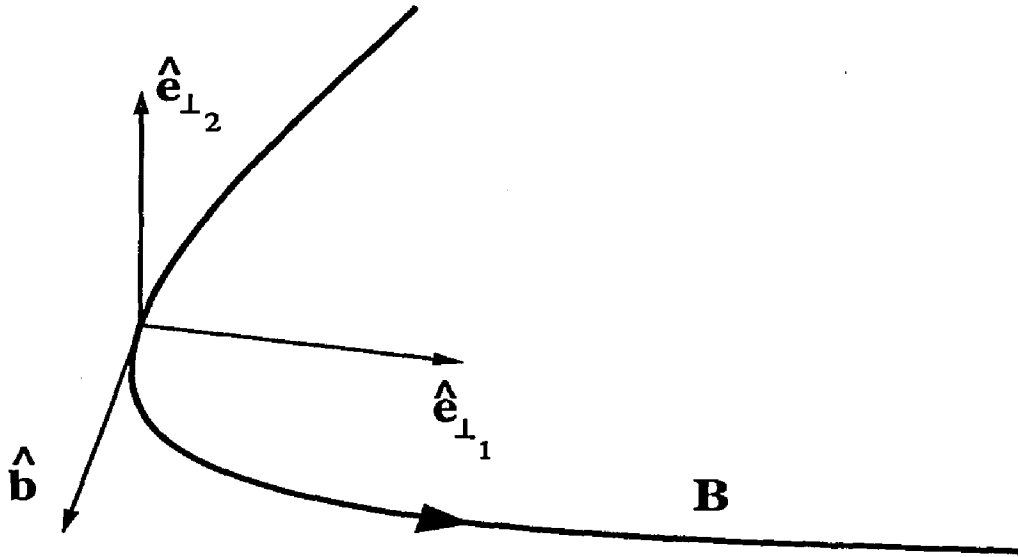


Figure 1.4.1. Unit Vectors $\hat{\mathbf{b}}$, $\hat{\mathbf{e}}_{\perp 1}$, and $\hat{\mathbf{e}}_{\perp 2}$.

Given the set of unit vectors (1.2.4a-c), and recalling that the components of the velocity are given by (1.4.4a-c), we can write \mathbf{v}_{\perp} as

$$\mathbf{v}_{\perp} = \frac{1}{B}[-x p_x \hat{\mathbf{x}} + \delta y p_y \hat{\mathbf{y}}] + \left[p_z + \frac{1}{2}(x^2 - \delta y^2) \right] \hat{\mathbf{z}} \quad (1.4.11)$$

In light of the above information, the magnetic moment μ defined in (1.2.2) is

$$\mu = \frac{1}{B^3} \left[x^2 p_x^2 + \delta^2 y^2 p_y^2 + B^2 \left(p_z + \frac{1}{2}(x^2 - \delta y^2) \right)^2 \right] \quad (1.4.12)$$

The quantity μ , as defined in (1.4.12), is a good adiabatic invariant if the magnetic field varies slowly in time and length scale over which the magnetic field varies is large compared to the particle's gyroradius. The gradient of B is

$$\nabla B = \frac{1}{B} (x \hat{\mathbf{x}} + \delta^2 y \hat{\mathbf{y}}).$$

Therefore the length scale L over which B changes significantly is

$$\begin{aligned} L &= \frac{B}{|\nabla B|} \\ &= B^3 (x^2 + \delta^4 y^2)^{-\frac{1}{2}}. \end{aligned} \quad (1.4.13)$$

In our dimensionless units defined above, particle's gyroradius ρ_g is simply

$$\rho_g = \frac{v_{\perp}}{B}.$$

Recalling the value of v_{\perp} given in (1.4.11), we find the particle's gyroradius to be

$$\rho_g = \frac{1}{B^2} \left[x^2 p_x^2 + \delta^2 y^2 p_y^2 + B^2 \left(p_z + \frac{1}{2}(x^2 - \delta y^2) \right)^2 \right]^{\frac{1}{2}}. \quad (1.4.14)$$

The ratio of ρ_g to L will determine how well the magnetic moment is conserved, and hence, how well guiding-center theory applies to the system. Recalling the definition of the magnetization function $\Upsilon(x, y, p_x, p_y, p_z)$ from (1.2.19), we find that Υ is a complicated function of the coordinates and momenta. Recall that when $\Upsilon \ll 1$, the particle will be magnetized, and μ will be a good invariant. When $\Upsilon \sim 1$, the adiabatic invariance of μ will begin to break, and the test particle will become demagnetized. Figure 1.4.2 illustrates surfaces of constant Υ for various field configurations. The shaded regions are the *unmagnetized regions*; i.e. regions where $\Upsilon \geq 1$.

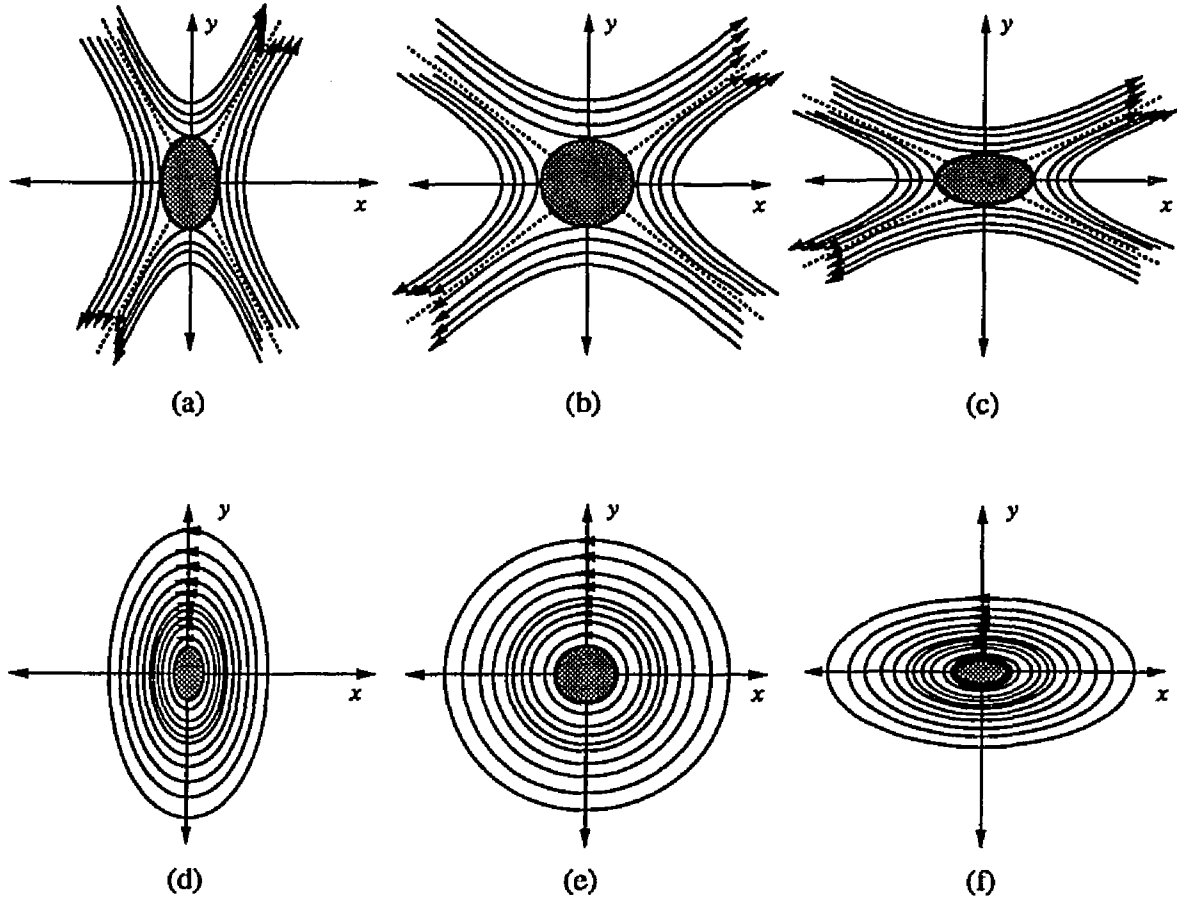


Figure 1.4.2 Unmagnetized Regions for Various δ :

(a) $\delta = \frac{1}{4}$, (b) $\delta = 1$, (c) $\delta = 4$, (d) $\delta = -\frac{1}{4}$, (e) $\delta = -1$, (f) $\delta = -4$.

In the case of open field line configurations (i.e. $\delta > 0$), the unmagnetized region can act as a scattering center. Recalling Figure 1.1.4, we see that if the uniform electric field $\epsilon > 0$ ($\epsilon < 0$), charged particles start in a region where $\Psi < 0$ ($\Psi > 0$), and will be carried in towards the unmagnetized region by the $\mathbf{E} \times \mathbf{B}$ drift:

$$\mathbf{v}_E = \frac{\epsilon \tilde{c}}{\delta^2 y^2 + x^2} (-x\hat{x} + \delta y\hat{y}). \quad (1.4.15)$$

Upon entering the unmagnetized region, the test particle will experience strong acceleration by the electric field, resulting in a sharp increase in its kinetic energy.

The particle will exit the unmagnetized region and drift away, carried by the $\mathbf{E} \times \mathbf{B}$ drift into a region where the flux function has changed sign from its original value.

The aforementioned motion shows an acute sensitivity to initial conditions, which was demonstrated by Moses, Finn, and Ling [21]. This sensitivity can be seen by starting an ensemble of test particles on a magnetic field line with $\Psi(x, y) = \Psi_0$, and evolving the individual particles forward until each of them encounters the outgoing flux surface $\Psi(x, y) = -\Psi_0$, and then measuring 1) the kinetic energy of the test particle, or 2) the travel time from the initial flux surface to the outgoing flux surface, i.e. the *time delay*. A plot of exit kinetic energy versus initial position along the initial flux surface (or *impact parameter*) is shown in Figure 1.4.3a. Note the fine structure in this graph, which persists when the plot is magnified in Figure 1.4.3b. This sensitivity to initial conditions is called *irregular* or *chaotic scattering* [33,34], which is a common occurrence in X-type null line configurations [21].

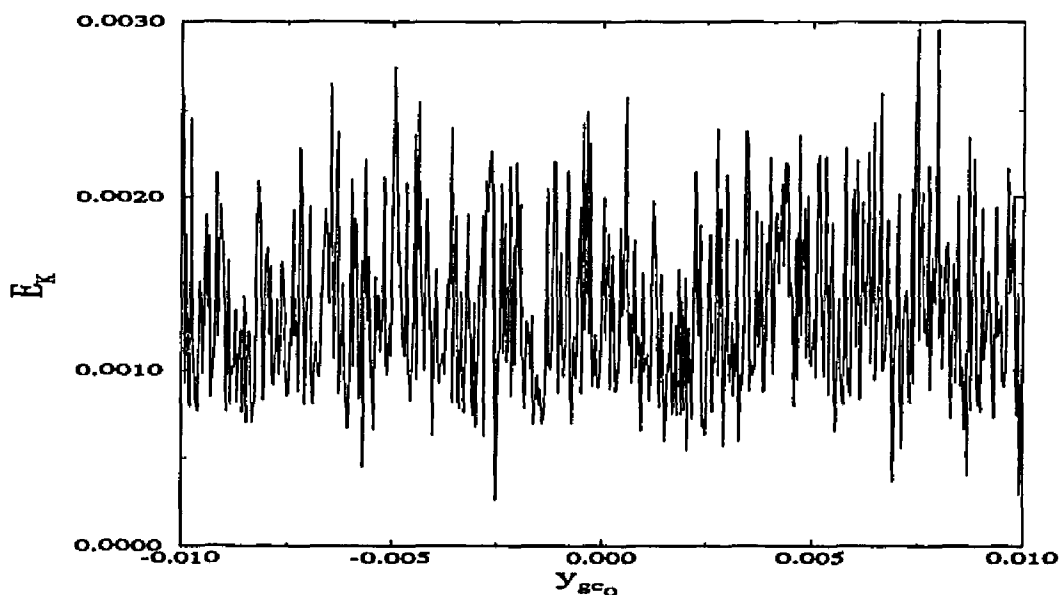


Figure 1.4.3a Final Kinetic Energy vs. Impact Parameter ($\delta = 1$).

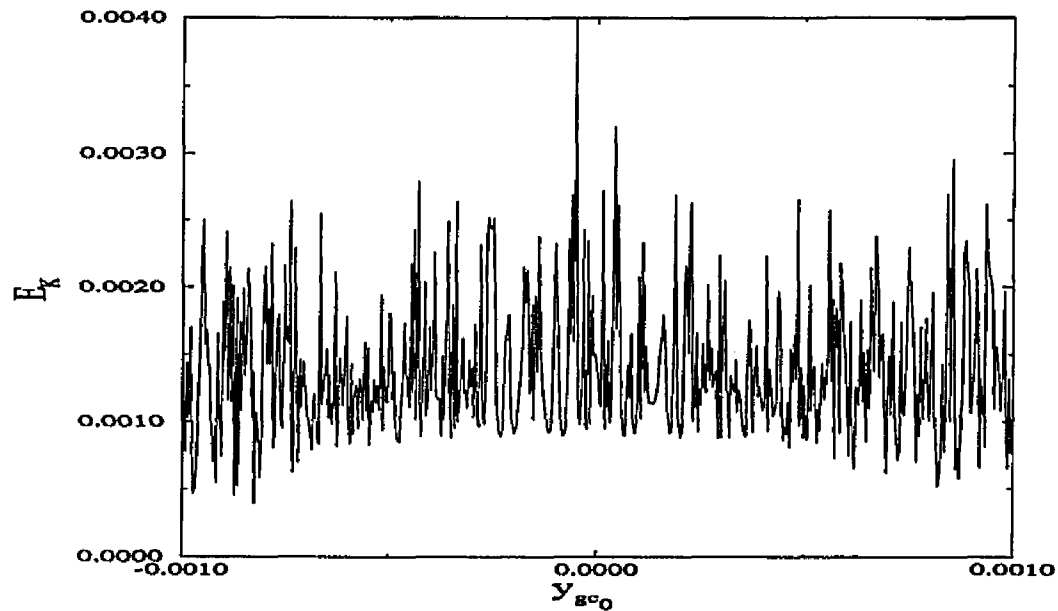


Figure 1.4.3b Detail of Figure 1.4.3a.

An estimate of the time scale on which a test particle passes from its initial flux surface $\Psi(x_0, y_0) = \Psi_0$ to an outgoing flux surface $\Psi(x, y) = -\Psi_0$ can be obtained by examining the implicit time dependence of the flux function $\Psi(x, y)$:

$$\left(\frac{d\Psi}{dt}\right)_{\mathbf{E} \times \mathbf{B}} = \frac{1}{2} \left(\frac{d}{dt}\right)_{\mathbf{E} \times \mathbf{B}} (\delta y^2 - x^2) = \delta y v_{E_y} - x v_{E_x}.$$

Recalling the value of v_E from (1.4.15), we find

$$\left(\frac{d\Psi}{dt}\right)_{\mathbf{E} \times \mathbf{B}} = \epsilon,$$

and thus the time scale on which the particle drifts into the vicinity of the null is $T_0 = \Psi_0/\epsilon$. The values of the time delay are thus on the order of $2T_0$.

In the case of closed field lines, the $\mathbf{E} \times \mathbf{B}$ drift can act as a strong focusing agent, and in chapters Four and Five, we will be investigating the sensitivity to initial conditions of particle dynamics in these configurations.

In summary, we wish to examine the effect of magnetic reconnection on plasma in the low-collisionality limit using *particle models*. The macroscopic behavior of the plasma in this limit may be linked to the integrability properties of the test particle equations of motion associated with the particle model. Analytical methods for examining such models exist; in particular, we will be applying *singularity analysis* to examine the integrability properties of (1.4.4a-f). These analytical tools will help us identify parameter régimes (i.e. sets of δ and ϵ), and hence, field structures, for which (1.4.4a-f) *may* be integrable. These analytical tools will be developed in the next chapter, and will be applied to particle motion during reconnection in Chapter Three.

CHAPTER TWO
INTEGRABILITY AND SINGULARITY ANALYSIS

§2.1 Dynamical Systems and Integrability

The term *integrability* has many subtly different meanings in the field of dynamical systems, and it is equally true that the term *dynamical system* also has many different interpretations. What follows is a short description of the multifold meanings of these terms, and their relationship to the problem at hand.

There are many types of dynamical systems; a few examples of which are listed below:

TYPE	EXAMPLE
System of O.D.E.'s	Hamilton's Equations
Partial Differential Equation	Nonlinear Schrödinger Equation
Integral Equation	Propagation of waves through an inhomogeneous medium
Finite Difference Equation	Quadratic Map

For our purposes, we will only consider dynamical systems that are represented by a system of first-order O.D.E.'s with independent variable t , and dependent variables $\{x_1, x_2, \dots, x_N\}$ of the form

$$\frac{dx_i}{dt} = F_i(x_1, x_2, \dots, x_N, t) \tag{2.1.1}$$

If the functions F_i are all independent of t , then the system (2.1.1) is called *autonomous*. In the case of higher-order ODE's, it is always possible to reduce them to a system of first-order ODE's. If the system (2.1.1) is not autonomous, it is possible to convert the system to an autonomous system by treating t as a dependent variable, and defining a new independent variable s ; a process that is simply that of extending the phase space of (2.1.1) [35].

In particular, we are interested in Hamiltonian systems in phase space with N degrees of freedom that have a Hamiltonian H , coordinates $\{q_1, q_2, \dots, q_N\}$, momenta $\{p_1, p_2, \dots, p_N\}$ and canonical time t :

$$H = H(q_1, q_2, \dots, q_N, p_1, p_2, \dots, p_N) \quad (2.1.2a)$$

$$\dot{q}_i = \frac{\partial H}{\partial p_i} \quad (2.1.2b)$$

$$\dot{p}_i = -\frac{\partial H}{\partial q_i}. \quad (2.1.2c)$$

If the Hamiltonian given in (2.1.2a) is independent of t , then the system (2.1.2a-c) is autonomous.

For autonomous Hamiltonian systems, the term integrability is related to— but not equivalent to—the issue of solvability of the differential equations themselves. Solvability is the ability to write down the solutions to the systems of O.D.E.'s in closed form, that is, in terms of elementary or special functions. A simple, but interesting example of a Hamiltonian system of this type is the pendulum:

$$H(q, p) = \frac{p^2}{2} + \cos(q) \quad (2.1.3a)$$

$$\frac{dq}{dt} = p \quad (2.1.3b)$$

$$\frac{dp}{dt} = \sin(q) \quad (2.1.3c)$$

The system (2.1.3b-c) is equivalent to the second order ODE

$$\frac{d^2 q}{dt^2} = -\sin(q).$$

This equation is solvable in terms of Jacobi elliptic functions [36].

The term *integrability*, in the context of Hamiltonian mechanics [37] is a property possessed by certain special types of Hamiltonian systems. Consider a system with N degrees of freedom with coordinates and momenta given by $\mathbf{q} = (q_1 \dots, q_N)$ and $\mathbf{p} = (p_1 \dots, p_N)$. For such a system, integrability is the existence of a set of $N - 1$ integrals of the motion $\{I_1, I_2, \dots, I_{N-1}\}$, which, along with the Hamiltonian H , are in involution:

$$\{I_i, I_j\} = 0, \quad \{I_i, H\} = 0, \quad \forall i, j \in \{1, 2, \dots, N - 1\}, \quad (2.1.4)$$

where $\{A, B\}$ is the Poisson bracket:

$$\{A, B\} = \frac{\partial A}{\partial q_i} \frac{\partial B}{\partial p_i} - \frac{\partial A}{\partial p_i} \frac{\partial B}{\partial q_i}, \quad (2.1.5)$$

with an implied summation over the repeated index i . These $N - 1$ integrals, or *actions* are global constants of the motion, and along with H , allow us to construct a set of N *angles* θ_i using the Hamilton-Jacobi procedure [37], thus providing a solution to the system in the action-angle representation. For a given Hamiltonian system (2.1.2a-c), the chances of actually finding the appropriate canonical transformation to these action-angle variables from the original variables is normally quite slim, and in most cases does not exist.

Autonomous Hamiltonian systems that possess a complete set of integrals that are in involution are said to possess the property of *Liouville integrability*. Liouville integrability is the definition of integrability most commonly used by physicists, and is the most restrictive definition of the term [38].

Another desirable property of systems that are Liouville integrable is the simplicity of their orbits in the action-angle representation. For such a system with N degrees of freedom, whose motion is *bounded*, the trajectories associated with a given value of H lie on a torus of genus N in the $2N$ -dimensional phase space.

The next least restrictive definitions involve the notion of *algebraic integrability*. This concept has been put forward by Yoshida [39,40,41] and Adler and Van Moerbeke [42]. A system is algebraically integrable if it is possible to construct $N - 1$ constants of the motion that are *rational* functions of the phase space coordinates. Note that there is no restriction that the constants of the motion are in involution. A diagnostic for this particular type of integrability lies in the system's Kowalevski exponents (which are defined in § 2.4); if the system's Kowalevski exponents are all rational, then the system under consideration is algebraically integrable.

A further refinement of algebraic integrability is the concept of *complete algebraic integrability*, as defined by Adler and van Moerbeke. An system with N degrees of freedom possesses complete algebraic integrability if it possesses $N - 1$ rational invariants that are in involution, and the solutions to the system can be expressed in terms of Abelian integrals [42]. This extra restriction allows for the construction of a rigorous connection between the results of singularity analysis

and the topological structure of the system's phase space trajectories. In particular, it can be shown that systems that possess complete algebraic integrability have trajectories that lie on a complex torus of genus $2N$ [42,43].

These previously discussed concepts of integrability are *global* in that they address a generic property of the system for the whole complex time domain. There are still less restrictive types of integrability, which include **1)** systems that allow the construction of analytic integrals for only limited domains in the complex t -plane, **2)** systems such as a particle in a potential decreasing sufficiently fast that the particle is asymptotically free [44], and **3)** systems that are integrable subject to certain constraints, such as a zero-energy constraint [45].

A less restrictive definition of integrability is *complex analytic integrability*. This definition of integrability is the one most commonly used by workers in the field of singularity analysis, is the property of a system that allows for the construction of the solutions to the equations of motion in terms of Laurent series. A diagnostic for this type of integrability is a test for the *Painlevé property*, which will be discussed in §2.3. This type of integrability contains no guarantees of the existence of a complete set of invariants in involution, nor does it tell us anything directly about the topological structure of the system's phase space trajectories.

§2.2 Singularity Analysis

The traditional approach to the integrability of systems of ODE's is to search for solutions to the equations in terms of elementary or known special functions, with the point of view that the system evolves in the real time domain. Another approach to this problem is to allow the time variable t to be complex, and then examine the local behavior of the differential equations and their solutions in the complex time plane, the idea being that if we can obtain a solution locally, it may be possible to construct a more global solution via analytic continuation applied to the local solution. This attack on the problem was originated by Cauchy [46], and was pushed further by Painlevé and his co-workers [47,48] The implementation of this approach demands the knowledge of the locations and types of singularities in the t -plane that the system possesses.

Classification of singularities

In terms of the *location* of the singularity, two general classes of singularities appear in the complex t -plane for systems of ODE's: *fixed* and *movable*. Fixed singularities are a consequence of the mathematical structure of the equations in question, while movable singularities have their positions determined by the initial conditions.

A simple example of a system that exhibits a fixed singularity in the complex time domain is [38]

$$(t - t_*) \frac{dx}{dt} = \lambda x.$$

This equation can be solved simply to obtain

$$x(t) = A(t - t_*)^\lambda,$$

where A is a constant. The singular point for this system is located at $t = t_*$, and the particular type of singular point that the function $x(t)$ possesses depends on the value of λ . If λ is a positive integer, the function $x(t)$ is holomorphic, and the point $t = t_*$ is a zero of $x(t)$. If λ is a negative integer, $t = t_*$ is a pole of $x(t)$. If λ is a rational number, then $t = t_*$ is an algebraic branch point of the system, and if λ is irrational, or has a nonzero imaginary part, then $t = t_*$ is a transcendental branch point.

Systems of linear ODE's can only possess fixed singularities [38,43,49]. When we examine nonlinear systems, however, it is possible to encounter *movable singularities*. Movable singularities are singularities whose position depends on the system's initial conditions. An example of a nonlinear system that has a movable singularity is the equation [38]

$$\frac{dx}{dt} = \lambda x^{1-\frac{1}{\lambda}},$$

where λ is a constant. The solution to this equation is

$$x(t) = (t - t_0)^\lambda.$$

In this case, the location of the singularity t_0 is not provided by the form of the differential equation, but rather by the initial condition; i.e. $t_0 = (-x_0)^{1/\lambda}$. The actual type of singularity at $t = t_0$ again depends on the value of λ , yielding an

analytic point for λ a positive integer, a movable pole for λ a negative integer, a movable algebraic branch point for λ rational, or a movable transcendental branch point for other values of λ not mentioned above.

Other types of singularities not mentioned above include essential singularities and logarithmic singularities. An essential singularity is best understood with reference to the Laurent series expansion of a function of a complex variable. Consider an function $f(t)$ that is analytic in some punctured neighborhood with radius ϵ and center $t = t_0$, with this point not in the domain of $f(t)$. In this neighborhood, f can be written as

$$f(t) = \sum_{n=-\infty}^{n=\infty} a_n(t - t_0)^n, \quad (2.2.1)$$

with the understanding that for some $n < 0$, $a_n \neq 0$. If there exists some value of n , $n = N$, $N < 0$ for which $a_n = 0$ for all values of $n < N$, then f has a removable pole of multiplicity N . If no such special value of n exists, f has an essential singularity at $t = t_0$. An example of an ODE that has an essential singularity is the equation

$$\frac{dx}{dt} = -\frac{x}{(t - t_0)^2}.$$

In this case the solution to this equation,

$$x(t) = C e^{\frac{1}{t-t_0}}$$

has an essential singularity at $t = t_0$.

In addition to the aforementioned *isolated* singularities, singularities may occur on curves in the complex plane, or even more complicated sets, such as the fractal illustrated in Figure 2.2.1.

Singularity Analysis and the Painlevé Property

Given the knowledge of the locations and types of singularities a system of ODE's possesses, it is natural to wonder whether or not this information can help determine the integrability properties of the system under consideration. Painlevé put forward the following conjecture:

Painlevé Conjecture: If a system of ODE's (2.1.1) has only poles as its movable singularities, the system may be more readily integrated than systems of ODE's that possess movable branch points or movable logarithmic singularities.

Systems that have this simple type of singularity structure are said to possess the *Painlevé property*. Further support for this conjecture can be found in the fact that many chaotic and nonintegrable solutions exhibit singularity structures that are complicated, either domains that are multi-sheeted, or infinitely-sheeted in the case of logarithmic singularities, or dense fractal sets of singularities in the complex plane, called *natural boundaries* [50]. These natural boundaries are particularly troublesome in that they act as barriers that often prevent the analytic continuation of local solutions. For example, consider the Hénon- Heiles system

$$H = \frac{1}{2}(p_1^2 + p_2^2) + q_1^2 q_2 + \frac{\epsilon}{3} q_2^3$$

Analytic continuation from a solution $\{\mathbf{q}(t), \mathbf{p}(t)\}$ leads to the discovery of a complicated singularity structure, as shown in Figure 2.1.1 [50]. The shape of the fractal barriers depicted in this figure are sensitive to the value of the parameter ϵ as well as the initial conditions.

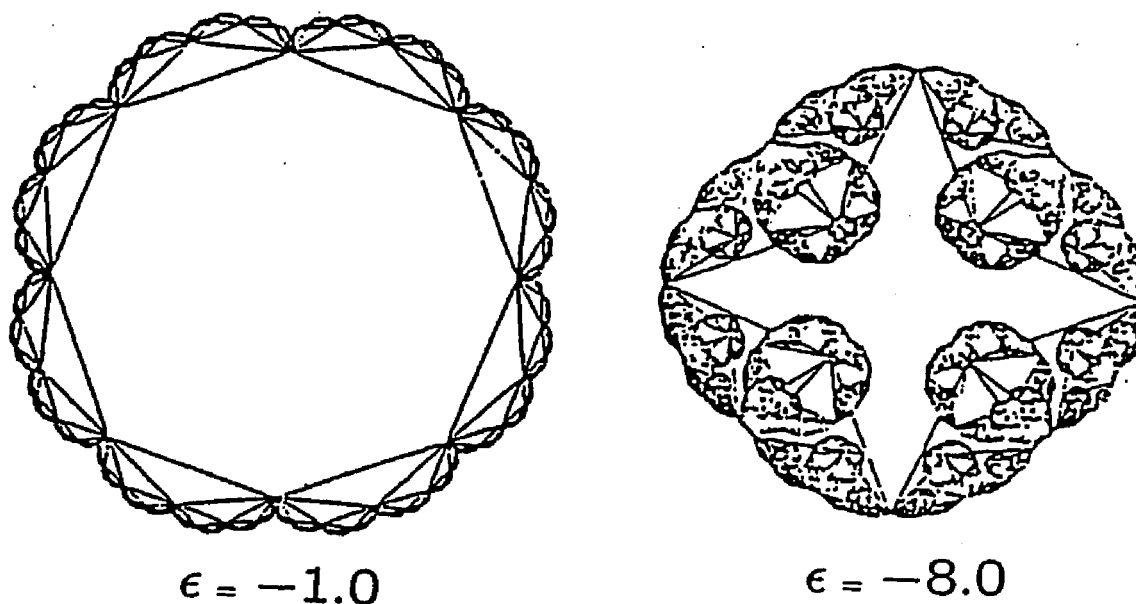


Figure 2.1.1. Natural Boundaries for the Hénon-Heiles System (From [50]).

Painlevé's initial approach to the study of the singularity structure of ODE's began with a study of first order differential equations of the form

$$\frac{dx}{dt} = f(x, t),$$

where f is a rational function of x , and analytic in t . His goal was to find all of the differential equations of this form that had only movable poles as their singularities. The only first-order ODE that possesses the Painlevé property is the Riccati equation [38,49]

$$\frac{dx}{dt} = f_0(t) + f_1(t)x + f_2(t)x^2, \quad (2.2.2)$$

where the functions f_i are all analytic functions of t . In fact, this equation can be

linearized by making the change of variable

$$x = -\frac{\dot{u}}{f_2(t)u},$$

and substituting this expression into (2.2.2), we get a linear second order ODE

$$\frac{d^2u}{dt^2} - \left(f_1(t) + \frac{\dot{f}_2(t)}{f_2(t)} \right) \frac{du}{dt} + f_0(t)f_2(t) = 0,$$

which is a linear, second order ODE, and thus possesses the Painlevé property, since linear ODE's can admit only fixed singularities.

Further work by Painlevé [48] focused on the nature of second-order ODE's of the form

$$\frac{d^2x}{dt^2} = F(t, x, \dot{x}), \quad (2.2.3)$$

where F is a function that is analytic in t , algebraic in x , and rational in \dot{x} . Through an exhaustive analysis of these systems, Painlevé et al discovered fifty basic types of ODE's of the form (2.2.3) that had all of their branch points and essential singularities fixed, having only poles as their movable singularities. Of these fifty classes, forty-four had solutions in terms of elementary functions, or could be integrated via quadratures or linearization, while the remaining six were irreducible, and could be solved only by the introduction of six new transcendental functions that are called the *Painlevé Transcendents* [49].

Various attempts have been made at classifying the singularity structure of higher-order ODE's [51-56], but such endeavors have met with less success, and currently there exists no complete scheme for classifying third-or-higher-order systems of ODE's that possess the Painlevé property [43]. Studies focusing on these

systems have also shown that they often exhibit dense singularity structures such as the natural boundaries discussed previously [38,57].

The significance of the Painlevé property lies in that it appears to be a sufficient, but not necessary, condition for a system of ODE's to be analytically integrable [38,49]. A rigorous proof of this assertion does not exist. Currently, however, there exists no counterexample to this conjecture [38]. Again, it is necessary to note that if a given system does not possess the Painlevé property, it may still be integrable, as we will see in the next section. This is of particular importance with respect to systems that possess movable branch points, but, through a change of dependent variable, can be transformed into systems possessing the Painlevé property. Such systems are often found to possess what is called the “weak-Painlevé” property, which will be discussed further in the next section.

Singularity Analysis “Success Stories”

In the application of singularity analysis on a system of ODE's of the form (2.2.1) we often find that the constant parameters associated with the system can often determine whether or not a system will possess the Painlevé property. This sensitivity to the values of the parameters associated with the model has presented itself in a number of interesting examples.

1) Kowalevskaya's study of the top [58], which is the first known application of singularity analysis to a physical problem, led to the discovery of a previously unknown integrable case for this system.

2) A study of the Hénon-Heiles system yielded a set of previously unknown

integrable cases that are linked to specific values of constant parameters associated with the model [59].

3) The discovery of an integrable case of the three-dimensional Lotka-Volterra system [60].

4) The discovery of parameter régimes that yield integrable cases for the Lorenz system [61]. Example 1) was found by evaluating the system's Kowalevski exponents, and is the approach that has evolved into Yoshida singularity analysis, while Examples 2) - 4) were found through the application of an algorithmic technique that was originally used to study the integrability properties of partial differential equations. This technique is called the Ablowitz-Ramani-Segur (ARS) algorithm, and is described in detail in the next section.

§2.3 The Ablowitz-Ramani-Segur (ARS) Algorithm

Consider a system of N differential equations

$$\frac{d^{\rho_i} w_i}{dt^{\rho_i}} = F_i(w_1, w_2, \dots, w_N), i = 1, 2, \dots, N. \quad (2.3.1)$$

The parameters ρ_i are the orders of the individual equations in the system; for example, a physical system's equations of motion, might have $N = 3$ and $\rho_i = 2, i = 1, 2, 3$ (Newtonian form), or $N = 6$, and $\rho_i = 1, i = 1, \dots, 6$ (Hamiltonian form).

Determining whether or not the system of nonlinear ordinary differential equations (2.3.1) possesses solutions that are expressible in terms of Laurent series about its movable nonessential singularities is a nontrivial task. The direct approach is to

assume that each of the functions we seek w_i has a Laurent series expansion about a given point t_0 of the form

$$w_i(t) = \alpha_i(t - t_0)^{\beta_i} \sum_{n=0}^{\infty} C_{in}(t - t_0)^n, \quad (2.3.2)$$

where the coefficients C_{in} are constants. Substitution of (2.3.2) into (2.3.1) provides us with the means to determine all of the C_{in} except for the N arbitrary constants that are sitting somewhere in the Laurent series. This process is highly laborious, and, in terms of its success rate, is a poor investment of our time.

Fortunately, however, there exists an algorithmic approach that eliminates many unsuitable candidate systems with much less effort: the Ablowitz - Ramani - Segur (ARS) Algorithm [38,49,62,63]. This algorithm was originally developed to determine whether or not a nonlinear PDE admits either algebraic or logarithmic branch points. The algorithm is a three-step process in which an equation or system of equations is examined near a hypothetical singularity in the complex time plane in terms of I) its leading-order behaviors, II) the powers in the series (2.3.2) at which arbitrary constants will arise, and III) the existence of nondominant logarithmic singularities. The steps I) - III) can be viewed as progressively finer sieves, with the amount of effort expended to carry out each step increasing dramatically. Still, nibbling at a problem employing the ARS algorithm is far better than biting off more than we can chew dealing with (2.3.2) from the outset.

What follows is a step-by-step description of the algorithm.

Step I: Leading-Order-Behaviors

Consider an arbitrary movable singular point t_0 of (2.3.1). In this step of the

algorithm, we wish to determine the leading-order behavior of (2.3.2). That is, we will determine the exponents β_i , and based on their values, decide on whether or not to continue on to step II. Define $\tau = t - t_0$, and approximate each of the solutions to (2.3.1) $w_i(t)$ by

$$w_i \sim \alpha_i \tau^{\beta_i}, \quad (2.3.3)$$

subject to the assumption that at least *one* of the β_i has $\text{Re}(\beta_i) < 0$. We now substitute (2.3.3) into (2.3.1), and order the terms in the resulting equations in powers of τ , searching for all sets of β_i such that two or more terms in each of the equations (2.3.1) balance at leading order in τ , with all other terms being higher-order in τ . Each choice of a set of suitable values of the β_i leads to a set of relations that define a corresponding set of α_i . Such a set of coefficients and exponents $\{\alpha_1, \dots, \beta_1, \dots, \beta_N\}$ is called a *leading-order-behavior* for the system (2.3.1). For a given system of differential equations, there may be a large number of possible leading order behaviors, and each one must be examined.

The values of the exponents β_i allow us to draw some preliminary conclusions about the system (2.3.1), using the following rules:

- 1) If all of the β_i are integers, then we continue on to step II of the algorithm.
- 2) If one or more of the exponents β_i are rational, and the rest are integers, then we still continue on to step II in hope that (2.3.1) may possess the *weak Painlevé* property, that is, the movable branch points are non-logarithmic and the solutions to (2.3.1) have as their domains finite-sheeted Riemann surfaces.
- 3) If any of the β_i are irrational or complex, the algorithm terminates at this

step, and the system does not possess the Painlevé property.

Great care must be taken in the implementation of step I to insure that *all* possible balances involving the β_i have been explored, as the omission of one possible leading-order behavior can lead to an erroneous result.

If we find a leading order behavior that passes step I of the test, we now know the leading order behavior of a candidate Laurent series expansion for each of the functions w_i , and we also know one of the system's integration constants, i.e. the location of the singularity t_0 . The next step of the algorithm will allow us to determine at which orders in the Laurent series we will expect the other integration constants to appear. These orders, r are called the *resonances* of the system, and the determination of them comprises the next step of the algorithm.

Step II: Resonances

We must perform this step for each of the leading-order-behaviors for (2.3.1) found in step I. For each of the leading-order-behaviors, we retain only the leading terms from the system (2.3.1) and substitute for w_i the expansion

$$w_i = \alpha_i \tau^{\beta_i} (1 + \gamma_i \tau^r), \quad (2.3.4)$$

where r is presumed positive. If $r < 0$, the leading order behavior for the system would have $w_i \sim \tau^{\beta_i+r}$, which violates the hypothesis for step I of the algorithm. As we shall see, the case $r = -1$ is a ubiquitous exception to this rule, and this is related to the fact that t_0 is a *movable* singularity.

Substituting (2.3.4) into the leading terms of (2.3.1), and retaining only terms

that are *linear* in the γ_i yields a linear system

$$\mathbf{Q}(r) \cdot \boldsymbol{\gamma} = 0, \quad (2.3.5)$$

where $\mathbf{Q}(r)$ is an $N \times N$ matrix of coefficients, whose elements are polynomials in r , and the vector $\boldsymbol{\gamma}$ is defined as $\boldsymbol{\gamma} \equiv \{\gamma_1, \dots, \gamma_N\}^T$.

What we wish to find are the values of r such that one or more of the γ_i are arbitrary. This will occur when the matrix $\mathbf{Q}(r)$ is singular, that is when

$$\det(\mathbf{Q}(r)) = 0. \quad (2.3.6)$$

The above equation is a polynomial equation in r , with the order of the polynomial being given by

$$\sum_{i=1}^N \rho_i,$$

where ρ_i is the order of the i^{th} differential equation in the set (2.3.1).

Solving for the roots of (2.3.6) gives us the values of the resonances r . When we can solve for the values of all of the resonances, we can draw some conclusions based on the values of the resonances from the following set of rules:

Rule 1: If we have $N - 1$ non-negative resonances in addition to a single resonance at $r = -1$ (see Rule 2), we have passed the resonance test and may proceed to step III.

Rule 2: We will *always* have $r = -1$ as a resonance. This is related to the fact that the t_0 is a *movable* singularity. We can see this by returning to the ansatz (2.3.3), replacing the variable τ with $\tau + d\tau$, and expanding the leading-order behaviors in powers of $d\tau$, and noting that the leading term in the expansion occurs at $\mathcal{O}((d\tau)^{\beta_i - 1})$.

Rule 3: For *each* occurrence of the root $r = 0$, one of the α_i is arbitrary.

Rule 4: Any resonance that has $Re(r) < 0$ leads to the termination of the algorithm, as it violates the assumption that the results of step I comprise the leading-order behavior of (2.3.1). The only permissible exception to this rule, of course, is the *single* occurrence of the resonance $r = -1$, as outlined in Rule 2.

Rule 5: Any resonance with $Re(r) > 0$, with r not an integer is indicative of a movable branch point, the algorithm usually terminates at this step. If r is real and rational, there may exist a simple coordinate transformation that can remove the branch point. Even if such a change of variable is not evident, Rule 6 may offer some help.

Rule 6: If some of the β_i are rational with the same denominator then positive rational resonances r with the same denominator as β_i indicate that the system is a candidate for possessing the *weak Painlevé property*.

The conclusion is this: if a singular expansion given by (2.3.2) possesses $N - 1$ nonnegative, integer resonances, or positive rational resonances in agreement with Rule 5, the expansion may be generic, and the system passes Step II of the algorithm. The next logical step is to test for the existence of nondominant logarithmic singularities, which is Step III of the algorithm.

Step III: Constants of Integration

Now that we know the orders in the expansions at which arbitrary constants—the integration constants—arise, we must now test to see if they do indeed appear as expected, and test for the occurrence of nondominant logarithmic singularities.

To perform this test, we begin by writing the desired solutions to (2.3.1) as

$$w_i(t) = \alpha_i \tau^{\beta_i} + \sum_{m=1}^{r_{max}} C_{im} \tau^{\beta_i+m}, \quad (2.3.7)$$

where r_{max} is the largest resonance found in step II. Substituting this expansion into the leading terms from (2.3.1), and balancing terms order-by-order in τ , we get a set of equations similar to (2.3.5), but with nonzero terms appearing on the right-hand side:

$$\mathbf{S}(m)\mathbf{C}_m = \mathbf{R}_m(t_0; \mathbf{C}_j), j = 1, \dots, m-1, \quad (2.3.8)$$

where m takes on the values $m = 1, \dots, r_{max}$ and the vector \mathbf{R} is defined as $\mathbf{R} \equiv (R_1, \dots, R_N)^T$. In order for us to find our desired constants of integration, the above relation (2.3.8) is subject to the following criteria:

- 1) For $1 \leq m < r_1$, (2.3.8) determines \mathbf{C}_m completely.
- 2) For $m = r_1$, we expect n_1 components of the vector \mathbf{C}_1 to be arbitrary, where n_1 is the multiplicity of the resonance. In order for this to happen, equation (2.3.8) must satisfy the following set of compatibility conditions:

$$\det(\mathbf{S}^{(k)}(r_1)) = 0, k = 1, \dots, N, \quad (2.3.9)$$

where the matrix $\mathbf{S}^{(k)}(r_1)$ is constructed by taking the matrix $\mathbf{S}(r_1)$ and replacing its k^{th} column by the vector $\mathbf{R}_m(t_0; \mathbf{C}_{r_1})$. This condition is reminiscent of Kramer's Rule for solving systems of linear equations by determinants, where a linear system such as (2.3.8) will have at least one arbitrary solution if the matrix $\mathbf{S}(m)$ has a null space. The conditions (2.3.9) are the same as insisting that the matrix $\mathbf{S}(r_1)$

has a null space, and that the dimension of this null space will be the same as the multiplicity of r_1 .

3) If the above condition 2) is satisfied, then, for $r_1 < m < r_2$, the equation (2.3.6) determine the components of \mathbf{C}_m completely.

4) We continue applying the procedure outlined in 1)-3), at each resonance up to the largest one r_{max} , bearing in mind that at any resonance that is a multiple root of (2.3.6) must be associated with a number of arbitrary constants equal to the root's multiplicity.

If the system in question satisfies the criteria defined above, we are finished, and if the collective leading-order behavior found in Step I contains only integer powers of τ then the system possesses the Painlevé property. If the system's leading-order- behaviors found in step I contain rational powers of τ , we are forced to alter the expansion (2.3.7) to account for this state of affairs. Say the exponents in the rational leading order behaviors to the system (2.3.1) (i.e. the β_i in equation (2.3.2)) have a common denominator N , we can make the change of variable $\tau \rightarrow \zeta \equiv \tau^{\frac{1}{N}}$. This transformation will alter the values of the resonances determined in step II by multiplying all of them by a factor of N , and the rules 1) - 6) stated in step II still apply, with the exception that the only negative resonance that the system possesses is at $r = -N$, rather than $r = -1$, and the resonances are all scaled by a factor of N . Should the modified system possess $N - 1$ nonnegative integer resonances then we can apply the test outlined in step III, with the ansatz (2.3.5)

rewritten as

$$w_i(\zeta) = \alpha_i \zeta^{N\beta_i} + \sum_{m=1}^{Nr_{max}} C_{im} \zeta^m. \quad (2.3.10)$$

Should this modified system satisfy the criteria outlined above, then the original system possesses the weak Painlevé property. Clearly, the amount of labor involved in verifying the singularity properties of such systems grows much faster than linearly in N . As we shall see in §3.2, it is easy to find examples where the application of step III of the algorithm becomes impracticable. In spite of this unpleasant situation, we can find comfort in the fact that if a system passes through the first two steps of the algorithm, it is often true that this partial fulfillment of the Painlevé property may be linked to partial integrability [38].

We may find, however, that for one or more of our resonances \tilde{r} , that the criteria 1) - 4) may break down. In this event, the system does not possess either form of the Painlevé property. This implies that the system may have nondominant logarithmic singularities. As a consequence of this, one or more of the expansions (2.3.7) may have to be rewritten to include logarithmic terms, e.g.:

$$w_i(t) = \alpha_i \tau^{\beta_i} + \sum_{m=1}^{\tilde{r}-1} C_{im} \tau^m + (C_{i\tilde{r}} + D_{i\tilde{r}} \ln(\tau)) \tau^{\beta_i + \tilde{r}} + \dots,$$

with higher-order terms in $\ln(\tau)$ possibly entering the expansion. Adding these logarithmic terms introduces new terms involving $D_{i\tilde{r}}$ into the relationships (2.3.8) and (2.3.9), allowing us to determine these new constants, by demanding that coefficients of the appropriate powers of τ vanish, while the $C_{i\tilde{r}}$ remain free.

Figure (2.3.1) contains a flowchart summarizing the ARS Algorithm.

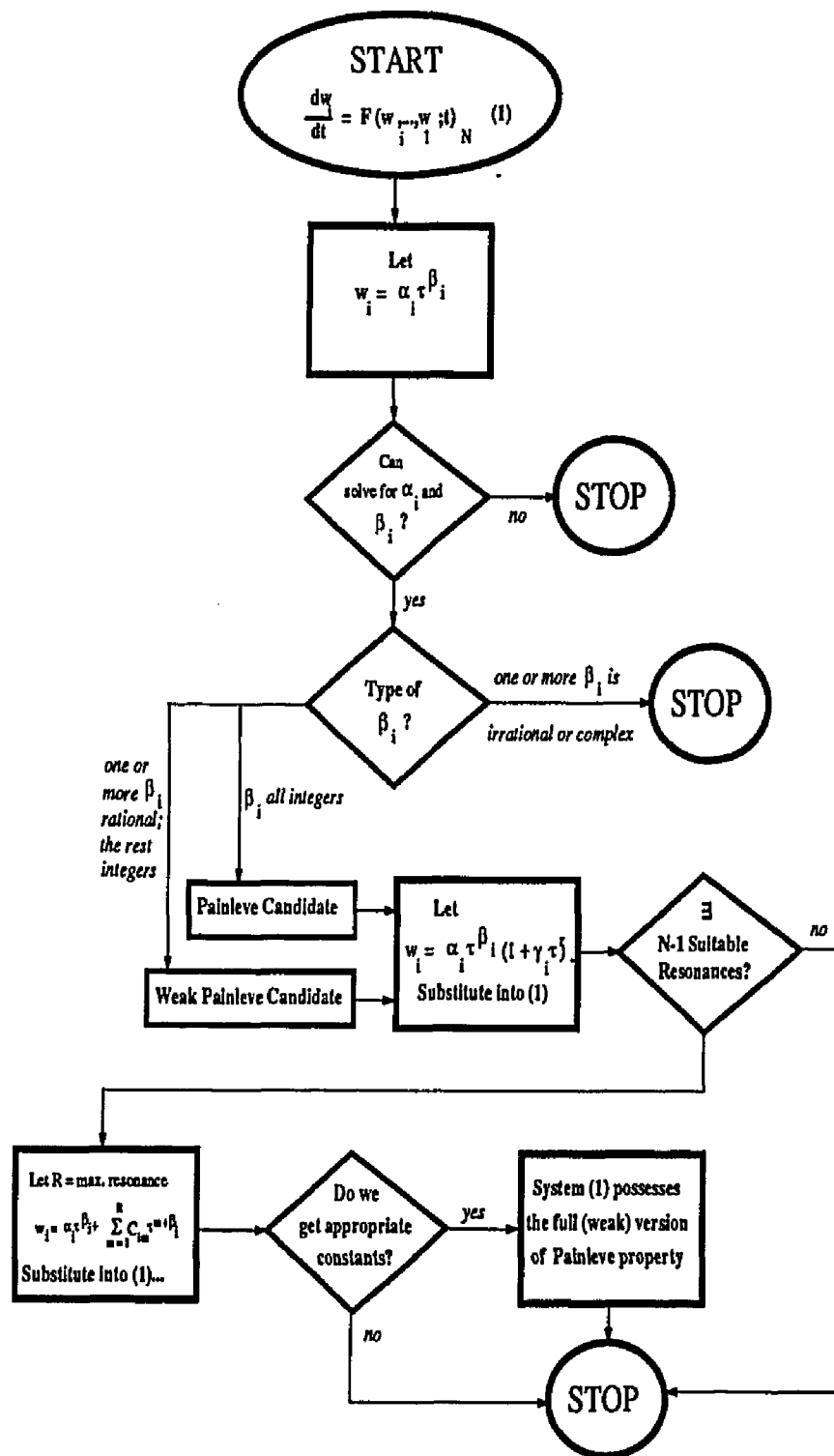


Figure 2.3.1. The Ablowitz-Ramani-Segur (ARS) Algorithm.

§2.4 Tests for Nonintegrability

The preceding sections of this chapter focused on the concept of integrability and tests for a certain type of integrability; i.e. complex analytic integrability. The results are encouraging in that many previously unknown integrable systems have been discovered via the application of singularity analysis and the ARS algorithm, but leave something to be desired in the lack of a rigorous connection between integrability and the Painlevé property. There is, of course, another approach that can help shed light on this problem. We could also search for a connection between certain types of singularity structures and nonintegrability. The main work in this area is the work of Yoshida [39-41] and Ziglin [64-66], who have showed that for a limited class of Hamiltonian systems, there is a method for testing for the nonintegrability as well as integrability of the system. Such methods are a test for the property of algebraic integrability, as outlined in § 2.1.

Yoshida's Method and Kowalevski Exponents

Consider an autonomous system of N ODE's of the form

$$\frac{dx_i}{dt} = F_i(x_1, \dots, x_N), i = 1, \dots, N \quad (2.4.1)$$

Suppose further that this system is invariant in form under the similarity transformation $t \rightarrow \sigma^{-1}t$ and $x_i \rightarrow \sigma^{g_i}x_i$ for $i = 1, \dots, N$, σ a constant, and the exponents g_i are rational numbers that are called the *weights* of the variables x_i . At this point a definition concerning functions of scaled variables is in order. A function

$\phi(x_1, \dots, x_N, t)$ is said to be *weighted homogeneous with weight M* if

$$\phi(\sigma^{g_1} x_1, \dots, \sigma^{g_N} x_N, \sigma^{-1} t) = \sigma^M \phi(x_1, \dots, x_N, t). \quad (2.4.2)$$

If the functions F_i are all weighted homogenous with weights M_i , it is possible to find particular solutions to (2.4.1)

$$x_i^{(s)}(t) = C_i t^{-g_i}, \quad g_i = M_i - 1, \quad (2.4.3a)$$

and the constants C_i are determined by

$$F_i(C_1, \dots, C_N) = -g_i C_i, \quad i = 1, \dots, N. \quad (2.4.3b)$$

There may exist many sets of solutions of the form (2.4.3a,b), and we will assume that there is at least one nontrivial solution of this form; i.e. that for some value of i , $g_i C_i \neq 0$. These solutions (2.4.3a,b) are called the *scaling solutions* for the system, and are analogous to the leading order behaviors obtained in step I of the ARS algorithm.

Given the set of particular solutions (2.4.3a-b) to equation (2.4.1), we can apply a variational technique to search for solutions that are “near” our scaling solutions by perturbing the scaling solutions via the introduction of a new set of variables h_i , and writing our dependent variables x_i as

$$x_i(t) = x_i^{(s)}(t) + h_i(t), \quad i = 1, \dots, N. \quad (2.4.4)$$

We can also expand the right-hand-side of (2.4.1) about the scaling solution, to first order in the h_i :

$$F_i(x_1, \dots, x_N) = F_i(x_1^{(s)}, \dots, x_N^{(s)}) + \sum_{j=1}^N \left. \frac{\partial F_i}{\partial x_j} \right|_{\mathbf{x}=\mathbf{x}^{(s)}} h_j, \quad (2.4.5)$$

where the vectors \mathbf{x} and $\mathbf{x}^{(s)}$ are defined by

$$\mathbf{x} = (x_1, \dots, x_N) \quad \text{and} \quad \mathbf{x}^{(s)} = (x_1^{(s)}, \dots, x_N^{(s)}).$$

Since the functions F_i are all homogeneous with weights $M_i = g_i + 1$, and recalling (2.4.2), it is possible to remove the time dependence from the arguments to the functions F_i and rewrite (2.4.5) as

$$F_i(x_1, \dots, x_N) = F_i(x_1^{(s)}, \dots, x_N^{(s)}) + \sum_{j=1}^N \left. \frac{\partial F_i}{\partial x_j} \right|_{\mathbf{x}=\mathbf{C}} t^{g_j - g_i - 1} h_j, \quad (2.4.6)$$

where the vector \mathbf{C} is defined by $\mathbf{C} = (C_1, \dots, C_N)$.

Substituting these expressions for the (2.4.4) and (2.4.6) into (2.4.1), we get

$$\frac{dh_i}{dt} = \sum_{j=1}^N \left. \frac{\partial F_i}{\partial x_j} \right|_{\mathbf{x}=\mathbf{C}} t^{g_j - g_i - 1} h_j. \quad (2.4.7)$$

Suppose that the solutions $h_i(t)$ of (2.4.7) take the form

$$h_i(t) = \eta_i t^{\rho - g_i}, \quad (2.4.8)$$

where ρ is a fixed number, and the η_i are constants. Substituting (2.4.8) into (2.4.7) yields an eigenvalue (ρ) - eigenvector ($\eta \equiv (\eta_1, \dots, \eta_N)^T$) problem:

$$(\rho - g_i)\eta_i = \sum_{j=1}^N K_{ij}\eta_j, \quad (2.4.9)$$

where the terms K_{ij} are the elements of the *Kowalevski matrix* \mathbf{K} , and are defined as

$$K_{ij} = \left. \frac{\partial F_i}{\partial x_j} \right|_{\mathbf{x}=\mathbf{C}} + \delta_{ij}g_i, \quad (2.4.10)$$

where δ_{ij} is the Kronecker delta symbol. The eigenvalues to (2.4.9), ρ are solutions to the characteristic equation

$$\det(\mathbf{K} - \rho\mathbf{I}) = 0. \quad (2.4.11)$$

If we can find solutions to (2.4.11), that is, if \mathbf{K} can be diagonalized, we call the eigenvalue spectrum $\{\rho_1, \dots, \rho_N\}$ the system's *Kowalevski exponents*, and the variational solutions $x_i(t)$ to (2.4.1) can be written as

$$x_i(t) = C_i t^{-g_i} + \eta_i t^{\rho - g_i} + \dots. \quad (2.4.12)$$

Again, we see a striking similarity between the Kowalevski exponents that are calculated in (2.4.11) and appear in the higher-order terms in (2.4.12), and the resonances, that are calculated in (2.3.6), and appear as the higher order term in the ansatz (2.3.4). Despite these analogies, it is important to note that the resonance spectrum for a system and its Kowalevski exponents are not the same thing. For homogeneous systems, the resonances and Kowalevski exponents will be the same, provided that the constants C_i in (2.4.3a,b) are *all* nonzero. In the event that some of the C_i are zero, the two concepts are still the same, up to some additive terms [38,39].

The relationship between a system's Kowalevski exponents and the issue of integrability is illustrated by a theorem due to Yoshida [40].

THEOREM 2.4.1: Consider a homogeneous system of the type (2.4.1). A necessary condition for the existence of algebraic integrals of the motion for this system is that all of the Kowalevski exponents calculated in (2.4.11) be rational

numbers. If any of the Kowalevski exponents associated with the system is irrational, or has a nonzero imaginary part, then (2.4.1) will not possess a complete set of algebraic integrals.

This is indeed a powerful result, if only applicable to a very restricted class of Hamiltonian systems. Ziglin [61] has made progress in extending the method by studying the integrability properties of the variational equations (2.4.7), and other work has been performed to relate these techniques to the issue of analytic integrability [41].

§2.5 Direct Methods for the Construction of Integrals

As we have seen earlier, integrability of an autonomous Hamiltonian system with N degrees of freedom given in (2.4.2a-c) is related to the existence of $N - 1$ functionally independent integrals $\{I_1, \dots, I_{N-1}\}$ that are in involution with each other and the system's Hamiltonian. Previous methods outlined in §2.2 – 2.4 have focused on the singularity properties of the system's solutions (the coordinates and momenta), or equivalently, of the integrals of the motion. Such methods are useful in determining whether or not a system is integrable, and can give clues to the Laurent series expansions of the system's solutions in the complex t -plane. Physicists, however, tend to be interested in the functional form of a system's integrals in terms of the system's coordinates and momenta; i.e. they seek expressions of the form

$$I_i = I_i(q_1, \dots, q_N, p_1, \dots, p_N). \quad (2.5.1)$$

One way to find these integrals, if they exist, is to make the assumption that the integrals have a certain type of functional dependence on the system's coordinates and momenta, and then insist that these ansätze for the integrals are in involution. The form of the integrals can take the form of polynomials, rational functions, *et cetera*, and will contain a large number of parameters that can be manipulated in order to satisfy the involution conditions given by (2.1.4).

The applicability of this method is limited by the fact that the integrals for a given system may not be of the form chosen, or, even if they are simply polynomials in the coordinates and momenta, they may be very high order polynomials, requiring considerable effort to implement the method. Still, some success stories exist, and a comprehensive review of these methods and examples where they have succeeded has been published by Hiertarinta [45] and Abraham-Shrauner [67].

Direct methods of the types outlined in reference [45] should be employed only if there is strong evidence that the system is indeed integrable. Sufficient evidence would constitute numerical studies of the system that indicate regular behavior, or positive results from Painlevé or Yoshida singularity analysis tests.

CHAPTER THREE
SINGULARITY ANALYSIS APPLIED TO
TEST-PARTICLE EQUATIONS OF MOTION

§3.1 A Simple Model and its Symmetries

A simple and commonly used model for particle motion near the neutral line in the Earth's magnetotail [20-22], which was discussed earlier in § 1.4, is a uniform electric field parallel to the z-axis, accompanied by a magnetic field whose components lie in the x-y plane:

$$\mathbf{E} = \epsilon \hat{z}, \quad (3.1.1a)$$

$$\mathbf{B} = \delta y \hat{x} + x \hat{y}, \quad (3.1.1b)$$

where δ and ϵ are constant parameters. Recall that for $\delta > 0$, the magnetic field has an X-type neutral line along the z-axis, while $\delta < 0$ produces an O-type neutral line along the z-axis. For $\delta = 0$, the magnetic field produced has a neutral sheet in the x - z plane, and taking the limit $\delta \rightarrow \infty$ leads to a null plane in the y - z plane.

Note that the magnetic field possesses a discrete $x - y$ symmetry. This symmetry will play a significant role when we examine the leading order behaviors of the system's equations of motion in § 3.2. One way to understand this symmetry is to consider the structure of the field lines more closely. For all values of δ , the field lines lie on the contours of a *flux function* $\Psi(x, y)$:

$$\Psi(x, y) = \frac{1}{2}(\delta y^2 - x^2).$$

In the case of elliptical and circular field lines, $\Psi(x, y)$ is always negative, and a particular field line may be identified with some value $\Psi(x, y) = -\Psi_0$. This allows us to express the field line as an ellipse:

$$\frac{x^2}{\sqrt{2\Psi_0}} + \frac{y^2}{\sqrt{2\Psi_0/|\delta|}} = 1.$$

For $|\delta| > 1$, the closed field line has as its major axis the x -axis, and its eccentricity e is given by

$$e = \sqrt{\frac{|\delta| - 1}{|\delta|}}.$$

If we take $|\delta| < 1$, the closed field line has as its major axis the y -axis, and now its eccentricity e is given by

$$e = \sqrt{1 - |\delta|}.$$

Now suppose that we have $|\delta'| < 1 = 1/|\delta|$, with $|\delta| > 1$. Substituting for δ' , we find that the e becomes

$$e = \sqrt{1 - |\delta'|} = \sqrt{1 - \frac{1}{|\delta|}} = \sqrt{\frac{|\delta| - 1}{|\delta|}},$$

and thus the transformation $\delta \rightarrow \delta^{-1}$ leads to a set of closed field lines with the same eccentricity. Note that both sets of field lines have the same orientation (i.e. same sense of rotation about the origin), as depicted in Figure 1.1.1.

For positive values of δ , the field lines form two sets of hyperbolae, whose asymptotes are the lines $y = \pm x/\sqrt{\delta}$ (Figure 3.1.1). The angles that these asymptotes form with the x and y axes are θ_1 and θ_2 , respectively, and are given by

$$\theta_1(\delta) = \arctan(\delta^{-\frac{1}{2}}) \quad \theta_2(\delta) = \arctan(\delta^{\frac{1}{2}}).$$

Note now that the transformation $\delta \rightarrow 1/\delta$ simply exchanges these angles and also preserves the directions of the field lines.

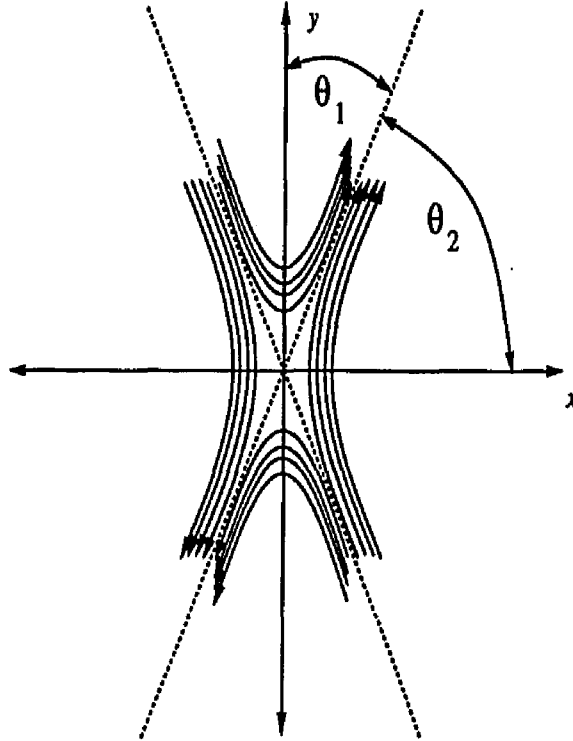


Figure 3.1.1. Angles θ_1 and θ_2 for an X-Line Field with $\delta = \frac{1}{4}$.

Recalling the results of § 1.4, a viable vector potential \mathbf{A} for \mathbf{B} is

$$\mathbf{A} = \frac{1}{2}(\delta^2 y^2 - x^2)\hat{\mathbf{z}} \equiv \Psi(x, y)\hat{\mathbf{z}}. \quad (3.1.2)$$

The Hamiltonian for a test particle can then be written as

$$H(x, y, z, p_x, p_y, p_z) = \frac{p_x^2 + p_y^2}{2} + \frac{(p_z - \Psi(x, y))^2}{2} - \kappa z, \quad (3.1.3)$$

where κ is the electric field strength. The Hamiltonian equations of motion for the test particle are:

$$\dot{x} = \frac{\partial H}{\partial p_x} = p_x \quad (3.1.4a)$$

$$\dot{y} = \frac{\partial H}{\partial p_y} = p_y \quad (3.1.4b)$$

$$\dot{z} = \frac{\partial H}{\partial p_z} = p_z - \Psi(x, y) = p_z + \frac{1}{2}(x^2 - \delta y^2), \quad (3.1.4c)$$

$$\dot{p}_x = -\frac{\partial H}{\partial x} = (\Psi(x, y) - p_z) \frac{\partial \Psi}{\partial x} = -x p_z + \frac{x(\delta y^2 - x^2)}{2} \quad (3.1.4d)$$

$$\dot{p}_y = -\frac{\partial H}{\partial y} = (\Psi(x, y) - p_z) \frac{\partial \Psi}{\partial y} = \delta y p_z - \frac{\delta y(\delta y^2 - x^2)}{2} \quad (3.1.4e)$$

$$\dot{p}_z = -\frac{\partial H}{\partial z} = \kappa. \quad (3.1.4f)$$

In view of the inherent symmetries of the magnetic field for this model, it is likely that these symmetries are related to the symmetries of H and the Hamiltonian equations of motion (3.1.4a-f). For $\delta \neq 0$, it is possible to rescale the coordinates, and replace δ with $1/\delta$, and the roles of the x and y motions will be exchanged. Given this symmetry, we will consider only values of the parameter δ that belong to the interval

$$-1 \leq \delta \leq 1.$$

As mentioned earlier, the case $\delta = 0$ ($\delta \rightarrow \infty$) leads to a magnetic field configuration that is a slab, with the plane $x = 0$ ($y = 0$) as a neutral sheet. The singularity analysis of this case is presented in Appendix Two and the properties of its trajectories are discussed in Chapter Five.

Note that the equation for p_z can readily be solved to get

$$p_z = \kappa t + p_{z_0},$$

where p_{z_0} is a constant. Eliminating p_z from the remaining equations (3.1.4a-e) we get

$$\dot{x} = p_x \quad (3.1.5a)$$

$$\dot{y} = p_y \tag{3.1.5b}$$

$$\dot{z} = (\kappa t + p_{z_0}) + \frac{1}{2}(x^2 - \delta y^2), \tag{3.1.5c}$$

$$\dot{p}_x = -x(\kappa t + p_{z_0}) + \frac{x(\delta y^2 - x^2)}{2}, \tag{3.1.5d}$$

$$\dot{p}_y = \delta y(\kappa t + p_{z_0}) - \frac{\delta y(\delta y^2 - x^2)}{2} \tag{3.1.5e}$$

The above reduction of the set (3.1.4a-f) to the set (3.1.5a-e) may appear to be of little importance, but is actually crucial to getting accurate results from the Painlevé analysis. This matter will be taken up again when we calculate the resonances in § 3.2.

Given the system of equations (3.1.5a-e), it is only logical to wonder whether or not they are nonintegrable for arbitrary values of δ and κ , or if there exist special field configurations (that is, particular values of δ and κ) for which the dynamics are integrable. In the next section, we will explore this issue by applying Painlevé singularity analysis to this system.

§3.2 Painlevé Property Test of (3.1.5a-e)

Given the equations of motion, we can now examine their singularity properties by applying the ARS algorithm to the system.

Step 1: Leading-Order Behaviors

Consider a singularity in the complex time plane located at some point t_0 . In the neighborhood of the singularity, we can approximate the leading order behaviors of the coordinates and momenta by

$$x = \alpha_x \tau^{\beta_x}, \quad y = \alpha_y \tau^{\beta_y}, \quad z = \alpha_z \tau^{\beta_z},$$

$$p_x = \alpha_{p_x} \tau^{\beta_{p_x}}, \quad p_y = \alpha_{p_y} \tau^{\beta_{p_y}},$$

where $\tau = (t - t_0)$, and the quantities $(\alpha_x, \alpha_y, \alpha_z, \alpha_{p_x}, \alpha_{p_y})$ and $(\beta_x, \beta_y, \beta_z, \beta_{p_x}, \beta_{p_y})$ are constants. Inserting these expressions into Hamilton's equations, we get

$$\frac{dx}{d\tau} = \alpha_x \beta_x \tau^{\beta_x - 1} = \alpha_{p_x} \tau^{\beta_{p_x}}, \quad (3.2.1a)$$

$$\frac{dy}{d\tau} = \alpha_y \beta_y \tau^{\beta_y - 1} = \alpha_{p_y} \tau^{\beta_{p_y}}, \quad (3.2.1b)$$

$$\frac{dz}{d\tau} = \alpha_z \beta_z \tau^{\beta_z - 1} = \kappa \tau + p_{z_0} + \frac{1}{2} \alpha_x^2 \tau^{2\beta_x} - \frac{1}{2} \delta \alpha_y^2 \tau^{2\beta_y}, \quad (3.2.1c)$$

$$\frac{dp_x}{d\tau} = \alpha_{p_x} \beta_{p_x} \tau^{\beta_{p_x} - 1} = -\alpha_x \tau^{\beta_x} (\kappa \tau + p_{z_0}) + \frac{1}{2} \delta \alpha_x \alpha_y^2 \tau^{2\beta_x + 2\beta_y} - \frac{1}{2} \alpha_x^3 \tau^{3\beta_x} \quad (3.2.1d)$$

$$\frac{dp_y}{d\tau} = \alpha_{p_y} \beta_{p_y} \tau^{\beta_{p_y} - 1} = \delta \alpha_y \tau^{\beta_y} (\kappa \tau + p_{z_0}) + \frac{1}{2} \delta \alpha_x^2 \alpha_y \tau^{2\beta_x + \beta_y} - \frac{1}{2} \delta^2 \alpha_y^3 \tau^{3\beta_y} \quad (3.2.1e)$$

The first two equations imply that $\beta_{p_x} = \beta_x - 1$, $\beta_{p_y} = \beta_y - 1$, $\alpha_{p_x} = \alpha_x \beta_x$, and $\alpha_{p_y} = \alpha_y \beta_y$. Using this information, we can simplify (3.2.1b-d) to get the system

$$\alpha_x \beta_x \tau^{\beta_x - 1} = p_{z_0} + \kappa \tau + \frac{1}{2} \alpha_x^2 \tau^{2\beta_x} - \frac{1}{2} \delta \alpha_y^2 \tau^{2\beta_y} \quad (3.2.2a)$$

$$\beta_x (\beta_x - 1) \tau^{-2} = -(\kappa \tau + p_{z_0}) + \frac{1}{2} \delta \alpha_y^2 \tau^{2\beta_y} - \frac{1}{2} \alpha_x^2 \tau^{2\beta_x} \quad (3.2.2b)$$

$$\beta_y (\beta_y - 1) \tau^{-2} = \delta (\kappa \tau + p_{z_0}) + \frac{1}{2} \delta \alpha_x^2 \tau^{2\beta_x} - \frac{1}{2} \delta^2 \alpha_y^2 \tau^{2\beta_y} \quad (3.2.2c)$$

It is now necessary to test *every* possible leading order behavior for the set of equations (3.2.2a-c). Upon examining (3.2.2a-c), it becomes clear that this is no small job. Counting the number of possible leading order balances for the system itself is something of a *monstre travail*. To this end, we must consider the set (3.2.2a-c) one at a time. This is an arduous task, and the details of the actual calculation are presented in Appendix One. What follows is a listing of the classes of acceptable leading order behaviors that we found.

Class I:

$$\begin{aligned} x &= \pm 2i\tau^{-1} & y &= \alpha_y \tau^{\beta_y} & z &= 2\tau^{-1} \\ p_x &= \mp 2i\tau^{-2} & p_y &= \beta_y \alpha_y \tau^{\beta_y - 1} \\ & & & \text{with} \end{aligned}$$

$$\beta_y^2 - \beta_y + 2\delta = 0, \quad \beta_y > -1.$$

Class II:

$$\begin{aligned}
 x &= \alpha_x \tau^{\beta_x} & y &= \pm \frac{2i}{\delta} \tau^{-1} & z &= -\frac{2}{\delta} \tau^{-1} \\
 p_x &= \beta_x \alpha_x \tau^{\beta_x - 1} & p_y &= \mp \frac{2i}{\delta} \tau^{-2}
 \end{aligned}$$

with

$$\beta_x^2 - \beta_x + \frac{2}{\delta} = 0, \quad \beta_x > -1.$$

Class III:

$$\begin{aligned}
 x &= \pm i \sqrt{4 + \alpha_y^2} \tau^{-1} & y &= \alpha_y \tau^{-1} & z &= 2\tau^{-1} \\
 p_x &= \mp i \sqrt{4 + \alpha_y^2} \tau^{-2} & p_y &= -\alpha_y \tau^{-2}
 \end{aligned}$$

Class IV:

$$\begin{aligned}
 x &= \pm \sqrt{\delta} \alpha_y \tau^\beta & y &= \alpha_y \tau^\beta & z &= \alpha_z \tau^{\beta_z} \\
 p_x &= \pm \beta \sqrt{\delta} \alpha_y \tau^{\beta-1} & p_y &= \beta \alpha_y \tau^{\beta-1}
 \end{aligned}$$

with $\beta < -1$, $\beta_z > 2\beta + 1$, and both α_y and α_z are arbitrary.

Class V:

$$\begin{aligned}
 x &= \pm \sqrt{\delta \alpha_y^2 - 2p_{z0}} & y &= \alpha_y & z &= \alpha_z \tau^{\beta_z} \\
 p_x &= 0 & p_y &= 0
 \end{aligned}$$

with $\beta_z > 1$, and both α_y and α_z are arbitrary.

Class VI:

$$\begin{aligned}
 x &= \pm\sqrt{\delta}\alpha_y\tau & y &= \alpha_y\tau & z &= \alpha_z\tau^{\beta_z} \\
 p_x &= \pm\sqrt{\delta}\alpha_y & p_y &= \alpha_y \\
 & \text{with } \beta_z > 3, \text{ and both } \alpha_y \text{ and } \alpha_z \text{ are arbitrary.}
 \end{aligned}$$

Now we examine in detail each of the above classes.

Class I: For this leading order behavior, the exponent β_y is determined by:

$$\beta_y^2 - \beta_y + 2\delta = 0, \quad (3.2.3)$$

with solutions given by

$$\beta_y = \frac{1 \pm \sqrt{1 - 8\delta}}{2}. \quad (3.2.4)$$

Since we require that β_y be real, we must have $\delta \leq 1/8$. The requirement that $\beta_y > -1$ is equivalent to requiring that $-1 < \delta \leq 1/8$, allowing both branches of (3.2.4) yield viable values of β_y . For values of $\delta < -1$, the “+” branch of (3.2.4) is still valid, and produces balances with $\beta_y > 2$.

As we mentioned in §2.3, all of the powers of the leading-order behaviors in a given class must be either integers (rationals) in order for the system to possess the Painlevé (weak Painlevé) property. These conditions will allow certain *discrete* values of δ . There exist four possibilities, based on the value of β_y .

Ia) β_y is an integer, and $\beta_y > -1$:

Let $\beta_y = J$, an integer. We know that given a value of J , (3.2.3) allows us to write δ as a function of J ,

$$\delta = \delta(J) = \frac{J(1 - J)}{2}, J \geq 2. \quad (3.2.5)$$

This implies that there is an infinite set of integer leading-order behaviors for β_y corresponding to δ given above. Below are some examples of the values of $\delta(J)$:

$$\delta(0) = 0, \quad \delta(1) = 0, \quad \delta(2) = -1,$$

$$\delta(3) = -3 \quad \delta(4) = -6 \quad \delta(5) = -10$$

$$\delta(6) = -15 \quad \delta(7) = -21 \quad \delta(8) = -28$$

For $J = 0, 1$, the resulting magnetic field is a neutral sheet field, with a neutral sheet in the plane $x = 0$. The resulting magnetic field geometry associated with the other values of δ correspond to elliptical O-line fields that are elongated along the x -axis.

Ib) β_y is rational, and $-1 < \beta_y < 0$.

Let $\beta_y = -M/N$, with M and N natural numbers, $M < N$. In this situation, there is also an infinite set of discrete values of δ , given by

$$\delta = \delta(M, N) = -\frac{M}{2N^2}(M + N) \quad (3.2.6)$$

A sampling of this set of $\delta(M, N)$ for $1 \leq M \leq 8$ and $M < N \leq 9$ is given in Table 3.1. Notice that once again we have values of δ that produce O-line magnetic fields, but the elliptical field lines are now elongated along the y -axis. Note also that the spectrum of values of δ for a fixed value of N lie in the range

$$-\frac{(N-1)(2N-1)}{2N^2} \leq \delta \leq -\frac{(N+1)}{2N^2},$$

thus as N gets large and $M \rightarrow N$, the field lines approach a circular geometry.

Table 3.1. Allowed Values of δ for Rational $\beta_y \in (-1, 0)$.

$\downarrow M \quad N \rightarrow$	2	3	4	5	6	7	8	9
1	$-\frac{3}{8}$	$-\frac{2}{9}$	$-\frac{5}{32}$	$-\frac{3}{25}$	$-\frac{7}{72}$	$-\frac{4}{49}$	$-\frac{9}{128}$	$-\frac{5}{81}$
2		$-\frac{5}{9}$	$-\frac{3}{8}$	$-\frac{7}{25}$	$-\frac{2}{9}$	$-\frac{9}{49}$	$-\frac{5}{32}$	$-\frac{11}{81}$
3			$-\frac{21}{32}$	$-\frac{12}{25}$	$-\frac{3}{8}$	$-\frac{15}{49}$	$-\frac{33}{128}$	$-\frac{2}{9}$
4				$-\frac{18}{25}$	$-\frac{5}{9}$	$-\frac{22}{49}$	$-\frac{3}{8}$	$-\frac{26}{81}$
5					$-\frac{55}{72}$	$-\frac{30}{49}$	$-\frac{65}{128}$	$-\frac{35}{81}$
6						$-\frac{39}{49}$	$-\frac{21}{32}$	$-\frac{5}{9}$
7							$-\frac{105}{128}$	$-\frac{56}{81}$
8								$-\frac{68}{81}$

Ic) β_y is rational, and $0 < \beta_y < 1$.

Let $\beta_y = M/N$, with M and N natural numbers, $M < N$. Again it is possible to express δ as a function of M and N :

$$\delta = \delta(M, N) = \frac{M(N - M)}{2N^2}. \quad (3.2.7)$$

Table 3.2 Lists a small sampling of these values of δ . Here we find that we have positive values of δ , which are associated with X-line magnetic field configurations, such as those shown in Figure 3.1.1a.

Table 3.2. Allowed Values of δ for Rational $\beta_y \in (0, 1)$.

$\downarrow M \quad N \rightarrow$	2	3	4	5	6	7	8	9	10
1	$\frac{1}{8}$	$\frac{1}{9}$	$\frac{3}{32}$	$\frac{2}{25}$	$\frac{5}{72}$	$\frac{3}{49}$	$\frac{7}{128}$	$\frac{4}{81}$	$\frac{9}{200}$
2		$\frac{1}{9}$	$\frac{1}{8}$	$\frac{3}{25}$	$\frac{1}{9}$	$\frac{5}{49}$	$\frac{3}{32}$	$\frac{7}{81}$	$\frac{2}{25}$
3			$\frac{3}{32}$	$\frac{3}{25}$	$\frac{1}{8}$	$\frac{6}{49}$	$\frac{15}{128}$	$\frac{1}{9}$	$\frac{21}{200}$
4				$\frac{2}{25}$	$\frac{1}{9}$	$\frac{6}{49}$	$\frac{1}{8}$	$\frac{10}{81}$	$\frac{3}{25}$
5					$\frac{5}{72}$	$\frac{5}{49}$	$\frac{15}{128}$	$\frac{10}{81}$	$\frac{1}{8}$
6						$\frac{3}{49}$	$\frac{3}{32}$	$\frac{1}{9}$	$\frac{3}{25}$
7							$\frac{7}{128}$	$\frac{7}{81}$	$\frac{21}{200}$
8								$\frac{4}{81}$	$\frac{2}{25}$
9									$\frac{9}{200}$

Id) β_y is rational, and $\beta_y > 1$.

Let $\beta_y = N/M$, with M and N natural numbers, $M < N$. Using (3.2.3) to define the values of δ that yield this behavior, we find

$$\delta = \delta(M, N) = \frac{N(M - N)}{2M^2}. \quad (3.2.8)$$

Table 3.3 lists the values of δ obtained from this relation. Once again, we have values of δ that produce O-line magnetic fields.

Table 3.3. Allowed Values of δ for Rational $\beta_y > 1$.

$\downarrow M \quad N \rightarrow$	2	3	4	5	6	7	8	9
1	-1	-3	-6	-10	-15	-21	-28	-36
2		$-\frac{3}{8}$	-1	$-\frac{15}{8}$	-3	$-\frac{35}{8}$	-6	$-\frac{63}{8}$
3			$-\frac{2}{9}$	$-\frac{5}{9}$	-1	$-\frac{14}{9}$	$-\frac{20}{9}$	-3
4				$-\frac{5}{32}$	$-\frac{3}{8}$	$-\frac{21}{32}$	-1	$-\frac{45}{32}$
5					$-\frac{3}{25}$	$-\frac{7}{25}$	$-\frac{12}{25}$	$-\frac{18}{25}$
6						$-\frac{7}{72}$	$-\frac{2}{9}$	$-\frac{3}{8}$
7							$-\frac{4}{49}$	$-\frac{9}{49}$
8								$-\frac{9}{128}$

Note that for $M = 1$, these values of δ are the same set as that given previously in Case Ai). Another interesting property of the δ -spectrum for this case can be seen by considering fixed N , and varying M . For fixed N and small M , say $M = 1$, the elliptical field lines are either circular ($N = 2$), or elongated along the y -axis ($N > 2$). The value of M for which the field lines switch their orientation is M_* , given by

$$M_* = \begin{cases} \frac{N}{2}, & \text{if } N \text{ even;} \\ \left[\frac{N}{2}\right] + 1, & N \text{ odd,} \end{cases}$$

where the notation $[x]$ indicates the greatest integer function of x .

Class II: Solving equations (3.2.3a-c) for the coefficients α_x , α_y , and α_z give us $\alpha_y = \pm 2i/\delta$, $\alpha_z = 2$, and α_x is arbitrary. The exponent β_x is determined by:

$$\beta_x^2 - \beta_x + \frac{2}{\delta} = 0, \quad (3.2.9)$$

with solutions given by

$$\beta_x = \frac{1 \pm \sqrt{1 - \frac{8}{\delta}}}{2}. \quad (3.2.10)$$

The condition that β_x be real requires either $\delta \geq 8$. The requirement that $\beta_x > -1$ manifests itself as follows: for the "–" branch of (3.2.10), we will get satisfactory values of β_x if $\delta < -1$ or $\delta \geq 8$, while the "+" branch of (3.2.10) gives us acceptable values of β_x for $\delta < 0$ or $\delta \geq 8$.

Again, we find that we can obtain satisfactory leading order behaviors for a *discrete* set of values of δ . There exist four classes of possibilities, based on the value of β_x . The set of allowed values of β_x is identical to the set of allowed values of β_y found for class I, and the corresponding values of δ are simply the reciprocals of the allowed values of δ calculated for class I.

IIa) β_x is an integer, and $\beta_x > -1$:

Let $\beta_x = J$, an integer. We know that given a value of J , (3.2.3) allows us to write δ as a function of J ,

$$\delta = \delta(J) = \frac{2}{J(1-J)}, \quad J \geq 2.$$

This implies that there is an infinite set of integer leading-order behaviors for β_y corresponding to δ given above. Below are some examples of the values of $\delta(J)$. Note that $\delta(J)$ is undefined for $\delta = 0, 1$, which is associated with a neutral sheet field along the x -axis.

$$\begin{aligned} \delta(2) &= -1, & \delta(3) &= -\frac{1}{3}, & \delta(4) &= -\frac{1}{6}, \\ \delta(5) &= -\frac{1}{10}, & \delta(6) &= -\frac{1}{15}, & \delta(7) &= -\frac{1}{21}, \\ \delta(8) &= -\frac{1}{28}, & \delta(9) &= -\frac{1}{36}, & \delta(10) &= -\frac{1}{45} \end{aligned}$$

These values of $\delta(J)$ are simply the reciprocals of those found for Case Ia), and the resulting magnetic field geometry associated with these values of δ correspond to elliptical O-line fields, but now the elongation is along the y -axis.

IIb) β_x is rational, and $-1 < \beta_x < 0$.

Let $\beta_x = -M/N$, with M and N natural numbers, $M < N$. In this situation, there is also an infinite set of discrete values of δ , given by

$$\delta = \delta(M, N) = -\frac{2N^2}{M(N + M)}$$

This leads to a set of $\delta < -1$ that form O-type neutral line fields. The values of $\delta(M, N)$ for this case is simply the reciprocal of the value of $\delta(M, N)$ obtained from Table 3.1.

IIc) β_x is rational, and $0 < \beta_x < 1$.

Let $\beta_x = M/N$, with M and N natural numbers, $M < N$. Again it is possible to express δ as a function of M and N :

$$\delta = \delta(M, N) = \frac{2N^2}{M(N - M)}$$

Now we have positive values of δ , which are associated with X-line magnetic field configurations with values of $\delta(M, N)$ that are the reciprocals of the corresponding entries in Table 3.2.

IIId) β_x is rational, and $\beta_x > 1$.

Let $\beta_x = N/M$, with M and N natural numbers, $M < N$. Again, we can use our equation for β_x to define the values of δ that yield this behavior, and we find

$$\delta = \delta(M, N) = \frac{2M^2}{N(M - N)}$$

The resulting magnetic field configurations for this case are again O-type neutral line fields, with $\delta(M, N)$ now given by the reciprocals of the corresponding entries in Table 3.3. Again, for fixed N , we can define M_* such that for fixed N , all $M < M_*(N)$, we will have $\delta < -1$, and for $M > M_*(N)$, we will have $-1 \leq \delta < 0$.

Class III: This class is associated with the circularly symmetric O-type field configuration, and passes the first step of the Painlevé analysis.

Class IV: This class of leading order behavior exists for all values of δ , and will be examined in more detail in step two of the algorithm.

Class V: One interesting aspect of this case is the situation in which $\alpha_x = \alpha_y = 0$. This forces the condition $p_{z_0} = 0$, and we get $\beta_z = 2$. This is simply the case of a particle starting at rest on the neutral line, and being accelerated down the neutral line by the electric field, simplifying the system's motion to

$$z(\tau) = \frac{\kappa}{2}\tau^2 + z_0,$$

where z_0 is a constant.

Class VI: This class also applies to all values of δ , and will be examined further in step Two.

Step 2: Resonances

Now we turn our attention to the question of at which order the integration constants will appear as we try to construct the coefficients of the Laurent series (2.2.1). To this end, we must solve for the *resonances* associated with the leading order behaviors for Classes I-VI. Recalling step II of the ARS algorithm, we expand

our coordinates and momenta found in (3.2.2a-e) as:

$$\begin{aligned}
 x &= \alpha_x \tau^{\beta_x} (1 + \gamma_x \tau^r) & p_x &= \alpha_{p_x} \tau^{\beta_{p_x}} (1 + \gamma_{p_x} \tau^r) \\
 y &= \alpha_y \tau^{\beta_y} (1 + \gamma_y \tau^r) & p_y &= \alpha_{p_y} \tau^{\beta_{p_y}} (1 + \gamma_{p_y} \tau^r) \\
 z &= \alpha_z \tau^{\beta_z} (1 + \gamma_z \tau^r)
 \end{aligned}$$

where r is presumed positive (with the exception of the ubiquitous resonance at $r = -1$) and the γ 's are constants. Substituting these expressions into (3.2.2a-e), and recalling the expressions for α_{p_x} , α_{p_y} , β_{p_x} , and β_{p_y} obtained from (3.2.1a-b), and retaining only terms up to those that are linear in the γ 's, we get

$$\alpha_x (\beta_x + r) \gamma_x \tau^{-1+\beta_x+r} - \alpha_x \beta_x \gamma_{p_x} \tau^{-1+\beta_x+r} = 0 \quad (3.2.11a)$$

$$\alpha_y (\beta_y + r) \gamma_y \tau^{-1+\beta_y+r} - \alpha_y \beta_y \gamma_{p_y} \tau^{-1+\beta_y+r} = 0 \quad (3.2.11b)$$

$$\begin{aligned}
 -p_{z_0} - \kappa \tau - \frac{\alpha_x^2 \tau^2 \beta_x}{2} + \frac{\alpha_y^2 \delta \tau^2 \beta_y}{2} + \alpha_x \beta_x \tau^{-1+\beta_x} - \alpha_x^2 \gamma_x \tau^{2\beta_x+r} + \\
 \alpha_y^2 \delta \gamma_y \tau^{2\beta_y+r} + \alpha_z (\beta_z + r) \gamma_z \tau^{-1+\beta_z+r} = 0
 \end{aligned} \quad (3.2.11c)$$

$$\begin{aligned}
 -(\alpha_x \beta_x \tau^{-2+\beta_x}) + \alpha_x \beta_x^2 \tau^{-2+\beta_x} + \alpha_x p_{z_0} \tau^{\beta_x} + \frac{\alpha_x^3 \tau^3 \beta_x}{2} + \alpha_x \kappa \tau^{1+\beta_x} - \\
 \frac{\alpha_x \alpha_y^2 \delta \tau^{\beta_x+2\beta_y}}{2} + \alpha_x \beta_x (\beta_x + r - 1) \gamma_{p_x} \tau^{\beta_x+r-2} + \alpha_x \gamma_x p_{z_0} \tau^{\beta_x+r} + \\
 \alpha_x \kappa \gamma_x \tau^{1+\beta_x+r} + \frac{3 \alpha_x^3 \gamma_x \tau^3 \beta_x+r}{2} - \frac{\alpha_x \alpha_y^2 \delta \gamma_x \tau^{\beta_x+2\beta_y+r}}{2} \\
 \alpha_x \alpha_y^2 \delta \gamma_y \tau^{\beta_x+2\beta_y+r} = 0
 \end{aligned} \quad (3.2.11d)$$

$$\begin{aligned}
& -(\alpha_y \beta_y \tau^{-2+\beta_y}) + \alpha_y \beta_y^2 \tau^{-2+\beta_y} - \alpha_y \delta p_{z_0} \tau^{\beta_y} + \frac{\alpha_y^3 \delta^2 \tau^{3\beta_y}}{2} - \alpha_y \delta \kappa \tau^{1+\beta_y} - \\
& \frac{\alpha_x^2 \alpha_y \delta \tau^{2\beta_x+\beta_y}}{2} + \alpha_y \beta_y (\beta_y + r - 1) \gamma_{p_y} \tau^{\beta_y+r-2} + \alpha_y \delta \gamma_y p_{z_0} \tau^{\beta_y+r} - \\
& \alpha_y \delta \kappa \gamma_y \tau^{1+\beta_y+r} - \alpha_x^2 \alpha_y \delta \gamma_x \tau^{2\beta_x+\beta_y+r} - \frac{\alpha_x^2 \alpha_y \delta \gamma_y \tau^{2\beta_x+\beta_y+r}}{2} + \\
& \frac{3 \alpha_y^3 \delta^2 \gamma_y \tau^{3\beta_y+r}}{2} = 0. \tag{3.2.11e}
\end{aligned}$$

For a given leading order behavior, we will find that the leading order terms that do not contain the γ_i cancel each other, as we expect, leaving only terms that are linear in the γ_i . This can be done regardless of the particular leading order behavior for only (3.2.11a) and (3.2.11b)

$$(r + \beta_x) \gamma_x - \beta_x \gamma_{p_x} = 0 \tag{3.2.12a}$$

$$(r + \beta_y) \gamma_y - \beta_y \gamma_{p_y} = 0, \tag{3.2.12b}$$

while the other equations must be examined on a case-by-case basis for each class of leading order behavior.

As was discussed in § 2.3, this system may be written as a linear system

$$\mathbf{Q} \cdot \boldsymbol{\gamma} = 0, \tag{3.2.13}$$

with the vector $\boldsymbol{\gamma}$ defined as $\boldsymbol{\gamma} = (\gamma_x, \gamma_y, \gamma_z, \gamma_{p_x}, \gamma_{p_y})^T$. The resonances will be the r roots of

$$\det(\mathbf{Q}(r)) = 0, \tag{3.2.14}$$

which is considered a polynomial equation in r . Given Equations (3.2.12a-b), (3.2.11c-e), and (3.2.13), we can now proceed to construct \mathbf{Q} for each class, and then evaluate the resonances using (3.2.14).

Class I: Recall that for this leading order behavior, we have $\alpha_x = 2$, $\alpha_z = -2$, and α_y is arbitrary, while $\beta_x = -1$, $\beta_z = -1$, and β_y is given by (3.2.4). The matrix $\mathbf{Q}(r)$ associated with this system is

$$\mathbf{Q}(r) = \begin{pmatrix} (r-1) & 0 & 0 & 1 & 0 \\ 0 & \alpha_y(\beta_y + r) & 0 & 0 & -(\alpha_y\beta_y) \\ 4 & 0 & -2 + 2r & 0 & 0 \\ -12i & 0 & 0 & 2i(2-r) & 0 \\ 4\alpha_y\delta & 2\alpha_y\delta & 0 & 0 & \alpha_y\beta_y(-1 + \beta_y + r) \end{pmatrix}. \quad (3.2.15)$$

Taking the determinant of (3.2.15), we find that the resonances satisfy

$$\det(\mathbf{Q}) = 8\alpha_y^2\beta_y(r-4)(r-1)(r+1)(\beta_y^2 - \beta_y + 2d - r + 2\beta_y r + r^2) = 0, \quad (3.2.16)$$

Recalling (3.2.3), we can rewrite (3.2.16) to find that the resonances are the r roots of

$$(r-4)(r-1)(r+1)r(r+2\beta_y-1) = 0, \quad (3.2.17)$$

meaning that the system's resonances for this case are $r = -1, 0, 1 - 2\beta_y, 1, 4$. Since α_y is arbitrary, we expected the resonance at $r = 0$, and the resonance at $r = 1 - 2\beta_y$ is in agreement with this system being a candidate for possessing the weak Painlevé property. Note here that since we wish that all of our resonances be either integers or positive rationals with the same denominator as β_y , we must have only values of β_y that fall in the range

$$-1 < \beta_y < \frac{1}{2}.$$

This leads to a further restriction on the admissible values of δ that lead to acceptable resonances. Case Ib) comes through this test unscathed, while we can keep only the values of δ for case Ic) that are associated with values of $\beta_y < \frac{1}{2}$. Table 3.4 is a summary of this narrowed class of field geometries.

Table 3.4. Allowed Values of δ for Rational $\beta_y \in (0, \frac{1}{2})$.

$\downarrow M \quad N \rightarrow$	3	4	5	6	7	8	9	10	11
1	$\frac{1}{9}$	$\frac{3}{32}$	$\frac{2}{25}$	$\frac{5}{72}$	$\frac{3}{49}$	$\frac{7}{128}$	$\frac{4}{81}$	$\frac{9}{200}$	$\frac{5}{121}$
2			$\frac{3}{25}$	$\frac{1}{9}$	$\frac{5}{49}$	$\frac{3}{32}$	$\frac{7}{81}$	$\frac{2}{25}$	$\frac{9}{121}$
3					$\frac{6}{49}$	$\frac{15}{128}$	$\frac{1}{9}$	$\frac{21}{200}$	$\frac{12}{121}$
4							$\frac{10}{81}$	$\frac{3}{25}$	$\frac{14}{121}$
5									$\frac{15}{121}$

Class II: Given the discrete symmetry discussed in §3.1, and the earlier arguments concerning the properties of this class in relation to class I, it is no surprise that we find that the system's resonances for this class are $r = -1, 0, 1 - 2\beta_x, 1, 4$. Since α_x is arbitrary, the resonance at $r = 0$ again is to be expected, and the resonance at $r = 1 - 2\beta_x$ is in agreement with this system being a candidate for possessing the weak Painlevé property. Note here that since we wish that all of our resonances be either nonnegative integers or positive rationals with the same denominator as β_y , so once again we find that we must have only values of β_x that fall in the range

$$-1 < \beta_x < \frac{1}{2}.$$

Clearly, all of the configurations connected to Class IIb) survive the resonance test. The above restriction on β_y immediately eliminates Classes IIa) and IIc) from

further consideration, and also eliminates the allowed values from Class Ic) that are associated with $\beta_y > \frac{1}{2}$. The surviving values of the field parameter δ for Class Ic) are the inverses of the entries in Table 3.4.

Class III: The matrix $\mathbf{Q}(r)$ associated with this class is

$$\mathbf{Q} = \begin{pmatrix} \alpha_x(r-1) & 0 & 0 & \alpha_x & 0 \\ 0 & \alpha_y(r-1) & 0 & 0 & \alpha_y \\ -\alpha_x & -\alpha_y^2 & 2(r-1) & 0 & 0 \\ -(2-\alpha_x)\alpha_x & \alpha_y^2\alpha_x & 0 & \alpha_x\alpha_y^2 & (2-r) & 0 \\ -\alpha_y\kappa & \alpha_y(\alpha_y^2-2) & 0 & 0 & \alpha_y(r-2) \end{pmatrix},$$

The determinant of $\mathbf{Q}(r)$ is thus

$$\det(\mathbf{Q}(r)) = -2\alpha_y^2\kappa(r-4)(r-3)(r-1)r(1+r) = 0. \quad (3.2.18)$$

Here we have integer resonances, indicating that this class of leading order behavior, which has integer leading order exponents may possess the Painlevé property. The disposition of this class regarding the Painlevé property will be determined in Step Three of the algorithm.

Class IV: Substituting this leading order behavior into (3.2.11a-e) we find the matrix \mathbf{Q} is

$$\mathbf{Q}(r) = \begin{pmatrix} \beta_x + r & 0 & 0 & -\beta_x & 0 \\ 0 & \beta_x + r & 0 & 0 & -\beta_x \\ 1 & -1 & 0 & 0 & 0 \\ -1 & 1 & 0 & 0 & 0 \\ 1 & -1 & 0 & 0 & 0 \end{pmatrix}. \quad (3.2.19)$$

The determinant of this matrix is clearly zero, and thus we are unable to obtain any information about the system's resonances. Therefore the algorithm terminates at this stage for this class.

Class V: Recalling the results of step I for this class, the matrix \mathbf{Q} from

equation (3.2.22) associated with this class is

$$\mathbf{Q} = \begin{pmatrix} r & 0 & 0 & 0 & 0 \\ 0 & r & 0 & 0 & 0 \\ \alpha_x^2 & -\delta\alpha_y^2 & 0 & 0 & 0 \\ -\alpha_x^2 & \delta\alpha_y^2 & 0 & 0 & 0 \\ \alpha_x^2 & -\delta\alpha_y^2 & 0 & 0 & 0 \end{pmatrix}. \quad (3.2.20)$$

The determinant of this matrix is also identically zero, indicating that we can not obtain the suitable number of resonances required for the system to pass through this step of the algorithm for this class. For class E, the algorithm terminates here, and the system does not possess either variety of the Painlevé property.

Class VI: For this class of leading order behavior, the matrix $\mathbf{Q}(r)$ becomes

$$\mathbf{Q}(r) = \begin{pmatrix} r+1 & 0 & 0 & -1 & 0 \\ 0 & r+1 & 0 & 0 & -1 \\ \alpha_x^2 & \delta\alpha_y^2 & 0 & 0 & 0 \\ r & 0 & 0 & 0 & 0 \\ 0 & r & 0 & 0 & 0 \end{pmatrix}. \quad (3.2.21)$$

Yet again, the determinant of $\mathbf{Q}(r)$ is identically zero, and the ARS algorithm terminates at this stage for this class, which possesses neither type of the Painlevé property.

Step 3: Constants of Integration

We now turn to the final step of the ARS algorithm: the construction of the constants of integration. Recall that this process is accomplished through further modification of the ansätze used to determine the system's leading order behaviors. The strategy is to construct the coefficients of the Laurent series representations of the coordinates and momenta from the leading orders β_i up to the orders associated with the largest positive resonance $(r_{max})_i$; $\beta_i + r_{max}$. Equation (2.3.7) is the recipe for this construction, and applying it to our dynamical system (3.2.1a-e), we find

that we must now expand our phase space coordinates as

$$x = \alpha_x \tau^{\beta_x} + \sum_{m=1}^{r_{max}} C_{1m} \tau^{\beta_x+m}, \quad (3.2.22a)$$

$$y = \alpha_y \tau^{\beta_y} + \sum_{m=1}^{r_{max}} C_{2m} \tau^{\beta_y+m}, \quad (3.2.22b)$$

$$z = \alpha_z \tau^{\beta_z} + \sum_{m=1}^{r_{max}} C_{3m} \tau^{\beta_z+m}, \quad (3.2.22c)$$

$$p_x = \beta_x \alpha_x \tau^{\beta_x-1} + \sum_{m=1}^{r_{max}} C_{4m} \tau^{\beta_x+m-1}, \quad (3.2.22d)$$

$$p_y = \beta_y \alpha_y \tau^{\beta_y-1} + \sum_{m=1}^{r_{max}} C_{5m} \tau^{\beta_y+m-1}, \quad (3.2.22e).$$

The next step in this process is the substitution of (3.2.22a-e) for a class of leading order behavior into the system (3.2.1a-e), and then solving for the coefficients C_{im} , working our way up order-by-order in the expansion for the equation. What follows are the results for our three surviving classes of leading order behaviors.

Classes I and II: The aforementioned strategy will work for for classes of leading order behavior that have integer resonances, such as class III, but will not work for situations in which one or more of the resonances are rational; i.e. classes I and II. For these classes, we must modify the expansions (3.2.22a-e) as described in § 2.3, and then carry out this process. If one or more of the resonances is rational, it is necessary to determine the lowest common denominator of the resonances. Call this denominator M . Now, we must modify the expressions (3.2.22a-e) to include the resonances in the orders of the expansion:

$$x = \alpha_x \tau^{\beta_x} + \sum_{m=1}^{Mr_{max}} C_{1m} \tau^{\beta_x + \frac{m}{M}}, \quad \text{et cetera.} \quad (3.2.23)$$

Clearly, even for small M this process is tedious, and as M gets larger, the process of constructing the constants becomes too laborious for pen and paper. A simple example will illustrate this dilemma.

Consider the case of Class I with $\beta_y = \frac{1}{3}$. The value of δ associated with this leading order behavior is $\delta = \frac{1}{9}$, and the resonances for this configuration are $r = -1, 0, \frac{1}{3}, 1, 4$. This means that some or all of the expansions (3.2.22a-e) must be modified to accomodate this condition. The most general approach is to rewrite (3.2.22a-e) as

$$x = \pm 2i\tau^{-1} + \sum_{m=1}^{12} C_{1m} \tau^{\frac{m}{3}-1} \quad (3.2.24a)$$

$$y = \alpha_y \tau^{\frac{1}{3}} + \sum_{m=1}^{12} C_{2m} \tau^{\frac{m+1}{3}} \quad (3.2.24b)$$

$$z = 2\tau^{-1} + \sum_{m=1}^{12} C_{3m} \tau^{\frac{m}{3}-1} \quad (3.2.24c)$$

$$p_x = \mp 2i\tau^{-2} + \sum_{m=1}^{12} C_{4m} \tau^{\frac{m}{3}-2} \quad (3.2.24d)$$

$$p_y = \frac{1}{3} \alpha_y \tau^{-\frac{2}{3}} + \sum_{m=1}^{12} C_{5m} \tau^{\frac{m-2}{3}}. \quad (3.2.24e)$$

The analysis of this simple example is lengthy, and it is not possible to find the arbitrary constants at the resonant orders in the expansion, indicating that this leading order behavior does not possess the weak Painlevé property.

In general, the analysis of these classes of leading order behaviors is quite complicated, and there exists no general way of guaranteeing that a particular leading order behavior in classes I or II will possess the weak Painlevé property.

Class III: This class lends itself well to the process of constructing the constants of integration. The system's resonances for this case are $r = -1, 0, 1, 3, 4$. The proper expansions to employ in this situation are

$$x = \alpha_x \tau^{-1} + \sum_{m=1}^4 C_{1m} \tau^{m-1} \quad (3.2.25a)$$

$$y = \alpha_y \tau^{-1} + \sum_{m=1}^4 C_{2m} \tau^{m-1} \quad (3.2.25b)$$

$$z = 2\tau^{-1} + \sum_{m=1}^4 C_{3m} \tau^{m-1} \quad (3.2.25c)$$

$$p_x = -\alpha_x \tau^{-2} + \sum_{m=1}^4 C_{4m} \tau^{m-2} \quad (3.2.25d)$$

$$p_y = -\alpha_y \tau^{-2} + \sum_{m=1}^4 C_{5m} \tau^{m-2}, \quad (3.2.25e)$$

where $\alpha_x = \pm \sqrt{\alpha_y^2 + 4}$.

Substituting these expressions into (3.2.1a-e), and enjoying the aid of the symbolic manipulator *Mathematica*, we find that for $m = 1$, we have

$$C_{41} = 0, \quad C_{51} = 0,$$

$$-i \sqrt{4 + \alpha_y^2} C_{11} - \alpha_y C_{21} = 0$$

$$-(6 + \alpha_y^2) C_{11} + i \alpha_y \sqrt{4 + \alpha_y^2} C_{21} - C_{41} = 0$$

$$i \alpha_y \sqrt{4 + \alpha_y^2} C_{11} + (\alpha_y^2 - 2) C_{21} - C_{51} = 0.$$

Solving for the unknown constants C_{11} , C_{21} , and C_{31} , we find

$$C_{11} = 0, \quad C_{21} = 0, \quad C_{31} \text{ is arbitrary.}$$

Note that $m = 1$ is a resonant order in the expansion, and, as expected, we have found an arbitrary constant associated with this order.

Moving on to $m = 2$, and substituting for the constants C_{i1} , we find

$$\begin{aligned} C_{42} &= C_{12}, & C_{52} &= C_{22}, \\ -i\sqrt{4 + \alpha_y^2} C_{12} - \alpha_y C_{22} + C_{32} - p_{z_0} &= 0 \\ -(6 + \alpha_y^2) C_{12} + i\alpha_y \sqrt{4 + \alpha_y^2} C_{22} + i\sqrt{4 + \alpha_y^2} p_{z_0} &= 0 \\ i\alpha_y \sqrt{4 + \alpha_y^2} C_{12} + (\alpha_y^2 - 2) C_{22} + \alpha_y p_{z_0} &= 0. \end{aligned}$$

Solving this set for the unknown constants C_{12} , C_{22} , and C_{32} , we find

$$\begin{aligned} C_{12} &= \frac{i}{6} p_{z_0} \sqrt{\alpha_y^2 + 4}, \\ C_{22} &= \frac{\alpha_y p_{z_0}}{6}, & C_{32} &= \frac{p_{z_0}}{3}, \end{aligned}$$

thus determining the constants fully, as we would expect, since $m = 2$ is not a resonant order in the expansion.

Continuing further, we substitute the values for the constants C_{i1} and C_{i2} , and at $m = 3$, the equations of motion yield the set of equations

$$\begin{aligned} C_{43} &= 2C_{13}, & C_{53} &= 2C_{23} = 0, \\ -i\sqrt{4 + \alpha_y^2} C_{13} - \alpha_y C_{23} + 2C_{33} - \kappa &= 0 \\ -(6 + \alpha_y^2) C_{13} + i\alpha_y \sqrt{4 + \alpha_y^2} C_{23} + C_{43} + i\sqrt{4 + \alpha_y^2} \kappa &= 0 \\ i\alpha_y \sqrt{4 + \alpha_y^2} C_{13} + (\alpha_y^2 - 2) C_{23} + C_{53} + \alpha_y \kappa &= 0. \end{aligned}$$

Solving the above equations for the unknown constants C_{13} , C_{23} , and C_{33} , we get

$$C_{23} = -\frac{1}{\alpha_y}(i\sqrt{4 + \alpha_y^2}C_{13} + \kappa) \quad C_{33} = 0,$$

and C_{13} is arbitrary, in agreement with the fact that $m = 3$ is a resonant order in the expansion.

Finally, we come to the largest positive resonant order, $m = 4$. Using the values of all of the constants determined previously, we find that the coefficients C_{i4} satisfy the equations

$$\begin{aligned} C_{44} &= 3C_{14}, \quad C_{54} = 3C_{24}, \\ -i\sqrt{4 + \alpha_y^2}C_{14} - \alpha_y C_{24} + 3C_{34} + \frac{p_{z_0}^2}{18} &= 0, \\ -(6 + \alpha_y^2)C_{14} + i\alpha_y\sqrt{4 + \alpha_y^2}C_{24} + 2C_{44} &= 0, \\ i\alpha_y\sqrt{4 + \alpha_y^2}C_{14} - 2C_{24} + \alpha_y^2 C_{24} + 2C_{54} &= 0. \end{aligned}$$

Solving the above set of equations for C_{14} , C_{24} , and C_{34} , we find

$$\begin{aligned} C_{14} &= \frac{\sqrt{4 + \alpha_y^2}i}{\alpha_y}C_{24}, \\ C_{34} &= -\frac{1}{3}\left[4\alpha_y C_{24} + \frac{p_{z_0}^2}{18}\right], \end{aligned}$$

and the coefficient C_{24} is arbitrary, consistent with the fact that $m = 4$ is a resonance in our expansion. Therefore we have satisfied the third step of the ARS algorithm, and Class III constitutes a leading order behavior (and field geometry) for which the system (3.1.5a-e) is integrable in the complex analytic sense of the word, as described in § 2.1. This case is of particular interest, due to the fact that the magnetic field,

and thus the test-particle Hamiltonian is cylindrically symmetric. This means that we know immediately that if we perform a canonical transformation on (3.1.4a-f) to take it to its representation in cylindrical coordinates, both the axial component of the momentum p_ϕ and the Hamiltonian (3.1.3) will be conserved quantities in involution. The results of this chapter tell us that the system is integrable in the complex analytic sense, which provides no guarantee of the existence of the third integral of the motion that we require to declare Class III to be integrable in the Liouville sense. This leads us to the natural question: *Does the third integral to (3.1.4a-f) exist, and if it does, what is it?* This question will be addressed in greater detail in Chapter Five.

§3.3 Yoshida Analysis of (3.1.4a-f)

Upon examination of the neutral-line field model (3.1.4a-f), we find an autonomous Hamiltonian system with three degrees of freedom. Although it is possible to eliminate p_z in favor of a time dependent constant, which was crucial to the successful Painlevé analysis of the model, we now will forgo such a simplification in order to test for the possibility that the system is algebraically integrable using Yoshida singularity analysis.

Recall the simple test-particle model for the reconnection field configuration discussed in § 3.1:

$$\frac{dx}{dt} = p_x \tag{3.3.1a}$$

$$\frac{dy}{dt} = p_y \tag{3.3.1b}$$

$$\frac{dz}{dt} = p_z + \frac{1}{2}(x^2 - \delta y^2), \tag{3.3.1c}$$

$$\frac{dp_x}{dt} = -xp_z + \frac{x(\delta y^2 - x^2)}{2} \quad (3.3.1d)$$

$$\frac{dp_y}{dt} = \delta y p_z - \frac{\delta y(\delta y^2 - x^2)}{2} \quad (3.3.1e)$$

$$\frac{dp_z}{dt} = \kappa. \quad (3.3.1f)$$

In order to carry out the Yoshida Analysis, we must know whether or not the test-particle equations of motion (3.1.4a-f) comprise a homogeneous system. In order to test this proposition, we apply the similarity transformation that was outlined in § 2.4:

$$t' = \sigma^{-1}t, \quad x' = \sigma^{g_1}x, \quad p_x' = \sigma^{g_4}p_x, \quad \text{etcetera.}$$

This transformation will affect the quantity dx/dt as follows:

$$\frac{dx}{dt} \rightarrow \frac{dx'}{dt'} = \sigma^{g_1+1} \frac{dx}{dt}.$$

Applying the above similarity transformation to (3.1.4a-f), we get

$$\sigma^{g_1+1} \frac{dx}{dt} = \sigma^{g_4} p_x \quad (3.3.2a)$$

$$\sigma^{g_2+1} \frac{dy}{dt} = \sigma^{g_5} p_y \quad (3.3.2b)$$

$$\sigma^{g_3+1} \frac{dz}{dt} = \sigma^{g_6} p_z + \frac{1}{2}(\sigma^{2g_1}x^2 - \delta\sigma^{2g_2}y^2), \quad (3.3.2c)$$

$$\sigma^{g_4+1} \frac{dp_x}{dt} = -\sigma^{g_1+g_6} xp_z + \frac{x(\delta\sigma^{2g_2}y^2 - \sigma^{2g_1}x^2)}{2} \quad (3.3.2d)$$

$$\sigma^{g_5+1} \frac{dp_y}{dt} = \delta\sigma^{g_2+g_6} yp_z - \frac{\delta\sigma^{g_2}y(\delta\sigma^{2g_2}y^2 - \sigma^{2g_1}x^2)}{2} \quad (3.3.2e)$$

$$\sigma^{g_6+1} \frac{dp_z}{dt} = \kappa. \quad (3.3.2f)$$

Enforcing the homogeneity condition (i.e. that both sides of an equation are collectively scaled by the same power of the parameter σ) on equations (3.3.2a-b) and (3.3.2f) leads us to the following conclusions:

$$g_4 = g_1 + 1, \quad , g_5 = g_2 + 1, \quad g_6 = -1. \quad (3.3.3)$$

Substituting for these exponents in (3.2.2c-e) gives us

$$\sigma^{g_3+1} \frac{dz}{dt} = \sigma^{-1} p_z + \frac{1}{2}(\sigma^{2g_1} x^2 - \delta \sigma^{2g_2} y^2), \quad (3.3.4a)$$

$$\sigma^{g_1+2} \frac{dp_x}{dt} = -\sigma^{g_1-1} x p_x + \frac{x(\delta \sigma^{2g_2} y^2 - \sigma^{2g_1} x^2)}{2} \quad (3.3.4b)$$

$$\sigma^{g_2+2} \frac{dp_y}{dt} = \delta \sigma^{g_2-1} y p_y - \frac{\delta \sigma^{g_2} y(\delta \sigma^{2g_2} y^2 - \sigma^{2g_1} x^2)}{2}. \quad (3.3.4c)$$

When we enforce the homogeneity condition on (3.3.4a-c), we find the set of conditions that must be satisfied:

$$g_3 + 1 = -1 = 2g_1 = 2g_2 \quad (3.3.5a)$$

$$g_1 + 2 = g_2 - 1 = 3g_1 = 2g_2 + g_1 \quad (3.3.5b)$$

$$g_2 + 2 = g_1 - 1 = 3g_2 = 2g_1 + g_2. \quad (3.3.5c)$$

Solving (3.3.5a) for g_3 , g_1 , and g_2 , gives us $g_3 = -2$, $g_1 = g_2 = -\frac{1}{2}$. These results are in clear contradiction with (3.3.5b,c), and thus the system (3.1.4a-f) is not invariant in form under the similarity transformation described above. This result tells us that Yoshida singularity analysis is not applicable to the system (3.1.4a-f).

§3.4 Summary

In our applications of singularity analysis to the neutral-line field model (3.1.5a-e), we have found two systems that are analytically integrable, as well as a host of other magnetic field configurations that may be partially integrable. The two analytically integrable systems are the cylindrically symmetric O-type neutral line ($\delta = -1$), and neutral sheet ($\delta = 0, \delta \rightarrow \infty$) configuration. The proof that the test-particle equations of motion for the neutral sheet configuration possess the Painlevé property is given in Appendix Two. Below is a listing of classes of configurations that lead to systems possessing the Painlevé property, as well as those that possibly possess the weak Painlevé property are presented below:

X-line Cases:

$$\delta(M, N) = \frac{M(N - M)}{2N^2}, \quad (3.4.1)$$

where M and N are natural numbers, and $M < N/2$.

O-line Cases:

$$\delta(M, N) = -\frac{M(N + M)}{2N^2}, \quad (3.4.2)$$

where M and N are natural numbers, and $M < N$.

Since these values of δ are generated by polynomial functions of rational numbers (i.e. the exponents in the leading order behaviors), and the rational numbers

are a dense set, the δ -spectra given in (3.4.1) and (3.4.2) are also dense sets. In the case of the X-line δ -spectrum, the values are dense in the interval $(0, 1/8)$, while the δ 's associated with the O-line fields are dense in the interval $(-1, 0)$. Invoking the discrete symmetry of (3.1.1a-f) discussed in § 3.1, it is possible to extend these results to values of $\delta \in (-\infty, -1)$ and $\delta \in (8, \infty)$. A summary of these results on the δ -parameter line is presented in Figure 3.4.1.

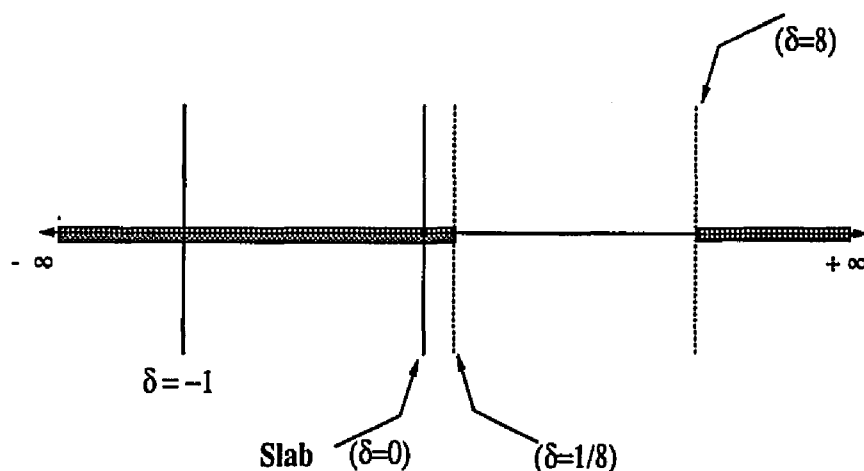


Figure 3.4.1. δ -Distribution of the Painlevé and Weak Painlevé Cases.

Given these results, it is only natural that we proceed to examine the orbits associated with the above system, and compare these special cases with configurations that do not pass the Painlevé property test. This topic will be explored in the next chapter for the cases that may possess the Painlevé property, while a discussion of the cases that do satisfy the Painlevé conjecture will be examined in Chapter Five.

CHAPTER FOUR
TRAJECTORIES, ASYMPTOTIC
BEHAVIOR AND INVARIANTS
PART I: THE WEAK PAINLEVÉ CANDIDATES

§4.1a Agenda for Testing the Singularity Analysis Results

The Painlevé singularity analysis carried out in §3.2 identified two systems that were analytically integrable—the circular O-line magnetic field geometry and the neutral sheet geometry—as well as two dense sets of geometries that passed through the first two steps of the ARS algorithm as weak Painlevé systems. The implementation of the third step of the ARS algorithm for the infinite sets of field geometries proved to be impractical, and thus we turn our attention to the task of testing by numerical means the results of the singularity analysis of the system

$$\dot{x} = p_x \tag{4.1.1a}$$

$$\dot{y} = p_y \tag{4.1.1b}$$

$$\dot{z} = p_z + \frac{1}{2}(x^2 - \delta y^2), \tag{4.1.1c}$$

$$\dot{p}_x = -xp_x + \frac{x(\delta y^2 - x^2)}{2} \tag{4.1.1d}$$

$$\dot{p}_y = \delta y p_z - \frac{\delta y(\delta y^2 - x^2)}{2} \tag{4.1.1e}$$

$$\dot{p}_z = \kappa, \tag{4.1.1f}$$

with a Hamiltonian H given by

$$H(x, y, z, p_x, p_y, p_z) = \frac{p_x^2 + p_y^2}{2} + \frac{1}{2} \left[p_z - \frac{1}{2}(\delta y^2 - x^2) \right]^2 - \kappa z. \tag{4.1.2}$$

This testing will be done via numerical experiments—that is, constructing the system's trajectories numerically for various values of the parameter δ , using initial conditions and field strengths that are similar, and then studying the resultant trajectories to answer the following questions:

Question I: Do the X-type neutral line and elliptical O-type neutral line geometries that satisfy (3.4.1) and (3.4.2) have trajectories that are more regular, or at least qualitatively different from trajectories associated with neighboring geometries that do not satisfy these conditions?

Question II: What are the properties of the dynamical systems associated with field geometries that yielded equations of motion possessing the Painlevé property? Do these systems possess closed-form solutions? Do they possess integrals in involution, thus making them integrable in the standard Hamiltonian sense?

The answers to Question I are presented in §4.2 and §4.3, where we discuss the properties of the motion of test particles in elliptical O-point and X-point magnetic fields. Chapter Five addresses the issues raised in Question II; §5.2 is an examination of the dynamics associated with the neutral sheet geometry, and §5.3 answers this question for the cylindrically symmetric field geometry.

§4.1b Plan of the Numerical Experiments

As we saw in §1.4, the process of charged particle acceleration during reconnection for X-type neutral line fields can be viewed in terms of a scattering problem in which charged particles scatter off of the *unmagnetized region*, where the test particle's magnetic moment μ is no longer an adiabatic invariant. In the case of elliptical O-type neutral line magnetic fields, the interesting behavior is related to the strong focussing of particles towards the neutral line and their subsequent acceleration.

We wish to examine the trajectories associated with the system (4.1.1a-f) under conditions that lead to reconnection—the X-line cases—or to strong focusing of the test particle towards the neutral line—the O-line cases. For both of these situations, we wish to have $\epsilon > 0$, which will produce $\mathbf{E} \times \mathbf{B}$ drifts of the types shown in Figure 1.1.4. For the X-line systems, this means that we will start our test particles in regions I or III in Figure 1.1.4, and the particles will drift in towards the neutral region, become demagnetized, scatter off of the unmagnetized region, and then drift away from the neutral line in either of the regions labelled II or IV.

The initial conditions for such numerical experiments are set by placing a test particle's guiding center at some coordinate $s_{0_{\theta c}}$ on a magnetic field line, which is a contour of constant flux function $\Psi(x, y) = (\delta y^2 - x^2)/2$. Identify this field line by the value $\Psi = \Psi_0$. We also will start our test particle in a region in which the magnetic moment μ is a good adiabatic invariant. We will also fix the particle's Hamiltonian (4.1.2) at a constant value H . Once we have determined the quantities H , Ψ_0 , $s_{0_{\theta c}}$, and μ , we can calculate the actual position of the particle in terms of its

coordinates (x, y, z) as functions of the quantities Ψ_0 and $s_{0,gc}$. This process involves wrapping our set of initial conditions around the field line in a helical fashion, with the radius of the helix being the test particle's gyroradius ρ_g , and the angle variable about the field line being the gyrophase angle ϕ , as shown in Figure 4.1.1.

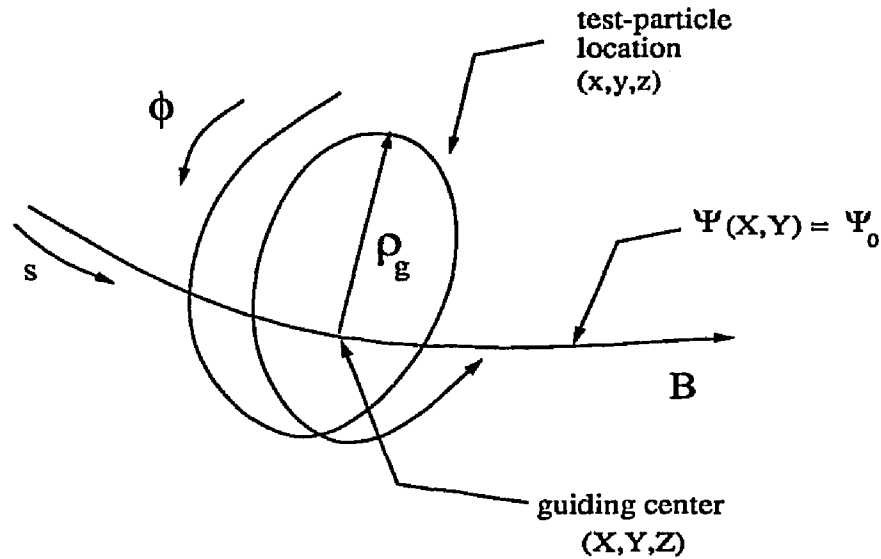


Figure 4.1.1. Initializing the Test Particle.

The momenta can be calculated through the knowledge of H and μ , which allow us to construct the parallel and perpendicular velocities

$$v_{\perp} = \sqrt{2\mu B} \quad (4.1.3a)$$

$$v_{\parallel} = \pm \sqrt{2(H - \mu B)}, \quad (4.1.3b)$$

where B is the local magnetic field strength.

Given the value of v_{\perp} , it is possible to compute the particle's gyroradius ρ_g by

(1.2.5d)

$$\rho_g = \frac{v_{\perp}}{B(x, y, z)}, \quad (4.1.4)$$

since we have $\Omega(x, y, z) = B(x, y, z)$ in our dimensionless variables. Now we choose the particle's gyrophase ϕ , which completely specifies the initial conditions for our test particle. Let X , Y , and Z be the coordinates of the particle's guiding center

$$X = X(s_{0_{gc}}, \Psi_0), \quad Y = Y(s_{0_{gc}}, \Psi_0), \quad Z = Z_0, \quad (4.1.5)$$

where Z_0 is a constant; for our numerical experiments, we shall take $Z_0 = 0$, unless stated otherwise. The particle's actual position (x, y, z) is given by

$$x = X(s_{0_{gc}}, \Psi_0) - \frac{B_y}{B_p} \rho_g \cos \phi - Z_0 \frac{B_z B_x}{B B_p} \rho_g \sin \phi \quad (4.1.6a)$$

$$y = Y(s_{0_{gc}}, \Psi_0) + \frac{B_x}{B_p} \rho_g \cos \phi - Z_0 \frac{B_z B_y}{B B_p} \rho_g \sin \phi \quad (4.1.6b)$$

$$z = Z_0 + \rho_g \sin \phi \frac{B_p}{B} \quad (4.1.6c)$$

where B_x , B_y , and B_z are the x , y , and z components of the magnetic field, respectively, B is the total magnetic field strength, and B_p is the magnitude of the magnetic field in the x - y plane, which is also called the *poloidal field strength*. The next step is to determine the x , y , and z components of the test particle's initial velocity. Again, we can construct these quantities from the parameters μ , H , the sign of v_{\parallel} , and the particle's gyrophase ϕ . This leads to

$$v_x = -v_{\parallel} \frac{B_x}{B_p} - \frac{B_z B_x}{B B_p} v_{\perp} \sin \phi - \frac{B_y}{B_p} v_{\perp} \cos \phi \quad (4.1.7a)$$

$$v_y = -v_{\parallel} \frac{B_y}{B_p} - \frac{B_z B_y}{B B_p} v_{\perp} \sin \phi + \frac{B_x}{B_p} v_{\perp} \cos \phi \quad (4.1.7b)$$

$$v_z = v_{\parallel} \frac{B_z}{B} + v_{\perp} \sin \phi \frac{B_p}{B} \quad (4.1.7c)$$

Finally, it is easy to obtain the particle's canonical momenta (p_x, p_y, p_z) from its velocities by adding the respective components of the magnetic vector potential **A**:

$$p_x = v_x + A_x(X, Y, Z), \quad p_y = v_y + A_y(X, Y, Z), \quad p_z = v_z + A_z(X, Y, Z).$$

It should be noted that the test particle was initialized assuming that the electric and magnetic field strengths were those evaluated at the particle's guiding center (X, Y, Z) . Once the particle's *actual* initial position is calculated using (4.1.6a-c), (4.1.7a-c) and (4.1.8), it will have slightly different values for these quantities than those originally supplied. These perturbed values will, in turn, affect the value of the Hamiltonian. The net change in E , B , μ and H will all be $\mathcal{O}(\rho_g)$, and as long as the test particle is initially magnetized, these differences between the guiding-center and actual-location initial conditions will be small. For this reason, all references to initial conditions in this chapter will refer to guiding-center initial conditions, unless otherwise specified.

§4.1c Simulations of Ensembles of Test Particles

The construction of single-particle trajectories, though illustrative, will be found inadequate for determining whether or not the system is chaotic in the sense that it displays a sensitivity to initial conditions. In order to examine this issue, we must integrate a large ensemble of test particles that have neighboring initial conditions and then calculate the kinetic energy of the particles in the ensemble after they have satisfied some suitable exit condition, which will be discussed shortly.

The integration schemes we employ are second-order momentum-implicit symplectic integration algorithms, which are derived and discussed in detail in Appendix Four. The advantage of using a symplectic scheme lies in the fact that the integration scheme is generated from the system's Hamiltonian, and thus will possess the same symmetries as H . It is generally considered that symplectic integration

schemes will preserve the topology of the phase space much better than standard numerical schemes, and symplectic schemes will often preserve the system's integrals to machine precision, a consequence of the algorithm having the same symmetries as the Hamiltonian. For the numerical experiments discussed in this Chapter, we use a timestep $\Delta t = 0.01$, and the relative error in the Hamiltonian, ϵ_H is of the order 10^{-4} after 150000 timesteps,

The type of diagnostic tool and exit condition may be one of two varieties:

Experiment No. 1: For X-type neutral lines, we can use the fact that the reconnection event is analogous to scattering, and test the system for chaotic scattering. This type of numerical experiment entails evolving the members of the ensemble until the individual particles cross an outgoing flux surface. This is the approach used by Moses, Finn, and Ling [21], and involves starting the particles in the vicinity of a magnetic field line identified by $\Psi(x, y) = \Psi_0$, and then integrating the test particle equations of motion until each particle passes through an outgoing flux surface, which is identified by $\Psi(x, y) = -\Psi_0$. Once the test particle has passed through this flux surface, the $\mathbf{E} \times \mathbf{B}$ drift will carry the test particle away from the unmagnetized region, and hence away from the region in which the particle experiences sudden acceleration along the neutral line. Upon crossing this “finish line,” we can employ one of two diagnostics to determine whether or not the system exhibits sensitivity to initial conditions:

Diagnostic A: Measure the test particle's kinetic energy as it crosses the outgoing flux surface. If the system is displaying sensitivity to initial conditions in

the form of chaotic scattering, then we should see this in a plot of test particle kinetic energy versus guiding-center position on the initial flux surface. This sensitivity should be visible on all length scales chosen along the initial conditions surface, such as the example presented in Figure 1.4.3, which is a plot of the final kinetic energy for test particles versus their initial guiding-center value of y .

Diagnostic B: Measure the amount of time t_d a test particle takes to reach the outgoing flux surface. This quantity is called the *time delay*, and will exhibit the same sort of structure as the kinetic energy curve used in Diagnostic A.

Experiment No. 2: For geometries that involve focusing of the test particles into the neutral line, such as the circular and elliptical field line geometries, or into a neutral plane, which is the case for the slab geometry, the flux function $\Psi(x, y)$ is negative everywhere in the x - y plane, and the exit condition used in Experiment No. 1 is not applicable. An alternative exit condition is integrating all of the particles for some long period of time T , where $T > \Psi_0/\epsilon$, and then measure the kinetic energy of each particle in the ensemble at $t = T$, plotting this quantity versus the particle's guiding-center position on the initial flux surface.

The initialization of an ensemble of test particles is accomplished using the same scheme as that outlined above. We wrap our initial conditions around a field line, changing the gyrophase ϕ as we step through the coordinate s_{gc_0} so that two neighboring test particles have coordinates given by

$$s_{gc_0}^{(n+1)} = s_{gc_0}^{(n)} + ds$$

$$\phi^{(n+1)} = \phi^{(n)} + \lambda ds,$$

where λ is a constant, and determines how tightly the initial conditions are wound around the field line.

§4.2 Properties of Trajectories in X-Line Configurations

The results of the Painlevé analysis done in §3.2 suggest that the dynamics associated with certain types of X-line fields may be partially integrable, or at least perhaps qualitatively different from that of their neighboring geometries. In particular, recall from (3.4.1) that the set of values of the magnetic field geometry parameter δ that yielded systems that passed through the first two stages of the ARS algorithm as "weak Painlevé" cases were given by the following rule

$$\delta(M, N) = \frac{M(N - M)}{2N^2}, \quad (4.2.1)$$

where M and N are natural numbers, and $M < N/2$. This gave us a dense set of values of δ on the interval $(0, 1/8)$. We also found, that we had an equivalent set of values of δ on the interval $(8, \infty)$, which were given by the inverses of the values stated in (4.2.1). The leading order behavior exponents for the coordinates (x, y, z) in such systems were given by

$$\beta_x = \beta_z = -1, \quad \beta_y = \frac{M}{N},$$

where M and N were natural numbers with $0 < M < \frac{N}{2}$, placing the values of β_y on the interval $(0, \frac{1}{2})$. Due to the increasing level of complexity involved in implementing the third step of the Painlevé analysis for such systems, we found it to be impractical to test for the weak Painlevé property systems associated with values

of $N \geq 4$, and thus are forced to rely on numerical means to determine whether or not there is anything special about the dynamics stemming from systems that have δ given by (4.2.1), as opposed to neighboring systems related to nearby values of δ that do not satisfy (4.2.1)

A logical place to begin this analysis is to examine trajectories related to values near $\delta = 1/8$. If the Painlevé analysis is indicating a change in behavior for the system, this value of δ is an effective separatrix in parameter space for the system, and we should see some qualitative difference in the system's trajectories as we vary δ in this neighborhood. To this end, we shall examine trajectories for three values of δ in the neighborhood of $\delta = 1/8$, while fixing the electric field strength at the value of κ to be 3.13×10^{-4} . The test particle was initialized by placing its guiding center on a flux surface of fixed value $\Psi_0 = -0.24$, and was given an initial magnetic moment of $\mu = 5.0 \times 10^{-3}$. The particle's initial momenta were set by calculating the perpendicular and parallel momenta as outlined in §4.1. We then employed our code XOSsim (whose listing can be found in Appendix Five) to evolve the particle, using a second order symplectic integration scheme such as the one outlined in §A4.3, and integrated equations (3.1.1a-f) for a period of time sufficient for the particle to scatter off of the unmagnetized region, and proceed away from the neutral line, which is of order $2\Psi_0/\epsilon$, as shown in § 1.4.

Test I $\delta = \frac{1}{8}$: Recall from (3.2.7) that this value of δ is linked to a leading order behavior exponent in y of $\beta_y = 1/2$, which was found to lead to a failure of the resonance test for the ARS algorithm, implying that the system (4.1.1a-f) does

not possess the weak Painlevé property. Setting $\delta = 1/8$, and fixing the values of μ , κ , and Ψ_0 at the values stated above, we integrated the system numerically. Figure 4.2.1 shows an x - y trajectory for this case, and an x - z trajectory is shown in Figure 4.2.2. In these figures, the test particle starts at $x \approx 0.6$, $y \approx 0.8$, and $z \approx 0$.

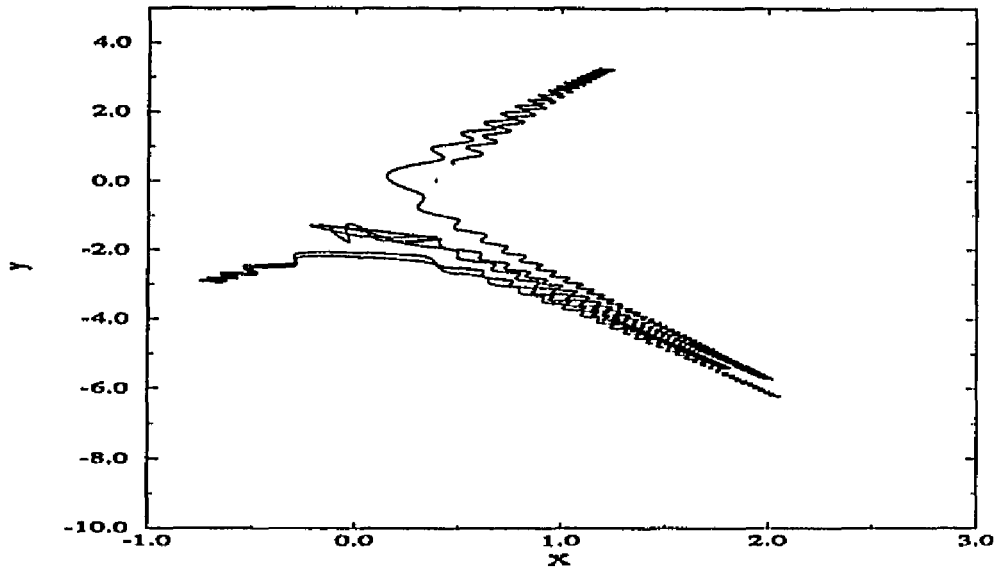


Figure 4.2.1. x - y Trajectory ($\delta = \frac{1}{8}$).

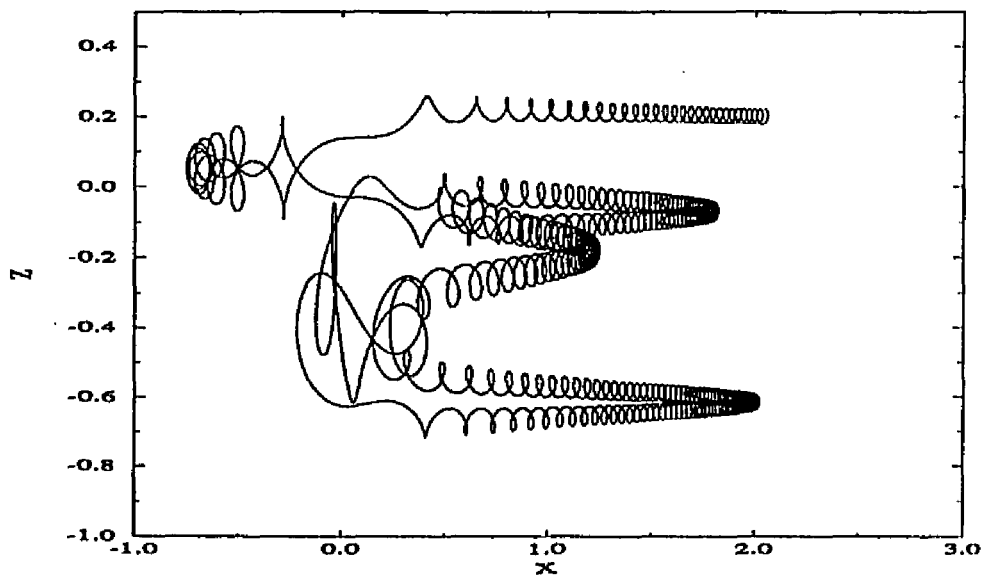


Figure 4.2.2. x - z Trajectory ($\delta = \frac{1}{8}$).

The phase space trajectories for the x and y motion have a similar structure, so we will concentrate on the x -motion, which is shown in Figure 4.2.3. The dark section at the right of this plot is simply the oscillation in x as the particle drifts in towards the unmagnetized region. As the particle enters the unmagnetized region, its motion becomes erratic, and then settles into a widened oscillation in x , as the test particle drifts away from the neutral line along the $-y$ direction.

The phase space motion for z is fairly simple, and is illustrated in Figure 4.2.4. Note the sudden jumps in z , which can be seen in both Figure 4.2.4 and Figure 4.2.2. These sudden increases in z occur when the particle becomes demagnetized and is accelerated by the electric field in the positive z -direction.

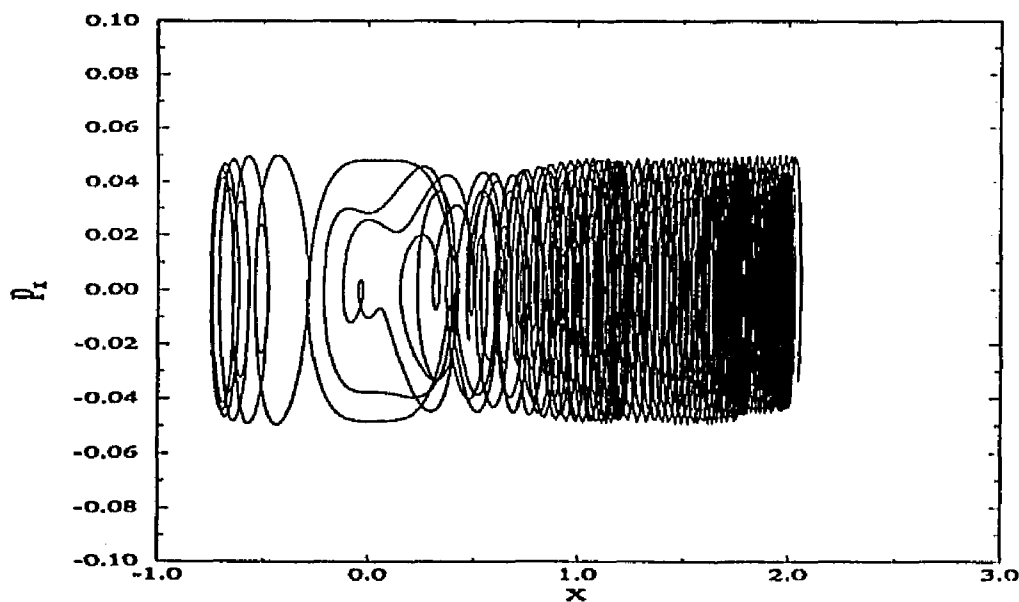


Figure 4.2.3. x -Phase Space Trajectory Trajectory ($\delta = \frac{1}{8}$).

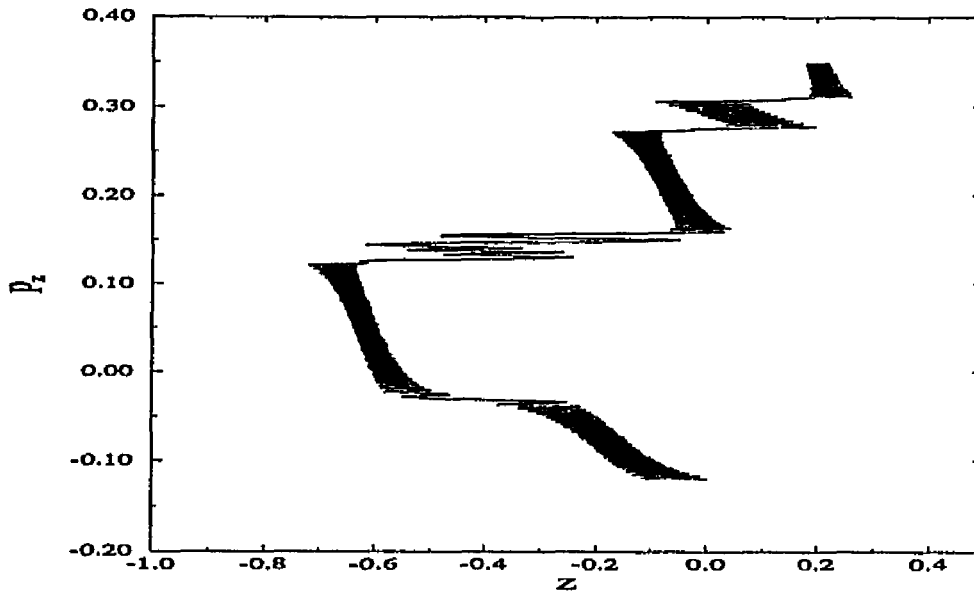


Figure 4.2.4. z -Phase Space Trajectory Trajectory ($\delta = \frac{1}{8}$).

The test particle began its journey in a domain in the phase space for which the particle is magnetized. As the particle is carried in towards the unmagnetized region by the $\mathbf{E} \times \mathbf{B}$ drift, it becomes unmagnetized, and this behavior can be seen by inspection of Figures 4.2.5a, which shows the time behavior of the magnetic moment μ . In the region between $t = 0$ and $t \approx 250$, the particle is magnetized and spirals about a field line, and the magnetic moment is conserved fairly well. In the neighborhood of $t \approx 250$, the test particle momentarily becomes demagnetized, and switches to oscillating about a different field line, and the value of μ oscillates about a different fixed value. At $t \approx 800$, the test particle becomes unmagnetized, and the invariance of μ breaks down until the particle becomes remagnetized at $t \approx 900$.

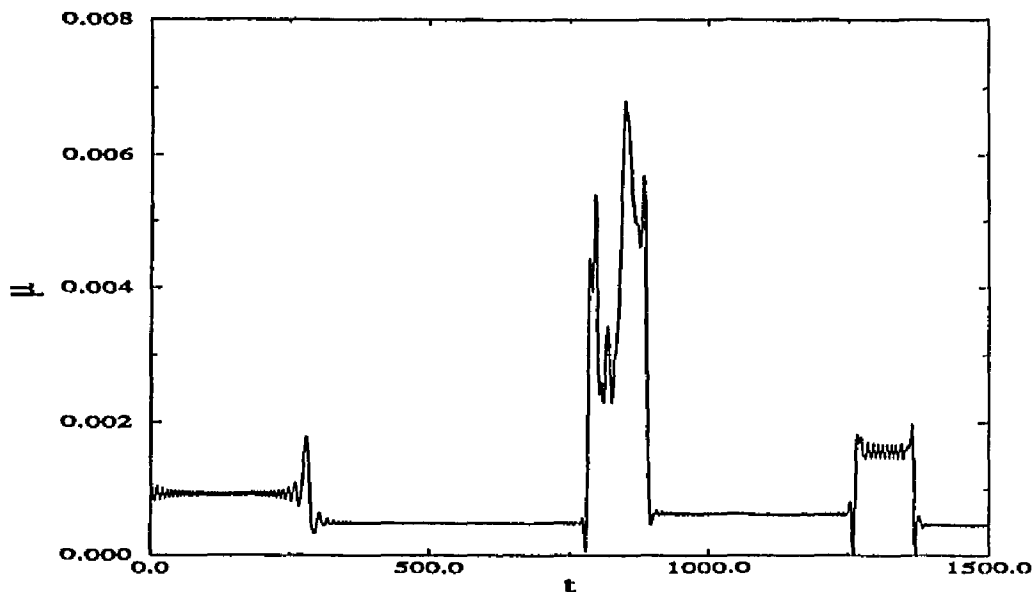


Figure 4.2.5. The Magnetic Moment μ vs. Time ($\delta = 1/8$).

The field configuration given by $\delta = 1/8, \kappa = 3.13 \times 10^{-4}$ yields the sensitivity to initial conditions seen in a system exhibiting chaotic scattering. Figure 4.2.6a shows the exit kinetic energy spectrum for an ensemble of 1000 particles, all initialized with the values of H, μ and stated above, but with $\Psi_0 = -0.48$. Figure 4.2.6b shows the exit kinetic energy spectrum for an ensemble of 1000 particles whose initial conditions lie on a small subset of the flux line used to generate Figure 4.2.6a. Further magnifications in this fashion show that the system is exhibiting a clear sensitivity to initial conditions.

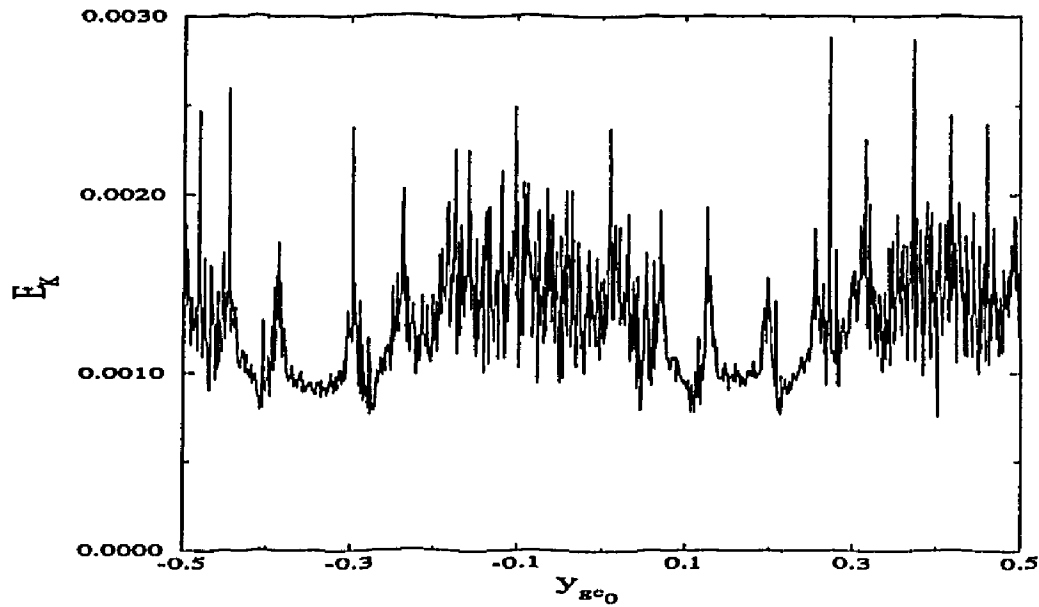


Figure 4.2.6a. Exit Kinetic Energy vs. Initial Position. ($\delta = 1/8$).

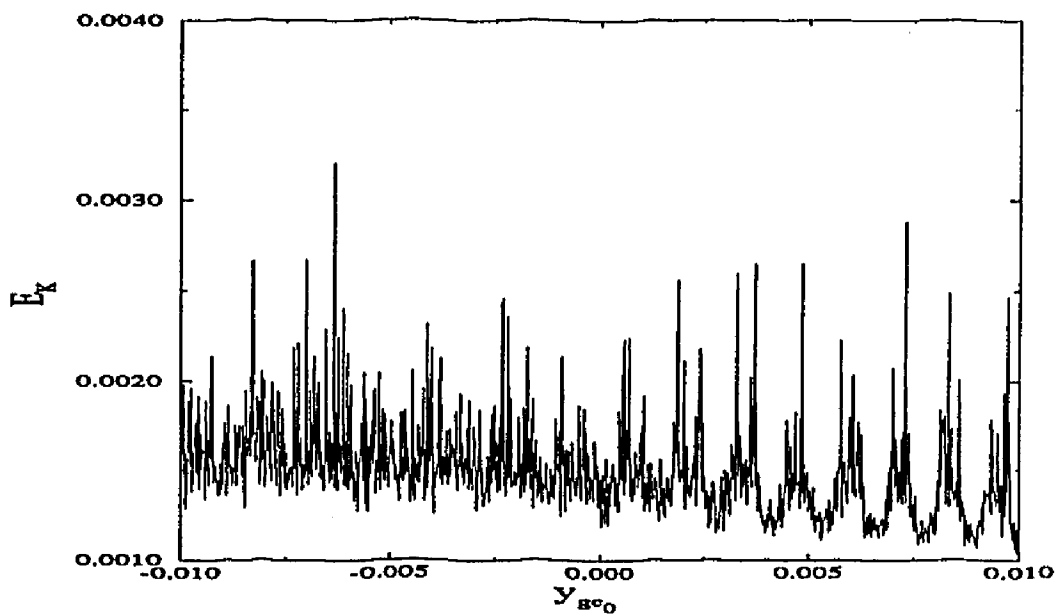


Figure 4.2.6b. Detail of Figure 4.2.6a.

Test II $\delta = \frac{15}{128}$: This value of δ satisfies (4.2.1), and is only $\frac{1}{128}$ less than our previous value of δ . The leading order behavior associated with the y -motion for

this case is $\beta = 3/8$, which allows the system to pass through step II of the ARS test, but the denominator for β_y is sufficiently large that it is well outside of the range of values of β for which we could carry out step III of the ARS algorithm for the system. Do we see any qualitative difference between the trajectories associated with this configuration and those for test I? If this particular value of δ is special, we should see some difference in the trajectories for the system. Once again, we present results for a fixed electric field strength $\kappa = 3.13 \times 10^{-4}$, and we hold μ fixed at 5×10^{-4} , and the initial flux surface corresponds to $\Psi_0 = -0.48$. Numerical integration of the system shows little difference in the system's phase space behavior, and no qualitative difference appears in the outgoing kinetic energy spectrum for a distribution of particles initialized about a single field line, as can be seen in Figure 4.2.7

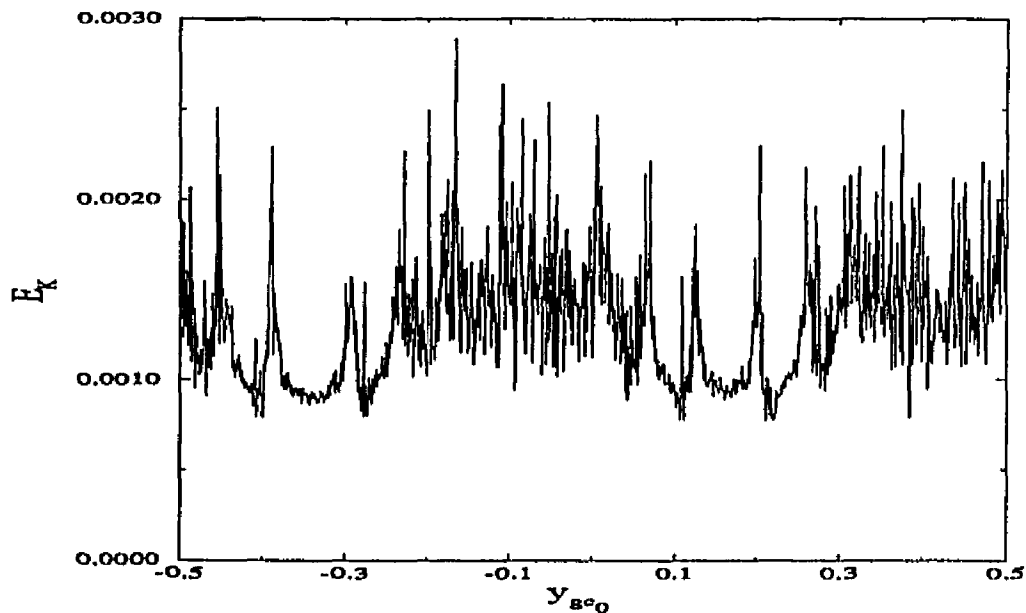


Figure 4.2.7. Exit Kinetic Energy vs. Initial Position. ($\delta = 15/128$).

Test III $\delta = \frac{17}{128}$: This value of δ does not satisfy (4.2.1), and yet is only

$\frac{1}{128}$ larger than our border value of $\delta = 1/8$. Recalling (3.2.7), we find that the leading-order behavior exponent for the y -motion is $\beta_y = (4 \pm i)/8$, meaning that the system for this value of δ will possess a transcendental branch point. The trajectories associated with this field configuration are also similar in structure to those associated with $\delta = 1/8$. The results of the numerical experiment conducted in the same fashion as it was in the previous two tests shows the same type of exit kinetic energy spectrum, complete with sensitivity to initial conditions (Figure 4.2.8).

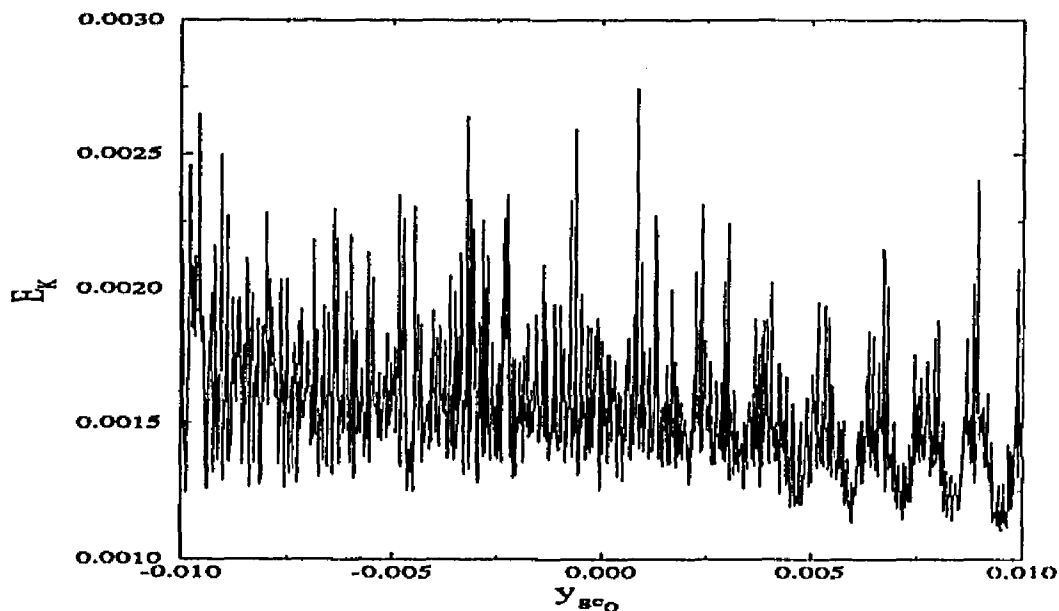


Figure 4.2.8. Exit Kinetic Energy vs. Initial Position. ($\delta = 17/128$).

Given the evidence presented in Figures 4.2.6-8, it seems that variations of the parameter δ about $\delta = 1/8$, shows no abrupt change in the character of the dynamics of the system. All of the above cases display a strong sensitivity to initial conditions. This is no serious indictment, however, of the Painlevé conjecture,

since we were comparing systems that might or might not *possibly* possess the weak Painlevé property, which is itself a weak indicator of possible integrability. In the region of the parameter space near $\delta = 1/8$, the condition (4.2.1) is not identifying any special dynamical systems.

The other interesting region of the δ -parameter space for X-lines to investigate is the limit that $\delta \rightarrow 0$. In this limit, we will find that as we decrease the value of δ , the motion of a charged particle becomes more regular as δ is decreased. This behavior is generic, and is true for all values of δ in this limit, regardless of whether or not δ satisfies (4.2.1). Given this insensitivity to the condition outlined in (4.2.1), we will examine trajectories for one value of δ that does satisfy (4.2.1), while performing chaotic scattering tests on values of δ in this region that do satisfy (4.2.1), as well as those that do not satisfy (4.2.1).

We begin with $\delta = 4.95 \times 10^{-3}$. This value of δ is associated with a value of $\beta_y = 1/100$. The trajectory plots presented in Figures 4.2.17-23 were generated from a set of initial conditions of $\mu = 5.0 \times 10^{-4}$, $\Psi_0 = 0.24$, $H = 10^{-3}$. The electric field strength was $\kappa = 3.13 \times 10^{-4}$. The motion, while complicated, is certainly less violent than the particle motion presented earlier in this section.

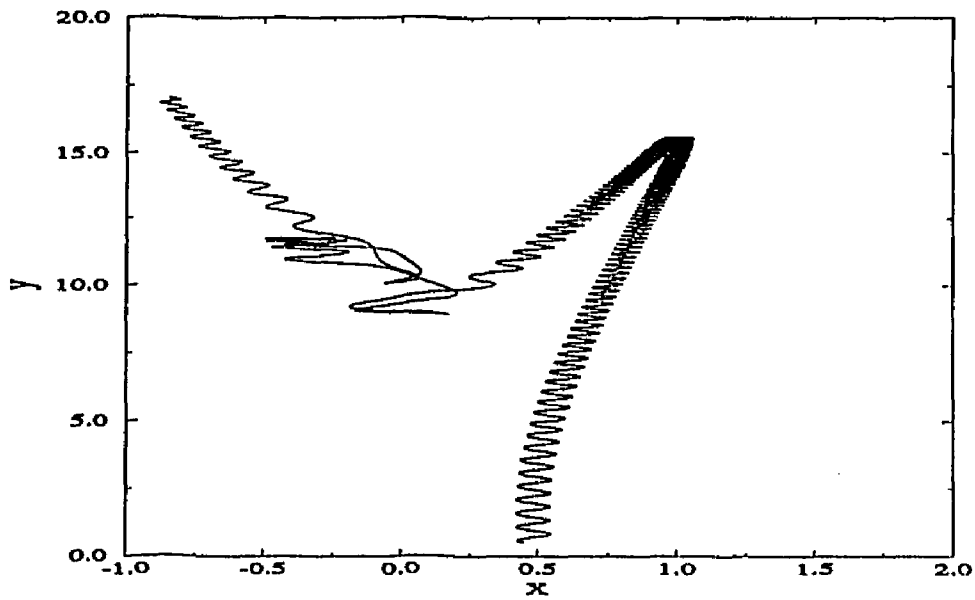


Figure 4.2.9. x - y Trajectory ($\delta = 4.95 \times 10^{-3}$).

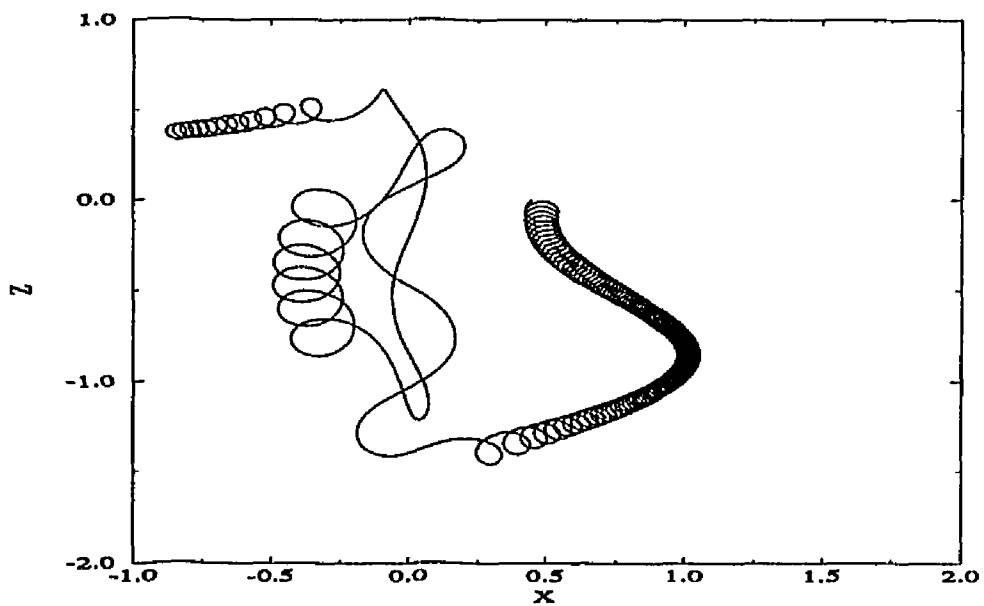


Figure 4.2.10. x - z Trajectory ($\delta = 4.95 \times 10^{-3}$).

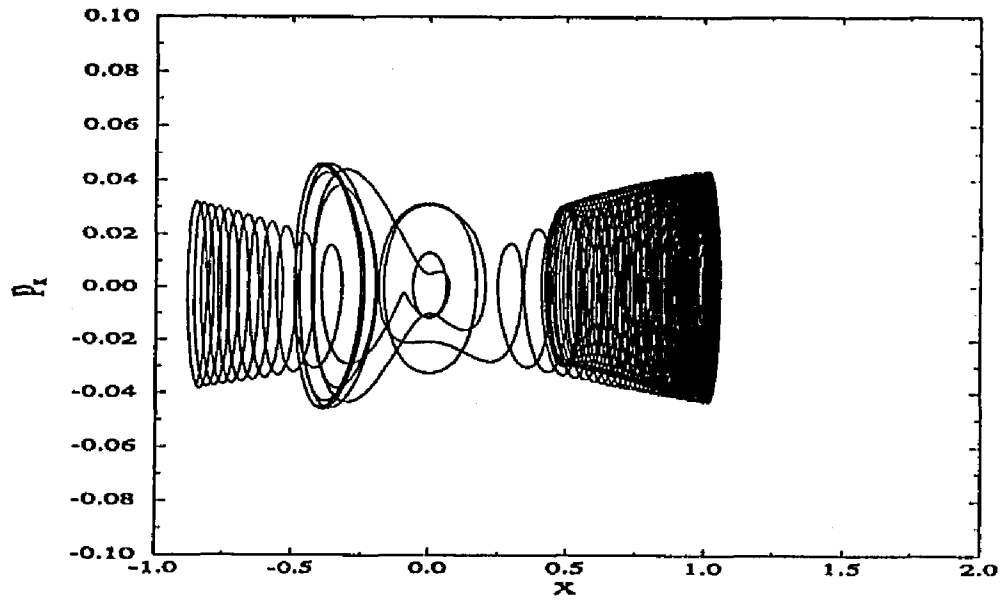


Figure 4.2.11. x -Phase Space Trajectory Trajectory ($\delta = 4.95 \times 10^{-3}$).

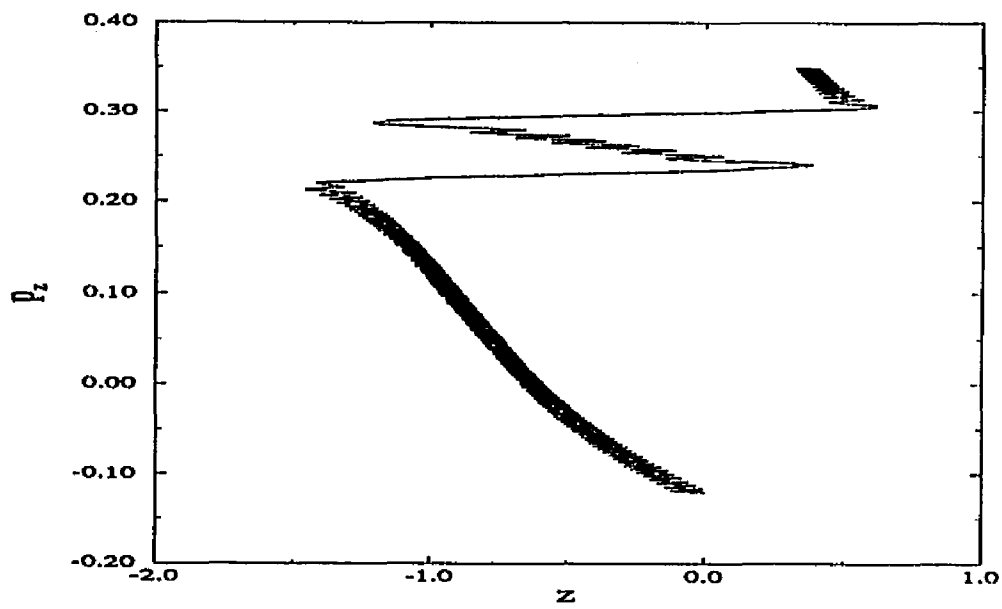


Figure 4.2.12. z -Phase Space Trajectory Trajectory ($\delta = 4.95 \times 10^{-3}$).

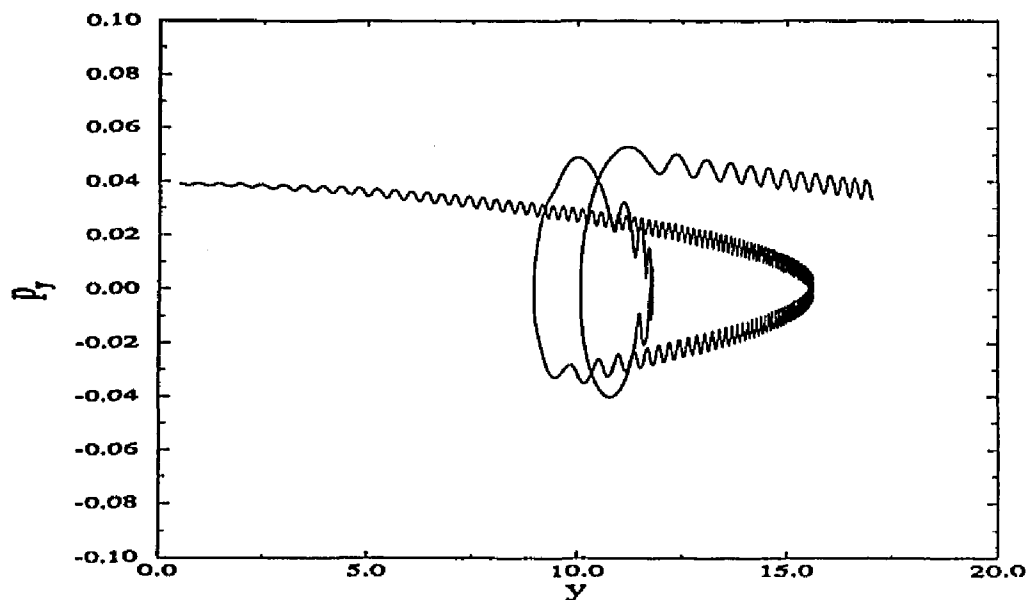


Figure 4.2.13. y -Phase Space Trajectory Trajectory ($\delta = 4.95 \times 10^{-3}$).

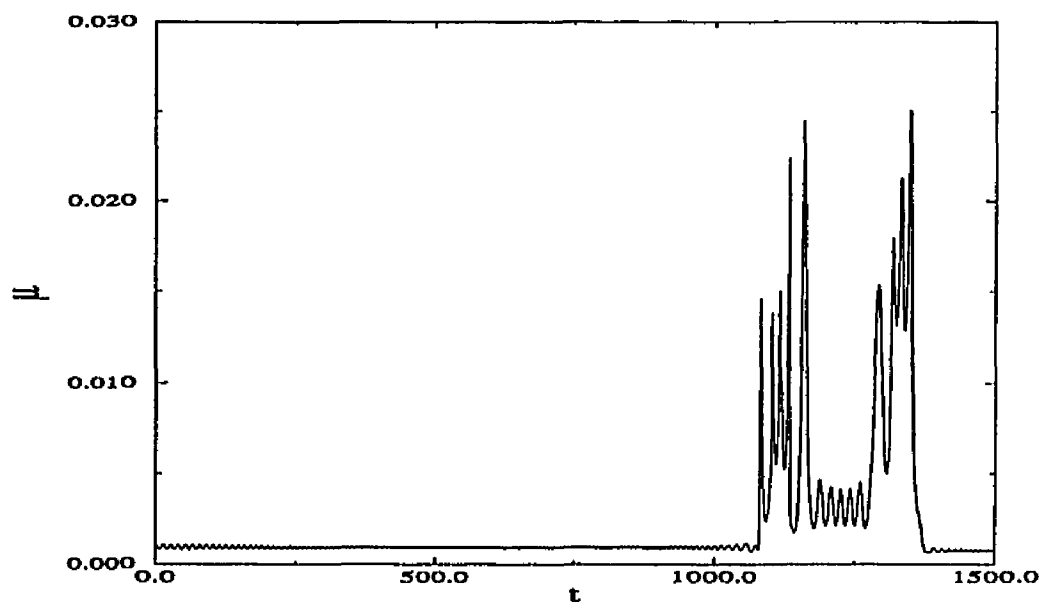


Figure 4.2.14. The Magnetic Moment μ vs. t ($\delta = 4.95 \times 10^{-3}$).

The chaotic scattering test results for $\delta = 4.95 \times 10^{-3}$ can be found in Figures 4.2.15a,b. Note that the structure of this graph is much less complicated than Figures 4.2.6-8, indicating a decreased sensitivity to initial conditions.

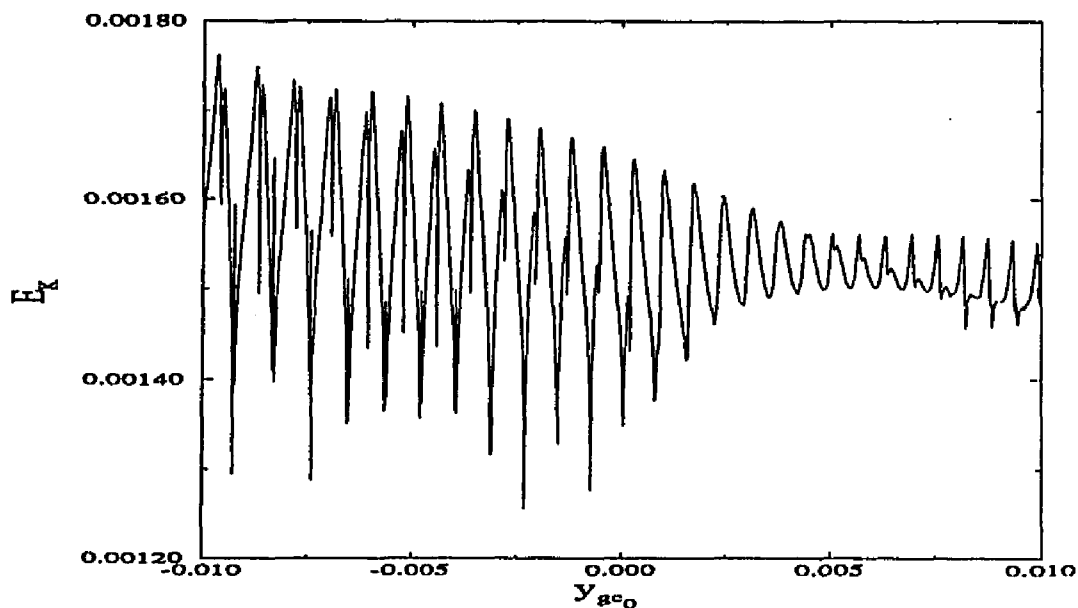


Figure 4.2.15a. Exit Kinetic Energy vs. y_{gc_0} ($\delta = 4.95 \times 10^{-3}$).

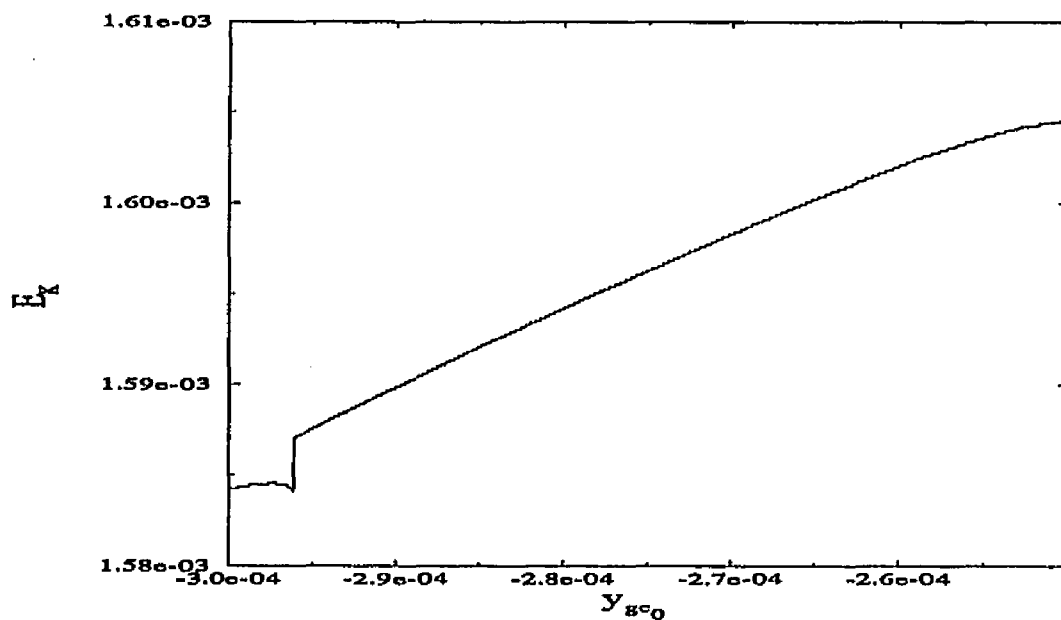


Figure 4.2.15b. Detail of Figure 4.2.15a.

Now let us choose a neighboring value of δ that does not satisfy (4.2.1) $\delta = 5.0 \times 10^{-3}$. Setting the initial flux Ψ_0 , μ , and H to the values used above, and performing the same numerical experiment, we arrive at Figure 4.2.16. Again,

we see very little sensitivity to initial conditions, and little qualitative difference between this graph and Figures 4.2.15a,b.

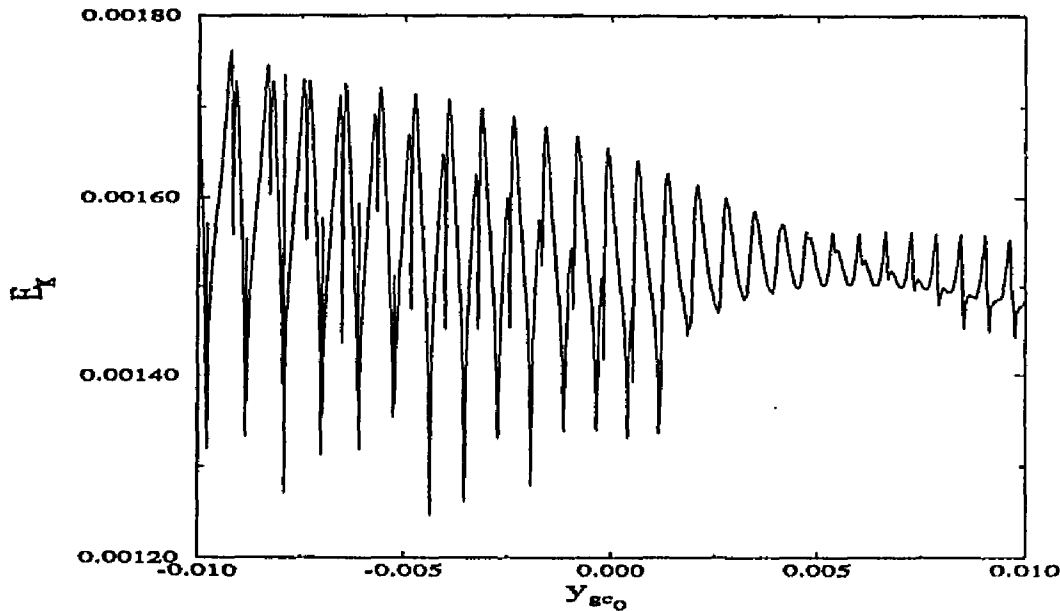


Figure 4.2.16. Exit Kinetic Energy vs. y_{gc_0} ($\delta = 5.0 \times 10^{-3}$).

Now we shall reduce δ even further to the value $\delta = 4.995 \times 10^{-4}$. Recalling (3.2.7), this value of δ corresponds to $\beta_y = 1/1000$. Again, we adopt the initial conditions $\Psi_0 = -0.24$, $H = 10^{-3}$, and $\mu = 5 \times 10^{-4}$. We also set $\kappa = 3.13 \times 10^{-4}$, and evolve the system forward over the reconnection time scale $2\Psi_0/\epsilon$. The resultant trajectories are yet more regular than the previous set shown in Figures 4.2.9-14. In particular, the phase space portrait of the y -motion indicates that p_y starts out as a quantity executing small oscillations about a slowly changing value, a condition which decays rapidly when the particle becomes demagnetized. The particle then becomes remagnetized, and p_y begins to oscillate about a different, slowly changing value.

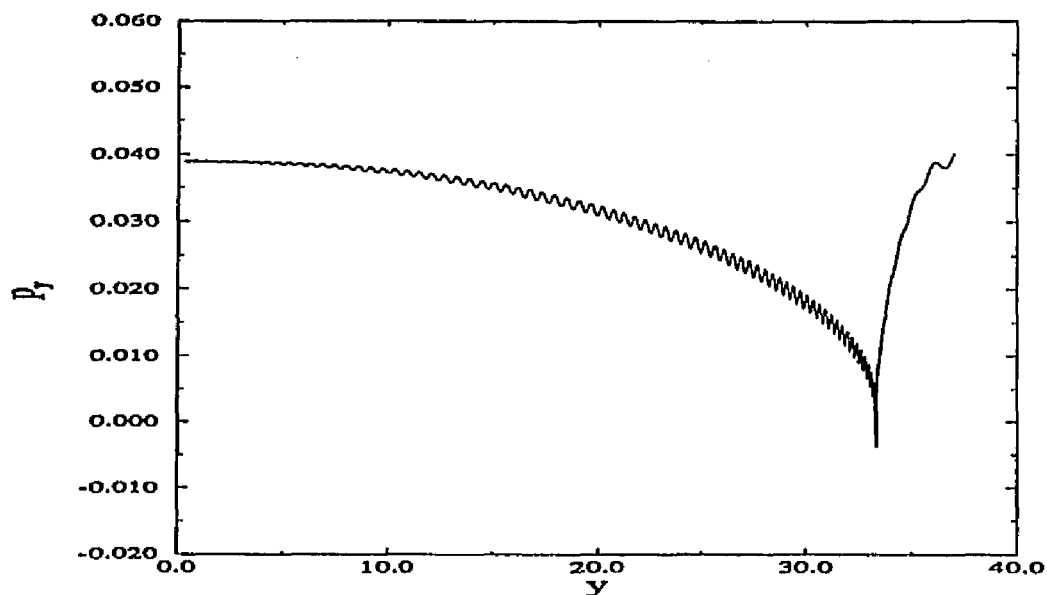


Figure 4.2.17. y -Phase Space Trajectory Trajectory ($\delta = 4.995 \times 10^{-4}$).

If we examine this configuration using the same chaotic scattering test used to generate Figures 4.2.15-16, we find that once again do not have extreme sensitivity to initial conditions.

Note that this increasingly regular behavior is simply a consequence of the fact that as $\delta \rightarrow 0$, the field geometry is approaching that of the slab configuration, which was shown in Appendix Two to possess the Painlevé property.

As mentioned in § 1.4, particles that pass through the vicinity of the null will experience sudden acceleration. This process can be seen clearly by examining the kinetic energy as a function of time. Figure 4.2.18 illustrates this effect for a member of the ensemble used to generate Figure 4.2.8 ($\delta = 17/128$), while Figure 4.2.19 is the kinetic energy time sequence for a test particle with $\delta = 4.95 \times 10^{-3}$. The downward trends in the kinetic energy that occur in these graphs are the result of

the ∇B drift and the curvature drift. Recalling (1.2.15) and (1.2.16), we have

$$\mathbf{v}_{\nabla B} \sim \frac{\mu}{qB^2}(\delta^3 y^2 - x^2)\hat{\mathbf{z}}$$

and

$$\mathbf{v}_C \sim \frac{\delta(H - \mu B)}{qB^4}(\delta y^2 - x^2)\hat{\mathbf{z}} = \frac{\delta(H - \mu B)}{qB^4}\Psi(x, y).$$

When $\Psi < 0$ and $0 < \delta < 1$, both of the above drift motions will carry the test particle into regions of higher electric potential, thus lowering the test particle's kinetic energy.

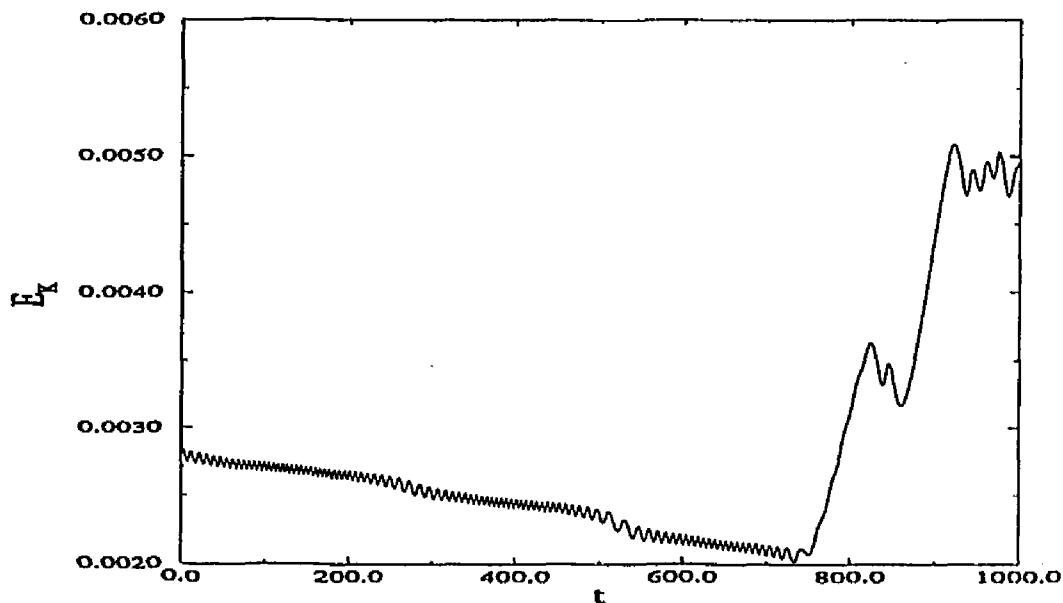


Figure 4.2.18. Test Particle Kinetic Energy vs. Time ($\delta = \frac{17}{128}$).

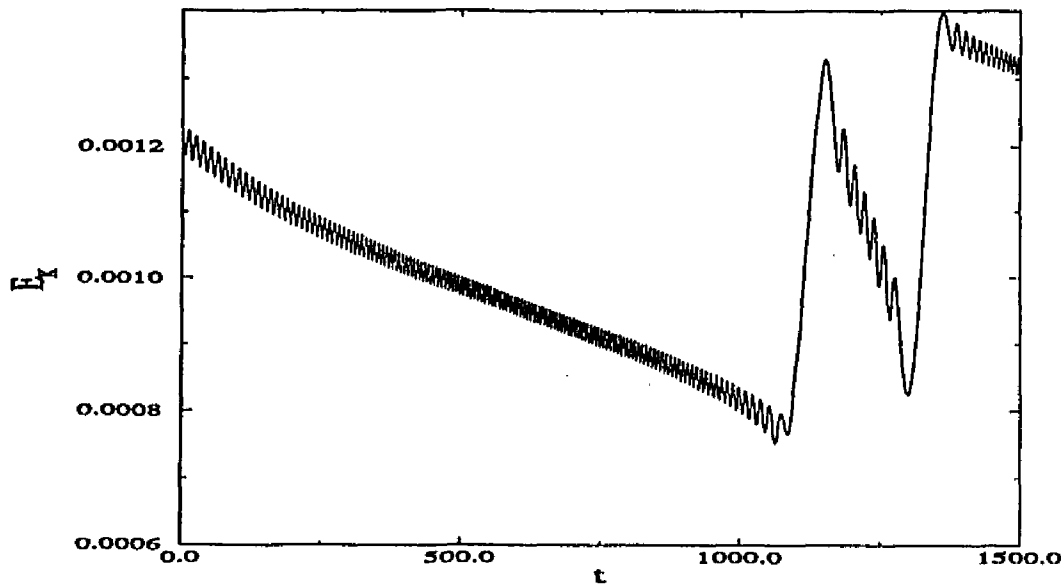


Figure 4.2.19. Test Particle Kinetic Energy vs. Time ($\delta = 4.95 \times 10^{-3}$).

§4.3 Properties of Trajectories in Elliptical O-Line Configurations

The results of the Painlevé analysis in §3.2 indicated a dense set of values of δ on the intervals $(-1, 0)$ and $(-\infty, -1)$ whose dynamics passed the first two steps of the ARS algorithm for the weak Painlevé property, implying that these systems might possibly be partially integrable. Kim and Cary [68] have studied test-particle motion in O-line magnetic fields with no electric field, which lead to the discovery of a numerical action integral for the motion in these fields. A similar integral exists for the motion in these fields when an electric field is introduced, and we shall demonstrate this shortly.

The set of values of δ that are of interest on the interval $(-1, 0)$ were stated in (3.4.2), and are given by

$$\delta(M, N) = -\frac{M(N + M)}{2N^2}, \quad (4.3.1)$$

where M and N are natural numbers, and $M < N$.

Recall the system's equations of motion (4.1.1). Depending on the sign of ϵ , we have two different asymptotic régimes in which we can find solutions to the system's equations of motion, and we can also calculate constants of the motion for the system.

Régime I: For $\epsilon < 0$, a charged test particle will execute an $\mathbf{E} \times \mathbf{B}$ drift that is directed outwards from the origin, which, after a sufficiently long period of time, will take the particle into a region in which both μ and J_{\parallel} are good invariants. These invariants, along with the system's constant Hamiltonian H , are sufficient to describe the particle's motion completely.

Régime II: $\epsilon > 0$. In this limit, the $\mathbf{E} \times \mathbf{B}$ drift will push charged particles inwards towards the neutral line, and if the system is allowed to evolve for a sufficiently long time, we can neglect the higher-order terms in the (4.1.1c-e), and can linearize the system, leading us to

$$\dot{x} = p_x \tag{4.3.2a}$$

$$\dot{y} = p_y \tag{4.3.2b}$$

$$\dot{z} = (\kappa t + p_{z_0}) \tag{4.3.2c}$$

$$\dot{p}_x = -x(\kappa t + p_{z_0}), \tag{4.3.2d}$$

$$\dot{p}_y = \delta y(\kappa t + p_{z_0}). \tag{4.3.2e}$$

In this linearized system, the motion in z is simply a free-fall in the electric field

$$z(t) = z_0 + p_{z_0}t + \frac{1}{2}\kappa t^2, \tag{4.3.3}$$

where z_0 is a constant.

The equations governing the x and y motion can be condensed into a pair of decoupled second-order ODE's

$$\frac{d^2x}{dt^2} + (\kappa t + p_{z_0})x = 0$$

$$\frac{d^2y}{dt^2} + |\delta|(\kappa t + p_{z_0})y = 0.$$

Introducing a *translated time variable* $\tau = t + p_{z_0}/\kappa$, we may rewrite the above equations to get

$$\frac{d^2x}{dt^2} + \kappa\tau x = 0 \quad (4.3.4a)$$

$$\frac{d^2y}{dt^2} + |\delta|\kappa\tau y = 0. \quad (4.3.4b)$$

This is quite useful indeed, since (4.3.4a,b) are just Airy equations. The solutions for to (4.3.4a) are the Airy functions $\text{Ai}(-\kappa\tau)$ and $\text{Bi}(-\kappa\tau)$, and the general solution for x in this régime is

$$x(\tau) = C_1 \text{Ai}(-\kappa\tau) + C_2 \text{Bi}(-\kappa\tau),$$

while the motion in y is described by

$$y(\tau) = D_1 \text{Ai}(-|\delta|\kappa\tau) + D_2 \text{Bi}(-|\delta|\kappa\tau).$$

The Airy functions $\text{Ai}(-\kappa\tau)$ and $\text{Bi}(-\kappa\tau)$ have asymptotic representations given by [69]

$$\begin{aligned} \text{Ai}(-\kappa\tau) = & \frac{1}{\sqrt{\pi\sqrt{\kappa\tau}}} \left[\sin\left(\zeta + \frac{\pi}{4}\right) \sum_{n=0}^{\infty} (-1)^n a_{2n} \zeta^{-2n} \right. \\ & \left. - \cos\left(\zeta + \frac{\pi}{4}\right) \sum_{n=0}^{\infty} (-1)^n a_{2n+1} \zeta^{-2n-1} \right] \end{aligned} \quad (4.3.5a)$$

and

$$\begin{aligned} \text{Bi}(-\kappa\tau) = & \frac{1}{\sqrt{\pi\sqrt{\kappa\tau}}} \left[\cos\left(\zeta + \frac{\pi}{4}\right) \sum_{n=0}^{\infty} (-1)^n b_{2n} \zeta^{-2n} \right. \\ & \left. + \sin\left(\zeta + \frac{\pi}{4}\right) \sum_{n=0}^{\infty} (-1)^n b_{2n+1} \zeta^{-2n-1} \right], \end{aligned} \quad (4.3.5b)$$

where $\zeta = \frac{2}{3}(\kappa\tau)^{3/2}$ and the coefficients a_n and b_n are constants. Keeping only the leading order terms in (4.3.5a,b) leads us to an asymptotic expression for $x(\tau)$, and using the same analysis, we can construct an asymptotic expression for $y(\tau)$.

$$x(\tau) = \frac{1}{\sqrt{\pi\sqrt{\kappa\tau}}} \left[C_1 \sin\left(\frac{2}{3}(\kappa\tau)^{3/2} + \frac{\pi}{4}\right) + C_2 \cos\left(\frac{2}{3}(\kappa\tau)^{3/2} + \frac{\pi}{4}\right) \right]. \quad (4.3.6a)$$

$$y(\tau) = \frac{1}{\sqrt{\pi\sqrt{|\delta|\kappa\tau}}} \left[D_1 \sin\left(\frac{2}{3}(|\delta|\kappa\tau)^{3/2} + \frac{\pi}{4}\right) + D_2 \cos\left(\frac{2}{3}(|\delta|\kappa\tau)^{3/2} + \frac{\pi}{4}\right) \right]. \quad (4.3.6b),$$

where D_1 and D_2 are also constants.

The behavior predicted by (4.3.6a,b) is oscillatory motion whose frequency is proportional to $\tau^{1/2}$ and amplitude which scales as $\tau^{-1/4}$. The frequency of the x -motion can be seen by examining the argument of the trigonometric functions in (4.3.6a), which is

$$\left[\left(\frac{2\kappa}{3} \right)^{3/2} \sqrt{\tau} \right] \tau + \frac{\pi}{4}.$$

This allows us to define a frequency in x , $\omega_x(\tau)$

$$\omega_x(\tau) = \left(\frac{2\kappa}{3} \right)^{3/2} \sqrt{\tau}. \quad (4.3.7a)$$

By a similar argument, we can define the frequency of the motion in y by

$$\omega_y(\tau) = \left(\frac{2\kappa|\delta|}{3} \right)^{3/2} \sqrt{\tau}. \quad (4.3.7b)$$

This scaling of the frequency agrees well with the log-log plot of $\omega_x(\tau)$ versus t , presented in Figure 4.3.1, which shows that in the interval between $t = 1000$ and $t = 1500$, the slope of the graph is approximately 0.53. The scaling of the amplitude can be seen by inspection of (4.3.6a,b), and is confirmed by a plot of the amplitude of x versus t (Figure 4.3.2)

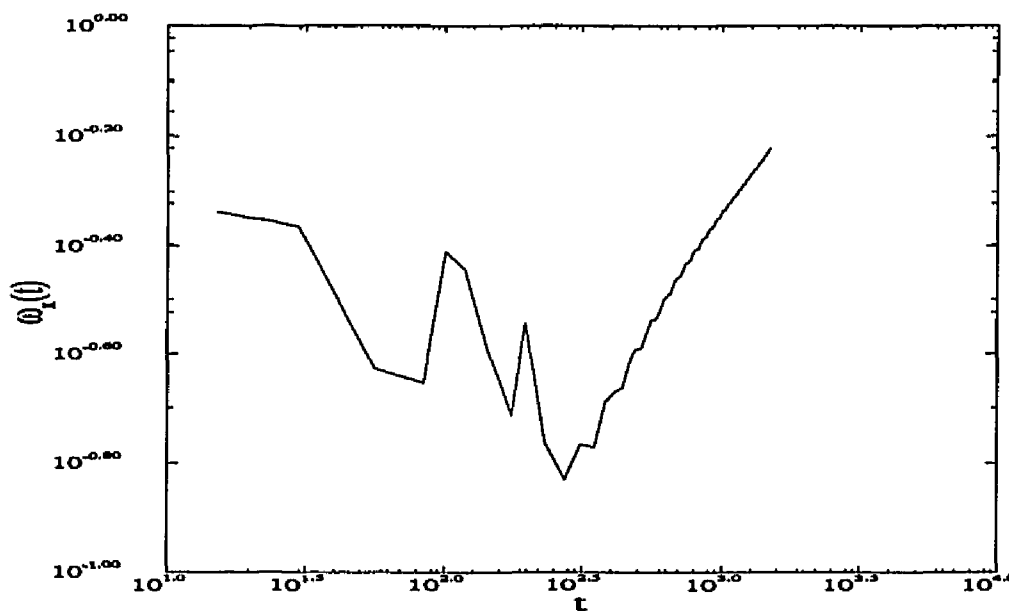


Figure 4.3.1. Frequency of the x -Oscillations ($\delta = -\frac{1}{8}$).

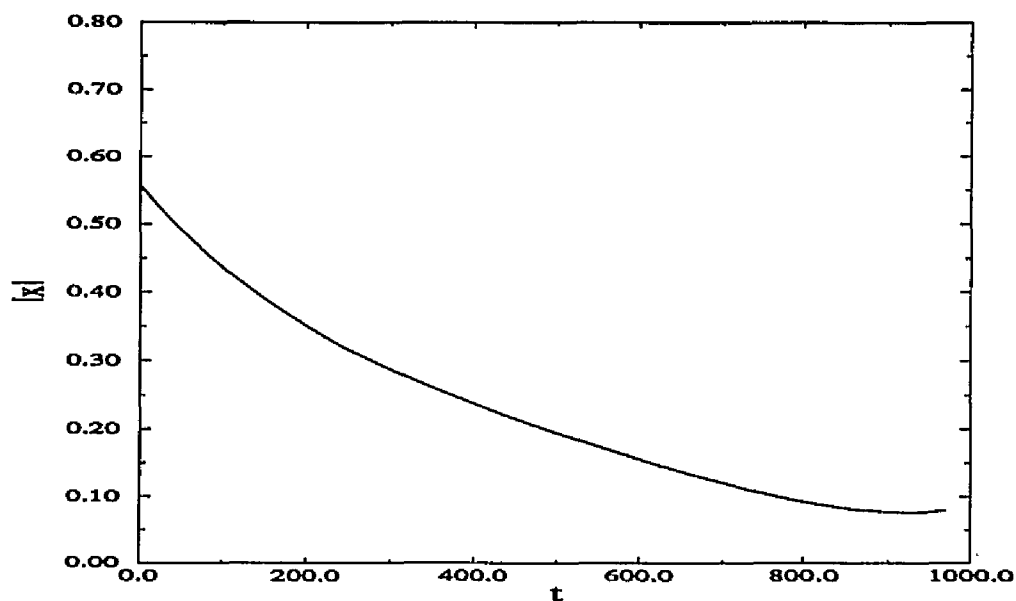


Figure 4.3.2. Amplitude of the x -Oscillations ($\delta = -\frac{1}{8}$).

The above analysis applies to *all* $\delta \in (-1, 0)$, as well as all $\delta \in (-\infty, -1)$, not just those values of δ that satisfy (4.3.1). The fact that (4.3.1) describes a *dense* set of δ on the interval $(-\infty, -1)$ may be related to the fact that it is possible to construct the asymptotic solutions (4.3.6a,b). A typical set of trajectories for the system in this limit are presented in Figures 4.3.3-7. The field configuration for these Figures is $\delta = \frac{1}{8}$, the electric field strength is set at $\kappa = 3.13 \times 10^{-4}$, and the initial value of the magnetic moment is $\mu = 5.0 \times 10^{-4}$.

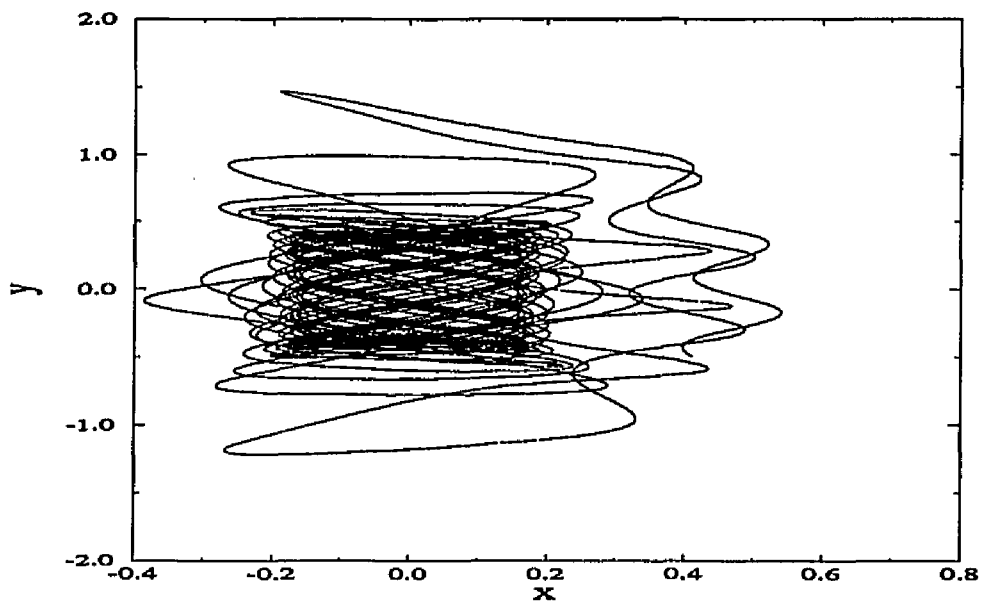


Figure 4.3.3. A Typical x - y Trajectory ($\delta = -\frac{1}{8}$)

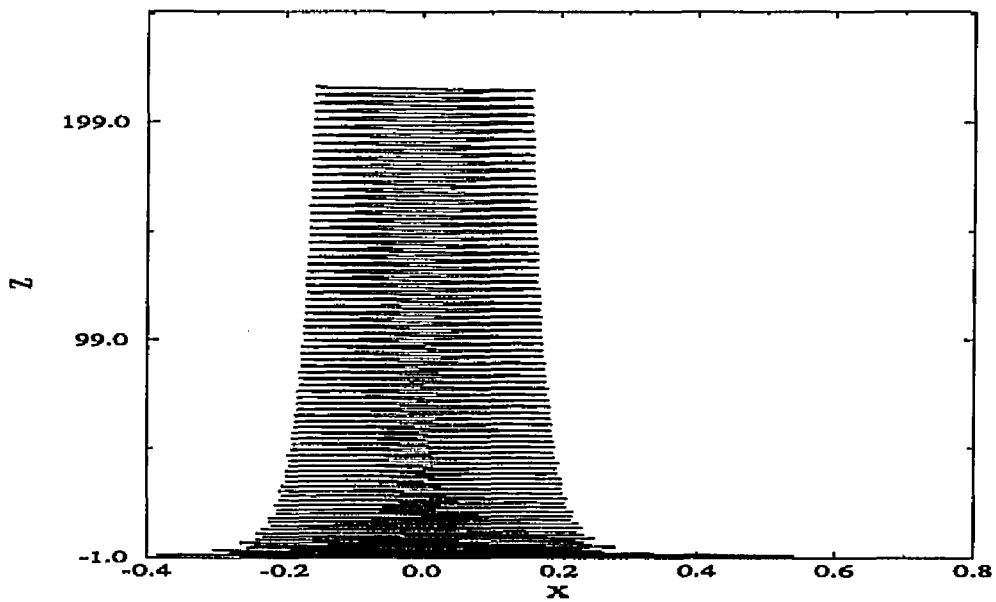


Figure 4.3.4. A Typical x - z Trajectory ($\delta = -\frac{1}{8}$).

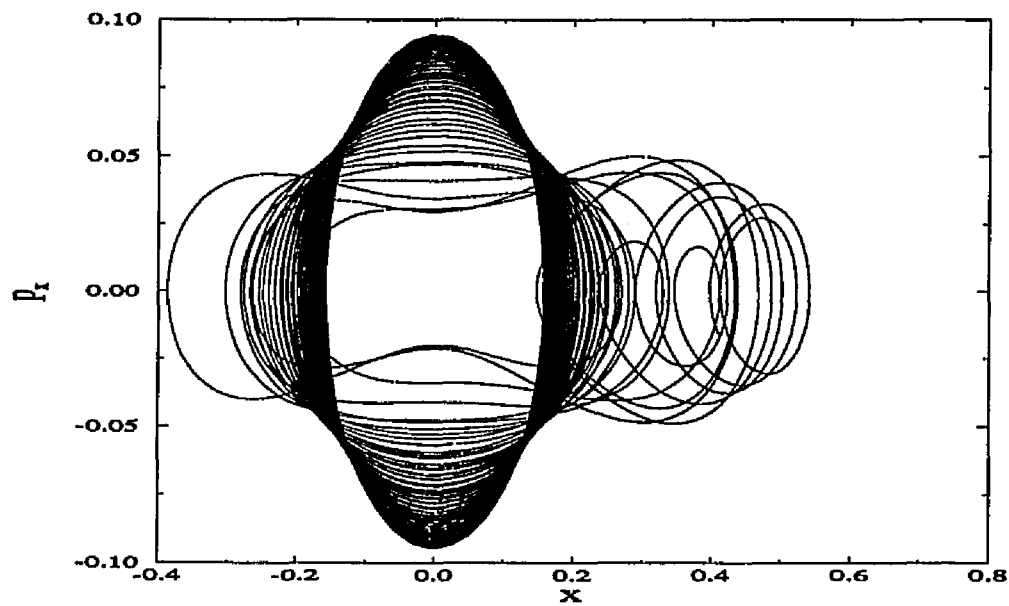


Figure 4.3.5. A Typical x -Phase Space Trajectory ($\delta = -\frac{1}{8}$).

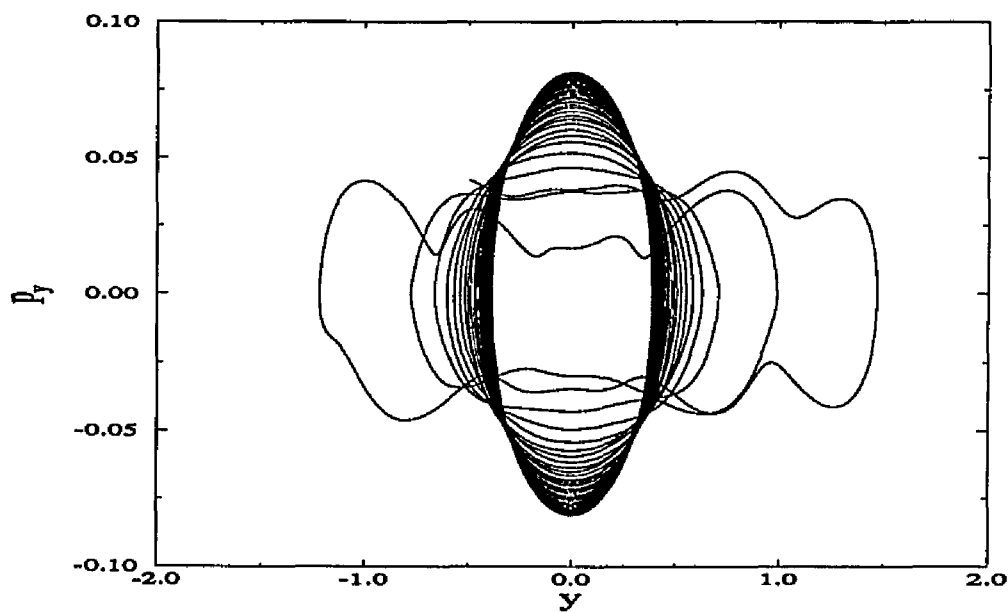


Figure 4.3.6. A Typical y -Phase Space Trajectory ($\delta = -\frac{1}{8}$).

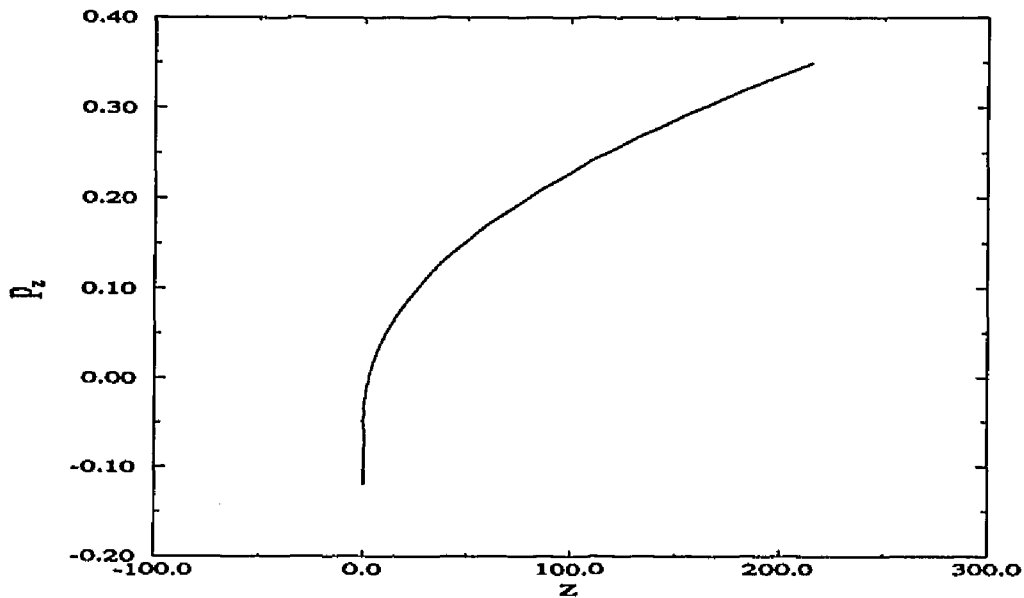


Figure 4.3.7. A Typical z -Phase Space Trajectory ($\delta = -\frac{1}{8}$).

There is no stark difference between the properties of the trajectories associated with values of δ that satisfy (4.3.1) and those that do not satisfy this relationship, with one exception: if $\delta = -(K^2/L^2)^{1/3}$, where K and L are natural numbers, with $K < L$, then the frequencies of the x and y motion become comensurate, i.e.

$$\frac{\omega_y}{\omega_x} = \frac{K}{L}. \quad (4.3.8)$$

In this case, the x - y trajectory resembles a Lissajous figure, such as the one shown in Figure 4.3.8, and we have quasiperiodic motion in x and y . The condition that a given value of δ that yield quasiperiodic trajectories leads to values of δ that do not satisfy (4.3.1).

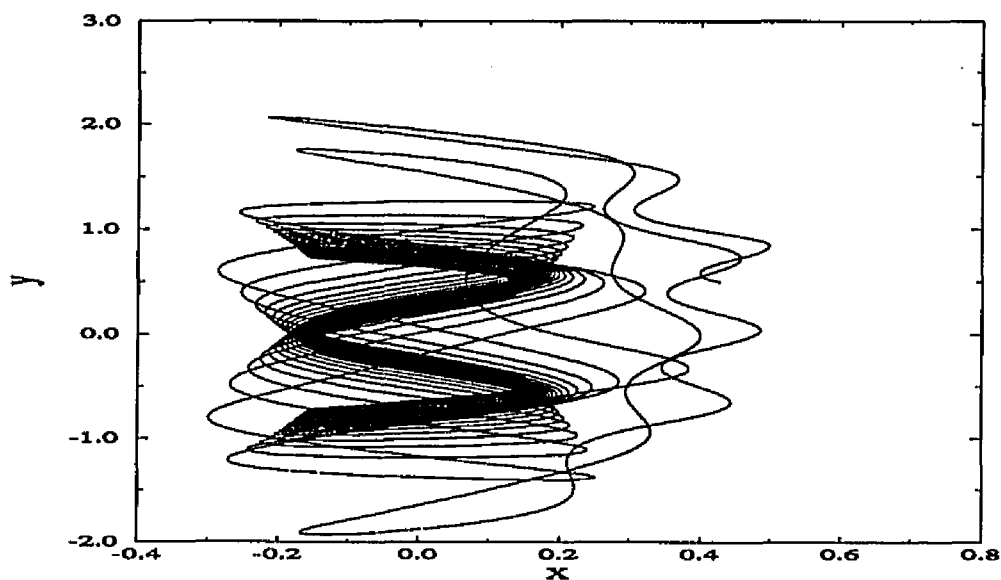


Figure 4.3.8. Quasiperiodic x - y Trajectory ($\delta = -\frac{1}{16}$)

As we saw with the X-line field configurations, as $\delta \rightarrow 0$, the dynamics of the system become more regular. This is also true of elliptical O-line field configurations, as can be seen in Figures 4.3.9-12, which are trajectory plots for $\delta = -4.95 \times 10^{-3}$, a value of δ that satisfies (4.3.1).

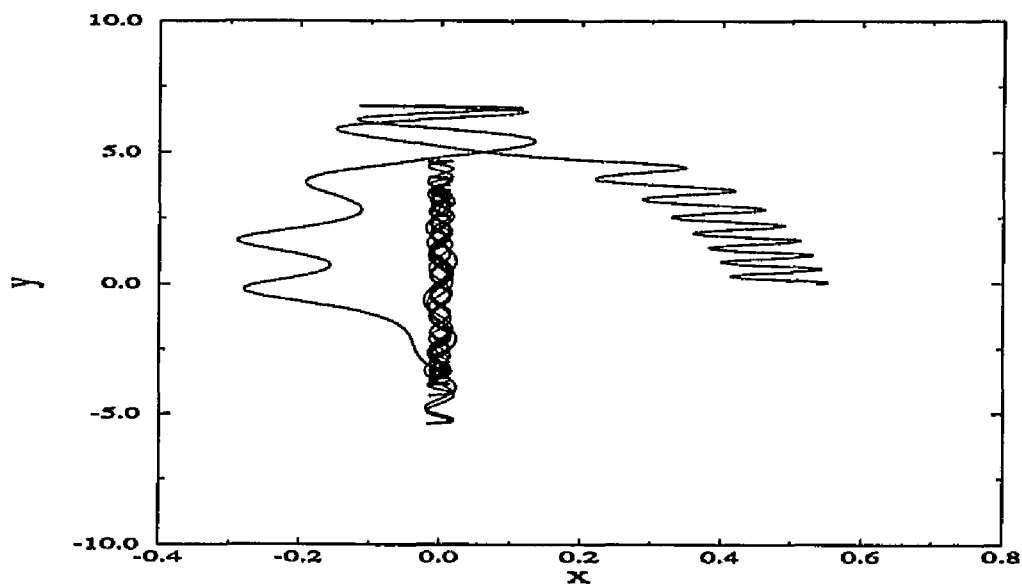


Figure 4.3.9. x - y Trajectory ($\delta = -4.95 \times 10^{-3}$)

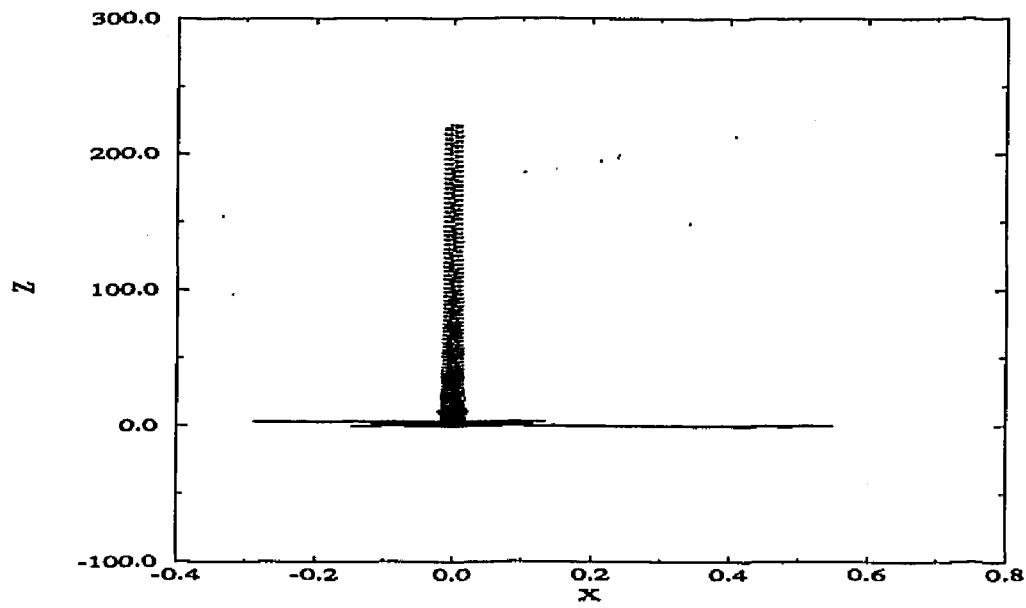


Figure 4.3.10. x - z Trajectory ($\delta = -4.95 \times 10^{-3}$).

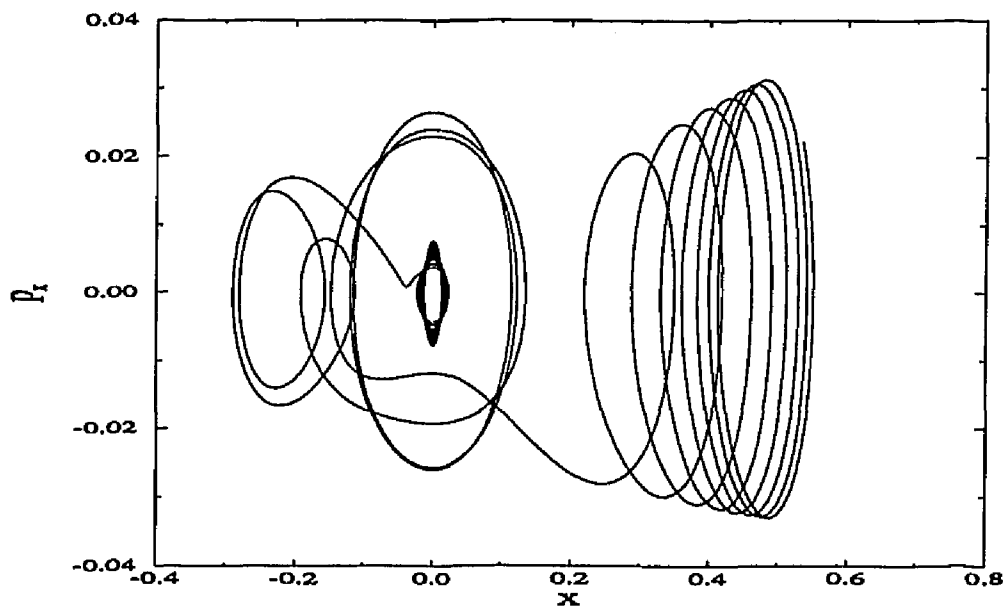


Figure 4.3.11. x -Phase Space Trajectory Trajectory ($\delta = -4.95 \times 10^{-3}$).

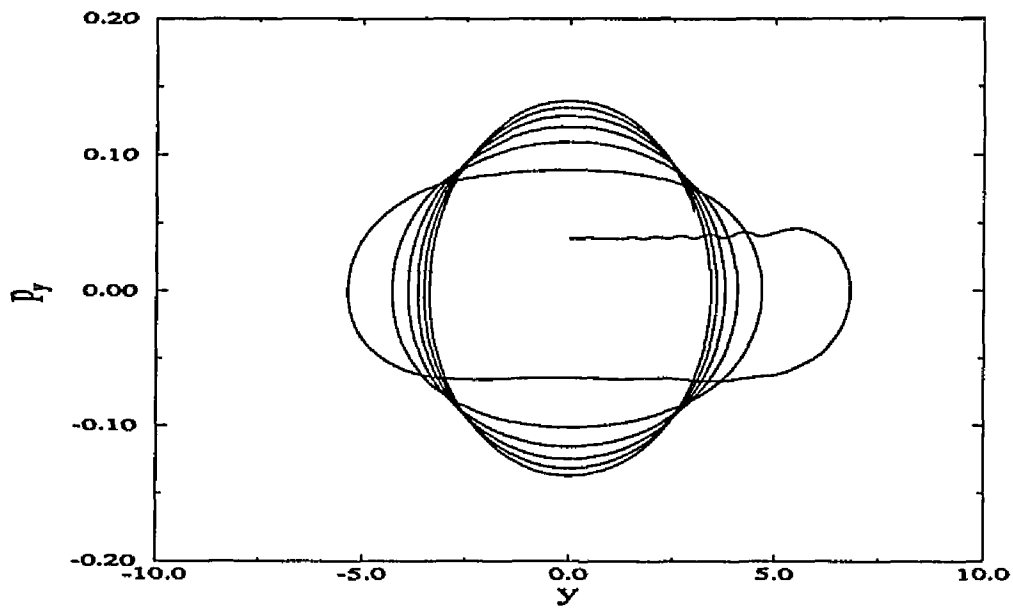


Figure 4.3.12. y -Phase Space Trajectory Trajectory ($\delta = -4.95 \times 10^{-3}$).

The condition (4.3.1) does not signal any generic change in behavior for the system. Any small value of δ (that is, $-1 \ll \delta < 0$) will yield regular dynamics, and as $\delta \rightarrow 0$, the system's behavior approaches that of the slab geometry, which, as we shall see in the next section, is integrable. Unlike the X-line cases in the previous section, note that we do not have a situation in which p_y approaches a constant value.

Given the ease with which we were able to construct asymptotic solutions to the equations of motion for the system for $\kappa > 0$, it would seem likely that the system may possess some constants of the motion in this régime. As the particle drifts in towards the neutral line, we lose the adiabatic invariant μ , as can be seen in Figure 4.3.13, and the parallel invariant defined in §1.2 by (1.2.23) also breaks down in this régime.

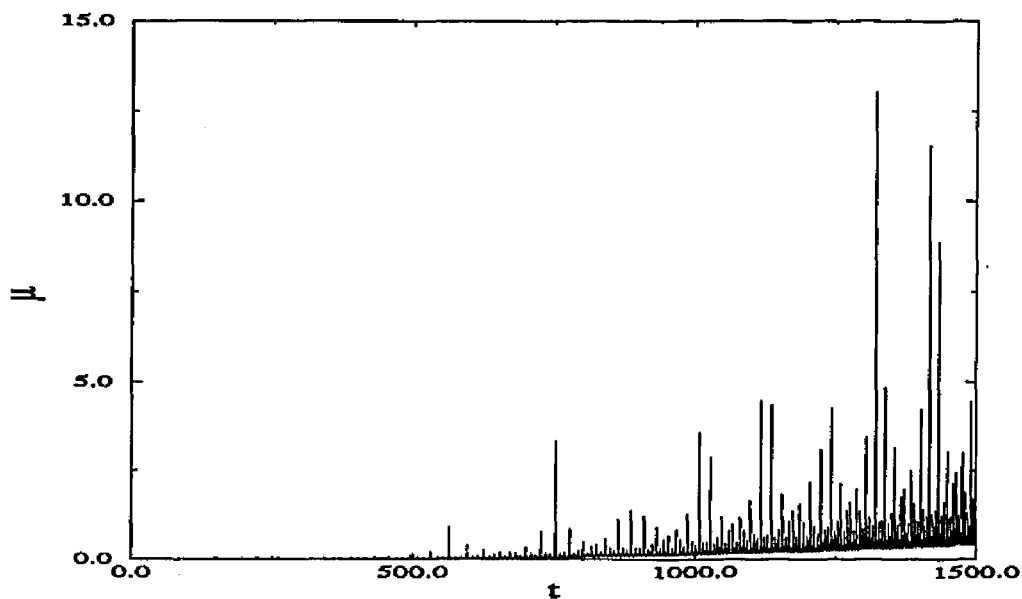


Figure 4.3.13. Magnetic Moment μ vs. time ($\delta = -\frac{1}{8}$).

We can, however, construct two new actions J_x and J_y , which are defined as

$$J_x = \int_{t_0}^{t_0+T_x} p_x dx \quad (4.3.9a)$$

$$J_y = \int_{t_0}^{t_0+T_y} p_y dy, \quad (4.3.9b)$$

where T_x and T_y are the periods of the x and y motion, respectively. Figures 4.3.14 and 4.3.15 show the values of these actions versus time, for the same set of parameters and initial conditions used to generate Figures 4.3.2-7.

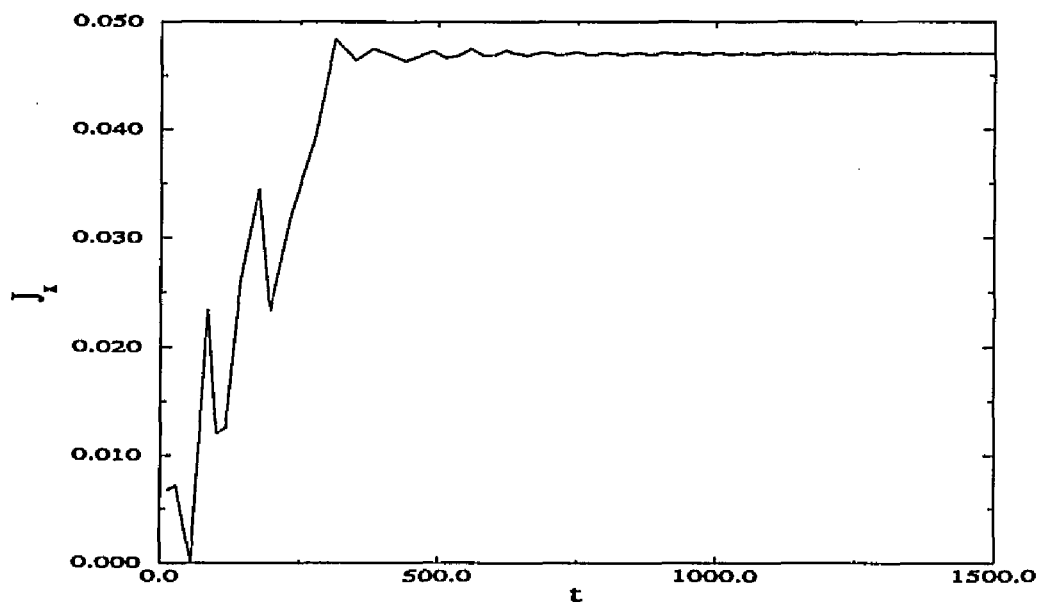


Figure 4.3.14. Action Integral in x , J_x , vs. Time ($\delta = -\frac{1}{8}$).

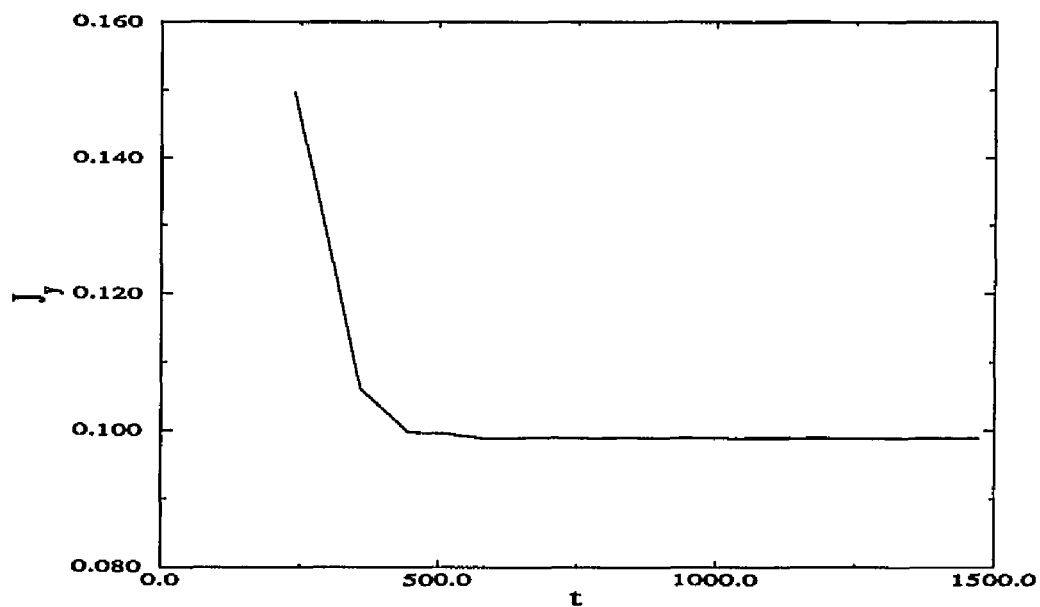


Figure 4.3.15. Action Integral in y , J_y , vs. Time ($\delta = -\frac{1}{8}$).

For all of the elliptic O-line cases, the fact that the test particle is focused into the unmagnetized region leads to a dramatic increase in the particle's kinetic

energy. This behavior is generic for these closed magnetic field geometries. The system's asymptotic solutions indicate that the test particle's kinetic energy will grow as a quadratic in t once the system enters the asymptotic régime. This can be seen by examining the Hamiltonian (4.1.2) and noting that the particle's position in z is given by (4.3.3). Examination of the linearized Hamiltonian yields a simple estimate of the test particle's kinetic energy

$$E_K = H + \kappa z(t) = H + \kappa \left[z_0 + p_{z_0} t + \frac{\kappa}{2} t^2 \right]. \quad (4.3.10)$$

Figure 4.3.16 shows a typical test-particle's kinetic energy plotted versus time, for $\delta = 1/8$, $\kappa = 3.13 \times 10^{-4}$, and $\mu = 5 \times 10^{-3}$, and Figure 4.3.17 is a log-log plot of a typical test particle's kinetic energy for $\delta = 1/16$, with the same values of electric field and initial magnetic moment.

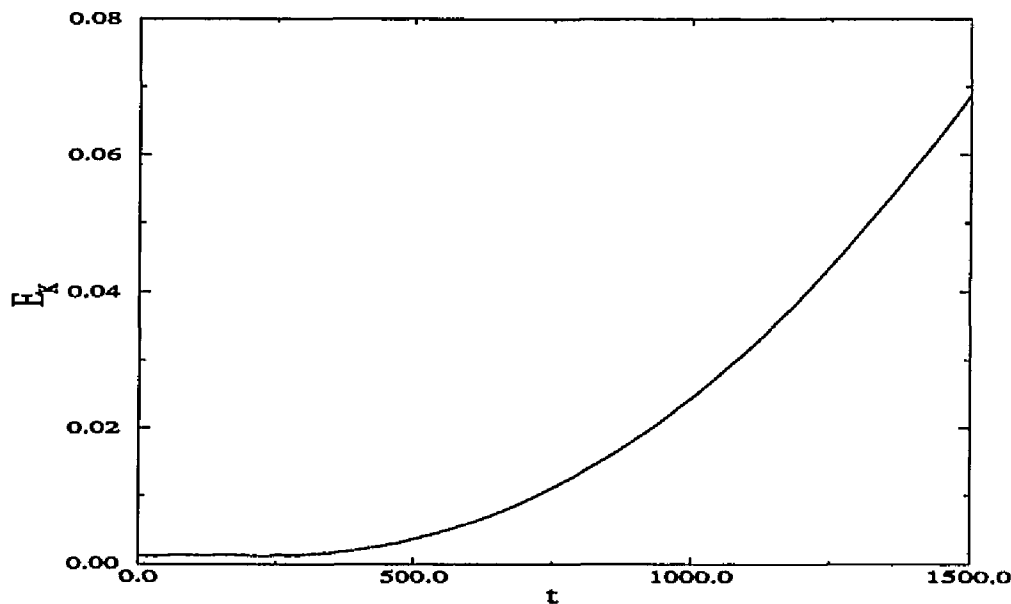


Figure 4.3.16. Test-Particle Kinetic Energy vs. Time ($\delta = -\frac{1}{8}$).

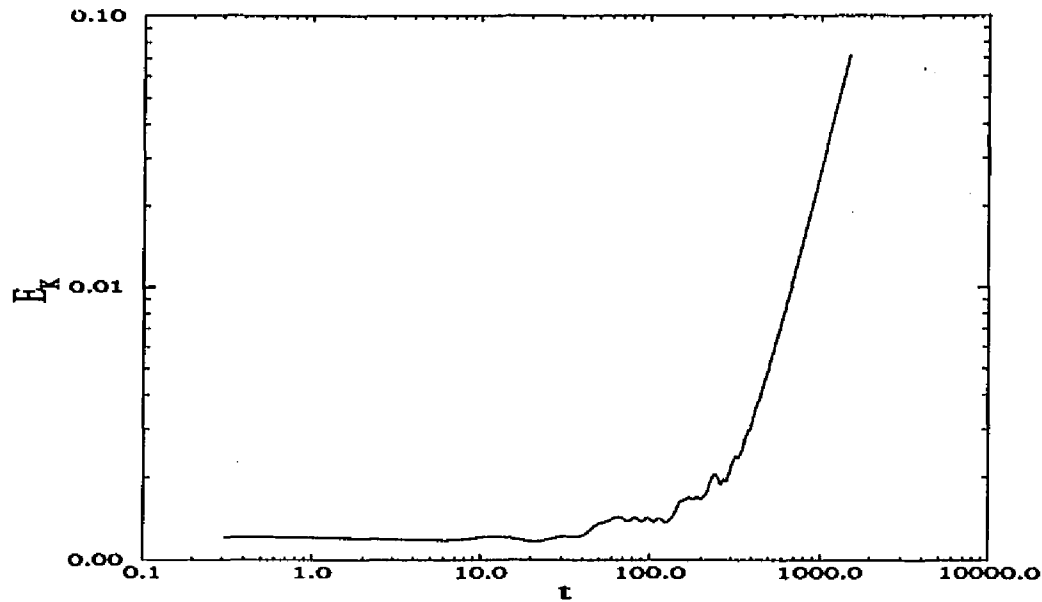


Figure 4.3.17. Log-log Plot of E_K vs. t ($\delta = -\frac{1}{16}$).

Finally, we turn our attention to the issue of sensitivity to initial conditions. Using diagnostic B outlined in § 4.1, we have examined elliptical O-line fields for various values of δ . The numerical experiments were performed using an ensemble with 1000 particles, and setting $H = 10^{-3}$, $\mu = 5 \times 10^{-4}$, $\Psi_0 = -0.48$, and $\kappa = 3.13 \times 10^{-4}$. The ensemble was integrated forward from $t = 0$ to $t = 1000$, and the test-particles' kinetic energies were calculated at $t = 1000$. The system showed large-scale structure in its kinetic energy spectrum (i.e. a sine wave), but still had some sensitivity to initial conditions superimposed over this orderly picture (Figure 4.3.18). These spikes are *not* numerical errors, since the typical final *relative* error in the Hamiltonian is on the order of 10^{-3} , much smaller than the displacements shown in Figure 4.3.18. Structure persists when we examine a small segment of the initial flux surface using an ensemble with the same population, as shown in Figure 4.3.19.

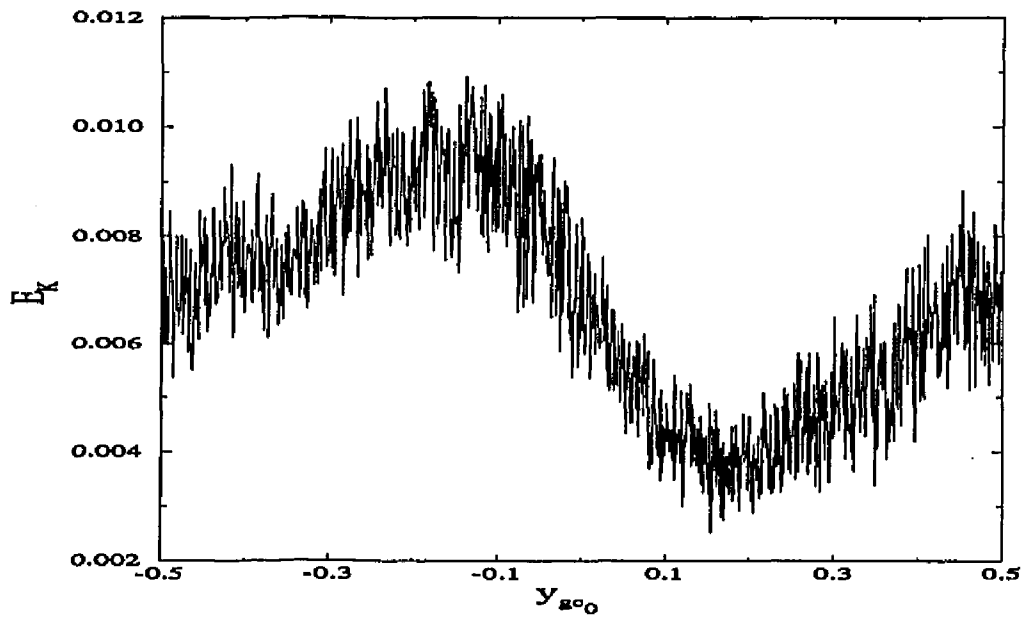


Figure 4.3.18. Exit Kinetic Energy vs. Initial Position ($\delta = -\frac{1}{8}$).

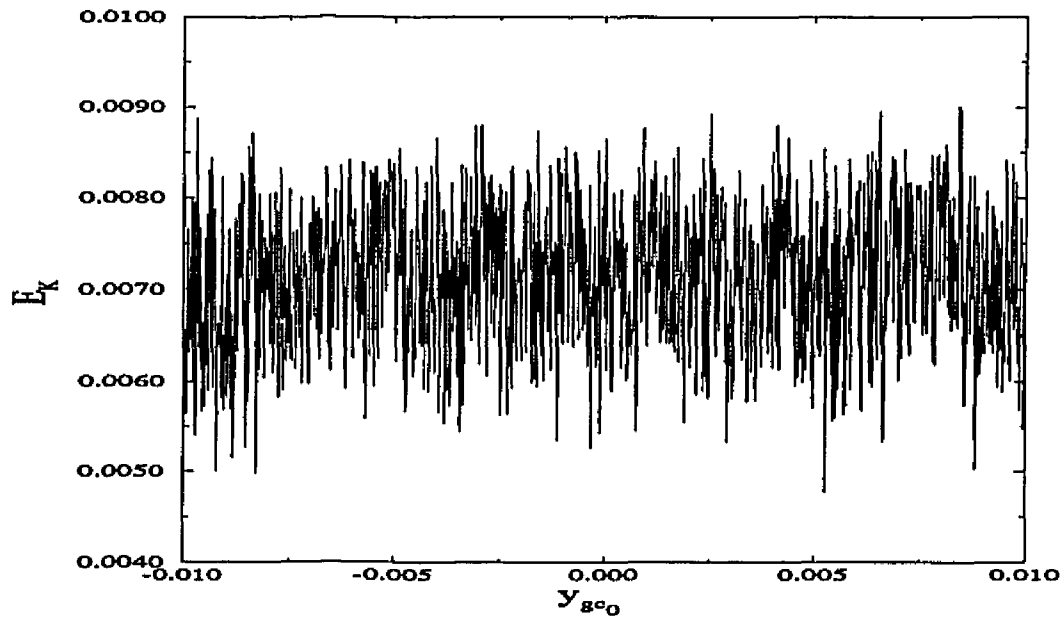


Figure 4.3.19. Detail of Figure 4.3.18.

§4.4 Summary of the Properties of the Weak Painlevé Candidates

We were unable to prove analytically whether or not the large classes of weak Painlevé candidates discovered in § 3.2 actually possess the weak Painlevé property. Numerical studies of single-particle trajectories and ensembles of particles have lead us to the following conclusions:

I: In the case of X-type neutral line configurations, the condition (4.2.1) did not identify any field configurations whose trajectories or sensitivities to ininial conditions were significantly different from neighboring field geometries (i.e. neighboring values of δ).

II: The O-type neutral line cases specified by the condition (4.3.1) form a dense set on the intervals $(-\infty, -1)$ and $(-1, 0)$. As we saw in §4.3, for $\epsilon > 0$, we could construct asymptotic solutions to the system (4.1.1a-f) in terms of Airy functions. We were also able to identify the numerical actions integrals J_x and J_y in this régime. The aforementioned constructions were possible for *all* values of δ on the intervals defined above, not just the values listed in (4.3.1). Furthermore, the weak Painlevé candidates did *not* include the quasiperiodic cases defined in (4.3.8). Finally, the dynamical systems associated with $\delta \in \{(-\infty, -1) \cup (-1, 0)\}$ showed no difference in their sensitivities to initial conditions with respect to the condition (4.3.1).

Drawing from the above results, it seems that the partial fulfillment of the weak Painlevé property criteria for the systems identified by (4.2.1) and (4.3.1) does not provide a dependable predictor of integrability. This should not be taken

as an indictment of the Painlevé conjecture, since the systems examined here do not satisfy the hypothesis of the conjecture. In the next chapter, we shall examine two field configurations which produce dynamical systems that possess the Painlevé property, and we shall get more satisfactory results.

CHAPTER FIVE
TRAJECTORIES, ASYMPTOTIC
BEHAVIOR AND INVARIANTS
PART II: CASES THAT POSSESS THE PAINLEVÉ PROPERTY

§5.1 What the Painlevé Property Implies

In Chapter Three, we found two cases for which the system (3.1.4a-e) possessed the Painlevé property: the neutral sheet ($\delta = 0$ and $\delta \rightarrow \infty$), and the circularly symmetric field line case ($\delta = -1$). Given the Painlevé conjecture stated in § 2.2, we expect these systems to be integrable in the complex analytic sense, that is, we will be able to construct Laurent series representations for the coordinates and momenta:

$$q_i(t) = \sum_{n=-\infty}^{\infty} a_i^{(n)} t^n$$
$$p_i(t) = \sum_{n=-\infty}^{\infty} b_i^{(n)} t^n,$$

where the coefficients $a_i^{(n)}$ and $b_i^{(n)}$ are constants. In this chapter, we will find that the aforementioned field configurations are indeed special, and we will find that they are integrable in the Hamiltonian sense in an extended phase space that includes the time as one of its canonical variables.

§5.2 The Neutral Sheet Configuration

The neutral sheet configuration can arise in two instances, depending on the value of δ : $\delta = 0$ and $\delta \rightarrow \infty$. The former case yields a neutral sheet in the plane $x = 0$, while the latter leads to a neutral sheet in the plane $y = 0$. The analysis for the case $\delta = 0$ is more transparent, and from our discussion in §3.1, it is equivalent to the situation $\delta \rightarrow \infty$. Thus, we shall only consider the case $\delta = 0$.

The Hamiltonian equations of motion (3.1.1a-f) for this system have been studied for the case of a neutral sheet in the y - z plane in Appendix Two, and setting $\delta = 0$ reduces them to

$$\dot{x} = p_x \tag{5.2.1a}$$

$$\dot{y} = p_y \tag{5.2.1b}$$

$$\dot{z} = p_z + \frac{x^2}{2}, \tag{5.2.1c}$$

$$\dot{p}_x = -xp_z - \frac{x^3}{2} \tag{5.2.1d}$$

$$\dot{p}_y = 0 \tag{5.2.1e}$$

$$\dot{p}_z = \kappa, \tag{5.2.1f}$$

with a Hamiltonian H , given by

$$H(x, y, z, p_x, p_y, p_z) = \frac{p_x^2 + p_y^2}{2} + \frac{1}{2} \left(p_z^2 + \frac{x^2}{2} \right)^2 - \kappa z. \tag{5.2.2}$$

The motion in y , described by (5.2.1b,e) is trivial, and y is given by

$$y(t) = p_y t + y_0, \tag{5.2.3}$$

As usual, p_z can be eliminated, and is

$$p_z(t) = \kappa t + p_{z0}, \quad (5.2.4)$$

where p_{z0} is a constant. Substituting (5.2.3) and (5.2.4) into (5.2.1a,c,d) gives us the system

$$\dot{x} = p_x \quad (5.2.5a)$$

$$\dot{z} = \kappa t + p_{z0} + \frac{x^2}{2}, \quad (5.2.5b)$$

$$\dot{p}_x = -x(\kappa t + p_{z0}) - \frac{x^3}{2}. \quad (5.2.5c)$$

The set (5.2.4a-c) tell us that the root dynamics of the system lies in the coordinate x , and given x , we can use (5.2.2), (5.2.3), and the system's Hamiltonian (4.1.2) to solve for z explicitly. Differentiating (5.2.5a) with respect to t and replacing \dot{p}_x by the expression found in (5.2.5c), we get

$$\frac{d^2x}{dt^2} + (\kappa t + p_{z0})x + \frac{x^3}{2} = 0. \quad (5.2.6)$$

Once again, this equation can be simplified by introducing a translated time variable

τ :

$$\tau = t + \frac{p_{z0}}{\kappa}, \quad \frac{d}{dt} = \frac{d}{d\tau}.$$

This transformation reduces (5.2.6) to

$$\frac{d^2x}{d\tau^2} + \kappa\tau x + \frac{x^3}{2} = 0. \quad (5.2.7)$$

In Appendix Two, the above equation (5.2.7) was shown to possess the Painlevé property, which means that it falls into one of the fifty classes of second order ODE's studied by Painlevé. In fact, (5.2.7) can be better understood by casting it in standard form [49]. This may be accomplished by applying the change of variables

$$\tau = (-\kappa)^{-1/3}\zeta \quad x = \pm 2i\sqrt[3]{\kappa}\chi,$$

which transforms (5.2.7) into the *second Painlevé transcendent* [49]:

$$\frac{d^2\chi}{d\zeta^2} = \zeta\chi + 2\chi^3. \quad (5.2.8)$$

The above equation (5.2.8) is integrable in the Liouville sense; i.e. it is possible to construct a Hamiltonian \mathcal{H} and second integral \mathcal{I} in an extended phase space that includes both χ and ζ as canonical coordinates [70]. A discussion of this procedure is found in § 5.4.

The solution to (5.2.7) in terms of the second Painlevé transcendent, though rigorous, is difficult to interpret from a physical point of view. We can, however, gain physical insight into the system's behavior by examining the asymptotic behavior of (5.2.7).

For $\epsilon > 0$, the particle trajectories associated with (5.2.5a-c) are forced into the plane $x = 0$ as t gets large. This is due to the action of the $\mathbf{E} \times \mathbf{B}$ drift. For sufficiently large τ , x will be small, and we can neglect the cubic term in (5.2.7), which leads to Airy's equation:

$$\frac{d^2x}{dt^2} + \kappa tx = 0. \quad (5.2.9)$$

The solutions for to (4.2.8) are the Airy functions $\text{Ai}(-\kappa\tau)$ and $\text{Bi}(-\kappa\tau)$, and the general solution for x in this régime is

$$x(\tau) = C_1 \text{Ai}(\tau) + C_2 \text{Bi}(\tau).$$

Recalling the arguments made in § 4.3 concerning the properties of Airy functions in the limit of increasing argument, we obtain an asymptotic expression for $x(\tau)$

$$x(\tau) = \frac{1}{\sqrt{\pi\sqrt{\kappa\tau}}} \left[C_1 \sin\left(\frac{2}{3}(\kappa\tau)^{3/2} + \frac{\pi}{4}\right) + C_2 \cos\left(\frac{2}{3}(\kappa\tau)^{3/2} + \frac{\pi}{4}\right) \right]. \quad (5.2.10)$$

The behavior predicted by (5.2.10) is oscillations with frequency proportional to $t^{3/2}$ and amplitude which scales as $t^{-1/4}$, which can be seen in Figures 5.2.1 and 5.2.2. Figure 5.2.2 is a plot of a typical particle trajectory, projected into the x - y plane. These results are in agreement with those of Speiser [71], who first published asymptotic results for charged particle motion near a neutral sheet.

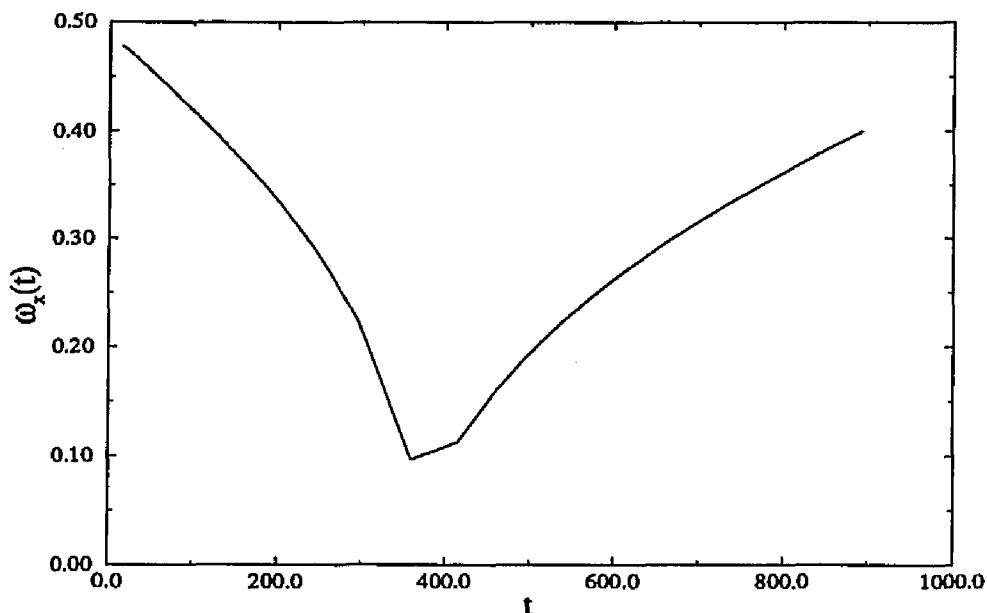


Figure 5.2.1. Frequency of the x -Oscillations in the Neutral Sheet.

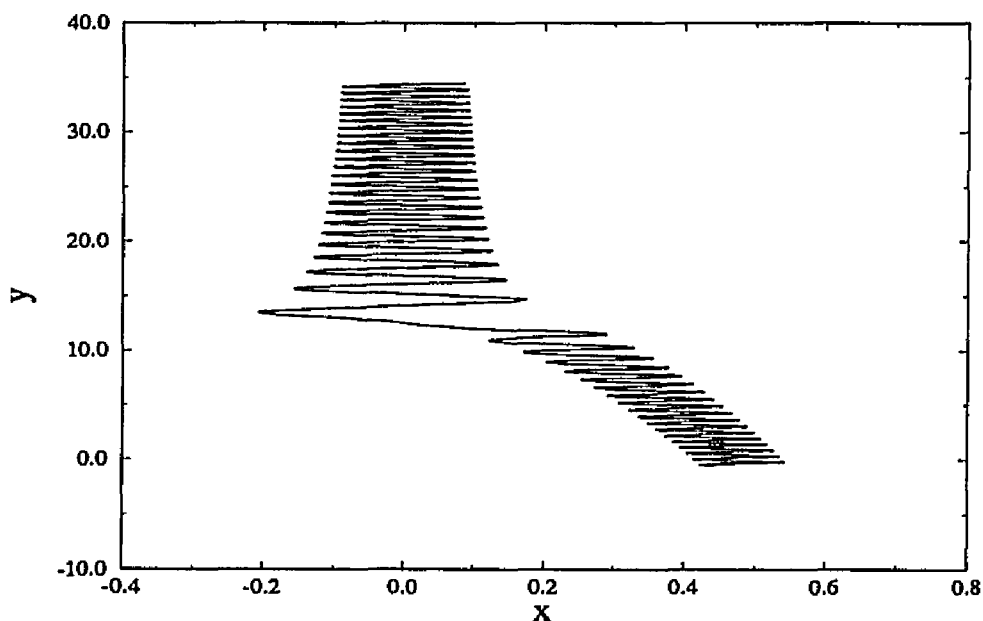


Figure 5.2.2. A Typical x - y Trajectory.

There are several invariants for particle motion in this régime, we already have two constants of the motion in H and p_y , as mentioned earlier. We also have the *time-dependent* constant of the motion $p_{z_0} = p_z - \kappa t$. The fact that the $\mathbf{E} \times \mathbf{B}$ drift

motion pushes the charged particle into the unmagnetized region tells us that μ will not be a good adiabatic invariant for the system. One quantity that is a good asymptotic constant of the motion that for the system is the action integral in x over one period of oscillation in x , which is defined by

$$\begin{aligned}
 J_x &= \oint p_x dx \\
 &= \int_{t=t_0}^{t=t_0+T} p_x^2 dt.
 \end{aligned}
 \tag{5.2.11}$$

The motivation for the existence of this action can be obtained by viewing Figure 5.2.3, which is an x -phase space trajectory plot. As the system evolves, the phase space trajectory approaches an elliptical orbit of constant area. The fact that this action is constant is demonstrated in Figure 5.2.4, which shows J_x versus t .

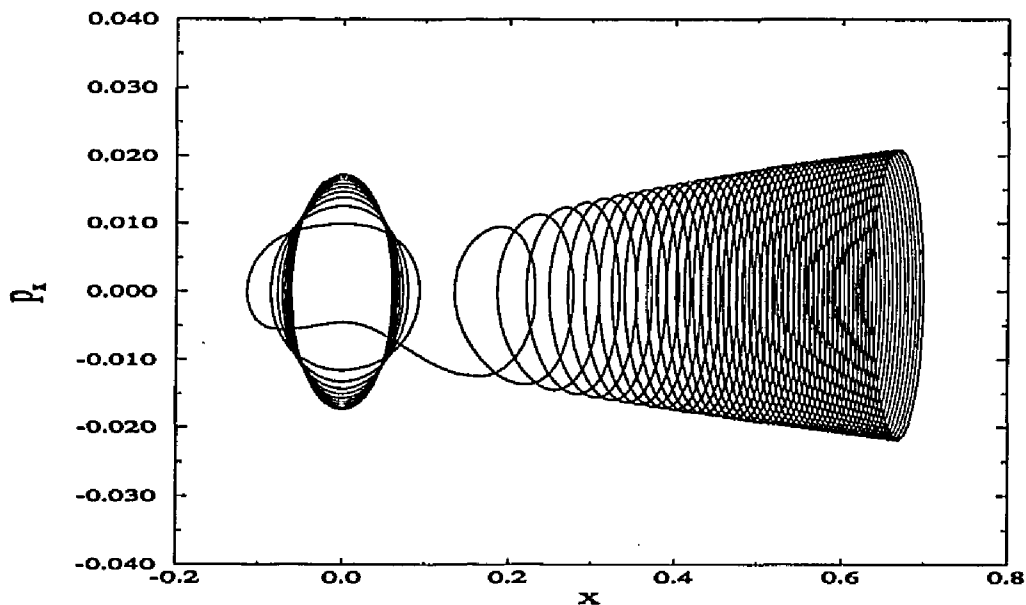


Figure 5.2.3. A Typical x -Phase Space Trajectory ($\epsilon > 0$).

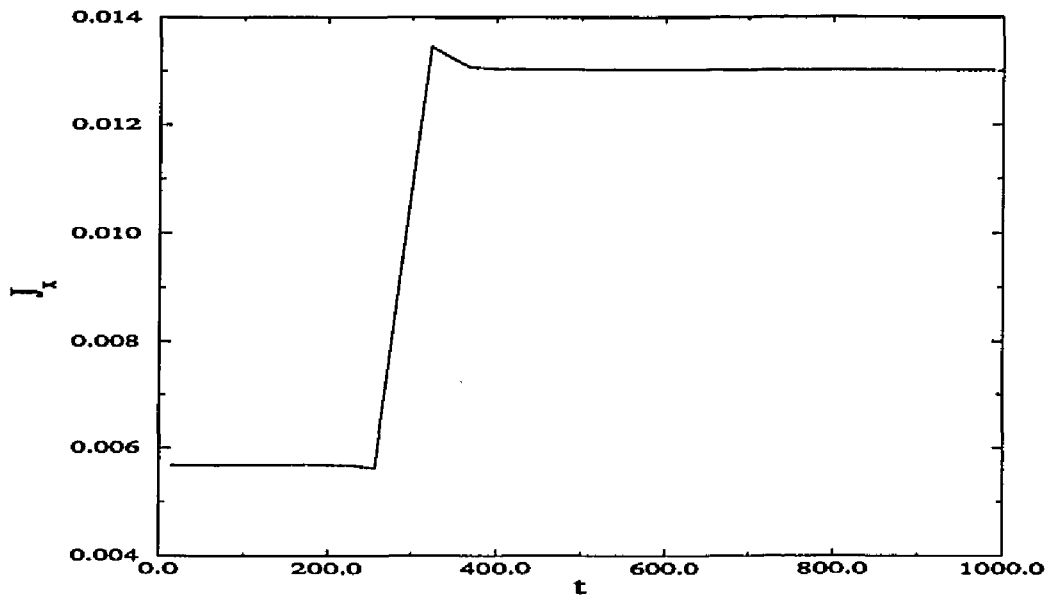
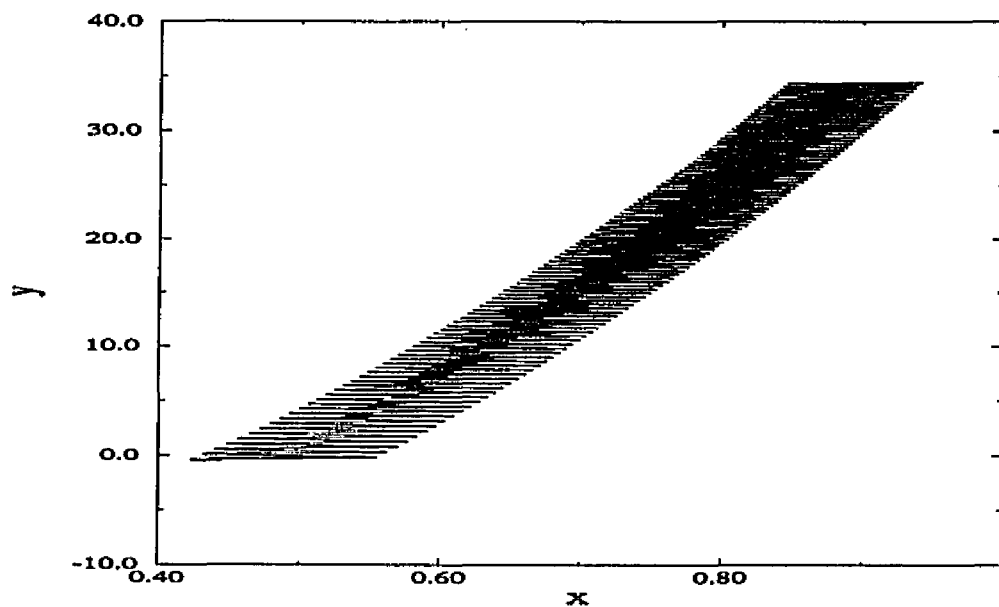
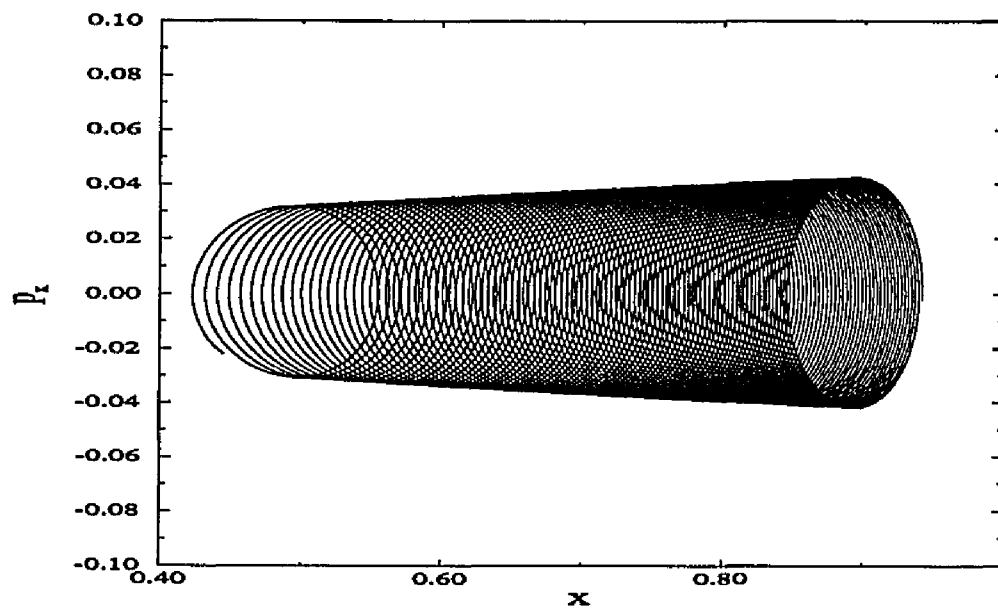


Figure 5.2.4. Action integral in x , J_x vs. Time ($\epsilon > 0$).

In the instance that $\epsilon < 0$, the $\mathbf{E} \times \mathbf{B}$ drift is away from the neutral plane. In this régime, x grows larger, which can be seen by inspection of Figure 5.2.5, which shows a typical x - y particle trajectory for this field configuration. This drift motion carries the test particle into a region in which guiding-center theory is valid; i.e. μ is a good adiabatic invariant.

An x -phase space portrait for the slab field configuration for $\epsilon < 0$ is shown in Figure 5.2.6, and once again, we have a phase space orbit that tends towards an ellipse of constant area, implying that it is possible to define an action identical to (5.2.11) for the system in this régime. A plot of J_x for $\epsilon < 0$ is shown in Figure 5.2.7, and it is no surprise that J_x tends towards a constant value. Finally, the fact that the test particle is moving away from the neutral sheet implies that the magnetic moment μ will tend towards being a conserved quantity, which is confirmed by

Figure 5.2.8.

Figure 5.2.5. A Typical x - y Trajectory ($\epsilon < 0$).Figure 5.2.6. A Typical x -Phase Space Trajectory ($\epsilon < 0$).

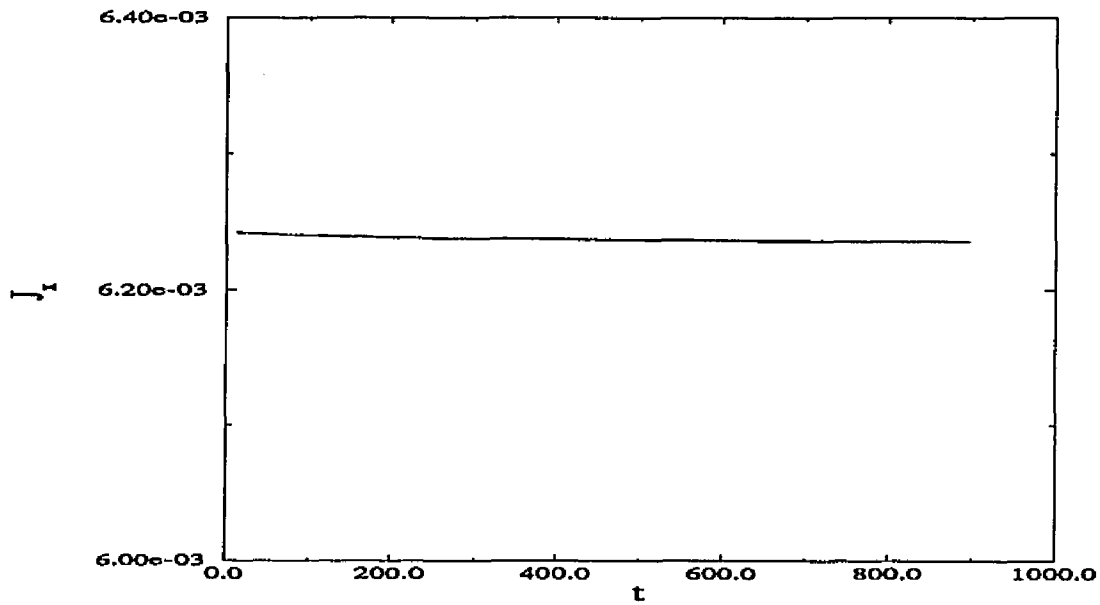


Figure 5.2.7. Action integral in x , J_x vs. Time ($\epsilon < 0$).

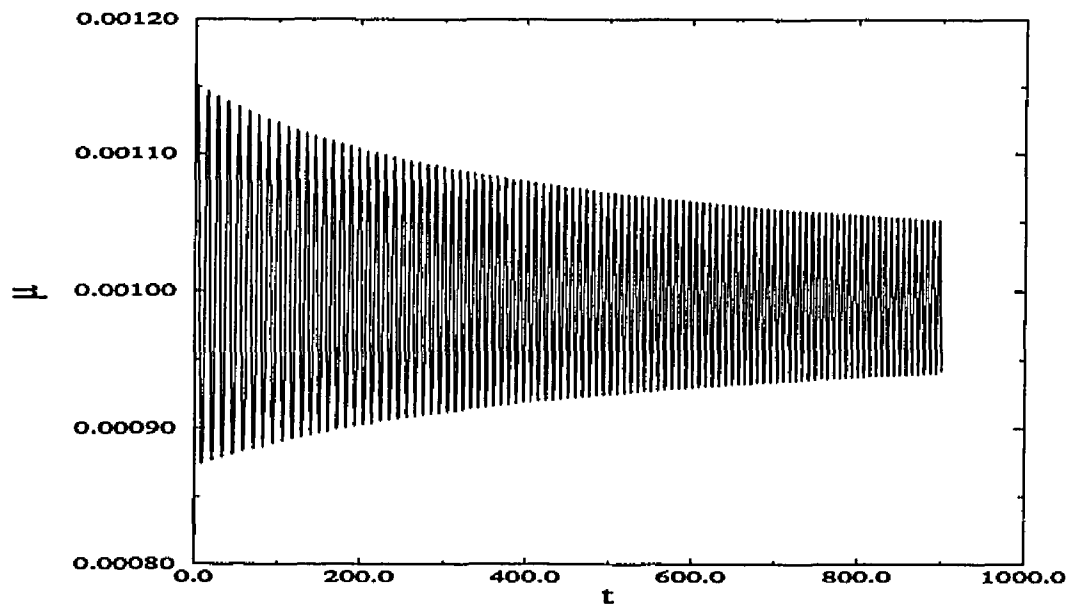


Figure 5.2.8. Magnetic Moment μ vs. Time ($\epsilon < 0$).

The system (5.2.1a-f) has two integrals in involution, namely H and p_y . We also have the time-dependent constant of the motion p_{z_0} , as well as the numerical invariant J_x . The fact that the x -motion of the system obeys the second Painlevé

transcendent means that we will be able to construct the third integral of the motion, thus rendering (5.2.1a-f) integrable in the Liouville sense. The construction of the remaining constant of the motion is nontrivial, and will be described in §5.4.

§5.3 The Circular O-Line Geometry

The other promising geometry identified by the Painlevé singularity analysis carried out in § 3.2 was the cylindrically symmetrical ($\delta = -1$) case. This configuration was found to possess particle dynamics that possessed the Painlevé property, meaning that the system of equations (3.1.4a-f) associated with this case should be analytically integrable.

In order to see this system's special properties more easily, it is necessary to transform to cylindrical coordinates. Since we wish to have a Hamiltonian system when we've accomplished this, we must use a canonical transformation to do this, or, equivalently, switch over to the Lagrangian formulation, perform the change of coordinates, and then construct the new Hamiltonian $H(\rho, \phi, z, p_\rho, p_\phi, p_z)$. Recall the Hamiltonian system given by (3.1.3) and (3.1.4a-f), with $\delta = -1$:

$$H(x, y, z, p_x, p_y, p_z) = \frac{p_x^2 + p_y^2}{2} + \frac{(p_z + \frac{1}{2}(x^2 + y^2))^2}{2} - \kappa z, \quad (5.3.1)$$

where ϵ is the electric field strength. The Hamiltonian equations of motion for the test particle are:

$$\dot{x} = p_x \quad (5.3.2a)$$

$$\dot{y} = p_y \quad (5.3.2b)$$

$$\dot{z} = p_z + \frac{1}{2}(x^2 + y^2), \quad (5.3.2c)$$

$$\dot{p}_x = -xp_z + \frac{x(y^2 - x^2)}{2} \quad (5.3.2d)$$

$$\dot{p}_y = -yp_z - \frac{y(y^2 + x^2)}{2} \quad (5.3.2e)$$

$$\dot{p}_z = \kappa. \quad (5.3.2f)$$

By using (5.3.2a-c), we can eliminate the momenta (p_x, p_y, p_z) in favor of the velocities $(\dot{x}, \dot{y}, \dot{z})$:

$$p_x = \dot{x} \quad p_y = \dot{y} \quad p_z = \dot{z} - \frac{1}{2}(x^2 + y^2).$$

This allows us to write the Hamiltonian as

$$H(x, y, z, \dot{x}, \dot{y}, \dot{z}) = \frac{1}{2}(\dot{x}^2 + \dot{y}^2 + \dot{z}^2) - \kappa z.$$

The Lagrangian for the system is thus

$$\begin{aligned} L(x, y, z, \dot{x}, \dot{y}, \dot{z}) &= xp_x + yp_y + zp_z - H(x, y, z, \dot{x}, \dot{y}, \dot{z}) \\ &= \frac{1}{2}(\dot{x}^2 + \dot{y}^2 + \dot{z}^2) - \frac{1}{2}(x^2 + y^2)\dot{z} + \kappa z. \end{aligned} \quad (5.3.3)$$

Now, we apply the simple transformation to cylindrical coordinates:

$$x = \rho \cos \phi \quad \dot{x} = \dot{\rho} \cos \phi - \rho \dot{\phi} \sin \phi$$

$$y = \rho \sin \phi \quad \dot{y} = \dot{\rho} \sin \phi + \rho \dot{\phi} \cos \phi.$$

$$z = z \quad \dot{z} = \dot{z}$$

This allows us to rewrite the system's Lagrangian as

$$L(\rho, \phi, z, \dot{\rho}, \dot{\phi}, \dot{z}) = \frac{1}{2}(\dot{\rho}^2 + \rho^2 \dot{\phi}^2 + \dot{z}^2 - \rho^2 \dot{z}) + \kappa z. \quad (5.3.4)$$

Given the above Lagrangian, we can calculate the canonical momenta p_ρ, p_ϕ , and p_z :

$$p_\rho = \frac{\partial L}{\partial \dot{\rho}} = \dot{\rho}, \quad (5.3.5a)$$

$$p_\phi = \frac{\partial L}{\partial \dot{\phi}} = \rho^2 \dot{\phi}, \quad (5.3.5b)$$

$$p_z = \dot{z} - \frac{\rho^2}{2}. \quad (5.3.5c)$$

Given these expressions for the momenta, we can use them to eliminate $\dot{\rho}$, $\dot{\phi}$, and \dot{z} from the Lagrangian (5.3.4), and thus we can construct the system's Hamiltonian in cylindrical coordinates via

$$H(\rho, \phi, z, p_\rho, p_\phi, p_z) = \rho p_\rho + \phi p_\phi + z p_z - L(\rho, \phi, z, p_\rho, p_\phi, p_z),$$

which gives the result

$$H(\rho, \phi, z, p_\rho, p_\phi, p_z) = \frac{1}{2} \left(p_\rho^2 + \frac{p_\phi^2}{\rho^2} + p_z^2 \right) + \frac{\rho^2 p_z}{2} + \frac{\rho^4}{8} - \kappa z. \quad (5.3.6)$$

Hamilton's equations are thus

$$\dot{\rho} = p_\rho \quad \dot{p}_\rho = \frac{p_\phi^2}{\rho^3} - \rho p_z - \frac{\rho^3}{2} \quad (5.3.7a, b)$$

$$\dot{\phi} = \frac{p_\phi}{\rho^2} \quad \dot{p}_\phi = 0 \quad (5.3.7c, d)$$

$$\dot{z} = p_z + \frac{\rho^2}{2} \quad \dot{p}_z = \kappa \quad (5.3.7e, f)$$

Clearly, the system (5.3.7a-f) is much more transparent than (5.3.2a-f), and in particular, we have p_ϕ as a constant of the motion, which is no great surprise, given the cylindrical symmetry of the magnetic and electric fields. As before, we still have the time-dependent constant of the motion p_{z_0} , and the Hamiltonian H is, of

course, also constant. These results agree with the notion of analytic integrability, but this set of constants are *not* a complete set of phase-space integrals, since p_{z_0} is a time-dependent quantity, and thus we have no guarantee that the system is Liouville integrable. In fact there exists a third integral, but its construction is nontrivial, and will be discussed in the next section.

The fact that p_ϕ is constant allows us to solve fully for the motion in ϕ to get

$$\phi(t) = p_\phi t + \phi_0, \quad (5.3.8)$$

where ϕ_0 is a constant. The system (5.3.7a-f) can be simplified further by noting that p_z is simply $p_z = \kappa t + p_{z_0}$, and thus

$$\dot{z} = \kappa t + p_{z_0} + \frac{\rho^2}{2}, \quad (5.3.9)$$

or, alternatively, we can use the fact that H is constant to solve for z explicitly:

$$z(t) = \frac{1}{2\kappa} \left[p_\rho^2 + \frac{p_\phi^2}{\rho^2} + \kappa^2 t^2 + 2p_{z_0} \kappa t + p_{z_0}^2 + \frac{\rho^2}{2} (p_{z_0} + \kappa t) + \frac{\rho^4}{4} - 2H \right]. \quad (5.3.10)$$

From (5.3.8) and (5.3.10), we see that the root dynamics of the system are in the ρ -motion, which is described by (5.3.7a,b). Using (5.3.7a) to substitute for p_ρ in (5.3.7b), we get a second order ODE for the radial motion

$$\frac{d^2 \rho}{dt^2} = \frac{p_\phi^2}{\rho^3} - \rho(\kappa t + p_{z_0}) - \frac{\rho^3}{2}. \quad (5.3.11)$$

As we have seen repeatedly during the past three sections, (5.3.11) can be simplified further by introducing a translated time variable $\tau = t + p_{z_0}/\kappa$. This transforms the above equation into

$$\frac{d^2 \rho}{d\tau^2} = \frac{p_\phi^2}{\rho^3} - \kappa\tau\rho - \frac{\rho^3}{2}. \quad (5.3.12)$$

We will call equation (5.3.12) the *radial equation*. This equation possesses many interesting features, the first of which is the fact that (5.3.12) possesses the Painlevé property, which is demonstrated in Appendix Three. Recalling the Painlevé conjecture, we have strong reason to believe that (5.3.12) is analytically integrable. Since this is a second order ODE which passes the Painlevé property test, it must fit into Painlevé's classification scheme. Following Ince [49], the radial equation may be put into standard form via the transformation $\rho = \sqrt{\xi}$, which puts (5.3.12) into the form

$$\frac{d^2 \xi}{dt^2} = \frac{1}{2\xi} \left(\frac{d\xi}{dt} \right)^2 + \frac{2p_\phi}{\xi} - 2\kappa\tau\xi - \xi^2. \quad (5.3.13)$$

The second step in this process is the application of the scaling transformation

$$\xi = \alpha\Xi \quad \text{and} \quad \tau = \beta T,$$

where $\alpha = \pm 2ip_\phi / \sqrt[3]{2\kappa}$ and $\beta = (2\kappa)^{-1/3}$, and defining the constant $\gamma = -\alpha\beta^2$ puts the radial equation into standard form:

$$\frac{d^2 \Xi}{dT^2} = \frac{1}{2\Xi} \left(\frac{d\Xi}{dT} \right)^2 + \frac{2p_\phi}{\xi} + 4\gamma\Xi - T\Xi - \frac{1}{2\Xi}. \quad (5.3.14)$$

This new equation is one of the fifty integrable classes of second order ODE's outlined by Painlevé. In fact it is standard form number XXXIV on page 340 of reference [43]. Note that if we set $p_\phi = 0$, we get the second Painlevé transcendent

(5.2.9). For $p_\phi \neq 0$, (5.3.14) has solutions given by

$$\Xi(T) = \frac{1}{2\gamma} \left[\frac{d\mathcal{P}_2}{dT} + \mathcal{P}_2^2 + \frac{1}{2}T \right], \quad (5.3.15)$$

where the function $\mathcal{P}_2(T)$ is the second Painlevé transcendent, which is the solution to equation (5.2.9). As we mentioned in the previous section, the second Painlevé transcendent is an integrable Hamiltonian system, and thus we are able to determine the third integral of the motion. The process of determining the integrals of the motion will be discussed in greater detail in § 5.4. It is interesting to note that an attempt was made to determine the the missing integral for (5.3.12) using direct methods, but no invariant that is a polynomial in the phase space variables was found [72].

The radial equation (5.3.12) exhibits interesting asymptotic behavior in three different asymptotic régimes: **I** $\epsilon > 0, \tau \rightarrow \infty$, **II** $\epsilon < 0, \tau \rightarrow \infty$, and $\tau \rightarrow 0$.

Régime I: If the parameter ϵ is positive, the $\mathbf{E} \times \mathbf{B}$ drift is directed inward, thus the system will tend to focus a charged particle in toward the neutral line, and as τ gets large, ρ shrinks, so we may neglect the $\mathcal{O}(\rho^3)$ term in (5.3.12), and we get an asymptotic form for the radial equation:

$$\frac{d^2\rho}{d\tau^2} - \frac{p_\phi^2}{\rho^3} + \kappa\rho\tau = 0.$$

If we make the assumption that

$$\left| \frac{1}{\rho} \frac{d\rho}{d\tau} \right| \gg 1, \quad (5.3.17)$$

then this equation has solutions with leading order behavior of the form:

$$\rho(\tau) = \sqrt{\frac{A + B \cos(\omega\tau^{3/2} + C)}{\sqrt{\tau}}},$$

where A , B , C , and ω are constants. A typical numerical ρ phase-space trajectory for this case with $\kappa = 0.01$ and $p_\phi = 1.0$ is shown in Figures 5.3.1. This plot suggests strongly that there is an invariant associated with the ρ -motion. Once again, it is possible to define an action J_ρ for the radial motion, using the same approach as we did in deriving J_x in the previous section:

$$\begin{aligned} J_\rho &= \oint p_\rho d\rho \\ &= \int_{t=t_0}^{t=t_0+T} p_\rho^2 dt. \end{aligned} \tag{5.2.17}$$

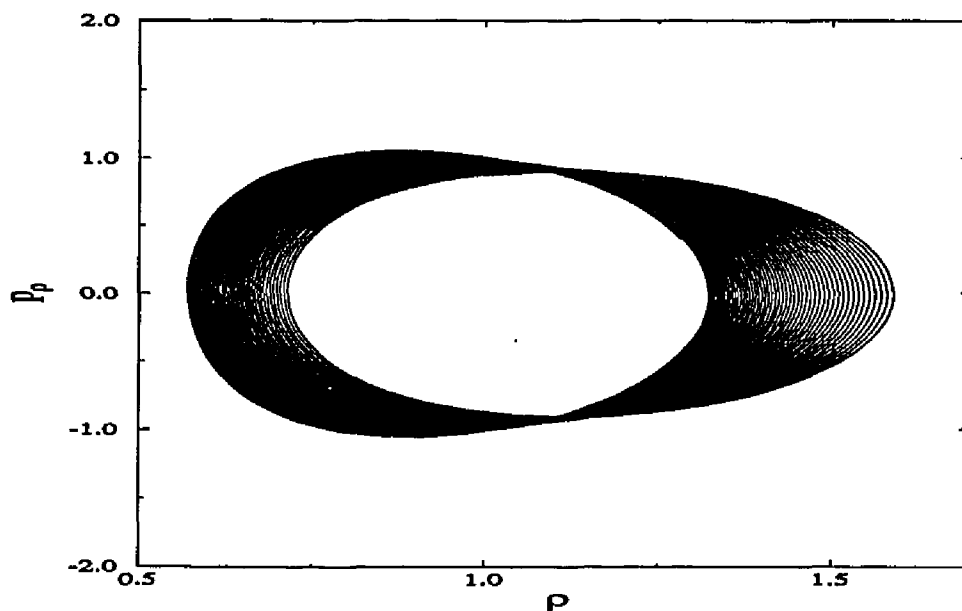


Figure 5.3.1. A Typical ρ -Phase Space Trajectory ($\epsilon > 0$).

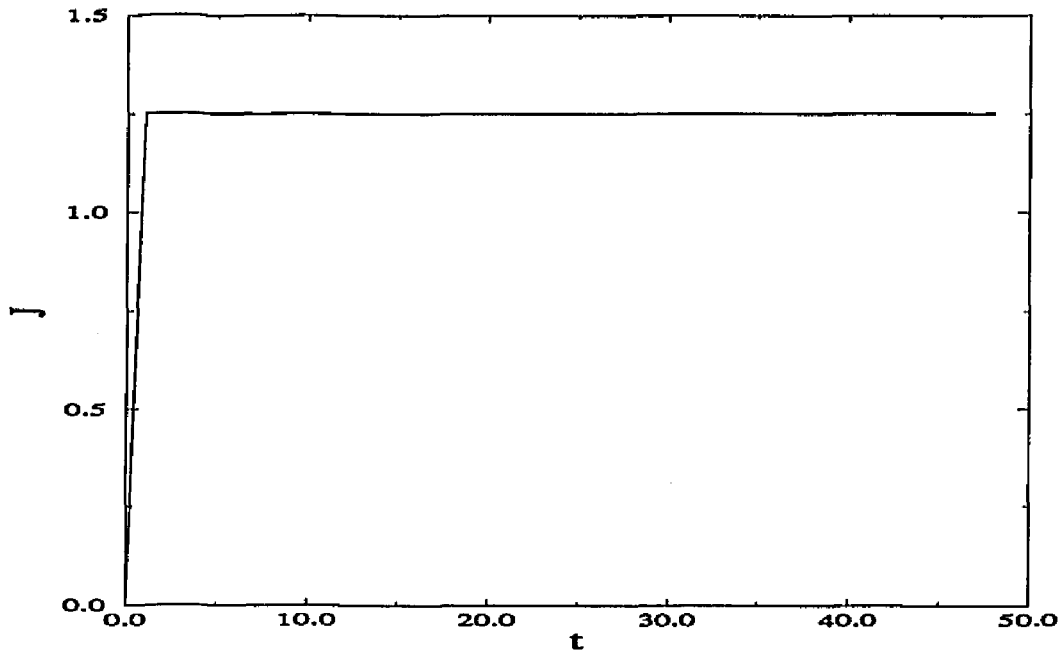


Figure 5.3.2. Radial Action integral J_ρ vs. Time ($\epsilon > 0$).

Régime II: Another possibility is that ϵ is negative. This field configuration will have an $\mathbf{E} \times \mathbf{B}$ drift that is directed away from the neutral line, leading to defocusing of the charged particles. As the system evolves, the value of ρ will increase, meaning that as long as the WKB condition (5.3.16) holds, we can ignore the ρ^{-3} term in (5.3.12), leaving us with

$$\frac{d^2 \rho}{d\tau^2} + \kappa \rho \tau + \frac{\rho^3}{2} = 0. \quad (5.3.18)$$

The above equation has asymptotic solutions of the form:

$$\rho(\tau) = \sqrt{\frac{A[\text{sn}(b(\tau)|m) - D]}{[\text{sn}(b(\tau)|m) - E]}},$$

where A, m, D , and E are constants.

Régime III: This is the zero-electric-field régime, but is also the case when we have $\tau = 0$, or, in terms of our previous time coordinate t' , the case of $t' = -p_{z_0}/\kappa$.

Taking this limit reduces (5.3.12) to

$$\frac{d^2 \rho}{d\tau^2} = \frac{p\phi^2}{\rho^3} - \frac{\rho^3}{2}. \quad (5.3.19)$$

Once again, the asymptotic solution to the radial equation in this limit will be in terms of Jacobi elliptic functions.

§5.4 More About the Second Painlevé Transcendent

As we have seen in § 5.2 and § 5.3, the second Painlevé transcendent plays a central role in understanding the dynamics in the neutral sheet and circular O-line field configurations. The actual method for solving this equation is quite complicated, and is similar to the method of *inverse scattering theory* (IST) [73-75]. Our goal in this section is not the actual construction of the solutions to (5.2.9) and (5.3.12), but rather to summarize the method by which the second Painlevé transcendent may be solved, as well as the identification of the “missing integral” for the neutral sheet problem, and an explanation of how we may be able to identify the third integral for the circular O-line configuration.

Recall that the second Painlevé transcendent is

$$\frac{d^2 q}{ds^2} = 2q^3 + sq - \nu, \quad (5.4.1)$$

where ν is a constant parameter. This equation can be shown to be the compatibility condition for a pair of linear operators, which in the vernacular of IST, are called the *Lax pair*, or *scattering problem*:

$$\frac{\partial}{\partial \zeta} \begin{pmatrix} V_1 \\ V_2 \end{pmatrix} = \mathcal{L} \begin{pmatrix} V_1 \\ V_2 \end{pmatrix} = \begin{pmatrix} -4i\zeta^2 - i(s + 2q^2) & 4\zeta q + \frac{\nu}{\zeta} + 2ir \\ 4\zeta q + \frac{\nu}{\zeta} - 2ir & 4i\zeta^2 + i(s + 2q^2) \end{pmatrix} \begin{pmatrix} V_1 \\ V_2 \end{pmatrix} \quad (5.4.2a)$$

$$\frac{\partial}{\partial s} \begin{pmatrix} V_1 \\ V_2 \end{pmatrix} = \mathcal{M} \begin{pmatrix} V_1 \\ V_2 \end{pmatrix} = \begin{pmatrix} -i\zeta & q \\ q & i\zeta \end{pmatrix} \begin{pmatrix} V_1 \\ V_2 \end{pmatrix}, \quad (5.4.2b)$$

where $r = \partial q / \partial s$. There exist solutions to this pair of equations as long the mixed partial derivatives of $V = (V_1, V_2)^T$ are equal, that is

$$\frac{\partial^2 V_1}{\partial \zeta \partial s} = \frac{\partial^2 V_1}{\partial s \partial \zeta}, \quad \text{etcetera.}$$

This leads to the compatibility condition for \mathcal{L} and \mathcal{M} , i.e. the operator equation

$$[\mathcal{L}, \mathcal{M}] = \frac{\partial \mathcal{L}}{\partial s} - \frac{\partial \mathcal{M}}{\partial \zeta}, \quad (5.4.3)$$

where $[\mathcal{L}, \mathcal{M}]$ is the ordinary matrix commutator. The above condition is equivalent to (5.4.1).

It is known from IST that the existence of a Lax pair (5.4.2) implies that the second Painlevé transcendent (5.4.1) is integrable in the Liouville sense. The actual technique for solving a differential equation using IST involves solving the scattering problem (in which the solution q to the differential equation plays the role of the potential) for its eigenvalue spectrum, which are called the *scattering data*. The evolution of these scattering data is followed in spectral space. Finally, an inverse transformation is performed to solve for the potential [73].

In the case of the second Painlevé transcendent, our scattering data arise in a slightly different fashion, and are related to the asymptotic behavior of the solutions to (5.4.2a). The two linearly independent WKB solutions $\psi^{(1)}(\zeta, s)$ and $\psi^{(2)}(\zeta, s)$ to the Lax pair (5.4.2a) have the following exponential behavior in the limit $\zeta \rightarrow \infty$:

$$\psi^{(1)}(\zeta, s) \sim \exp \left[\frac{4i\zeta^3}{3} + is\zeta \right] \quad (5.4.4a)$$

$$\psi^{(2)}(\zeta, s) \sim \exp\left[-\frac{4i\zeta^3}{3} - is\zeta\right]. \quad (5.4.4b)$$

In the limit $\zeta \rightarrow \infty$, the solutions $\psi^{(1)}$ and $\psi^{(2)}$ will display *Stokes phenomenon*; i.e. the general solution to the scattering problem will be dominated strongly by one of the individual solutions $\psi^{(1)}$ or $\psi^{(2)}$. This will lead to the division of the complex plane into six sectors in this region, with the leading edge of each section defined by

$$S_j = \left\{ \zeta : |\zeta| > \rho, \frac{(j-1)\pi}{3} \leq \arg(\zeta) < \frac{j\pi}{3} \right\},$$

where ρ is taken as given. The initial lines of the sectors are called the *anti-Stokes lines*, while the lines on which the asymptotic solutions given in (5.4.2a,b) maximally dominant or recessive are called the *Stokes lines*, with the Stokes line in the j^{th} sector defined by the argument values

$$\arg(\zeta) = \frac{(2j+1)\pi}{6}.$$

In sectors S_1 , S_3 , and S_5 , $\tilde{\psi}^{(1)}$ is the dominant solution to (5.4.2), while $\tilde{\psi}^{(2)}$ is dominant in sectors S_2 , S_4 , and S_6 . The sectoring of the complex ζ - plane near $\zeta = \infty$ is shown in Figure 5.4.1.

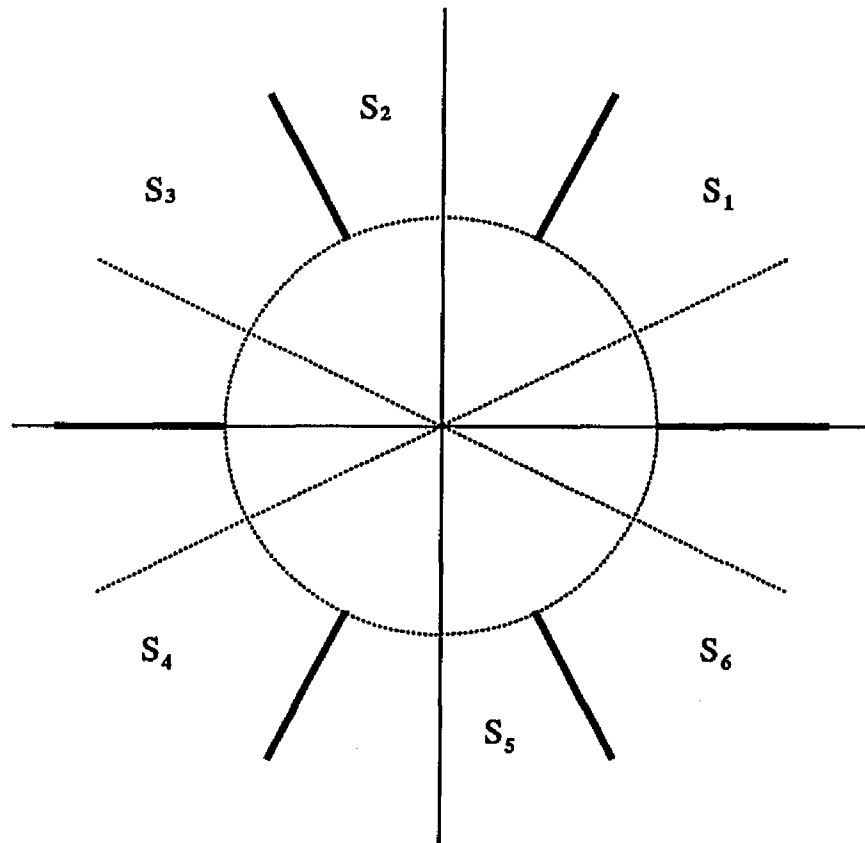


Figure 5.4.1. Sectoring of the Complex ζ -Plane Near $\zeta = \infty$.

The anti-Stokes lines delineate the borders between regions in which $\tilde{\psi}^{(1)}$ and $\tilde{\psi}^{(2)}$ exchange roles as the dominant/recessive asymptotic solutions to (5.4.2a). If we start with an asymptotic solution in one region, and wish to extend it analytically into another region, we will find that this extension is not the same as an asymptotic solution that is computed locally in that region. One way to cast light onto the transformation properties of the asymptotic expansions is to introduce the fundamental matrix solution Ψ_j , which has as its columns the local solutions $\psi_j^{(1)}$ and $\psi_j^{(2)}$, where the subscript j indicates the sector with which the solution is

associated.

$$\Psi_j \equiv \{\psi_j^{(1)}, \psi_j^{(2)}\} \sim \{\tilde{\psi}_j^{(1)}, \tilde{\psi}_j^{(2)}\}. \quad (5.4.5)$$

The relationship between two neighboring asymptotic expansions, say Ψ_j and Ψ_{j+1} can be expressed as a matrix product

$$\Psi_{j+1} = A_j \Psi_j, \quad (5.4.6)$$

where the matrices A_j are called the *Stokes multiplier matrices*. The Stokes matrices are triangular,

$$A_1 = \begin{pmatrix} 1 & 0 \\ a & 1 \end{pmatrix} = A_4^T \quad (5.4.7a)$$

$$A_2 = \begin{pmatrix} 1 & b \\ 0 & 1 \end{pmatrix} = A_5^T \quad (5.4.7b)$$

$$A_3 = \begin{pmatrix} 1 & 0 \\ c & 1 \end{pmatrix} = A_6^T, \quad (5.4.7c)$$

and their nontrivial entries a , b , and c are called the *Stokes multipliers*. These three quantities a , b , and c , satisfy the relation [70]

$$a + b + c + abc = 2i \sin(\nu\pi), \quad (5.4.8)$$

thus only two of them are independent. The transform data are independent of s , and it can be shown [70] that any two of the Stokes parameters $\{a, b, c\}$ can be used to generate all of the transform data. This implies that the second Painlevé transcendent is a Liouville integrable system in an extended phase space whose coordinates are q and s , and has a canonical time σ , i.e.

$$q_1 \equiv q \quad q_2 \equiv s \quad (5.4.9a)$$

$$p_1 \equiv \frac{dq}{ds} \quad p_2 = -H, \quad (5.4.9b)$$

where

$$H \equiv \frac{1}{2}(p^2 + sq^2) - \nu q, \quad (5.4.9c)$$

is the Hamiltonian for Painlevé II. The extended phase-space Hamiltonian \mathcal{H} associated with (5.4.8) is

$$\mathcal{H} = \frac{1}{2}(p_1^2 + q_2 q_1^2) - \nu q_1 + p_2 \quad (5.4.10)$$

The extended phase-space Hamiltonian \mathcal{H} is a conserved quantity, and the actual evolution of the Painlevé II system occurs on the submanifold $\mathcal{H} = 0$. The Stokes data are related to this Hamiltonian, and one of the Stokes parameters, say a , along with \mathcal{H} are the two integrals for the Hamiltonian system (5.4.9-10), and in particular,

$$\{a, \mathcal{H}\} = 0,$$

meaning that (5.4.9-10) is an integrable Hamiltonian system in the Liouville sense.

Recall that the growth or decay rate of q as $\zeta \rightarrow \pm\infty$ is governed by the exponential factor $e^{\pm 4i\zeta^3/3}$. In the neighborhood of $\zeta = \infty$, the ζ part of the scattering problem has two linearly independent solutions with asymptotic expansions given by

$$\psi^{(1)}(\zeta, s) \sim \tilde{\psi}^{(1)} = e^{-\frac{4i\zeta^3}{3} - i\zeta s} \left(1 - \frac{i}{2\zeta}(q_s^2 - sq^2 - q^4 + 2\nu q) + \dots \right) \quad (5.4.11a)$$

$$\psi^{(2)}(\zeta, s) \sim \tilde{\psi}^{(2)} = e^{\frac{4i\zeta^3}{3} + i\zeta s} \left(1 + \frac{i}{2\zeta}(q_s^2 - sq^2 - q^4 + 2\nu q) + \dots \right). \quad (5.4.11b)$$

The actual determination of the solution $q(s)$ is accomplished by relating the Stokes data a and b to q via the inverse problem. Flaschka and Newell have

solved the scattering problem by using a technique developed by Birkhoff [76] to recast the differential equations in (5.4.2) as singular integral equations that involve the Stokes parameters explicitly. In particular,

$$\begin{aligned} \psi^{(1)}(\zeta)e^{\theta(\zeta)} &= \begin{pmatrix} 1 \\ 0 \end{pmatrix} - \text{Res}\left(\frac{\psi^{(1)}e^{\theta(\xi)}}{\xi - \zeta}, \xi = 0\right) + \frac{a}{2\pi i} \int_{C_{42}} \frac{\psi^{(2)}e^{\theta}}{\xi - \zeta} \\ &\quad + \frac{b}{2\pi i} \int_{C_{46}} \frac{\psi^{(2)}e^{\theta}}{\xi - \zeta} + \frac{bc}{2\pi i} \int_{C_{64}} \frac{\psi^{(1)}e^{\theta}}{\xi - \zeta} \end{aligned} \quad (5.4.12a)$$

and

$$\begin{aligned} \psi^{(2)}(\zeta)e^{-\theta(\zeta)} &= \begin{pmatrix} 0 \\ 1 \end{pmatrix} - \text{Res}\left(\frac{\psi^{(2)}e^{-\theta(\xi)}}{\xi - \zeta}, \xi = 0\right) + \frac{b}{2\pi i} \int_{C_{53}} \frac{\psi^{(1)}e^{-\theta}}{\xi - \zeta} \\ &\quad + \frac{c}{2\pi i} \int_{C_{51}} \frac{\psi^{(1)}e^{-\theta}}{\xi - \zeta} + \frac{ab}{2\pi i} \int_{C_{53}} \frac{\psi^{(2)}e^{-\theta}}{\xi - \zeta} \end{aligned} \quad (5.4.12b)$$

The contours along which the integrations in (5.4.12a,b) are performed appear in Figure 5.4.2; e.g. C_{46} approaches $\zeta = \infty$ along C_4 , travels from C_4 to C_6 , counter-clockwise along the contours γ_4 and γ_5 , and then exits from the singular region along C_6 .

These equations are linear integral equations for $\psi^{(1)}$ and $\psi^{(2)}$. Recalling our asymptotic solutions $\psi^{(1)}$ and $\psi^{(2)}$ from (5.4.11a,b), it is possible to solve for the potential $q(s)$:

$$\begin{aligned} q(s) &= 2i \lim_{\zeta \rightarrow \infty} \zeta \psi^{(2)}_1 e^{-\theta} \\ &= -2i \lim_{\zeta \rightarrow \infty} \zeta \psi^{(1)}_2 e^{\theta}. \end{aligned} \quad (5.4.13)$$

Given this value of $q(s)$, we may use the other components $\psi^{(1)}_1$ and $\psi^{(2)}_2$ to determine q_s , thus we can solve the initial value problem associated with the second Painlevé transcendent in terms of the Stokes multipliers.

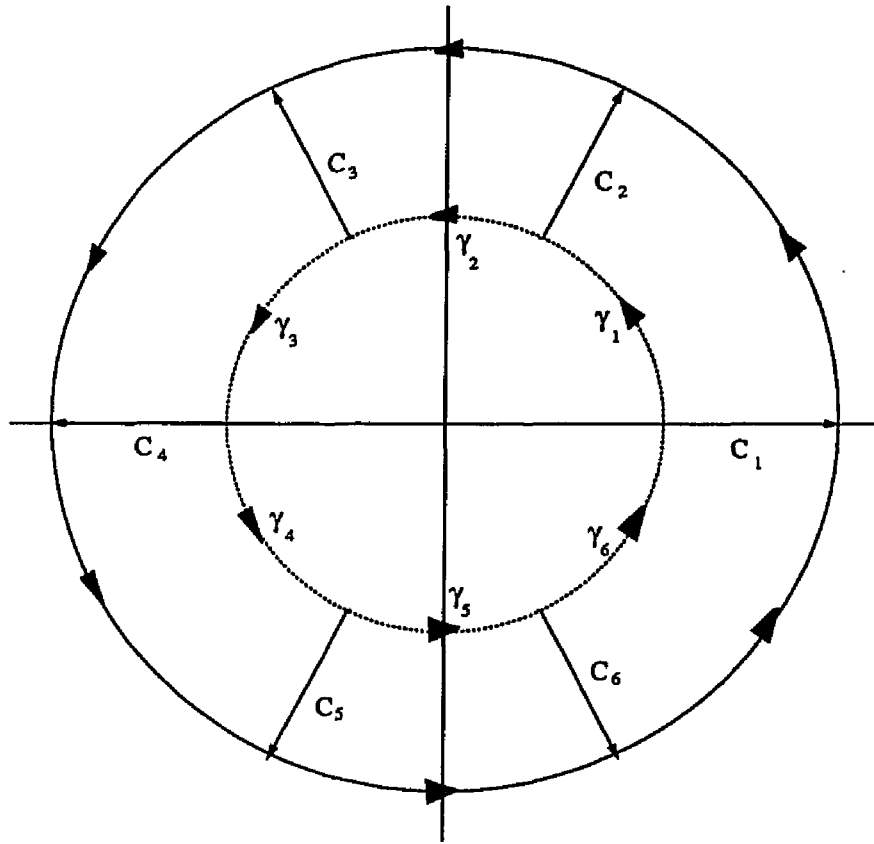


Figure 5.4.2. Contours for the Inverse Problem.

The argument given above demonstrates that the second Painlevé transcendent and members of the Painlevé II family (which includes the radial equation (5.3.12)), is an integrable dynamical system in the Liouville sense. The independent Stokes parameters a and b are functions of the phase space coordinates, and are the integrals of the system. The exact dependence of these quantities on the phase space coordinates is not clear, and will be the subject of further study. We have already explored the asymptotic régime $q(s) \rightarrow 0$ as $s \rightarrow \infty$, which lead us to asymptotic solutions to the transcendent in terms of Airy functions. This was done in §5.2. There are other well-known special cases in which asymptotic solutions to Painlevé

If have been derived, the most straightforward of these is the *linear limit*.

The Linear Limit

Let $\nu = 0$ (which is precisely the case for the x -motion in the neutral sheet configuration), and furthermore, let the Stokes parameters a , b , and c all be small.

In this case, we can linearize (5.4.12a) in terms of the Stokes data, and $\psi^{(1)}$ becomes

$$\psi^{(1)}e^\theta = \begin{pmatrix} 0 \\ 1 \end{pmatrix} + \frac{a}{2\pi i} \begin{pmatrix} 1 \\ 0 \end{pmatrix} \int_{C_{42}} \frac{e^{2\theta(\xi)} d\xi}{\xi - \zeta} + \frac{b}{2\pi i} \begin{pmatrix} 0 \\ 1 \end{pmatrix} \int_{C_{46}} \frac{e^{2\theta(\xi)} d\xi}{\xi - \zeta}. \quad (5.4.14)$$

From (5.4.13) we have

$$\begin{aligned} q &= \frac{a}{\pi} \int_{C_{42}} \exp\left(\frac{8i\zeta^3}{3} + 2i\zeta s\right) ds + \frac{b}{\pi} \int_{C_{46}} \exp\left(\frac{8i\xi^3}{3} + 2i\xi s\right) d\xi \\ &= \left(a + \frac{b}{2}\right) \text{Ai}(s) - \frac{ib}{2} \text{Bi}(s). \end{aligned} \quad (5.4.15)$$

Setting $\nu = 0$, and linearizing the condition (5.4.8) yields the following restriction on the Stokes parameters:

$$a + b + c = 0.$$

If we require $q(s)$ to be real, we get $c = -a^*$, $b = a^* - a$. Such constraints on spectral data are not unusual in the field of IST, and is simply the analogue of the *reality constraint* imposed when solving systems via IST [77]. Employing this constraint, we get

$$q(s) = \text{Re}(a)\text{Ai}(s) + i \text{Im}(a)\text{Bi}(s). \quad (5.4.16)$$

The above solution (5.4.16) is merely the *leading-order* solution in the linear limit. Higher-order corrections to (5.4.16) may be determined by constructing the von Neumann series for the transcendent, which is a procedure analogous to the Born approximation in quantum mechanics. This is beyond the scope of the current discussion, and will be the subject of future work.

§5.5 Exact Solutions to the Kinetic Equation

Given the fact that we are able to find integrals to the test particle equations of motion for the neutral sheet and circular O-line configurations, it is likely that we will be able to find exact solutions to the collisionless kinetic equation

$$\frac{\partial f}{\partial t} + \dot{\mathbf{q}} \cdot \frac{\partial f}{\partial \mathbf{q}} + \dot{\mathbf{p}} \cdot \frac{\partial f}{\partial \mathbf{p}} = 0. \quad (5.5.1)$$

As we saw in the previous section, the x -motion for the neutral sheet configuration is integrable in terms of the second Painlevé transcendent, and is integrable in the Hamiltonian sense in an extended phase space which includes the time t as one of its canonical coordinates. The radial motion for the circular O-line is also solvable in terms of the second Painlevé transcendent, but its Hamiltonian structure is more complicated. Thus, we shall concentrate on how one may solve (5.5.1) for the neutral sheet configuration.

In the eight-dimensional extended phase space for the slab configuration, we have the canonical coordinates $\{x, y, z, t, p_x, p_y, p_z, -H\}$, where H is the Hamiltonian defined in (5.2.2) and s is the canonical time in the extended phase space. The constants of the motion for this system are the extended phase space \mathcal{H} , p_y , the initial z -momentum $p_{z_0} = p_z - \kappa t$, and the Stokes data a . Since the slab configuration forms a Liouville integrable system in the extended phase space, a special class of solutions to (5.5.1) \mathcal{F} are completely determined in that \mathcal{F} is an arbitrary function of the constants of the motion:

$$\mathcal{F} = \mathcal{F}(\mathcal{H}, p_y, p_{z_0}, a). \quad (5.5.2)$$

The solutions described by (5.5.2) are *equilibrium solutions* to the kinetic equation in the eight-dimensional extended phase space described above. The *physical* evolution of the system takes place on the six-dimensional submanifold of the extended phase-space corresponding to $\mathcal{H} = 0$. It is possible to obtain solutions to the physical kinetic equation (5.5.1) by projecting the equilibrium solutions $\mathcal{F}(\mathcal{H}, p_y, p_{z_0}, a)$ that lie in the extended eight-dimensional phase space down to the six-dimensional physical phase space via a procedure similar to that used in wave-kinetic theory [78,79]. This procedure will be carried out in future work, and is beyond the scope of the present discussion. The important thing to note is that this reduction procedure will produce *exact* time-dependent solutions to (5.5.1).

APPENDIX ONE

**DETERMINATION OF THE LEADING-
ORDER BEHAVIORS FOR (3.2.2a-c)**

Consider the system of equations (3.2.2a-c), which contain all the information about the singularity structure of (3.1.4a-f)

$$\alpha_z \beta_z \tau^{\beta_z - 1} = p_{z_0} + \kappa \tau + \frac{1}{2} \alpha_x^2 \tau^{2\beta_x} - \frac{1}{2} \delta \alpha_y^2 \tau^{2\beta_y} \quad (A1.1a)$$

$$\beta_x (\beta_x - 1) \tau^{-2} = -(\kappa \tau + p_{z_0}) + \frac{1}{2} \delta \alpha_y^2 \tau^{2\beta_y} - \frac{1}{2} \alpha_x^2 \tau^{2\beta_x} \quad (A1.1b)$$

$$\beta_y (\beta_y - 1) \tau^{-2} = (\kappa \tau + p_{z_0}) + \frac{1}{2} \delta \alpha_x^2 \tau^{2\beta_x} - \frac{1}{2} \delta^2 \alpha_y^2 \tau^{2\beta_y} \quad (A1.1c)$$

It is now necessary to test *every* possible leading order behavior for the set of equations (A1.1a-c). Upon examining (A1.1a-c), it becomes clear that this is not a trivial task. Counting the number of possible leading order balances for the systems itself is something of a task. To this end, we must consider the set (A1.1a-c) one at a time.

Let us begin our search with (A1.1b). We will find that we will have a number of cases that are dependent on the value of p_{z_0} and κ , as well as the value of β_x . Beginning with the assumption that β_x is not zero or one, we must examine the following version of (A1.1b):

$$\beta_x (\beta_x - 1) \tau^{-2} = \frac{1}{2} \delta \alpha_y^2 \tau^{2\beta_y} - \frac{1}{2} \alpha_x^2 \tau^{2\beta_x} \quad (A1.2)$$

This equation has three terms, so the number of possible balances is the sum of the

number of two-term balances plus the one three-term balance:

$$\text{Number of possible balances} = \binom{3}{2} + \binom{3}{3} = 4,$$

where the notation $\binom{n}{m}$ is simply the binomial coefficient, which determines the number of possible combinations of n objects, taken m at a time:

$$\binom{n}{m} = \frac{n!}{m!(n-m)!}.$$

(A1.2) has the following cases associated with it:

Case B1: $\beta_x = -1$ and $\beta_y > -1$. Then

$$\beta_x(\beta_x - 1) = -\frac{\alpha_x^2}{2}.$$

Case B2: $\beta_y = -1$ and $\beta_x > -1$. Then

$$\beta_x(\beta_x - 1) = \frac{\delta}{2}\alpha_y^2.$$

Case B3: $\beta_x = \beta_y$ and $\beta_x < -1$. Then

$$\alpha_y = \pm \frac{\alpha_x}{\sqrt{\delta}}.$$

Case B4: $\beta_x = \beta_y = -1$. Then

$$\alpha_y = \pm \sqrt{\frac{4 + \alpha_x^2}{\delta}}.$$

Now suppose that $\beta_x = 0$. Then (A1.2) becomes

$$-p_{z0} - \frac{1}{2}\alpha_x^2 + \frac{1}{2}\delta\alpha_y^2\tau^2\beta_y = 0. \quad (\text{A1.3})$$

If the $\mathcal{O}(1)$ term is nonzero, i.e. $\alpha_x^2 \neq -2p_{z0}$, there is only one possible balance, namely

Case B5: $\beta_y = 0$, $\beta_x = 0$ and $\alpha_x^2 \neq -2p_{z0}$. Then α_x and α_y satisfy

$$\alpha_y = \pm \sqrt{\frac{2p_{z0} + \alpha_x^2}{\delta}}.$$

If the $\mathcal{O}(1)$ term in (A1.2) is in fact zero, we must include the subdominant electric field term, and (A1.2) becomes

$$-\kappa\tau + \frac{1}{2}\delta\alpha_y^2\tau^{2\beta_y} = 0. \quad (\text{A1.4})$$

Clearly, there exists only one dominant balance for this situation:

Case B6: $\beta_y = \frac{1}{2}$, and

$$\alpha_y = \pm \sqrt{\frac{2\kappa}{\delta}}.$$

Next, suppose that $\beta_x = 1$. This causes the LHS term in (A1.1b) to vanish, leaving us with

$$-(\kappa\tau + p_{z0}) + \frac{1}{2}\delta\alpha_y^2\tau^{2\beta_y} - \frac{1}{2}\alpha_x^2\tau^2 = 0. \quad (\text{A1.5})$$

Yet again we must consider the values of various parameters as we search for the balances of this equation. If the initial z -momentum, p_{z0} is nonzero, the leading order in the above equation is $\mathcal{O}(1)$, and we have

Case B7: $p_{z0} \neq 0$, $\beta_y = 0$, and

$$\alpha_y = \pm \sqrt{\frac{2p_{z0}}{\delta}}.$$

If the initial z -momentum is zero, but the electric field is nonzero, then the leading order balance is at $\mathcal{O}(\tau)$:

Case B8: $p_{z0} = 0$, $\kappa \neq 0$, and $\beta_y = \frac{1}{2}$. Then

$$\alpha_y = \pm \sqrt{\frac{2\kappa}{\delta}}.$$

Finally, there is the case that both the initial z -momentum and electric field are zero:

Case B9: $p_{z0} = 0$, $\kappa = 0$, and $\beta_y = 1$. Then

$$\alpha_y = \pm \sqrt{\frac{\alpha_x}{\delta}}.$$

Finally, we must examine the possible balances present in (A1.1c). Again, we will find that we will have a number of cases that depend on specific values of p_{z0} and κ , as well as the value of β_y . We will begin with the assumption that β_y is not zero or one. Then we must examine the following version of (A1.1c) for $p_{z0} \neq 0$, which will have an $\mathcal{O}(\tau^{-2})$ present:

$$\beta_y(\beta_y - 1)\tau^{-2} = \frac{1}{2}\delta\alpha_x^2\tau^{2\beta_x} - \frac{1}{2}\delta^2\alpha_y^2\tau^{2\beta_y}. \quad (\text{A1.6})$$

Yet again, this equation will have three two-term balances and one three-term balance associated with it. These cases are the following:

Case C1: $\beta_x = -1$ and $\beta_y > -1$. Then

$$\beta_y(\beta_y - 1) = \frac{\delta}{2}\alpha_x^2.$$

Case C2: $\beta_y = -1$ and $\beta_x > -1$. Then

$$\alpha_y^2 = \frac{-4}{\delta^2}.$$

Case C3: $\beta_x = \beta_y$ and $\beta_y < -1$. Then

$$\alpha_y = \pm \frac{\alpha_x}{\sqrt{\delta}}.$$

Case C4: $\beta_x = \beta_y = -1$. Then

$$\alpha_x = \pm \sqrt{\frac{4 + \delta^2 \alpha_y^2}{\delta}}.$$

Now suppose that $\beta_y = 0$, which will cause the $\mathcal{O}(\tau^{-2})$ term to vanish. There will be an $\mathcal{O}(1)$ term present in the balances, and as long as this term is nonzero, i.e. $\alpha_y^2 \neq \frac{2p_{z0}}{\delta^2}$, (A1.6) becomes

$$p_{z0} + \frac{1}{2}\delta\alpha_x^2\tau^{2\beta_x} - \frac{1}{2}\delta^2\alpha_y^2 = 0. \quad (\text{A1.7})$$

This situation leads to only one possible balance:

Case C5: $\beta_y = 0$, $\beta_x = 0$ and $\alpha_y^2 \neq \frac{2p_{z0}}{\delta^2}$. Then α_x and α_y satisfy

$$\alpha_y = \pm \frac{1}{\delta} \sqrt{\delta\alpha_x^2 + 2p_{z0}}.$$

If the $\mathcal{O}(1)$ term in (A1.7) is in fact zero, we must include the subdominant electric field term, and (A1.7) becomes

$$\kappa\tau + \frac{1}{2}\delta\alpha_x^2\tau^{2\beta_x} - \frac{1}{2}\delta^2\alpha_y^2 = 0. \quad (\text{A1.8})$$

Clearly, there exists only one dominant balance for this situation:

Case C6: $\beta_x = \frac{1}{2}$, and

$$\alpha_x^2 = -\frac{2\kappa}{\delta}.$$

Next, suppose that $\beta_y = 1$. This also causes the LHS term in (A1.1b) to vanish, but also introduces an $\mathcal{O}(\tau^2)$ term, leaving us with

$$p_{z0} + \kappa\tau + \frac{1}{2}\delta\alpha_x^2\tau^{2\beta_x} - \frac{1}{2}\delta^2\alpha_y^2\tau^2 = 0. \quad (\text{A1.9})$$

Yet again we must consider the values of various parameters as we search for the balances of this equation. If the Initial z -momentum, p_{z0} is nonzero, the leading order in the above equation is $\mathcal{O}(1)$, and we have

Case C7: $p_{z0} \neq 0$, $\beta_x = 0$, and

$$\alpha_x^2 = -\frac{2p_{z0}}{\delta}.$$

If the initial z -momentum is zero, but the electric field is nonzero, then the leading order balance is at $\mathcal{O}(\tau)$:

Case C8: $p_{z0} = 0$, $\kappa \neq 0$, and $\beta_x = \frac{1}{2}$. Then

$$\alpha_x^2 = -\frac{2\kappa}{\delta}.$$

Finally, there is the case that both the initial z -momentum and electric field are zero:

Case C9: $p_{z0} = 0$, $\kappa = 0$, and $\beta_x = 1$. Then

$$\alpha_y = \pm\sqrt{\frac{\alpha_x}{\delta}}.$$

Now that we have determined all of the possible leading-order-behaviors for the individual equations, we must determine which combinations of these possibilities will lead to a viable leading order behavior for the system as a whole. The testing

of these candidate balances has to be done carefully and systematically. Note that we have a total of $35 \times 9 \times 9 = 2835$ possible combinations of these balances for the system. In order to ensure a thorough examination, we shall record our progress in tabular form via the construction of *Filters*, i.e. a set of tables that evaluate the possible leading order behaviors of two of the above equations with respect to each other. This insures that we explore all of the possible leading-order behaviors associated with the system.

Table A1.1. Filter Comparing (A1.1a) and (A1.1b).

(A1.1b) →	(A1.1c) ↓	B1	B2	B3	B4	B5	B6	B7	B8	B9
		C1		■	■	■	■	■	■	■
C2	■		■	■	■	■	■	■	■	■
C3	■	■		■	■	■	■	■	■	■
C4	■	■	■		■	■	■	■	■	■
C5	■	■	■	■		■	■	■	■	■
C6	■	■	■	■	■	■	■	■	■	■
C7	■	■	■	■	■	■	■	■	■	■
C8	■	■	■	■	■	■	■	■	■	■
C9	■	■	■	■	■	■	■	■	■	

The rows of Filter A1.1 correspond to possible leading-order behaviors of equa-

tion (A1.1b), and its columns are identified the possible dominant balances associated with (A1.1c). The shaded boxes in the filter indicate combinations of cases that contradict each other, while the white regions indicate an agreement between the exponents in the leading-order-behaviors for the two equations.

Clearly there are only six instances in which the equations (A1.1b) and (A1.1c) have leading order behaviors that agree. These cases are:

Case BC1: $\beta_x = -1$ and $\beta_y > -1$. Then (A1.1b) and (A1.1c) become

$$\alpha_x = \pm 2i \quad (\text{A1.10a})$$

$$\beta_y(\beta_y - 1) + 2\delta = 0. \quad (\text{A1.10b})$$

Using these conditions, (A1.1a) becomes

$$\alpha_z \beta_z \tau^{\beta_z - 1} = p_{z0} + \kappa \tau + \frac{\alpha_x^2}{2} \tau^{-2} - \frac{\delta \alpha_y^2}{2} \tau^{2\beta_y}.$$

Since $\beta_y > -1$, we find that $\beta_z = -1$ and $\alpha_z = 2$.

Case BC2: $\beta_y = -1$ and $\beta_x > -1$. Then (A1.1b) and (A1.1c) become

$$\alpha_y = \pm \frac{2i}{\delta} \quad (\text{A1.11a})$$

$$\beta_x(\beta_x - 1) + \frac{2}{\delta} = 0. \quad (\text{A1.11b})$$

Again, substitution of these parameters into (A1.1a) yields a simple relation

$$\alpha_z \beta_z \tau^{\beta_z - 1} = p_{z0} + \kappa \tau + \frac{\alpha_x^2}{2} \tau^{2\beta_x} - \frac{\delta \alpha_y^2}{2} \tau^{-2}.$$

We know that $\beta_x > -1$, thus $\beta_z = -1$ and $\alpha_z = -\frac{2}{\delta}$.

Case BC3: $\beta_y = \beta_x < -1$. Then (A1.1b) and (A1.1c) reduce to the same relation:

$$\alpha_y = \pm \frac{\alpha_x}{\sqrt{\delta}} \quad (\text{A1.12})$$

Upon examination of (A1.1a), we get

$$\alpha_z \beta_z \tau^{\beta_z - 1} = p_{z0} + \kappa \tau + \frac{1}{2}(\alpha_x^2 - \delta \alpha_y^2) \tau^{2\beta_x}.$$

Yet again, the leading order is $\mathcal{O}(\tau^{2\beta_x})$, and we recover (A1.12) if $\beta_z > 2\beta_x + 1$. If $\beta_z = 2\beta_x + 1$, then we must conclude that $\alpha_x = 0$ or $\beta_x = 0$. Since β_x is clearly negative, we have $\alpha_x = 0$, which violates the hypothesis of the ARS algorithm.

Case BC4: $\beta_y = \beta_x = -1$. Then (A1.1b) and (A1.1c) imply

$$\delta \alpha_y^2 - \alpha_x^2 = 4 \quad (\text{A1.13a})$$

$$\delta^2 \alpha_y^2 - \delta \alpha_x^2 = 4, \quad (\text{A1.13b})$$

which are in agreement if and only if $\delta = -1$. Substituting the results of this case into (A1.1a), we get

$$\alpha_z \beta_z \tau^{\beta_z - 1} = p_{z0} + \kappa \tau - 2\tau^{-2}.$$

If $\beta_z = -1$ then $\alpha_z = 2$. If $\beta_z > -1$, then (A1.1a) becomes at leading order

$$0 = \frac{1}{2}(\alpha_x^2 - \delta \alpha_y^2) = 2,$$

which is clearly a contradiction, and we do not get an acceptable leading order behavior for this case.

Case BC5: $\beta_y = \beta_x = 0$, $\alpha_y \neq \pm \frac{\sqrt{2p_{z0}}}{\delta}$, and $\alpha_x \neq \pm i\sqrt{2p_{z0}}$. Then (A1.1b) and (A1.1c) imply

$$\delta\alpha_y^2 - \alpha_x^2 = 2p_{z0} \quad (\text{A1.14a})$$

$$-\delta\alpha_y^2 + \alpha_x^2 = -\frac{2p_{z0}}{\delta}, \quad (\text{A1.14b})$$

which are in agreement if and only if either $\delta = 1$ or $p_{z0} = 0$. If we set $\delta = 1$ in (A1.1a), we get

$$\alpha_z\beta_z\tau^{\beta_z-1} = p_{z0} + \kappa\tau + \frac{1}{2}(\alpha_x^2 - \alpha_y^2).$$

If $\beta_z > 1$, then α_z is arbitrary. If $\beta_z = 1$, however, then $\alpha_z = 0$, and the basic hypothesis of the ARS algorithm is violated.

Setting $p_{z0} = 0$ in (A1.1a) yields

$$\alpha_z\beta_z\tau^{\beta_z-1} = \kappa\tau + \frac{1}{2}(\alpha_x^2 - \delta\alpha_y^2).$$

The leading order balance in this relation is at $\mathcal{O}(1)$. If $\beta_z > 1$, then α_z is arbitrary. If, on the other hand, $\beta_z = 1$, (A1.14a,b) now both imply $\alpha_x^2 - \delta\alpha_y^2 = 0$, and thus $\beta_z = 1$ leads to the conclusion that $\alpha_z = 0$, which again contradicts the ARS algorithm's hypothesis.

Case BC6: $\beta_x = \beta_y = 1$, $p_{z0} = 0$ and $\kappa = 0$. In this situation, (A1.1b) and (A1.1c) reduce to the same relation:

$$\alpha_y = \pm \frac{\alpha_x}{\sqrt{\delta}}. \quad (\text{A1.15})$$

For this case, (A1.1a) becomes

$$\alpha_z\beta_z\tau^{\beta_z-1} = \frac{1}{2}(\alpha_x^2 - \delta\alpha_y^2)\tau^2.$$

If $\beta_z > 3$, then α_z is arbitrary, and we get (A1.15) once again, yielding a viable leading order behavior. If, however, $\beta_z = 3$, then we are forced to conclude that $\alpha_z = 0$, leading to a contradiction with our hypothesis.

Upon examination of the Cases BC1-BC6 and their subcases, we find that there exist six classes of viable leading order behaviors for this system. They are the following:

Class I: $\beta_x = -1, \beta_y > -1, \beta_z = -1$. Then $\alpha_x = \pm 2i$, α_y is arbitrary, $\beta_y(\beta_y - 1) + 2\delta = 0$, and $\alpha_z = 2$.

Class II: $\beta_x > -1, \beta_y = -1, \beta_z = -1$. Then $\alpha_y = \pm \frac{2i}{\delta}$, α_x is arbitrary, $\beta_x(\beta_x - 1) + 2\delta = 0$, and $\alpha_z = -\frac{2}{\delta}$.

Class III: $\beta_x = \beta_y = -1, \beta_z = -1$. Then $\delta = -1$, $\alpha_x = \pm i\sqrt{4 + \alpha_y^2}$, α_y is arbitrary, and $\alpha_z = 2$.

Class IV: $\beta_x = \beta_y < -1, \beta_z = 2\beta_x + 1$. Then $\alpha_x = \pm\sqrt{\delta}\alpha_y$, with both α_y and α_z arbitrary.

Class V: $\beta_x = \beta_y = 0, \beta_z > 1$, with the conditions that $p_{z0} = 0$ or $\delta = 1$. There is also the pair of constraints $\alpha_y \neq \pm\sqrt{\frac{2p_{z0}}{\delta}}$ and $\alpha_x \neq \pm\sqrt{2p_{z0}}$. Then $\beta_z > 1$, $\alpha_x = \pm\sqrt{2p_{z0} + \alpha_y^2}$, with both α_y and α_z arbitrary.

Class VI: $\beta_x = \beta_y = 1, \beta_z > 3$, with the conditions $p_{z0} = 0$ and $\kappa = 0$. Then $\alpha_x = \pm\sqrt{\delta}\alpha_y$ and both α_y and α_z arbitrary.

APPENDIX TWO
THE SLAB ($\delta = 0$) GEOMETRY

Here we consider the special case of $\delta = 0$ in equations (3.1.1a-b). As mentioned in §3.1, the magnetic field configuration produced is that of a neutral sheet, with \mathbf{B} and \mathbf{E} given by

$$\mathbf{E} = \epsilon \hat{\mathbf{z}} \tag{A2.1a}$$

$$\mathbf{B} = x \hat{\mathbf{y}}, \tag{A2.1b}$$

where ϵ is a constant. A vector potential for this field combination is

$$\mathbf{A} = -\frac{x^2}{2} \hat{\mathbf{z}}, \tag{A2.2}$$

and the scalar potential for the electric field is simply

$$\Phi(x, y, z) = -\epsilon z. \tag{A2.3}$$

The system's Hamiltonian is thus

$$H(x, y, z, p_x, p_y, p_z) = \frac{p_x^2 + p_y^2}{2} + \frac{1}{2} \left(p_z^2 + \frac{x^2}{2} \right)^2 - \kappa z, \tag{A2.4}$$

The system's equations of motion in Hamiltonian form are

$$\dot{x} = p_x \tag{A2.5a}$$

$$\dot{y} = p_y \tag{A2.5b}$$

$$\dot{z} = p_z + \frac{x^2}{2}, \quad (\text{A2.5c})$$

$$\dot{p}_z = -xp_z - \frac{x^3}{2} \quad (\text{A2.5d})$$

$$\dot{p}_y = 0 \quad (\text{A2.5e})$$

$$\dot{p}_z = \kappa. \quad (\text{A2.5f})$$

Things are considerably more simple than the system (3.1.4a-f). Note that p_y is a constant and that (A2.5b) can be integrated to give

$$y(t) = p_y t + y_0, \quad (\text{A2.6})$$

where y_0 is a constant. We also can solve for p_z explicitly, just as we did in §3.1:

$$p_z(t) = \kappa t + p_{z0}, \quad (\text{A2.7})$$

where p_{z0} is a constant. The only nontrivial parts of the system (A2.5a-f) that remain are the equations

$$\dot{x} = p_x \quad (\text{A2.8a})$$

$$\dot{z} = \kappa t + p_{z0} + \frac{x^2}{2}, \quad (\text{A2.8b})$$

$$\dot{p}_x = -x(\kappa t + p_{z0}) - \frac{x^3}{2}. \quad (\text{A2.8c})$$

The above system (A2.8a-c) does indeed possess the Painlevé property. This can be seen by applying the ARS algorithm to (A2.8a-c). The only viable leading order behavior for this system is

$$x = \pm 2i\tau^{-1}, \quad p_x = \mp 2i\tau^{-2}, \quad z = 2\tau^{-1}.$$

Using the technique outlined in § 2.3, we can calculate the resonances associated with the above leading order behavior, and find that they are -1 , 1 , and 4 .

Finally, it is possible to recover the remaining constants of integration as required by the algorithm. Using the ansatz (2.3.7), we write the phase space coordinates x , z , and p_x as

$$x = \pm 2i\tau^{-1} + \sum_{m=1}^4 C_{1m}\tau^{m-1}, \quad (\text{A2.9a})$$

$$z = 2\tau^{-1} + \sum_{m=1}^4 C_{2m}\tau^{m-1}, \quad (\text{A2.9b})$$

$$p_x = \mp 2i\tau^{-2} + \sum_{m=1}^4 C_{3m}\tau^{m-2}, \quad (\text{A2.9c})$$

Substituting the expansions (A2.9a-c) into (A2.8a-c), and solving for the coefficients C_{im} , we find:

$$C_{11} = C_{31} = 0, \quad C_{21} \text{ arbitrary,}$$

$$C_{12} = C_{32} = \frac{ip_{z_0}}{3}, \quad C_{22} = \frac{p_{z_0}}{3},$$

$$C_{13} = \frac{i\kappa}{2}, \quad C_{23} = -\kappa, \quad C_{33} = i\kappa,$$

$$C_{14} \text{ arbitrary,} \quad C_{34} = 3C_{14},$$

$$\text{and } C_{24} = \frac{1}{3} \left[2iC_{14} - \frac{p_{z_0}^2}{18} \right].$$

Note that we have an arbitrary coefficient entering at each resonant order in the expansion, and thus we have shown that the neutral sheet magnetic field configuration admits test-particle equations of motion that possess the Painlevé property.

Therefore, by the Painlevé conjecture stated in § 2.2, the system of equations (A2.8a-c) are integrable in the complex analytic sense of the word. Furthermore, since we have a good constant of the motion p_y , and also a time-dependent constant of the motion p_{z_0} , it is very likely that the system (A2.1a-f) is also analytically integrable.

The fact that the system of equations (A2.8a-c) are analytically integrable is little surprise, when the motion in x is considered in greater detail.

We can also test the system (A2.5a-f) using Yoshida analysis, but to do this, we consider the reduced x - z system (A2.5a), (A2.5c,d), and (A2.5f). The first step is to determine whether or not this system is invariant under the scaling transformation

$$\begin{aligned} x' &= \sigma^{g_1} x & z' &= \sigma^{g_2} z & t' &= \sigma^{-1} t \\ p_x' &= \sigma^{g_3} p_x & p_z' &= \sigma^{g_4} p_z & \frac{d}{dt'} &= \sigma \frac{d}{dt} \end{aligned} \quad (\text{A2.10})$$

Under this transformation, (A2.5a), (A2.5c,d), and (A2.5f) become

$$\sigma^{g_1+1} \dot{x} = \sigma^{g_3} p_x \quad (\text{A2.11a})$$

$$\sigma^{g_2+1} \dot{z} = \sigma^{g_4} p_z + \frac{\sigma^{2g_1} x^2}{2}, \quad (\text{A2.11b})$$

$$\sigma^{g_3+1} \dot{p}_x = -\sigma^{g_1+g_4} x p_z - \frac{\sigma^{3g_1} x^3}{2} \quad (\text{A2.11c})$$

$$\sigma^{g_4+1} \dot{p}_z = \kappa. \quad (\text{A2.11d})$$

The condition that the reduced x - z system is invariant under the scaling transformation (A2.10) is thus the following set of conditions on the exponents g_i :

$$g_3 = g_1 + 1, \quad g_2 + 1 = g_4 = 2g_1,$$

$$g_3 + 1 = g_1 + g_4 = 3g_1, \quad g_4 = -1.$$

These conditions can be simplified to give

$$g_2 + 1 = -1 = 2g_1, \quad (\text{A2.12a})$$

$$g_1 + 2 = g_1 - 1 = 3g_1. \quad (\text{A2.12b})$$

Solving (A2.12a) yields $g_1 = -\frac{1}{2}$ and $g_2 = -2$. This result is clearly incompatible with (A2.12b), and thus the reduced dynamical system (A2.5a), (A2.5c,d), and (A2.5f) is not homogeneous, and thus Yoshida singularity analysis is not applicable in this situation.

As we have seen in § 5.4, the slab field configuration does indeed possess fairly simple dynamics, which is consistent with the results of Painlevé singularity analysis.

Another interesting thing to note is that the addition of a uniform axial field B_z to the slab configuration will also yield Hamiltonian equations of motion that possess the Painlevé property.

APPENDIX THREE

PROOF THAT THE RADIAL EQUATION

(5.3.11) POSSESSES THE PAINLEVÉ PROPERTY

The radial equation (5.3.11) was derived in §5.3, and is

$$\frac{d^2 \rho}{dt^2} = \frac{p_\phi^2}{\rho^3} - \rho(\kappa t + p_{z_0}) - \frac{\rho^3}{2}. \quad (\text{A3.1})$$

Our goal is to demonstrate that this differential equation possesses the Painlevé property.

Recalling the ARS algorithm described in § 2.3, we begin by finding the viable leading-order behaviors for (A3.1). Suppose that (A3.1) possesses a singularity $t = t_*$ in the complex t -plane, and let $\rho = \alpha\tau^\beta$, where $\tau = t - t_*$. Substituting this expression into (A3.1), we get

$$\beta(\beta - 1)\alpha\tau^{\beta-2} = p_\phi^2 \alpha^3 \tau^{-3\beta} - \kappa\alpha\tau^{\beta+1} - p_{z_0}\alpha\tau^\beta - \frac{\alpha^3}{2}\tau^{3\beta}. \quad (\text{A3.2})$$

The process of finding the leading order behaviors for (A3.2) is quite simple compared to the task that we undertook in §3.2. For $\beta \neq 0$ and $\beta \neq 1$, the $\mathcal{O}(\tau^\beta)$ and $\mathcal{O}(\tau^{\beta+1})$ terms may be neglected, leaving us with

$$\beta(\beta - 1)\alpha\tau^{\beta-2} = p_\phi^2 \alpha^3 \tau^{-3\beta} - \frac{\alpha^3}{2}\tau^{3\beta}. \quad (\text{A3.3})$$

For (A3.3) there exist three possible balances

Case i: $\beta - 2 = -3\beta < 3\beta$. Then $\beta = \frac{1}{2}$, and $\alpha^4 = -4p_\phi^2$.

Case ii: $\beta - 2 = 3\beta < -3\beta$. Then $\beta = -1$, and $\alpha^4 = -4p_\phi^2$.

Case iii: $\beta - 2 > 3\beta = -3\beta$. Then $\beta = 0$, in contradiction to our original assumption.

Now, suppose $\beta = 0$. or $\beta = 1$. Then (A3.2) becomes

$$p_\phi^2 \alpha^3 \tau^{-3\beta} - \kappa \alpha \tau^{\beta+1} - p_{z_0} \alpha \tau^\beta - \frac{\alpha^3}{2} \tau^{3\beta} = 0. \quad (\text{A3.4})$$

Case iv: If $\beta = 0$, then all of the terms except the electric field term (i.e. the $\kappa \alpha \tau^{\beta+1}$ term) in (A3.4) balance, and α satisfies

$$\alpha^6 + 2\alpha^4 p_{z_0} - 2p_\phi^2 = 0.$$

This polynomial equation contains only even powers of α , and the substitution $A = \alpha^2$ allows us to write it as a cubic in A , which can be solved by radicals:

$$A^3 + 2A^2 p_{z_0} - 2p_\phi^2 = 0.$$

Case v: For $\beta = 1$, (A3.4) becomes

$$p_\phi^2 \alpha^3 \tau^{-3} - \kappa \alpha \tau^2 - p_{z_0} \alpha \tau - \frac{\alpha^3}{2} \tau^3 = 0,$$

and there exists no leading order balance for this case.

Having determined the viable leading order behaviors to (A3.1), we turn our attention to the system's resonances. Recalling (2.3.3), we write our dependent variable as

$$\rho = \alpha \tau^\beta (1 + \gamma \tau^r), \quad (\text{A3.5})$$

where r is presumed positive or equal to -1, and the parameters α and β were determined in the first step of the algorithm. Substitution of this extended expansion

will give us the means of solving for r ; that is, the resonances of the system for each particular leading order behavior.

Case i: $\alpha^4 = -4p_\phi^2$ and $\beta = \frac{1}{2}$ Substitution of (A3.5) into (A3.1) for this case gives us, to leading order,

$$\alpha\gamma\left(r + \frac{1}{2}\right)\left(r - \frac{1}{2}\right) = -3p_\phi^2\alpha^3\gamma,$$

which reduces to a quadratic in r

$$r^2 - \frac{1}{4} + 3\alpha^2 p_\phi^2 = 0.$$

Recalling the value of α for this leading order behavior, we find $\alpha^2 = \pm 2ip_\phi$, and thus our equation for r becomes

$$r^2 - \frac{1}{4} \pm 6ip_\phi^3 = 0.$$

The resonances are the r roots of the above polynomial equation, and are given by

$$r = \frac{1}{2} \left[\frac{1}{4} \pm \sqrt{\frac{1}{16} \mp 24ip_\phi^3} \right].$$

For real p_ϕ , we will not have real roots unless $p_\phi = 0$, in which case $r = \{1/4, 0\}$.

Clearly we can not obtain nonnegative integer resonances, nor will we have $r = -1$ as a resonance. For this case, the algorithm terminates at this stage.

Case ii: Here we have $\beta = -1$ and $\alpha = \pm 2i$. Substituting (A3.5) into (A3.1) for this leading order behavior gives us the equation

$$\alpha\gamma(r-1)(r-2) = -\frac{3}{2}\alpha^3\gamma,$$

which reduces to a quadratic for r :

$$r^2 - 3r - 4 = 0,$$

which has roots $r = -1$ and $r = 4$. Thus this leading order behavior yields acceptable resonances, and passes this level of the Painlevé test.

Case iv: This was the case of $\beta = 0$, and α was defined above in terms of a cubic in $A = \alpha^2$. Using this set of parameters in (A3.5), and substituting into (A3.1) gives us at leading order

$$-3p_\phi^2 - \alpha^4 p_{z_0} - \frac{3}{2}\alpha^6 = 0,$$

or, using the above expression for α , we get

$$\alpha^4 p_{z_0} - 3p_\phi^2 = 0.$$

Clearly, this equation contains no information about the resonances, and the algorithm terminates at this stage.

Having determined all of the resonances for the system's possible leading order behaviors, we take up the task of constructing the constants of integration for the one leading order behavior—Case ii—that has passed through both of the first two steps of the algorithm. This case has one nonnegative resonance at $r = 4$, and at this order in the Laurent series expansion for $\rho(t)$, we expect an arbitrary constant to appear. In order to see whether or not this will happen, we expand the solution to (A3.1), $\rho(\tau)$ as a truncated series as defined by (2.3.7):

$$\rho(\tau) = \pm 2i\tau^{-1} + \sum_{m=1}^4 C_{im}\tau^m, \quad (\text{A3.6})$$

where the coefficients C_{im} are constants that are determined by substitution of (A3.6) into (A3.1). Substituting (A3.6) into (A3.1), and balancing order by order in τ gives us a set of equations for the coefficients C_{im} :

$$\begin{aligned}
 -6 C_{11} &= 0 \\
 3 i C_{11}^2 - 6 C_{12} - 2 i p_{z_0} &= 0 \\
 \frac{C_{11}^3}{2} + 6 i C_{11} C_{12} - 4 C_{13} - 2 i \kappa - C_{11} p_{z_0} &= 0 \\
 \frac{3 C_{11}^2 C_{12}}{2} + 3 i C_{12}^2 + 6 i C_{11} C_{13} - C_{11} \kappa - C_{12} p_{z_0} &= 0
 \end{aligned} \tag{A3.7a-d}$$

The first of these equations implies that $C_{11} = 0$, which reduces (A3.7b) in the set to

$$-6 C_{12} - 2 i p_{z_0} = 0.$$

Solving for C_{12} , we get $C_{12} = -\frac{i}{3} p_{z_0}$, which, when substituted into (A3.7c) yields

$$-4 C_{13} - 2 i \kappa = 0.$$

Thus $C_{13} = -\frac{i}{2} \kappa$, and substitution of this result into the (A3.7c) in the set reduces it to zero identically, leaving us with an arbitrary C_{14} , which is precisely what we would expect at this resonant order in the expansion. Note that we could have seen this immediately by inspection of (A3.7d), since there is no term involving C_{14} in this equation. Therefore, the radial equation (A3.1), or (5.3.11), possesses the Painlevé property.

APPENDIX FOUR

SYMPLECTIC INTEGRATION

§A4.1 Introduction

In the study of the behavior of systems of ordinary differential equations, it is often advantageous, or simply necessary, to turn to numerical methods. In particular, the dynamical systems discussed in this thesis either 1) did not possess closed-form solutions, or 2) had exact solutions that are difficult to interpret physically.

There exist many techniques for integrating systems of O.D.E.'s, and when the system in question happens to be Hamiltonian, we have at our disposal a wealth of techniques that can be tailor-made to fit the problem. Given the thrust of our work so far, we would like to use a method that does its best to respect the phase space structure of our system, that is, we wish our method to be *symplectic*. Thus we turn to the technique of symplectic integration.

Symplectic integration was first introduced by De Vogelaere [80], and extended to general Hamiltonians by Channell [81] and Ruth [82]. Further exploration of this technique has been made by Forest [83], and others [84,85]. Other symplectic methods involve the use of Lie transforms [86], which are used extensively by accelerator physicists, or operator splitting [87].

The basic method is simple. Consider a system in Hamiltonian form with coordinates q_1, \dots, q_N and momenta p_1, \dots, p_N , and the system's Hamiltonian H is

$H = H(q_1, \dots, q_N, p_1, \dots, p_N)$. The equations of motion in Hamiltonian form are:

$$\dot{q}_i = \frac{\partial H}{\partial p_i} \quad (A4.1.1a)$$

and

$$\dot{p}_i = -\frac{\partial H}{\partial q_i}. \quad (A4.1.1b)$$

The Hamiltonian differential equations are then replaced by a symplectic mapping that is generated using a near-identity canonical transformation. Express a time step from time $t = t_0$ to $t = t_0 + \Delta t$ as a canonical transformation from a set of coordinates and momenta (q_i, p_i) at time t_0 to the new set (Q_i, P_i) at $t = t_0 + \Delta t$.

The chief advantage to symplectic techniques is that they are natural outgrowths of the system's Hamiltonian and tend to possess the same symmetries as the Hamiltonian from which they spring. The trajectory manifold resulting from the mapping remains close to the system's true trajectory manifold. Very often, symplectic mappings with fairly large timesteps will preserve a system's integrals with startling precision, allowing greater speed and accuracy when compared to more standard numerical integration techniques [88]. As is often the case with a "standard" finite-difference scheme, such as the Runge-Kutta method, the quality-control portion of the integration routine is the testing of the integrity of the system's constants of the motion; a process which often forces the routine to cut the timestep size and re-do the step. A symplectic scheme by contrast, is simply the iteration of a mapping that shares the symmetries of the system in question, and a symplectic mapping that is order n in the timestep Δt will normally preserve the system's

Hamiltonian to $\mathcal{O}((\Delta t)^{n+1})$ automatically. When a Hamiltonian system possesses a continuous symmetry (e.g. azimuthal symmetry), the integral of the motion associated with this symmetry (e.g. angular momentum) will often be preserved to machine precision. We will return to this question of accuracy in the next section.

§A4.2 Constructing Symplectic Schemes

Consider a canonical transformation of the third kind. In this case the generating function is $S = F_3(Q_1, \dots, Q_N, p_1, \dots, p_N)$, and P_i and q_i are given by

$$q_i = -\frac{\partial S}{\partial p_i} \quad (\text{A4.2.1a})$$

and

$$P_i = -\frac{\partial S}{\partial Q_i}. \quad (\text{A4.2.ab})$$

Now, expand S as a Taylor series in Δt :

$$S = \sum_{m=0}^{\infty} S_m(p, Q) \frac{(\Delta t)^m}{m!}. \quad (\text{A4.2.2})$$

Note that $S_0(Q, p) = -\mathbf{Q} \cdot \mathbf{p}$, the identity transformation. The next step is to derive the higher-order terms in the generating function. To this end, note that substituting (A4.2.2) into (A4.2.1b) allows us to write the new momentum P_i as

$$P_i = p_i - \sum_{m=1}^{\infty} \frac{(\Delta t)^m}{m!} \frac{\partial S_m}{\partial Q_i}. \quad (\text{A4.2.3})$$

We can write the total time derivative of the new momentum P_i as

$$\dot{P}_i = \frac{\partial P_i}{\partial t} + \dot{\mathbf{Q}} \cdot \frac{\partial P_i}{\partial \mathbf{Q}}. \quad (\text{A4.2.4})$$

Recalling the expansion for P_i and Hamilton's equations, we can write (A4.2.3) as

$$\sum_{m=1}^{\infty} \frac{(\Delta t)^{m-1}}{(m-1)!} \frac{\partial S_m}{\partial Q_i} + \sum_{m=1}^{\infty} \frac{(\Delta t)^m}{m!} \frac{\partial^2 S_m}{\partial \mathbf{Q} \partial Q_i} \cdot \left(\frac{\partial}{\partial \mathbf{P}} \right) H(\mathbf{Q}, \mathbf{P}) = -\frac{\partial}{\partial Q_i} H(\mathbf{Q}, \mathbf{P}). \quad (\text{A4.2.5})$$

We wish to determine \mathbf{Q} and \mathbf{P} such that they agree with the solutions of (A4.1.1) to some order in Δt . Given the above expression for P_i , we can write the vector \mathbf{P} as

$$\mathbf{P} = \mathbf{p} - \sum_{m=1}^{\infty} \frac{(\Delta t)^m}{m!} \frac{\partial S_m}{\partial \mathbf{Q}}.$$

or

$$\mathbf{P} = \mathbf{p} + \Delta \mathbf{P},$$

where

$$\Delta \mathbf{P} = - \sum_{m=1}^{\infty} \frac{(\Delta t)^m}{m!} \frac{\partial S_m}{\partial \mathbf{Q}}.$$

Expanding the arguments of the Hamiltonian in eqn (A4.2.5), we get

$$\sum_{m=0}^{\infty} \frac{(\Delta t)^m}{m!} \frac{\partial S_{m+1}}{\partial Q_i} = \sum_{m=1}^{\infty} \frac{(\Delta t)^m}{m!} \frac{\partial^2 S_m}{\partial \mathbf{Q} \partial Q_i} \cdot \sum_{j=0}^{\infty} \frac{(\Delta \mathbf{P} \cdot \frac{\partial}{\partial \mathbf{P}})^j}{j!} \frac{\partial H}{\partial \mathbf{P}} - \sum_{j=0}^{\infty} \frac{(\Delta \mathbf{P} \cdot \frac{\partial}{\partial \mathbf{P}})^j}{j!} \frac{\partial H}{\partial Q_i}. \quad (\text{A4.2.6})$$

Expanding the powers of $\Delta \mathbf{P}$, and collecting terms order by order in Δt allows us to derive the first two orders of the generating function S .

$$S_1 = H(\mathbf{p}, \mathbf{Q}), \quad (\text{A4.2.7a})$$

and

$$S_2 = - \left(\frac{\partial}{\partial \mathbf{Q}} H(\mathbf{p}, \mathbf{Q}) \right) \cdot \left(\frac{\partial}{\partial \mathbf{p}} H(\mathbf{p}, \mathbf{Q}) \right). \quad (\text{A4.2.7b})$$

A general, but complicated version of eqn (A4.2.6) can be derived by expanding the powers of $\Delta\mathbf{P}$ using the binomial theorem and identifying like powers of Δt . This expression can be found in reference [88].

Returning to the question of how well a symplectic algorithm will preserve the Hamiltonian for a given system, consider a simple Hamiltonian of the form

$$H(q, p) = \frac{p^2}{2} + V(q).$$

Applying (A4.2.7a,b) to construct a first-order symplectic scheme, we find the explicit mapping

$$\begin{aligned} Q &= q + p\Delta t + \mathcal{O}(\Delta t^2) \\ P &= p - \frac{\partial V}{\partial q}\Delta t + \mathcal{O}(\Delta t^2). \end{aligned}$$

This mapping is exactly symplectic; i.e. $dQ \wedge dP = 0$, but the system's Hamiltonian is preserved only to first order in Δt :

$$H(P, Q) = \frac{p^2}{2} + V(q) + \left(\frac{\partial V}{\partial q}\Delta t \right)^2,$$

and thus,

$$H(P, Q) - H(p, q) \sim \mathcal{O}(\Delta t^2).$$

EXAMPLE: Consider a Hamiltonian of the form

$$H = \frac{1}{2}(p_x^2 + p_y^2 + p_z^2) + \frac{x^2}{2} + \cos(y) + z. \quad (\text{A4.2.8})$$

Note here that the dynamics for this Hamiltonian are completely separable; the motion in x is a harmonic oscillator, the y -motion is a pendulum, and the motion

in z is a free-fall. The system can be broken down into three separate systems with individual Hamiltonians given by:

$$H_x = \frac{p_x^2 + x^2}{2},$$

$$H_y = \frac{p_y^2}{2} + \cos(y),$$

$$H_z = \frac{p_z^2}{2} + z.$$

Hamilton's equations for this system are

$$\dot{x} = p_x, \tag{A4.2.9a}$$

$$\dot{y} = p_y, \tag{A4.2.9b}$$

$$\dot{z} = p_z, \tag{A4.2.9c}$$

$$\dot{p}_x = -x, \tag{A4.2.9d}$$

$$\dot{p}_y = \sin(y), \tag{A4.2.9e}$$

$$\dot{p}_z = -1. \tag{A4.2.9f}$$

Applying equations (A4.2.7a,b), we can construct the generating function S , which is good to third order in the time step Δt :

$$\begin{aligned}
S(X, Y, Z, p_x, p_y, p_z) = & -(Xp_x + Yp_y + Zp_z) + \Delta t \left(\frac{p_x^2 + p_y^2 + p_z^2}{2} + \right. \\
& \left. \frac{X^2}{2} + \cos(Y) + z \right) - \frac{(\Delta t)^2}{2} (Xp_x - p_y \sin(Y) + p_z).
\end{aligned} \tag{A4.2.10}$$

The symplectic mapping generated by S given above is:

$$x = X - \Delta t p_x + \frac{(\Delta t)^2}{2} X, \tag{A4.2.11a}$$

$$y = Y - \Delta t p_y - \frac{(\Delta t)^2}{2} \sin(Y), \tag{A4.2.11b}$$

$$z = Z - \Delta t p_z - \frac{(\Delta t)^2}{2}, \tag{A4.2.11c}$$

$$P_x = p_x - \Delta t X + \frac{(\Delta t)^2}{2} p_x, \tag{A4.2.11d}$$

$$P_y = p_y - \Delta t \sin(Y) - \frac{(\Delta t)^2}{2} p_y \cos(Y), \tag{A4.2.11e}$$

$$P_z = p_z - \Delta t. \tag{A4.2.11f}$$

Note that this mapping is implicit in the new coordinates (X, Y, Z) . The x and z components of this mapping can be inverted by inspection:

$$X = \frac{x + \Delta t p_x}{1 - \frac{(\Delta t)^2}{2}} \tag{A4.2.12a}$$

and

$$Z = z + p_z \Delta t. \tag{A4.2.12b}$$

The motion in y is another matter altogether; equation (A4.2.11b) is transcendental in Y , and must be inverted numerically using a root-finding method such as Newton's method. This is generally the case.

There is, however, another way of generating the mapping in a fashion that avoids the difficulties encountered above. Instead of using a canonical transformation of the third kind, suppose we try evolving the system via a canonical transformation of the second kind, where we step from coordinates (\mathbf{q}, \mathbf{p}) at time t to a new set of coordinates (\mathbf{Q}, \mathbf{P}) at time $t + \Delta t$, with a generating function $F = F(\mathbf{q}, \mathbf{P})$. The new coordinates and old momenta are thus given by:

$$Q_i = \frac{\partial F}{\partial P_i} \quad (\text{A4.2.13a})$$

$$p_i = \frac{\partial F}{\partial q_i}. \quad (\text{A4.2.13b})$$

Once again, we can express F as a power series in the timestep Δt .

$$F = \sum_{m=0}^{\infty} F_m(p, Q) \frac{(\Delta t)^m}{m!}. \quad (\text{A4.2.14})$$

Note now that $F_0(Q, p) = -\mathbf{q} \cdot \mathbf{P}$, the identity transformation. As before, the object is to determine the higher-order contributions to the generating function F . This process is essentially the same as the one outlined above. Using (A4.2.13a,b), the new coordinates Q_i can be written as

$$Q_i = q_i + \sum_{m=1}^{\infty} \frac{(\Delta t)^m}{m!} \frac{\partial F_m}{\partial Q_i}. \quad (\text{A4.2.15})$$

Now we can write the total time derivative of the new coordinate Q_i as

$$\dot{Q}_i = \frac{\partial Q_i}{\partial t} + \dot{\mathbf{P}} \cdot \frac{\partial Q_i}{\partial \mathbf{P}}. \quad (\text{A4.2.16})$$

Substituting the expansion (A4.2.15) for Q_i into (A4.2.16), and using Hamilton's equations to eliminate $\dot{\mathbf{P}}$, we get

$$\sum_{m=1}^{\infty} \frac{(\Delta t)^{m-1}}{(m-1)!} \frac{\partial F_m}{\partial P_i} + \sum_{m=1}^{\infty} \frac{(\Delta t)^m}{m!} \frac{\partial^2 F_m}{\partial \mathbf{P} \partial P_i} \cdot \left(\frac{\partial}{\partial \mathbf{Q}} \right) H(\mathbf{Q}, \mathbf{P}) = \frac{\partial}{\partial P_i} H(\mathbf{Q}, \mathbf{P}). \quad (\text{A4.2.16})$$

Given the above expression for Q_i , we can write the vector \mathbf{Q} as

$$\mathbf{Q} = \mathbf{q} + \sum_{m=1}^{\infty} \frac{(\Delta t)^m}{m!} \frac{\partial F_m}{\partial \mathbf{P}}.$$

or

$$\mathbf{Q} = \mathbf{q} + \Delta \mathbf{Q},$$

where

$$\Delta \mathbf{Q} = \sum_{m=1}^{\infty} \frac{(\Delta t)^m}{m!} \frac{\partial F_m}{\partial \mathbf{P}}.$$

As before, we simply expand the arguments of H in terms of $\Delta \mathbf{Q}$, which leads us to a result very similar to (A4.2.6):

$$\sum_{m=0}^{\infty} \frac{(\Delta t)^m}{m!} \frac{\partial F_{m+1}}{\partial P_i} = \sum_{m=1}^{\infty} \frac{(\Delta t)^m}{m!} \frac{\partial^2 F_m}{\partial \mathbf{P} \partial P_i} \cdot \sum_{j=0}^{\infty} \frac{(\Delta \mathbf{Q} \cdot \frac{\partial}{\partial \mathbf{Q}})^j}{j!} \frac{\partial H}{\partial \mathbf{Q}} + \sum_{j=0}^{\infty} \frac{(\Delta \mathbf{Q} \cdot \frac{\partial}{\partial \mathbf{Q}})^j}{j!} \frac{\partial H}{\partial P_i}. \quad (\text{A4.2.17})$$

again, it is possible to derive a general expression for F_m for any order m , but for our purposes, we shall be interested in only the first two orders of F :

$$F_1 = H(\mathbf{q}, \mathbf{P}), \quad (\text{A4.2.18a})$$

and

$$F_2 = \left(\frac{\partial}{\partial \mathbf{P}} H(\mathbf{q}, \mathbf{P}) \right) \cdot \left(\frac{\partial}{\partial \mathbf{q}} H(\mathbf{q}, \mathbf{P}) \right). \quad (\text{2.2.18b})$$

Armed with this scheme, let's return to our specimen system, whose Hamiltonian is given by equation (A4.2.10). To second order in Δt , the generating function F is

$$\begin{aligned}
 F(x, y, z, P_x, P_y, P_z) = & xP_x + yP_y + zP_z + \\
 \Delta t \left(\frac{P_x^2 + P_y^2 + P_z^2}{2} + \frac{x^2}{2} + \cos(y) + z \right) + & \\
 \frac{(\Delta t)^2}{2} (xP_x - P_y \sin(y) + P_z). & \quad (A4.2.19)
 \end{aligned}$$

Now note that the second-order symplectic mapping that F generates is implicit in the new momentum \mathbf{P} , and is given by:

$$p_x = P_x + \Delta t x + \frac{(\Delta t)^2}{2} P_x, \quad (A4.2.20a)$$

$$p_y = P_y - \Delta t \sin(y) - \frac{(\Delta t)^2}{2} P_y \cos(y), \quad (A4.2.20b)$$

$$p_z = P_z + \Delta t. \quad (A4.2.20c)$$

$$X = x + \Delta t P_x + \frac{(\Delta t)^2}{2} x, \quad (A4.2.20d)$$

$$Y = y + \Delta t P_y - \frac{(\Delta t)^2}{2} P_y \sin(y), \quad (A4.2.20e)$$

$$Z = z + \Delta t P_z + \frac{(\Delta t)^2}{2}, \quad (A4.2.20f)$$

Note that unlike the mapping (A4.2.11) this mapping is easily inverted to be made explicit. Solving (A4.2.20a-c) for the new momenta, we get

$$P_x = \frac{p_x - x\Delta t}{1 + \frac{(\Delta t)^2}{2}}, \quad (A4.2.21a)$$

$$P_y = \frac{p_y - \sin(y)\Delta t}{1 + \frac{(\Delta t)^2}{2} \cos(y)}, \quad (A4.2.21b)$$

$$P_z = p_z - \Delta t. \quad (\text{A4.2.21c})$$

Figures A4.2.1 - A4.2.3 illustrate how well this algorithm preserves the individual Hamiltonians H_x , H_y , and H_z . The data for these graphs were generated using the symplectic scheme (A4.2.21a-c) and (A4.2.20d-f) with the initial conditions $x = 1$, $y = \pi/2$, $z = 0.5$, $p_x = 1.0$, $p_y = 1.0$, and $p_z = 1.0$. The size of the time step was fixed at $\Delta t = 10^{-2}$. It is interesting to note that a second-order numerical integration scheme would be expected to introduce relative errors in the Hamiltonian on the order of $(\Delta t)^3$. Our graphs, however, tell us quite a different story. In the case of H_x , the instantaneous relative error ϵ_{H_x} oscillates between -2.5×10^{-9} and 2.5×10^{-9} , cancelling itself out on average. The map for the y-motion shows some growth in the relative error, which is unfortunate, but still, the relative error after 100000 steps is still small. The freefall motion in z shows some dissipative behavior, but only on the order of 10^{-7} after 100000 steps.

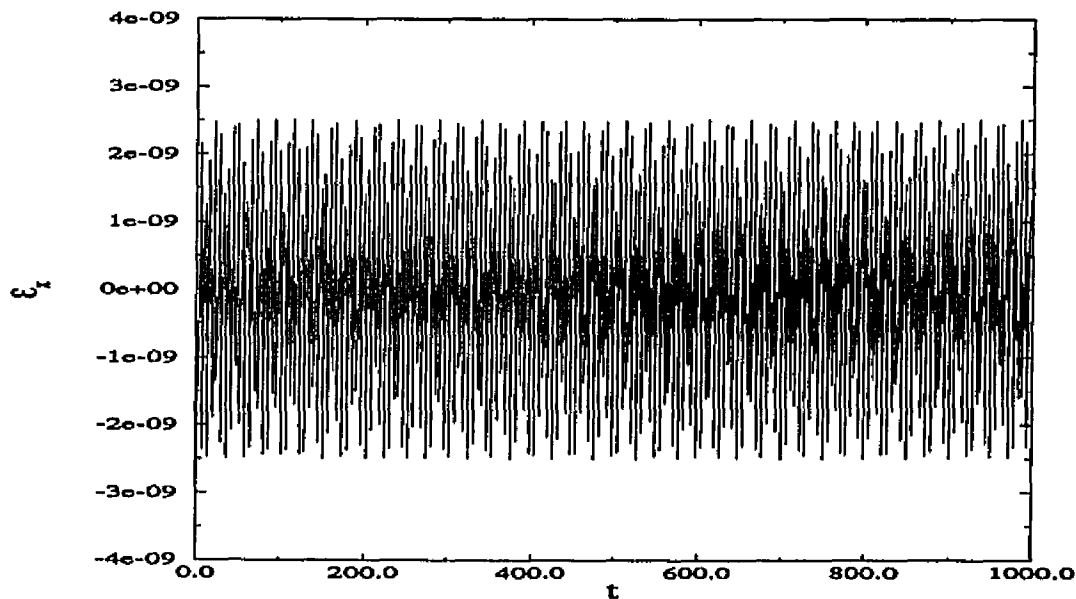


Figure A4.2.1. Relative Error in H_x vs. Time.

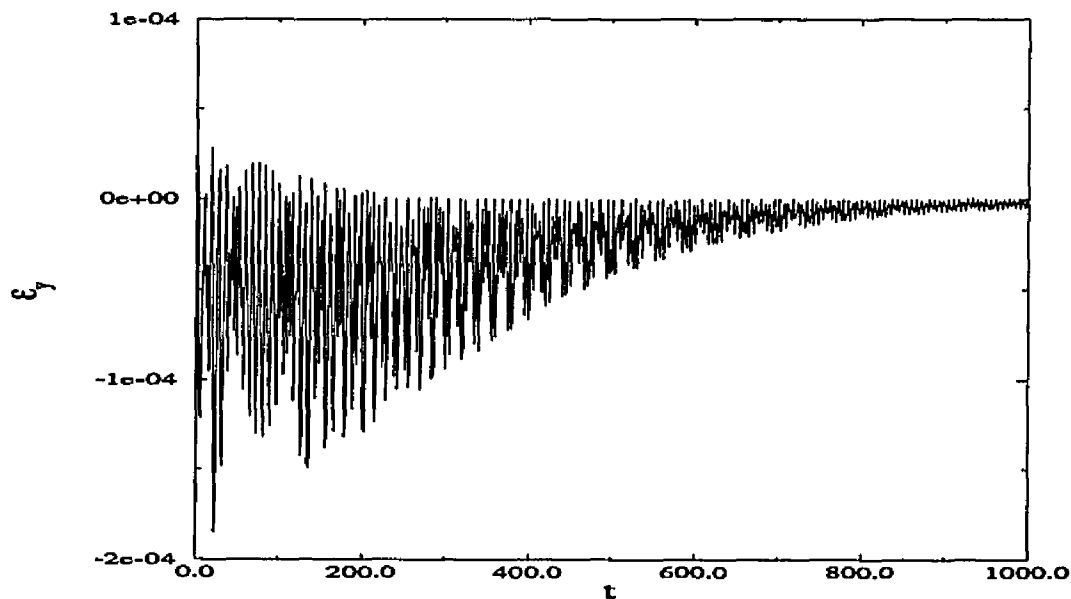


Figure A4.2.2. Relative Error in H_y vs. Time.

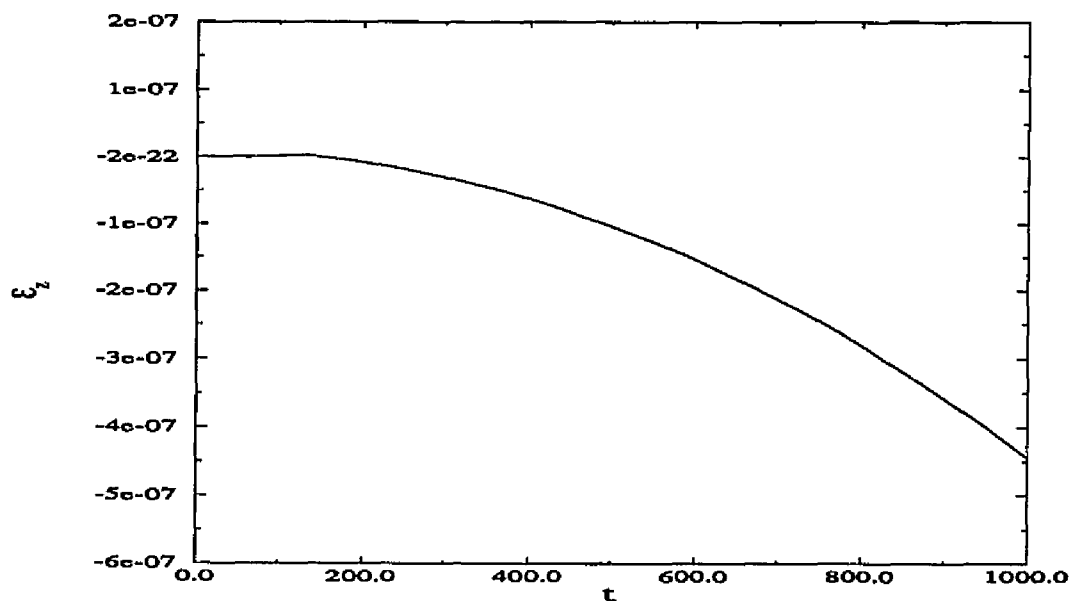


Figure A4.2.3. Relative Error in H_x vs. Time.

Given what we've seen with this simple example, it would appear that for Hamiltonians of the type typically encountered (i.e. $H = \text{kinetic energy} + \text{potential energy}$), using canonical transformations of the second kind to generate the symplectic mapping would be a superior technique in that it is more easily inverted.

The fact that most Hamiltonians for physical systems tend to contain terms that are either linear or quadratic in the momenta, but often contain terms that are cubic, quartic, quintic, or even rational in the coordinates tells us we will normally have better luck using canonical transformations of the second kind to create symplectic integration algorithms that are easily invertible, and hence fast, since we probably won't need to call in a root-finding routine to invert the scheme. To understand why this is so, consider a Hamiltonian of the form

$$H(\mathbf{q}, \mathbf{p}) = \frac{\mathbf{p} \cdot \mathbf{p}}{2} + \mathbf{p} \cdot \mathbf{V}(\mathbf{q}) + U(\mathbf{q}), \quad (\text{A4.2.22})$$

where the functions \mathbf{V} and U are either polynomials in \mathbf{q} or rational functions of \mathbf{q} . If we construct a symplectic scheme of the type generated by (A4.2.7), the generating function $S(\mathbf{Q}, \mathbf{p})$ is

$$\begin{aligned} S(\mathbf{Q}, \mathbf{p}) = & -\mathbf{Q} \cdot \mathbf{p} + \Delta t \left(\frac{\mathbf{p} \cdot \mathbf{p}}{2} + \mathbf{p} \cdot \mathbf{V}(\mathbf{Q}) + U(\mathbf{Q}) \right) - \\ & \frac{(\Delta t)^2}{2} \left([(\mathbf{p} + \mathbf{V}(\mathbf{Q})) \cdot \nabla_{\mathbf{Q}}][\mathbf{p} \cdot \mathbf{V}(\mathbf{Q})] + \nabla_{\mathbf{Q}} U(\mathbf{Q}) \right). \end{aligned} \quad (\text{A4.2.23})$$

with the symplectic mapping scheme for the i^{th} conjugate pair given by

$$\begin{aligned} q_i = & Q_i - \Delta t(p_i + V_i) + \\ & \frac{(\Delta t)^2}{2} [\partial_i(\mathbf{p} \cdot \mathbf{V}) + (\mathbf{V} \cdot \nabla)V_i(\mathbf{p} \cdot \partial_i \mathbf{V}) + [(\mathbf{p} + \mathbf{V}) \cdot \nabla]V_i + \partial_i U] \end{aligned} \quad (\text{A4.2.24a})$$

$$P_i = p_i - \Delta t(\mathbf{p} \cdot (\partial_i \mathbf{V}) + \partial_i U \cdot \partial_i \mathbf{V}) + [(\partial_i \mathbf{V}) \cdot \nabla]U + \frac{(\Delta t)^2}{2} [(\mathbf{p} + \mathbf{V}) \cdot \nabla][\mathbf{p} \cdot \mathbf{V} + U] + (\mathbf{p} + \mathbf{V}) \cdot \nabla(\partial_i U).$$

(A4.2.24b)

If the functions V_i and U are polynomials, but more complicated than linear functions in the coordinate Q , the inversion of the symplectic mapping has the potential of being a difficult task; for each component of the mapping that is not explicit, we will have at least two branches of the inverted mapping, meaning that we will be faced with one of two things: 1) if the equations (A4.2.24) are solvable in radicals for Q , we could write out the roots explicitly, and test to see which one is associated with the timestep, or 2) if (A4.2.24) is a quintic or higher-order polynomial in Q , we are faced with inverting the mapping via a numerical root-finding routine. In either case, our numerical scheme will be slowed down.

Now consider the same system with a symplectic scheme generated by equation (A4.2.18). The generating function F for the timestep is

$$F(\mathbf{q}, \mathbf{P}) = -\mathbf{q} \cdot \mathbf{P} + \Delta t \left(\frac{\mathbf{P} \cdot \mathbf{P}}{2} + \mathbf{P} \cdot \mathbf{V}(\mathbf{q}) + U(\mathbf{q}) \right) - \frac{(\Delta t)^2}{2} \left([(\mathbf{P} + \mathbf{V}(\mathbf{q})) \cdot [\nabla_{\mathbf{q}}]][\mathbf{P} \cdot \mathbf{V}(\mathbf{q}) + \nabla_{\mathbf{q}}U(\mathbf{q})] \right).$$

(A4.2.25)

The symplectic mapping is then

$$\begin{aligned}
 Q_i &= q_i - \Delta t(P_i + V_i) + \\
 &\frac{(\Delta t)^2}{2} [\partial_i(\mathbf{P} \cdot \mathbf{V}) + (\mathbf{V} \cdot \nabla)V_i(\mathbf{P} \cdot \partial_i \mathbf{V}) + \\
 &[(\mathbf{P} + \mathbf{V}) \cdot \nabla]V_i + \partial_i U] \tag{A4.2.26b}
 \end{aligned}$$

$$\begin{aligned}
 p_i &= P_i - \Delta t(\mathbf{P} \cdot (\partial_i \mathbf{V}) + \partial_i U) + \\
 &\frac{(\Delta t)^2}{2} [(\mathbf{P} + \mathbf{V}) \cdot \nabla][\mathbf{P} \cdot \partial_i \mathbf{V}] + [(\partial_i \mathbf{V}) \cdot \nabla](\mathbf{P} \cdot \mathbf{V} + U) + (\mathbf{P} + \mathbf{V}) \cdot \nabla(\partial_i U)]. \tag{A4.2.26}
 \end{aligned}$$

From (A4.2.26) we see that we have a relation for \mathbf{P} that is quadratic in \mathbf{P} . , Thus, for a one-dimensional system, we can solve for \mathbf{P} using the quadratic formula, and then check the two branches to see which one is the appropriate one for the mapping. Notice that the term in (A4.26) that is quadratic in \mathbf{P} takes the form

$$P_j P_k \partial_i \partial_j V_k.$$

Thus, if the i^{th} component of the mapping if the components of \mathbf{V} satisfy the condition

$$\partial_i \partial_j V_k = 0, \quad \forall i, j, k. \tag{2.2.27}$$

If the condition (A4.2.27) applies for all of the components of \mathbf{V} , then the mapping (A4.2.26) is linear in \mathbf{P} . The condition (A4.2.27) is highly restrictive, but if it applies, then the implicit mapping is completely invertible by inspection. If this condition applies for some component of \mathbf{V} , then this portion of the map can be inverted via the quadratic formula. No such guarantee exists for the scheme generated

by (A4.2.7), thus leading us to conclude that for Hamiltonians with complicated potentials or electromagnetic terms, such as the Hamiltonians (1.4.7) and the reduced radial system derived in §5.3, a momentum-implicit scheme is a good choice for constructing a second-order symplectic integration algorithm.

§A4.3 Numerical Scheme for Equations (1.4.8a-f)

Now we will apply the momentum-implicit method generated by (A4.2.18) to derive a symplectic mapping for the system (1.4.8a-f). Recall from (1.4.7) that the Hamiltonian is

$$H(x, y, z, p_x, p_y, p_z) = \frac{p_x^2 + p_y^2 + p_z^2}{2} + \frac{\alpha}{2}(p_x y - p_y x) + \frac{p_z}{2}(x^2 - \delta y^2) + \frac{\alpha^2}{8}(x^2 + y^2) + \frac{1}{8}(x^2 + \delta y^2)^2 - \kappa z, \quad (\text{A4.3.1})$$

where α is a constant that specifies the z -component of the magnetic field. For the work done in this thesis, $\alpha = 0$.

Applying the momentum-implicit method, we get the symplectic map

$$p_z = P_z - \kappa(\Delta t) \quad (\text{A4.3.2a})$$

$$p_x = P_x + \frac{(\Delta t)}{2} \left(-\alpha P_y + \frac{\alpha^2 x}{2} + 2P_z x + x(x^2 - \delta y^2) \right) + \frac{(\Delta t)^2}{2} \left(P_x P_z - \kappa x + \frac{P_x}{2}(3x^2 - \delta y^2) + \frac{\alpha P_z(1 + \delta)y}{2} - \delta P_y x y - \frac{\delta P_x y^2}{2} + \frac{3\alpha(1 + \delta)x^2 y}{4} - \frac{\alpha\delta(1 + \delta)y^3}{4} \right) \quad (\text{A4.3.2b})$$

$$\begin{aligned}
p_y = P_y + (\Delta t) & \left(\frac{\alpha P_x}{2} + \frac{\alpha^2 y}{4} - \delta P_z y - \frac{\delta x^2 y}{2} + \frac{\delta^2 y^3}{2} \right) + \\
\frac{(\Delta t)^2}{2} & \left(-\delta P_y P_z + \frac{\alpha(1+\delta)P_z x}{2} + \frac{\delta}{2} P_y (3\delta y^2 - x^2) - \delta P_x x y + \right. \\
& \left. \frac{\alpha(1+\delta)x^3}{4} + \delta \kappa y - \frac{3\alpha\delta(1+\delta)xy^2}{4} \right) \quad (A4.3.2c)
\end{aligned}$$

$$X = x + (\Delta t) \left(P_x + \frac{\alpha y}{2} \right) + \frac{(\Delta t)^2}{2} x \left(P_z + \frac{1}{2}(x^2 - \delta y^2) \right) \quad (A4.3.2d)$$

$$Y = y + (\Delta t) \left(P_y - \frac{\alpha x}{2} \right) + \frac{(\Delta t)^2}{2} \delta y \left(-P_z + \frac{1}{2}(\delta y^2 - x^2) \right) \quad (A4.3.2e)$$

$$\begin{aligned}
Z = z + (\Delta t) & \left(P_z + \frac{1}{2}(x^2 - \delta y^2) \right) + \frac{(\Delta t)^2}{2} \left(-\kappa + P_x x - \delta P_y y + \frac{\alpha(1+\delta)xy}{2} \right). \\
& \quad (A4.3.2f)
\end{aligned}$$

This mapping is quite easily inverted; the only nonlinear terms in the momenta involve $P_x P_z$ and $P_y P_z$. Note that since P_z can be obtained explicitly from (A4.3.2a), the equations (A4.3.2b) and (A4.3.2c) can also be solved trivially to obtain P_x and P_y . Thus the symplectic scheme can be made entirely explicit. To illustrate this, we write (A4.3.2a) and (A4.3.2b) as the matrix equation

$$\mathbf{C}(P_x, P_x)^T = \mathbf{R},$$

or

$$\begin{pmatrix} C_{11} & C_{12} \\ C_{21} & C_{22} \end{pmatrix} \begin{pmatrix} P_x \\ P_y \end{pmatrix} = \begin{pmatrix} R_1 \\ R_2 \end{pmatrix}. \quad (A4.3.3)$$

where the elements of \mathbf{C} and \mathbf{R} are given by

$$C_{11} = 1 + \frac{(\Delta t)^2}{2} \left(P_z + \frac{1}{2}(3x^2 - \delta y^2) \right),$$

$$\begin{aligned}
C_{12} &= -\frac{\alpha(\Delta t)}{2} - \frac{(\Delta t)^2}{2}\delta xy, \\
C_{21} &= \frac{\alpha(\Delta t)}{2} - \frac{(\Delta t)^2}{2}\delta xy, \\
C_{22} &= 1 + \frac{(\Delta t)^2}{2} \left(-\delta P_z + \frac{\delta}{2}(3x^2 - \delta y^2) \right), \\
R_1 &= p_x - \frac{(\Delta t)}{2} \left(\frac{\alpha^2 x}{2} + 2P_z x + x(x^2 - \delta y^2) \right) - \\
&\frac{(\Delta t)^2}{2} \left(-\kappa x + \frac{\alpha P_z (1 + \delta)y}{2} + \frac{3\alpha(1 + \delta)x^2 y}{4} - \frac{\alpha\delta(1 + \delta)y^3}{4} \right) \\
R_2 &= p_y - (\Delta t) \left(\frac{\alpha^2 y}{4} - \delta P_z y - \frac{\delta x^2 y}{2} + \frac{\delta^2 y^3}{2} \right) - \\
&\frac{(\Delta t)^2}{2} \left(\frac{\alpha(1 + \delta)P_z x}{2} + \frac{\alpha(1 + \delta)x^3}{4} + \delta\kappa y - \frac{3\alpha\delta(1 + \delta)xy^2}{4} \right).
\end{aligned}$$

A minimal amount of linear algebra allows us to complete the inversion of the mapping for P_x and P_y :

$$P_x = \frac{C_{22}R_1 - C_{12}R_2}{\det(\mathbf{C})} \quad (\text{A4.3.3a})$$

$$P_y = \frac{C_{11}R_2 - C_{21}R_1}{\det(\mathbf{C})} \quad (\text{A4.3.3b})$$

Thus the symplectic stepping scheme is thus comprised of equations, (A4.3.2a), (A4.3.3a-b), and (A4.3.2d-f). This integration scheme is identical to the one used to conduct the numerical studies on the fully three dimensional system (1.4.8a-f). Figure (A4.3.1) shows the performance of the routine in time for typical particle out of an ensemble of test-particles used in one of the simulations conducted for this system. The step size was $\Delta t = 10^{-2}$. After nearly 200000 steps, the relative error in the Hamiltonian ϵ_H has climbed to a peak value of 1.7×10^{-4} .

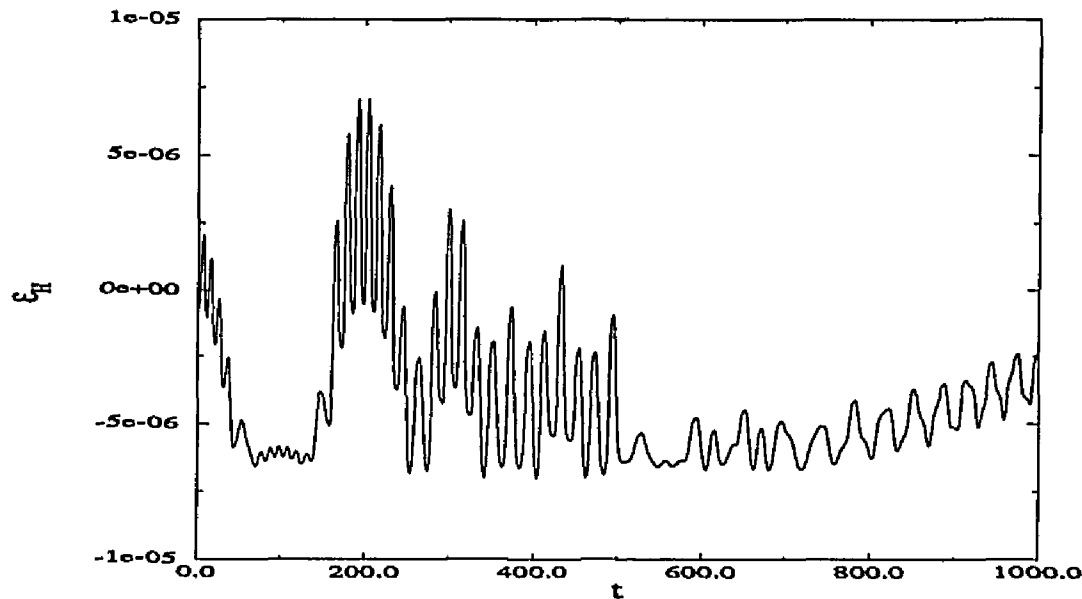


Figure A4.3.1. Relative Error in H vs. Time.

§A4.4 Symplectic Scheme for the Reduced System (5.3.12)

Now we turn our attention to the task of the numerical integration the reduced equation derived in §5.3. Recall the radial equation (5.3.12):

$$\frac{d^2 \rho}{dt^2} + \eta t \rho + \frac{\rho^3}{2} - \frac{1}{\rho^3} = 0, \quad (\text{A4.4.1})$$

where η is a constant. Once again we will employ a symplectic scheme. The first task towards this end is to write (A4.4.1) in Hamiltonian form. Let's rename ρ q and define the canonical momentum p by $p = \dot{q}$. This gives us the system

$$\dot{q} = p, \quad (\text{A4.4.2a})$$

$$\dot{p} = \frac{1}{q^3} - \frac{q^3}{2} - \eta t q. \quad (\text{A4.4.2b})$$

We can now define a nonautonomous Hamiltonian H by integrating (A4.4.2a) with respect to p and (A4.4.2b) with respect to q :

$$H(q, p, t) = \frac{p^2}{2} + \frac{1}{2} \left(\eta t q^2 + \frac{q^4}{4} + \frac{1}{q^2} \right) \quad (\text{A4.4.3})$$

The Hamiltonian system (A4.4.2a,b) and (A4.4.3) is nonautonomous; i.e. the Hamiltonian is explicitly time-dependent. In order to proceed with the construction of a symplectic integration scheme, we must extend the phase space of the system, and then apply the techniques outlined in §A4.2. This extension of the phase space is achieved via a canonical transformation of the second kind [29], with the “old” phase space coordinates being (q, p, t, H) , and the new set of phase space coordinates will be denoted (q_1, q_2, p_1, p_2) with the new extended phase space Hamiltonian K , and new canonical time ζ . Define the new phase space coordinates as:

$$q_1 = q,$$

$$q_2 = t,$$

$$p_1 = p,$$

$$p_2 = -H(q, p, t).$$

The generating function for the extension is F , given by

$$F = p_1 q + p_2 t.$$

The new Hamiltonian K is given by

$$K(q_1, q_2, p_1, p_2) = H + \frac{\partial F}{\partial t}.$$

Thus

$$K(q_1, q_2, p_1, p_2) = \frac{p_1^2}{2} + p_2 + \frac{1}{2} \left(\eta q_2 q_1^2 + \frac{q_1^4}{4} + \frac{1}{q_1^2} \right).$$

(A4.4.4)

Now that we have a system that is autonomous in ζ , we may take up the task of constructing the symplectic integrator. The generating function F is given by

$$F(q_1, q_2, P_1, P_2) = P_1 q_1 + P_2 q_2 + \frac{(\Delta\zeta)}{2} \left(P_1^2 + 2P_2 + \frac{1}{q_1^2} + \frac{q_1^4}{4} + \eta q_1^2 q_2 \right) + \frac{(\Delta\zeta)^2}{2} \left(-\frac{P_1}{q_1^3} + \frac{\eta q_1^2}{2} + \frac{P_1 q_1^3}{2} + \eta P_1 q_1 q_2 \right). \quad (\text{A4.4.5})$$

Using (A4.2.18) to process F , we get the symplectic mapping

$$p_1 = P_1 + \Delta\zeta \left(-q_1^{-3} + \frac{q_1^3}{2} + \eta q_1 q_2 \right) + \frac{\Delta\zeta^2}{2} \left(\frac{3P_1}{q_1^4} + \eta q_1 + \frac{3P_1 q_1^2}{2} + \eta P_1 q_2 \right) \quad (\text{A4.4.6a})$$

$$p_2 = P_2 + \frac{\Delta\zeta \eta q_1^2}{2} + \frac{\Delta\zeta^2 \eta P_1 q_1}{2} \quad (\text{A4.4.6b})$$

$$Q_1 = q_1 + \Delta\zeta P_1 + \frac{\Delta\zeta^2}{2} \left(\frac{-1}{q_1^3} + \frac{q_1^3}{2} + \eta q_1 q_2 \right) \quad (\text{A4.4.6c})$$

$$Q_2 = q_2 + \Delta\zeta \quad (\text{A4.4.6d})$$

The above mapping is linear in P_1 and P_2 , and as such can be made explicit by noting that the (A4.4.6a) involves only linear terms in P_1 , and has no dependence on P_2 . This gives us

$$P_1 = \frac{p_1 - \Delta\zeta \left(-q_1^{-3} + \frac{q_1^3}{2} + \eta q_1 q_2 \right) - \frac{(\Delta\zeta)^2}{2} \eta q_1}{1 + \frac{(\Delta\zeta)^2}{2} \left(\eta q_1 q_2 + \frac{3}{2} q_1^2 + \frac{3}{q_1^4} \right)} \quad (\text{A4.4.7})$$

Also, note that the expression (A4.4.6b) for P_2 is also unnecessary, in that we have a closed-form expression for P_2 ; it is simply the old one-dimensional phase space

Hamiltonian H defined by (A4.4.3), but evaluated at the new values Q_1 and P_1 of the radial phase space variables.

The numerical performance of this integration scheme is quite stunning, indeed. Figure (A4.4.1) shows the extended phase space Hamiltonian $K(q_1, q_2, p_2, p_2)$ versus time. Ideally, we expect the value of K to be zero, but would be prepared to accept it being as large as $(\Delta\zeta)^3 = 10^{-6}$. What we find, however, is that K oscillates with an amplitude on the order of 10^{-16} .

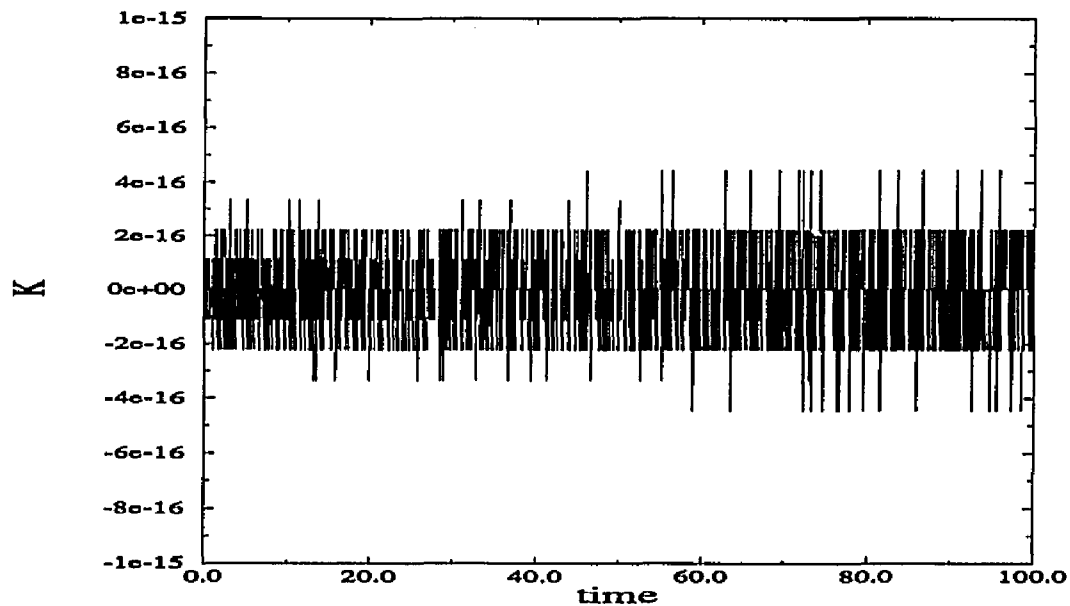


Figure A4.4.1. Extended Phase Space Hamiltonian vs. Time.

APPENDIX FIVE
COMPUTER SIMULATION CODE XOSSIM.F

The following computer code was developed and run on Sun and IBM workstations, as well as CRAY II computers. Though the variable declaration statements are the data type `real`, the code was always compiled using the implicit double precision option, meaning that all of our real floating point arithmetic was done using the data type `real*8`.

XOSsim

program XOSsim

```

*****
* *****
* * This code calculates particle trajectories for reconnection
* * fields, including X- and O-type neutral lines, as well as
* * neutral plane fields.
* * The magnetic field is taken to be:
* *  $B_x = \delta * y$ ,  $B_y = x$ ,  $B_z = \alpha = \text{constant}$ .
* * The electric field is  $E_z = \epsilon$ 
* ***** 10
*****
      parameter (nmps = 50001)
      parameter(nbins = 100)
c
      real kappa,length,mass
c
      real x0(nmps),y0(nmps),z0(nmps),px0(nmps),py0(nmps),
& pz0(nmps),t(nmps),dt(nmps),x(nmps),y(nmps),z(nmps),
& px(nmps),py(nmps),pz(nmps),h(nmps),herr(nmps),
& ham0(nmps),efin(nmps),amufin(nmps),tfin(nmps),
& esubl(nbins),hamfin(nmps),qguide(nmps),curre(nmps),
& effin(nmps)
c
      integer ifin(nmps),nsurf(nmps),num(nbins)
common /fields/ alfa,b0,delta,efield,kappa
common /slab/ xunif,yunif,ymax,ifxu,ifyu,iflat
common /intpars/ dtmin,nitmax
c
c open input & output files...
c
      open(95, file='upsilon.d')
      open(97, file='omegax.d')
      open(98, file='omegay.d')
      open(99, file = 'jy.d')
      open(7, file='muout.d')
      open(8, file='hamout.d')
      open(9, file='reclog.d')
      open(14, file='xpx.d')
      open(15, file = 'ypy.d')
      open(16, file='zpz.d')
      open(17, file='efin.d')
      open(18, file='tfin.d')
      open(19, file='mufin.d')
      open(20, file='hist.d')
40

```

```

        open(21, file='enot.d')
        open(22, file='jx.d')
        open(30, file='xy.d')
        open(31, file='xz.d')
        open(32, file='yz.d')
        open(33, file='xyz.d')
        open(34, file='hamfin.d')
        open(47, file='ftefin.d')
open(4, file='XOSsim.d')
open(13, file='inout.d')
open(69, file='isurf.d')
open(70, file='isurf2.d')
open(71, file='fluxs.d')
open(73, file='gcs.d')
open(74, file='stuff.d')
open(75, file='rho0.d')
open(76, file='rhop.d')
open(77, file='rhoz.d')
open(78, file='phi.d')
open(79, file='vperp.d')
open(80, file='vpar.d')
open(81, file='munot.d')
open(91, file='tunmag.d')
open(96, file='ke.d')
c
c Read in parameters...
c
read(4,2) alfa,b0,delta,efield
read(4,5) ymax,ifxu,ifyu,iflat
read(4,3) h0,amu0
read(4,3) psi0,dpsi
read(4,4) xmin,xmax
read(4,*) znot
read(4,4) phiof0,phscale
if(delta .lt. 0.) then
  if(ifyu .eq. 1) then
    xmin = -0.5*sqrt(abs(2. * psi0))
    xmax = 0.5*sqrt(abs(2. * psi0))
  endif
  if(ifxu .eq. 1) then
    ymin = -0.5*sqrt(abs(2. * psi0 / delta))
    ymax = 0.5*sqrt(abs(2. * psi0 / delta))
  endif
endif
endif

```

```

if(delta .eq. 0.) then
  if(ifxu .eq. 1) then
    ymin = xmin
    ymax = xmax
    xunif = sqrt(abs(2. * psi0))
  endif
  if(ifyu .eq. 1) then
    yunif = sqrt(abs(2. * psi0))
  endif
endif
if(delta .gt. 0.) then
  if(ifxu .eq. 1) then
    ymin = xmin
    ymax = xmax
  endif
endif
psimin = psi0 - dpsi
psimax = psi0 + dpsi
  read(4,6) iran,iexb,iprints,inoint,iact
2  format(4(e12.5,1x))
3  format(2(e11.4,1x))
4  format(2(e17.10,1x))
5  format(e9.2,3(1x,i1))
6  format(5(i1,1x))
  read(4,2001) nparts,ntype
  write(9,2301) nparts,ntype
  read(4,2002) jmax,ntrial,nitmax,nord,icut,
&  iprint,iprints,i3d,icsonly,itest,ihist
  write(9,2302) jmax,ntrial,nitmax,nord,icut,
&  iprint,iprints,i3d,icsonly,itest,ihist
  read(4,2007) t0,dt0,tmax
  read(4,2006) dtfudge,hfudge
  read(4,2006) q,mass
read(4,*) rmax
read(4,*) tinc
  write(9,2305) rmax,tinc
read(4,*) isptraj
if(isptraj .eq. 1) then
  read(4,*) xs0,ys0,zs0,pxs0,pys0,pzs0
  xs = xs0
  ys = ys0
  zs = zs0
  pxs = pxs0
  pys = pys0

```

```

        pzs = pzs0
        call hamilt(xs,ys,zs,pxs,pys,pzs,hs0)
        hs = hs0
        ts = ts0
        dts = dt0
        herrs = hs0 * (dts ** (nord+1))
        nspec = 1
endif
ifail = 0
ifintot = 0
pi = acos(-1.0)
twopi = 2.0 * pi
phscale = phscale * twopi
tiny = 1.0e-14
c = 2.99792458e10
qe = 4.8032068e-10
pmass = 1.6726231e-24
emass = 9.1093897e-28
if(ntype .eq. 1) then
    mass = mass * pmass
    q = qe
endif
if(ntype .eq. 2) then
    mass = mass * emass
    q = -qe
endif
omega0 = q * b0 / (mass * c)
length = 100.
kappa = q * efield / (mass * length *
&zomega0**2)
    write(9,2310) b0,delta,alfa,efield,q,mass
    write(9,2312) length,omega0,kappa
    write(9,2316) tmax,dt0,tolf,tolx
    write(9,2318) h0,amu0,psi0,znot,xmin,xmax,
&zphiof0,phimax
c
c    call up the initialization routine INIT...
c
if(isptraj .ne. 1) then
    call init(xmin,xmax,nparts,h0,amu0,psi0,znot,x0,
&zy0,z0,px0,py0,pz0,ham0,qguide,ekbar0,phiof0,phscale,
&ziexb,iran,iprints,np)
c
c    check to see if integration of the trajectories is

```

```

c      desired...If only a set of particles about a flux
c      surface is wanted, inoint is one...
c
c      if(inoint .ne. 1) then
c
c      set size of minimum step, dsmin
c
c      dtmin = dtfudge * dt0**(nord + 1)
c
c      do 100 n=1,np
c
c      herr(n) = ((abs(dt0))**(nord+1)) * ham0(n) * hfudge
c
c      set up values of coordinates & momenta for use in
c      the integration scheme...
c
c      x(n)= x0(n)
c      y(n)= y0(n)
c      z(n)= z0(n)
c      px(n)= px0(n)
c      py(n)= py0(n)
c      pz(n)= pz0(n)
c      t(n) = t0
c      dt(n) = dt0
c      h(n) = ham0(n)
c      ifin(n) = 0
c
c      100 continue
c
c      ifintot = 0
c
c      begin integration...
c
c      write(6,*) np
c      do 1000 n=1,np
c
c      call the particle pusher for this particle...
c
c      ifail = 0
c      psif = psi0
c      call parpush(n,x(n),y(n),z(n),px(n),py(n),pz(n),t(n),dt(n),h(n),
c      &ham0(n),herr(n),efin(n),eftfin(n),tfin(n),amufin(n),ifail,ifin(n),
c      &icsonly,itest,icut,rmax,tmax,tinc,jmax,curre(n),psi0,psimin,

```

```

&psimax,nsurf(n))
c
    ifintot = ifintot + ifin(n)
    if(ifail .ne. 0) write(6,2320) n,ifail
c
c    calculate the final hamiltonian
c
    call hamilt(x(n),y(n),z(n),px(n),py(n),pz(n),hamfin(n))
1000 continue
c
c    determine max & min values of the final kinetic
c    energy for the distribution...y
c
    if((iprint .eq. 1) .or. (ihist .eq. 1)) then
        ektot = 0.
        ekmax = 0.
        ekmin = 1.e10
        nspec = 2
c
c    Write out final quantities, and determine the most
c    energetic particle...
c
        ekavf = 0.
        ekavft = 0.
        current = 0.
    do 1100 n=1,np
        if(itest .eq. 5) write(47,2005) qguide(n),eftfin(n)
        write(17,2005) qguide(n),efin(n)
        write(18,2005) qguide(n),tfin(n)
        write(19,2005) qguide(n),amufin(n)
        herr(n) = (hamfin(n) - ham0(n)) / ham0(n)
        write(34,2005) qguide(n),herr(n)
        ekavf = ekavf + efin(n) / float(np)
        if(itest .eq. 5) then
            ekavft = ekavft + eftfin(n) / float(np)
        endif
        current = current + curre(n) / float(np)
c
    if(efin(n) .gt. ekmax) then
        nspec = n
        ekmax = efin(n)
    endif
    if(efin(n) .lt. ekmin) then
        nmin = n

```



```

        emin = efn(n)
        endif
1100    continue
        emax = efn(nspec)
        emin = efn(nmin)
    endif
    if(ihist .eq. 1) then
        erange = emax - emin
        deltae = erange / float(nbins)
        do 1150 l=1,nbins
            esubl(l) = efn(nmin) + float(l) * delatae
            num(l) = 0
1150        continue
            do 1200 n=1,np
                lbino = int((efn(n) - emin) / deltae) + 1
                num(lbino) = num(lbino) + 1
1200            continue
                do 1250 m=1,nbins
                    write(20,2015) esubl(m),num(m)
1250                continue
            endif
c          This is where the single particle trajectory control jumps in...
        endif
c
        if((iprint .eq. 1) .or. (isptraj .eq. 1)) then
            tnext = ts + tinc
c
c          if this is not a s.p. trajectory, initialize xs, et cetera...
c
            if(isptraj .eq. 0) then
                xs = x0(nspec)
                ys = y0(nspec)
                zs = z0(nspec)
                pxs = px0(nspec)
                pys = py0(nspec)
                pzs = pz0(nspec)
                ts = t0
                dts = dt0
                hs0 = ham0(nspec)
                hs = hs0
                herrs = herr(nspec)
                iystart = 0
                ixstart = 0
                nyper = 0
            endif
        endif
    endif

```

270

280

290

300

```

        nxper = 0
        txp = 0.
        typ = 0.
        xdsn = pxs + 0.5 * alfa * ys
        ydsn = pys - 0.5 * alfa * xs
    endif
c
c   Write out first line of trajectory data file .
c
        write(14,2005) xs,pxs
        write(15,2005) ys,pys
        write(16,2005) zs,pzs
        write(20,2005) ts,dts
        write(30,2005) xs,ys
        write(31,2005) xs,zs
        write(32,2005) ys,zs
c
c
c       if(i3d .eq. 1) write(33,2008) xs,ys,zs
c
c   do 1300 j=1,jmax
c       if(idone .ne. 1) then
c           call step(xs,ys,zs,pxs,pys,pzs,ts,dts,xsn,ysn,
&zsn,pxsn,pysn,pzsn,hs,hs0,hsn,herrs,nit,ntrial,
&icut,ifail)
c
c           if(ifail .eq. 1) write(9,2100) n,nit,dt,j
c           xds = xdsn
c           yds = ydsn
c           xdsn = pxsn + 0.5 * alfa * ysn
c           ydsn = pysn - 0.5 * alfa * xsn
c           if(iact .ne. 0) then
c               if(ixstart .eq. 1) then
c                   dx = xsn - xs
c                   pxavg = 0.5 * (pxs + pxsn)
c                   actx = actx + pxavg * dx
c                   if(xds*xdsn .le. 0.) then
c                       nxper = nxper + 1
c                       if(mod(nxper,2) .eq. 0) then
c                           write(22,2005) ts,actx
c                           taux = ts - txp
c                           txp = ts
c                           if(taux .ne. 0.) then
c                               omegax = twopi / taux
c                           else

```

310

320

330

340

350

```

        omegax = 0.0
        endif
        write(97,2005) ts,omegax
        actx = 0.
    endif
endif
endif
if(iystart .eq. 1) then
    dy = ysn - ys
    pyavg = 0.5 * (pys + pysn)
    acty = acty + pyavg * dy
    if(yds*ydsn .le. 0.) then
        nyper = nyper + 1
        if(mod(nyper,2) .eq. 0) then
            write(99,2005) ts,acty
            tauy = ts - typ
            if(tauy .ne. 0.) then
                omegay = twopi / tauy
            else
                omegay = 0.0
            endif
            typ = ts
            write(98,2005) ts,omegay
            acty = 0.
        endif
    endif
endif
endif
if(ixstart .eq. 0) then
    if(xds*xdsn .le. 0.) then
        nxper = 0
        actx = 0.
        txp = ts
        ixstart = 1
    endif
endif
if(iystart .eq. 0) then
    if(yds*ydsn .le. 0.) then
        nyper = 0
        actx = 0.
        typ = ts
        iystart = 1
    endif
endif
endif
endif

```

```

c
c  evaluate the particle unmagnetization function epsilon...
c
    vx = pxsn - ax(xsn,ysn,zsn)
    vy = pysn - ay(xsn,ysn,zsn)
    vz = pzsn - az(xsn,ysn,zsn)
    eknow = vx*vx + vy*vy + vz*vz
    bx = bex(xsn,ysn,zsn)
    by = bwhy(xsn,ysn,zsn)
    bz = bzee(xsn,ysn,zsn)
    bt = sqrt(bx*bx + by*by + bz*bz)
    vpa = (vx*bx + vy*by + vz*bz) / bt
    vper = sqrt(2.*abs(ho - vpa*vpa))
    gyrorho = vper / bt
    amus = vper * gyrorho
    gbob = sqrt((delta**4)*ysn*ysn + xsn*xsn) / (bt*bt + tiny)
    epsilon = gyrorho * gbob
    write(95,2005) ts,epsilon
c
c  update trajectory data
c
    xs= xsn
    ys= ysn
    zs= zsn
    pxs= pxsn
    pys= pysn
    pzs= pzsn
    herrs = (hsn - hs0) / hs0
    hs = hsn
c
c  Pause to print out trajectory number nspec (if desired).
c
    if(ts .ge. tnext) then
    tnext = ts + tinc
    write(7,2005) ts,amus
    write(96,2005) ts,eknow
    write(8,2005) ts,herrs
    write(14,2005) xs,pxs
    write(15,2005) ys,pys
    write(16,2005) zs,pzs
    write(20,2005) ts,dts
    write(30,2005) xs,ys
    write(31,2005) xs,zs
    write(32,2005) ys,zs

```

```

c          if(i3d .eq. 1) then
c              write(33,2008) xs,ys,zs
c          endif
          endif
          if(ts .ge. tmax) idone = 1
      endif
c
1300  continue
c
      endif
c
          write(9,2075) nparts,ifintot
          write(9,2200) nspec
          heatr = ekavf / ekbar0
          if(itest .eq. 5) then
              heatftr = ekavft / ekbar0
              write(9,2265) ekavft,heatftr
          endif
          write(9,2205) ekavf,heatr
          write(9,2206) tmax,current
          write(9,2207) ifxu,ifyu,iflat,xunif,yunif
c
c      format statements
c
2000  format(6(e16.10,1x))
2001  format(i6,1x,i1)
2002  format(i6,2(1x,i2),8(1x,i1))
2003  format(3(f7.3,1x))
2005  format(2(e18.12,2x))
2006  format(2(e8.2,1x))
2007  format(3(e8.2,1x))
2008  format(3(e16.10,1x))
2010  format(6(e9.3,1x))
2015  format(e16.10,1x,i6)
2075  format('Out of a total of ',i6,' particles, ',i6,
&' completed their runs ',/'and exited the scattering
& region. ')
2100  format(10x,'Out of luck, cowboy--Particle number ',i6,
& ' stalled after ',i4,' shots with dt = ',e16.10,'and
& j = ',i6)
2200  format('Trajectory data corresponds to particle # ',i6)
2205  format('Average Final Kinetic Energy = ',e12.6,/'Ratio
& of final to initial kinetic energies = ',e12.6)
2206  format('Average current at time t = ',e12.6,' is j = ',

```

```

&el2.6)
2207 format('Orientation and I.S. type parameters : ',/'ifxu = ',
&i1,10x,'ifyu = ',i1,10x,'iflat = ',i1,/'xunif = ',e14.8,10x,
&'yunif = ',e14.8)
2265 format('Average Fixed Time Final Kinetic Energy = ',e12.6,/'Ratio
& of fixed time final to initial kinetic energies = ',e12.6) 490
2301 format('Simulation of ',i6,' particles.',/'ntype = ',i1)
2302 format('Max. no. of steps : ',i6,/'ntrial = ',i2,
&5x,'nitmax = ',i2,5x,'nord = ',i1,5x,'icut = ',i1,/'
&'iprint = ',i1,5x,'iprints = ',i1,5x,'i3d = ',i1,/'
&'icsonly = ',i1,5x,'itest = ',i1,5x,'ihist = ',i1)
2305 format('Radius of the NULL BALL = ',e10.4,/'Time
&interval between trajectory points = ',e10.4)
2310 format('Field parameters : ',/'B0 = ',e9.3,5x,'delta = ',
&e9.3,5x,'alfa = ',e9.3,5x,'E0 = ',e9.3,/'q = ',e9.3,
&' esu',10x,'m = ',e9.3,' g') 500
2312 format('Scale length = ',e11.5,' cm',/'Omega0 = ',
&e11.5,10x,'kappa = ',e11.5)
2316 format('tmax = ',e9.3,10x,'dt0 = ',e9.3,/'tolf = ',
&e9.3,10x,'tolx = ',e9.3)
2318 format('Flux surface parameters:',/'H0 = ',e9.3,10x,
&'Mu0 = ',e9.3,/'Psi0 = ',e9.3,10x,'z0 = ',e9.3,/'
&'xmin = ',e9.3,10x,'xmax = ',e9.3,/'phiof0 = ',e10.4,
&10x,'phscale = ',e10.4)
2320 format('Particle number ',i6,' crapped out with ifail = ',
&i1) 510
c
endif
c
end
*****
***** PARPUSH *****
*****
subroutine parpush(n,xo,yo,zo,pxo,pyo,pzo,to,dto,ho,ha0,hepa,parpush
&ekf,ftkf,tf,amuf,ifail,ifinish,icsonly,itest,icut,rmax,tmax,tinc,
&jmax,curr,psinot,psimin,psimax,next) 520
real kappa
common /fields/ alfa,b0,delta,efield,kappa
common /slab/ xunif,yunif,ymax,ifxu,ifyu,iflat
c
c This is the particle pusher. This routine pushes single particles
c for the chaotic scattering calculation. It uses one of three different
c types of tests to trap the particle, each of which is signaled by a
c particular value of the integer itest.

```

```

c
c   if itest = 1, push until a particular z-value is reached.           530
c
c   if itest = 2, push until a particular time tmax is reached.
c
c   if itest = 3, push the particle until it scatters out to a
c   distance rmax from the origin.
c
c   if itest = 4, the initial surface is single-valued in x, psinot>0,
c   and we require that the particle pass through the field line separatrix
c   reaching an outgoing flux surface psi = -psinot.
c
c
c   if itest = 5, the initial surface is single-valued in y, psinot<0,
c   and we require that the particle pass through the field line separatrix
c   reaching an outgoing flux surface psi = -psinot.
c
c
c   if itest = 6, we are using the time diagnostic--push the particles
c   until a time t=tmax is reached. This diagnostic is applicable to the
c   closed field line (i.e. elliptical and circular) cases. This is the
c   same diagnostic as the case itest=2, except that this flag allows us to
c   calculate a final value of <vz>, which is proportional to the current.
c
c
c   if itest = 7, we are considering the case of the slab (delta=0)
c   configuration, and we push the particle until it has drifted a
c   distance ymax along the y-axis (note that for the slab, py = constant).
c
c
c   ipsid = 0
c   do 3000 j=1,jmax
c
c   ARE WE DEAD? If ifail =1, the answer is yes.
c   If isconly=1, then we only want chaotic scattering
c   data, so the code will stop when all of the particles
c   have satisfied the appropriate exit condition.
c   Satisfaction of the appropriate exit condition for a
c   particular particle is signified by setting the flag
c   ifinish equal to 1.
c
c   if(((ifail .eq. 0) .or. (iconly .ne. 1)) .and.
c   & (ifinish .ne. 1)) then
c
c   Take a step of size dt...
c
c   call step(xo,yo,zo,pxo,pyo,pzo,to,dto,xn,yn,zn,pxn,

```

```

&pyn,pzn,ho,ha0,hnew,herro,nit,ntrial,icut,ifail)
c
  if(ifail .eq. 1) write(9,3100) n,nit,dt,j
  if(ifail .eq. 2) write(6,*) to,xo,xn,yo,yn
c
c   Now that we have the coordinates at the new point, check to see if
c   any poincare surfaces of section have been crossed, and if so, write
c   this information to the appropriate file... 580
c
c   for now, just reset coordinates & momenta to new values, as well
c   as h & t:
c
  xo = xn
  yo = yn
  zo = zn
  pxo = pxn
  pyo = pyn
  pzo = pzn 590
  ho = hnew
c
c   check to see whether the particle is magnetized or
c   unmagnetized...
c
  vx = pxo - ax(xo,yo,zo)
  vy = pyo - ay(xo,yo,zo)
  vz = pzo - az(xo,yo,zo)
  bx = bex(xo,yo,zo)
  by = bwhy(xo,yo,zo) 600
  bz = bzee(xo,yo,zo)
  bt = sqrt(bx*bx + by*by + bz*bz)
  vpa = (vx*bx + vy*by + vz*bz) / bt
  vper = sqrt(2.*abs(ho - vpa*vpa))
  gyrorho = vper / bt
  gbob = sqrt((delta**4)*yo*yo + xo*xo) / (bt*bt + tiny)
  upsilon = gyrorho * gbob
  if(iunmag .ne. 1) then
    if(upsilon .ge. 1.) then
      iunmag = 1 610
      tunmag = to
      nunmag = nunmag + 1
    endif
  else
    if(upsilon .lt. 1) then
      iunmag = 0

```



```

        ttunmag = to - tunmag
    endif
endif
c
c
c      check to see if the particle satisfies "exit" condition
c      on this step, and keep a running tally on how many particles
c      have exited the scattering region by summing up values of ifinish.
c
    if(itest .eq. 1) then
        if(z0 .ge. zmax) then
            ifinish = 1
            ifintot = ifintot + 1
            call kefin(xo,yo,zo,pxo,pyo,pzo,ekf,amuf)
            if(efin .eq. 0.) write(6,3200) xo,yo,zo,pxo,
&pyo,pzo
            tf = to
        endif
    endif
c
    if(itest .eq. 2) then
        if(to .ge. tmax) then
            ifinish = 1
            call kefin(xo,yo,zo,pxo,pyo,pzo,ekf,amuf)
            if(ekf .eq. 0.) write(6,3200) xo,yo,zo,pxo,pyo,pzo
            call hamilt(xo,yo,zo,pxo,pyo,pzo,hf)
            write(91,*) n,nunmag,ttunmag
            tf = to
        endif
    endif
c
    if(itest .eq. 3) then
        r = sqrt(xn*xn + yn*yn + zn*zn)
        if(r .ge. rmax) then
            ifinish = 1
            call kefin(xo,yo,zo,pxo,pyo,pzo,ekf,amuf)
            tf = to
        endif
    endif
    if(itest .eq. 4) then
        psinow = 0.5 * (delta * yn * yn - xn * xn)
        if(psinow .le. -psinot) then
            ifinish = 1
            call kefin(xo,yo,zo,pxo,pyo,pzo,ekf,amuf)
            tf = to

```

```

        if(xo .lt. 0.) nexit = 3
        if(xo .gt. 0.) nexit = 1
    endif
endif
if(itest .eq. 5) then
    psinow = 0.5 * (delta * yn * yn - xn * xn)
    if(psinow .ge. -psinot) then
        ifinish = 1
        call kefin(xo,yo,zo,pxo,pyo,pzo,ekf,amuf)
        tf = to
        if(xo .lt. 0.) nexit = 3
        if(xo .gt. 0.) nexit = 1
    endif
endif
if(itest .eq. 6) then
    psinow = 0.5 * (delta * yn * yn - xn * xn)
    if((psinow .le. psimin) .and. (ifinish .ne. 1)) then
        call kefin(xo,yo,zo,pxo,pyo,pzo,ekf,amuf)
        tf = to
        if(xo .lt. 0.) nexit = 3
        if(xo .gt. 0.) nexit = 1
    endif
    if(to .ge. tmax) then
        call kefin(xo,yo,zo,pxo,pyo,pzo,eftkf,amuf)
        ifinish = 1
        curr = vz
    endif
endif
if(itest .eq. 7) then
    if(abs(yo) .ge. ymax) then
        call kefin(xo,yo,zo,pxo,pyo,pzo,ekf,amuf)
        tf = to
        ifinish = 1
    endif
endif
c
endif
c
3000 continue
3100 format(10x,'Out of luck, cowboy--Particle number ',i4,
& ' stalled after ',i4,' shots with dt = ',e16.10,'and
& j = ',i5)
3200 format(6(e16.10,1x))
return

```

end

```

*****
***** STEP *****
*****
c
c   This is the stepper for the integration scheme.                                710
c
c   subroutine step(q1,q2,q3,p1,p2,p3,s,ds,q1n,q2n,q3n,p1n,p2n,p3n, step
&   hnow,hnot,hnew,dhmax,nit,ntrial,icut,ifail)
c   real kappa
c   common /fields/ alfa,b0,delta,efield,kappa
c   common /intpars/ dtmin,nitmax
*****
*****
c   If icut = 0: turn off the error control; topology, not
c   numbers is the key...                                                            720
c
c   If icut = 1: test to see if the Hamiltonian is conserved within
c   reasonable limits...If the step is unsuccessful, cut the step
c   size in half. If the step is successful, try doubling the stepsize
c   on the next run...
*****
*****
c   if(icut .eq. 0) then
c       call symmap(q1,q2,q3,p1,p2,p3,s,ds,q1n,q2n,q3n,p1n,p2n,
&   p3n,ntrial,ifail)                                                                730
c       call hamilt(q1n,q2n,q3n,p1n,p2n,p3n,hnew)
c   endif
c   if(icut .eq. 1) then
c       do 2500 i=1,nitmax
c       call symmap(q1,q2,q3,p1,p2,p3,s,ds,q1n,q2n,q3n,p1n,p2n,
&   p3n,ntrial,ifail)
c       call hamilt(q1n,q2n,q3n,p1n,p2n,p3n,hnew)
c       if(abs((hnew - hnow) / hnot) .gt. abs(dhmax)) then
c           s = s - ds
c           nit = nit + 1                                                            740
c           ds = ds / 2.
c           if((abs(dt).le.abs(dtmin)) .or. (i .eq. nitmax)) then
c               ifail = 1
c           endif
c       else
c           nit = 0
c           ds = 2. * ds
c       return

```

```

endif
2500 continue
endif
return
end

```

```

*****
***** HAMILT *****
*****

```

```

subroutine hamilt(q1,q2,q3,p1,p2,p3,hamil)          hamilt
real kappa
common /fields/ alfa,b0,delta,efield,kappa
hx = 0.5 * (p1 - ax(q1,q2,q3))**2                760
hy = 0.5 * (p2 - ay(q1,q2,q3))**2
hz = 0.5 * (p3 - az(q1,q2,q3))**2
hamil = hx + hy + hz + potl(q1,q2,q3)
return
end

```

```

*****
***** POTL *****
*****

```

```

real function potl(q1,q2,q3)                      potl
real kappa                                       770
common /fields/ alfa,b0,delta,efield,kappa
potl = -kappa * q3
return
end

```

```

*****
***** SYMMAP *****
*****

```

```

c
c   Here is the symplectic map...
c
c   subroutine symmap(q1,q2,q3,p1,p2,p3,s,ds,q1n,          780
&  q2n,q3n,p1n,p2n,p3n,ntrial,ifail)                    symmap
real kappa
common /fields/ alfa,b0,delta,efield,kappa

```

```

c
c   The following symplectic integration scheme takes us from the
c   phase-space vector (q1,q2,q3,p1,p2,p3) at time s to the vector
c   (q1n,q2n,q3n,p1n,p2n,p3n) at time s + ds. This
c   scheme is an explicit and second-order in ds.

```

```

c
c   Definitions of useful combinations of variables that show
c   up repeatedly in the mapping equations...

```

```

c
    q12 = q1 * q1
    dq22 = delta * q2 * q2
    dq1q2 = delta * q1 * q2
    ds2 = ds*ds
    q1o2 = 0.5 * q1
    q2o2 = 0.5 * q2
    alfa2 := alfa*alfa
c
c
    Take step dt forward in time...
c
    s = s + ds
c
    First, step the momenta...
    p3n = p3 + kappa*ds
c
c
    The stepping in px & py is implicit, but linear. Write it
c
    in matrix form AP = R, and invert A to get the new momenta
c
    P. First, write down the elements of A...
c
    a11 = 1. + 0.25*ds2*(2.*p3n + 3.*q12 - dq22)
    a12 = -0.5*ds*(alfa + ds*dq1q2)
    a21 = a12 + alfa
    a22 = 1. - 0.25*delta*ds2*(2.*p3n + q12 - 3.*dq22)
    det = a11*a22 - a12*a21
c
    Now the right-hand-side vector R...
    term1 = kappa*ds - 2.*p3n - q12 + dq22
    r1 = p1 + 0.5*ds*q1*(-0.5*alfa2 + term1) +
    &alfa*q2*ds2*(-2.*p3n - 3.*q12 + dq22)*(1. + delta)/8.
    r2 = p2 + 0.5*ds*q2*(-0.5*alfa2 - delta*term1) +
    &alfa*q1*ds2*(1. + delta)*(-2.*p3n - q12 + 3.*dq22)/8.
c
c
    Now, invert A to get p1n & p2n...
c
    p1n = (a22*r1 - a12*r2) / det
    p2n = (-a21*r1 + a11*r2) / det
c
    now, the coordinates...
    *****
    q1n = q1 + ds*(p1n + alfa*q2o2) + 0.5*ds2*q1o2*(2.*p3n + q12
    & dq22)
c
    q2n = ds*(p2n - alfa*q1o2) + q2 + 0.5*delta * ds2 * q2o2*
    & (-2.*p3n - q12 + dq22)
    *****
    q3n = 0.5*ds2*(-kappa + p1n*q1 - delta*p2n*q2 + alfa*q1*

```

```

&      q2o2 + alfa*dq1q2/2.) + 0.5*ds*(2.*p3n + q12 -
&      dq22) + q3
return
end

```

840

```

*****
***** KEFIN *****
*****

```

```

c
c      kefin computes the final kinetic energy of the particle...
c

```

```

subroutine kefin(q1,q2,q3,p1,p2,p3,energy,amuf)      kefin
real kappa
common /fields/ alfa,b0,delta,efield,kappa
xdot = p1 + 0.5 * alfa * q2                        850
ydot = p2 - 0.5 * alfa * q1
zdot = p3 + 0.5 * (q1*q1 - delta*q2 *q2)
energy = 0.5 * (xdot**2 + ydot**2 + zdot**2)
vtot2 = 2. * energy
bt = btot(q1,q2,q3)
vpa = xdot * (bex(q1,q2,q3) / bt) + ydot *
&(bwhy(q1,q2,q3) / bt) + zdot * (bzee(q1,q2,q3) / bt)
vper2 = vtot2 - vpa * vpa
amuf = vper2 / (2. * bt)
return
end

```

860

```

*****
***** INIT *****
*****

```

```

subroutine init(qmin,qmax,nparts,h0,amu0,psi0,znot,q10,q20,      init
&q30,p10,p20,p30,hami0,qgc,ekavg0,phiof0,phisca,iexb,iran,
&ziprints,np)

```

```

*****
*****
**      INIT   This code sets up an ensemble of nparts+1      870
**      particles on an energy surface h0, all particles
**      having the same initial magnetic moment amu0 and all
**      particles residing on the same flux surface psi0 (i.e.
**      on the same field line.  The code drops a set of guiding
**      centers on the initial psi0 surface, and then winds
**      them about this line by incrementing the gyrophase phi.
**      The code computes the parallel and perpindicular velocities
**      for the test particles, as well as their canonical momenta.
**      It also checks to be sure that this process places the
**      particles within an energy shell of thickness 2. * hittol.      880

```

```

*****
*****
parameter(nmps = 50001)
  real q10(nmps),q20(nmps),q30(nmps),p10(nmps),p20(nmps),
&p30(nmps),vpar(nmps),xgc(nmps),ygc(nmps),vparp(nmps),
&vper(nmps),v3(nmps),hami0(nmps),vpa2(nmps),vx(nmps),
&vy(nmps),vz(nmps),v4(nmps),energy0(nmps),qgc(nmps)
  real kappa
  common /fields/ alfa,b0,delta,efield,kappa
  common /slab/ xunif,yunif,ymax,ifxu,ifyu,iflat
c
c   define the constants pi & twopi
c
c   pi = acos(-1.)
c   twopi = 2. * pi
c
c   define error tolerance hittol...
c
c   hittol = 1.e-2 * h0
c   ekavg0 = 0.
c
c   Now, set all of the z--values...
c
c   do 9 i=1,nparts
c     q30(i) = znot
9   continue
c
c   find center of the flux surface.
c
c   qcent = (qmin + qmax ) / 2.
c   if((ifyu .eq. 1) .and. (delta .ne. 0.))then
c     xcent = qcent
c     if(delta .gt. 0.) then
c       ycent = yxsurf(xcent,psi0)
c     endif
c     if(delta .lt. 0.) then
c       ycent = yosurf(xcent,psi0)
c     endif
c   endif
c   if((ifxu .eq. 1) .and. (delta .ne. 0.)) then
c     ycent = qcent
c     if(delta .gt. 0.) then
c       xcent = xxsurf(ycent,psi0)

```

```

endif
if(delta .lt. 0.) then
  xcent = xosurf(ycent,psi0)
endif
endif
if(delta .eq. 0.) then
  if(ifxu .eq. 1) then
    ycent = qcent
    xcent = xunif
  endif
  if(ifyu .eq. 1) then
    xcent = qcent
    ycent = yunif
  endif
endif
endif
c
c calculate the total magnetic field at the center of the
c distrubution
c
  bpcent = bpol(xcent,ycent,znot)
  bcent = btot(xcent,ycent,znot)
c
c calculate the parallel & perpindicular velocities
c at the center of the distribution.
c
  vp2cent = vpar2(h0,amu0,xcent,ycent,znot)
  if(vp2cent .lt. 0.) then
    write(13,15) vp2cent
15    format('Parallel velocity at center of distribution
&         is imaginary; vp2cent = ',l10.4)
    ifail = 1
  endif
  if(ifail .ne. 1) then
    vpcent = sqrt(vp2cent)
    vperpc = vperp(amu0,xcent,ycent,znot)
c
c vpcp is the component of the parallel velocity that lies
c in the x-y plane...
c
  vpcp = vpcent * bpcent / bcent
c
c initialize gyrophase phi to value phi0
c
  phi0 = phiof0 + qlmin * phisca

```



```

c
      dq0 = (qmax - qmin) / float(nparts)
      dphi0 = phisca * dq0
c
c   Here is the loop that initializes the particles...
c
      np = 0
      do 600 n=1,nparts+1
c
c   set guiding center position xgc(n),ygc(n).
c   if ifyu = 1, a distribution that is single-valued in
c   y is desired...
c
      if((delta .ne. 0.) .and. (ifyu .eq. 1)) then
        xgc(n) = qmin + float(n-1) * dq0
        qgc(n) = xgc(n)
        if(xgc(n) .le. qmax) then
          if(delta .gt. 0.) then
            ygc(n) = yxsurf(xgc(n),psi0)
          endif
          if(delta .lt. 0.) then
            ygc(n) = yosurf(xgc(n),psi0)
          endif
        endif
      endif
c
c   For ifxu = 1, we
c   set up a distribution that is single-valued in y...
c
      if((delta .ne. 0.) .and. (ifxu .eq. 1)) then
        ygc(n) = qmin + float(n-1) * dq0
        qgc(n) = ygc(n)
        if(ygc(n) .le. qmax) then
          if(delta .gt. 0.) then
            xgc(n) = xxsurf(ygc(n),psi0)
          endif
          if(delta .lt. 0.) then
            xgc(n) = xosurf(ygc(n),psi0)
          endif
        endif
      endif
c
c   Set up I.C.s if a slab configuration is desired...
c

```

970

980

990

1000

1010

```

        if(delta .eq. 0.) then
c
c   I.C.'s along a line xgc = constant...
c
            if(ifxu .eq. 1) then
                ygc(n) = qmin + float(n-1) * dq0
                qgc(n) = ygc(n)
                xgc(n) = xunif
            endif
c
c   I.C.'s along a line ygc = constant...
c
            if(ifyu .eq. 1) then
                xgc(n) = qmin + float(n-1) * dq0
                qgc(n) = xgc(n)
                ygc(n) = yunif
            endif
c
c   write(73,500) xgc(n),ygc(n)
c   bp = bpol(xgc(n),ygc(n),q30(n))
c   bt = btot(xgc(n),ygc(n),q30(n))
c
c   calculate parallel and perpendicular components of v:
c
c   vper(n) = vperp(amu0,xgc(n),ygc(n),q30(n))
c   vpa2(n) = vpar2(h0,amu0,xgc(n),ygc(n),q30(n))
c
c   test to be sure that vpa2 > 0.
c   if the condition is satisfied, this i.c. is viable, so
c   load it, calculating the total and poloidal components of
c   vpar & vper...
c
c   if(vpa2(n) .ge. 0.) then
c       q10(n) = xgc(n)
c       if(iran .ne. 0) then
c           vpar(n) = ((-1.)**n) * sqrt(vpa2(n))
c       else
c           vpar(n) = sqrt(vpa2(n))
c       endif
c       vparp(n) = vpar(n) * bp / bt
c
c   calculate increment in gyrophase, dphi...
c   assume dphi < twopi...

```



```

        write(71,501) q10(np),q20(np),q30(np),p10(np),p20(np),p30(np)
500     format(2(e16.10,1x))
501     format(6(e16.10,1x))
        else
            write(13,*) n,xgc(n),vpa2(n)
        endif
c
c     an endif used to be here...
c
600     continue
        write(13,662) np,nparts
c
c     rescale ekavg0, now that we know np
c
        if (np .ne. 0) ekavg0 = ekavg0 / float(np)
c
        endif
c
662     format(i4,1x,'particles successfully placed out of
&a total of ',i4,' initial conditions.')
668     format('foul-up on particle # ',i4,2x,'x = ',
&ze12.6,2x,'ham0 = ',e12.6)
c
c     clean up the arrays for the coordinates and momenta;
c     wipe out all entries with index greater than np...
c
        do 700 n=np+1,nmps
            q10(n) = 0.
            q20(n) = 0.
            q30(n) = 0.
            p10(n) = 0.
            p20(n) = 0.
            p30(n) = 0.
            hami0(n) = 0.
            xgc(n) = 0.
700     continue
c
c     return
c     end
*****
***** Magnetic Field Components... *****
*****
real function bex(q1,q2,q3)
real kappa

```

1150

1160

1170

1180

bex

```

common /fields/ alfa,b0,delta,efield,kappa
bex = delta * q2
return
end

```

1190

```

*****

```

```

real function bwhy(q1,q2,q3)
common /fields/ alfa,b0,delta,efield,kappa
bwhy = q1
return
end

```

bwhy

```

*****

```

```

real function bzee(q1,q2,q3)
real kappa
common /fields/ alfa,b0,delta,efield,kappa
bzee = alfa
return
end

```

bzee

1201

```

*****

```

```

***** Components of the Vector Potential... *****

```

```

*****

```

```

real function ax(q1,q2,q3)
real kappa
common /fields/ alfa,b0,delta,efield,kappa
ax = -0.5 * alfa * q2
return
end

```

aX

1210

```

*****

```

```

real function ay(q1,q2,q3)
real kappa
common /fields/ alfa,b0,delta,efield,kappa
ay = 0.5 * alfa * q1
return
end

```

ay

1220

```

*****

```

```

real function az(q1,q2,q3)
real kappa
common /fields/ alfa,b0,delta,efield,kappa
az = 0.5 * (delta * q2 * q2 - q1 * q1)
return
end

```

aZ

```

*****

```

```

***** Poloidal and Total Magnitudes for the Magnetic Field... *****

```

```

*****

```

```

real function bpol(q1,q2,q3)
real kappa
common /fields/ alfa,b0,delta,efield,kappa
bpol = sqrt(bex(q1,q2,q3)**2 + bwhy(q1,q2,q3)**2)
return
end

```

bpol

```

real function btot(q1,q2,q3)
real kappa
common /fields/ alfa,b0,delta,efield,kappa
btot = sqrt(bpol(q1,q2,q3)**2 + bzee(q1,q2,q3)**2)
return
end

```

btot

1240

***** Definition of the flux surface that is single-valued in y... *****

*****--First, an X-Point... *****

```

real function xxsurf(q2,psi)
real kappa
common /fields/ alfa,b0,delta,efield,kappa
arg = 2.0 * abs(psi) + delta * q2 * q2
xxsurf = sqrt(arg)
return
end

```

xxsurf

1250

***** O-Point surface that is single-valued in y... *****

```

real function xosurf(q2,psi)
real kappa
common /fields/ alfa,b0,delta,efield,kappa
arg = (2. * abs(psi) + delta * q2 * q2)
xosurf = sqrt(arg)
return
end

```

xosurf

1260

***** Definition of an X-line flux surface that is single-valued *****

***** in x... *****

```

real function yxsurf(q1,psi)
real kappa
common /fields/ alfa,b0,delta,efield,kappa
arg = (2. * psi + q1 * q1) / delta
yxsurf = sqrt(arg)

```

yxsurf

1271

REFERENCES

- [1] Giovanelli, R. G., *Nature*, **158**, 81 (1946).
- [2] Giovanelli, R. G., *Mon. Not. Roy. Ast. Soc.*, **107**, 338 (1947).
- [3] Giovanelli, R. G., *Mon. Not. Roy. Ast. Soc.*, **108**, 163 (1948).
- [4] Hones, E. W., Jr. (ed.), *Magnetic Reconnection in Space and Laboratory Plasmas*, Geophysical Monograph No. 30, American Geophysical Union, Washington, D.C. (1984).
- [5] Gold, T. and Hoyle, F., *Mon. Not. Roy. Ast. Soc.*, **120**, 89 (1960).
- [6] Parker, E. N., *Astrophys. J., Suppl. Ser.*, **8**, 177 (1963).
- [7] Axford, W. I., *Rev. Geophys. Space Phys.*, **7**, 421 (1969).
- [8] Nishida, A., *Geophys. Res. Lett.*, **10**, 451 (1983).
- [9] Coppi, B., Laval, G., and Pellat, R., *Phys. Rev. Lett.*, **16**, 1207 (1966).
- [10] Neidner, M. B. and Brandt, J. C., *Astrophys J.*, **223**, 655 (1969).
- [11] Galeev, A., Rosner, R., and Vaiana, G., *Astrophys. J.*, **229**, 318 (1979).
- [12] Rosenbluth, M. N., and Rutheford, P. H., in *Fusion*, Teller, E. M. (ed.). New York: Academic Press (1981).

- [13] Boyd, T. J. M. and Sanderson, J. J., *Plasma Dynamics*. New York: Barnes and Noble (1969).
- [14] Greene, J. M., *JGR*, **93**, 8583 (1988).
- [15] Dungey, J. W. *Phil. Mag.*, **44**, 725 (1953).
- [16] Dungey, J. W. *J. Atmos. Terr.*, **40**, 231 (1978).
- [17] Vasyliunas, V. M., *Rev Geophys. Space Phys.*, **13**, 303 (1975).
- [18] Hockney, R. W, *Computer Simulation Using Particles*. New York: IOP Publishing Ltd. (1988).
- [19] Martin, R. F., In *Modelling Magnetospheric Plasma*, Geophys. Monograph Series No. 44. Washington, D.C.: AGU (1988).
- [20] Martin, R. F., *J. Geophys. Res.*, **91**, 11985 (1986).
- [21] Moses, R. W., Finn, J. M., and Ling, K. M., In publication.
- [22] Deeg, H-J., Borovsky, D. E., and Duric, N., *Phys. Fluids B.*, 2660 (1991).
- [23] Alfvén, H., *J. Geophys. Res.*, **73**, 4379 (1968).
- [24] Stern, D. P., *J. Geophys. Res.*, **84**, 63 (1979).
- [25] Dragt, A. J. and Finn, J. M. *JGR*, **81**, 2327 (1976).
- [26] White, R. B., Boozer, A. H., and Hay, R., *Phys. Fluids*, **25**, 575 (1982).
- [27] Northrup, T. G., *The Adiabatic Motion of Charged Particles*, Interscience, New York (1963).

- [28] Kruskal, M. D., *J. Math. Phys.*, **3**, 806 (1962).
- [29] Christofilos, N. C., *J. Geophys. Res.*, **64**, 869 (1959).
- [30] Van Allen, J. A., Ludwig, G. H., Ray, E. C., and Mc Ilwainm C. E., *ARS J.*, **28**, 588 (1958).
- [31] Fowler, T. K., in *Fusion*, Teller, E. M. (ed). New York: Academic Press (1981).
- [32] Fukao, S., Ugai, M., and Tsuda, T., *Rep. Ionos. Res. Space Res. Japan*, **29**, 132 (1975).
- [33] Eckhardt, B., *Physica*, **33D**, 89 (1988).
- [34] Bleher, S., Ott, E., and Grebogi, C., *Phys. Rev. Lett.*, **63**, 919 (1989).
- [35] Lichtenberg, A. J. and Lieberman, M. A., *Regular and Stochastic Motion*. Heidelberg: Springer-Verlag (1986).
- [36] Lin, C. C. and Siegel, L. A., *Mathematics Applied to Deterministic Problems in the Natural Sciences*, Macmillan, New York (1974).
- [37] Goldstein, H., *Classical Mechanics*. Reading, Massachusetts: Addison-Wesley (1980).
- [38] Kruskal, M. D., Ramani, A., and Grammaticos, B., *Singularity Analysis and its Relation to Complete, Partial, and Non-integrability*, Proceedings of the NATO Advanced Study Institute on Partially Integrable Nonlinear Evolution Equations and Their Physical Applications, Les Houches (1989).

- [39] Yoshida, H., *Celest Mech.*, **31**, 363 (1983).
- [40] Yoshida, H., *Celest Mech.*, **31**, 381 (1983).
- [41] Yoshida, H., Grammaticos, B., and Ramani, A. *Acta Appl. Math*, **8**, 75 (1987).
- [42] Adler, M. and van Moerbecke, P., *Algebraically Integrable Systems: a Systematic Approach, Perspectives in Mathematics*, Academic Press, New York (1988).
- [43] Ramani, A., Grammaticos, and Bountis, T., *Phys. Reports*, **180**, 159 (1989).
- [44] Flaschka, H., *Phys. Lett.*, **A131**, 505 (1988).
- [45] Hietarinta, J., *Phys. Reports*, **147**, 87 (1987).
- [46] Cauchy, A. L., *C. R. Acad. Sc. Paris*, **9-11, 14, 15, 23** (1839-46).
- [47] Painlevé, P., *Acta Math.*, **25**, 1 (1902).
- [48] Gambier, B., *Acta Math.*, **33**, 1 (1910).
- [49] Ince, E. I., *Ordinary Differential Equations*. London: Dover (1956).
- [50] Bessis, D., *An Introduction to Kowalevski's Exponents*, Proceedings of the NATO Advanced Study Institute on Partially Integrable Nonlinear Evolution Equations and Their Physical Applications, Les Houches (1989).
- [51] Bessis, D. and Chafee, N., *On the Existence and Nonexistence of Natural Boundaries for Nonintegrable Dynamical Systems in Chaotic Dynamics and*

- Fractals*, M. Barnsley and S. Demko, (eds.). New York: Academic Press, (1986).
- [52] Chazy, J., *Acta Math.*, **34**, 317 (1911).
- [53] Garnier, R., *Ann. Ec. Norm.*, **27**, 1 (1912).
- [54] Bureau, F. J., *Ann. Math.*, **44**, 229 (1964).
- [55] Bureau, F. J., *Ann. Math.*, **46**, 1 (1964).
- [56] Bureau, F. J., *Ann. Math.*, **94**, 344 (1972).
- [57] Frisch, U. and Thual, O., *Natural Boundaries For the Kuramoto Model*, in *Workshop on Combustion, Flames, and Fires*, Les Houches, France (1984).
- [58] Kowalevski, S., *Acta Math., Acad. Sci. Hun.*, **14** (1890).
- [59] Chang, Y. F., Tabor, M., and Weiss, J., *J. Math Phys.*, **23**, 531 (1982).
- [60] Grammaticos, Moulin-Ollagnier, J., Ramani, A., Strelcyn, J. M., and Wojciechowski, S., in publication.
- [61] Segur, H; *Lectures at International School "Enrico Fermi"*, Varenna, Italy (1980).
- [62] Ablowitz, M. J., Ramani, A., and Segur, H., *Lett. Nuovo Cimento*, **23**, 333 (1978).
- [63] Ablowitz, M. J., Ramani, A., and Segur, H., *J. Math. Phys.*, **21**, 715 (1980).
- [64] Ziglin, S. L., *Funct. Anal. Appl.*, **16**, 181 (1983).

- [65] Ziglin, S. L., *Funct. Anal. Appl.*, **17**, 6 (1983).
- [66] Ziglin, S. L., *Trans. Moscow Math. Soc.*, **12**, 1 (1983).
- [67] Abraham-Shrauner, B., *J. Math. Phys.*, **31**, 1627 (1990).
- [68] Kim, J. S. and Cary, J. R., *Phys. Fluids*, **26**, 2167 (1983).
- [69] Abramowitz, M. and Stegun, I. A., *Handbook of Mathematical Functions*.
London: Dover (1972).
- [70] Flaschka, H. and Newell, A. C., *Commun. Math. Phys.*, **76**, 65 (1980).
- [71] Speiser, T. W., *J. Geophys. Res.*, **70**, 4219 (1965).
- [72] Abraham-Shrauner, B., Private Communication.
- [73] Ablowitz, M. J. and Segur, H., *Solitons and the Inverse Scattering Transform*. Philadelphia: SIAM (1981)
- [74] Its, A. R. and Novokshenov, V. Y., *The Isomonodromic Deformation Method in the Theory of Painlevé Expansions*, Lecture Notes in Mathematics, No. 1191, Springer-Verlag, Heidelberg (1980).
- [75] Fokas, A. S. and Ablowitz, M. J., *J. Math. Phys.*, **23**, 203 (1982).
- [76] Birkhoff, G. D., *Trans. AMS*, **10**, 436 (1909).
- [77] Tracy, E. R., Chen, H. H., Lee, Y. C., *Phys. Rev. Lett*, (1984).
- [78] Mc Donald, S. W. and Kaufmann, A. N., *Phys. Rev.*, **32A**, 1708 (1985).
- [79] Neil, A. J., Ph. D. Thesis, College of William and Mary (1992).

- [80] De Vogelaere, R., *Methods of Integration which Preserve the Contact Transformation Property of Hamiltonian Equations*, Dept. Mathematics, Univ. of Notre Dame report 4 (1956).
- [81] Channell, P. J., *Symplectic Integration Algorithms*, LANL Report AT-6:ATN-83-9 (1983).
- [82] Ruth, R. D., *IEEE Trans Nuc. Sci.*, **30**, 2669 (1983).
- [83] Forest, E. and Ruth, R. D., *Physica*, **43D**, 105 (1990).
- [84] Mc Lachlan, R. I. and Atela, P., *Nonlinearity*, **5**, 551 (1992).
- [85] Kang, F., and Qin, M-Z., *Comp. Phys. Commun.*, **65**, 173 (1991).
- [86] Dragt, A. J. and Finn, J. M., *J. Math. Phys.*, **17**, 2215 (1976).
- [87] Qian, S., and Lee, Y. C., *The Split Operator Method*, preprint, Dept. of Physics and Astronomy, University of Maryland.
- [88] Channell, P. J. and Scovel, C., *Nonlinearity*, **3**, 231 (1990).

VITA

Jay Walter Larson was born on August 14, 1962 at 10:54 P. M. Central Daylight Time. His parents are Joyce Elva Rockne Larson and Walter John Larson.

At age five Jay entered Hoak Elementary School in Des Moines. In fourth grade, the author won first place in the fourth-sixth grade category in the Iowa Pollution Poster Contest, which gave him an opportunity to meet Governor Robert Ray, who complimented Mr. Larson on his "good manners." Fifth and sixth grades were spent at Wright Elementary School, and grades seven through nine were spent at Brody Junior High. In tenth grade, Mr. Larson entered Norwalk High School in Norwalk, Iowa. By the end of his junior year, Jay had become restless, and finished his high school diploma during August, 1979 at the Area XI Community College in Ankeny, Iowa.

In the fall of 1979, the author entered Drake University in Des Moines, Iowa, where he majored in both physics and mathematics, also taking a minor in French. In May, 1984, Jay graduated from Drake University, and entered the Graduate Program in Physics at The College of William and Mary in August, 1984. In May, 1986, the author earned the M.S. Degree in Physics. On April 14, 1992, Mr. Larson successfully defended his dissertation, *Painlevé Singularity Analysis Applied to Charged Particle Dynamics During Reconnection*, thus gaining a Ph. D. Degree in Physics.